Paper-Based Analytical Devices

with Simplified Signal Detection for Medical Screening

August 2017

YAMADA, Kentaro

A Thesis for the Degree of Ph.D. in Engineering

Paper-Based Analytical Devices with Simplified Signal Detection for Medical Screening

August 2017

Graduate School of Science and Technology

Keio University

YAMADA, Kentaro

Table of Contents

Chapter 1 General introduction to medical diagnosis on paper-based analytical devices

This chapter is based on
"Paper-Based Inkjet-Printed Microfluidic Analytical Devices",
Kentaro Yamada; Terence G. Henares; Koji Suzuki; Daniel Citterio,
Angewandte Chemie, International Edition, **2015**, *54*, 5294−5310.

"Toward practical application of paper-based microfluidics for medical diagnostics: state-of-the-art and challenges",
Kentaro Yamada; Hiroyuki Shibata; Koji Suzuki; Daniel Citterio,
Lab on a Chip, **2017**, *17*, 1206−1249.

1.1. Short history of paper-based chemical analysis

Although there might be some unaccounted-for examples, the oldest confirmed paper-based analytical device is the litmus paper invented in the 17th century by the Irish chemist Robert Boyle.[1] This surprisingly old device is still around as a well-known simple solution acidity checker, as commonly seen in a science experimental class at elementary schools. The latter half of the 19th century brought the origination of urine testing strips, another example of paper-based analytical devices still in use in modern medical diagnosis. In 1850, the French chemist Jules Maumené has developed a first urine test strip for sugar detection by impregnating sheep's wool with $SnCl_2$,[2] but his system did not grow popular despite its simplicity. In 1883, the English physiologist George Oliver marketed his urine test papers by describing the usefulness of reagent-loaded porous materials (filter paper, linen, and other similar fabrics) requiring only contact with a specimen to inspect albumin, sugar, and total acidity relying on color change.[3] He stressed that eliminated reagent solution handling and instant re-hydration of the pre-deposited reagents leads to manageable, handy yet accurate tests performable by busy practitioners. Despite urine sugar tests being dominated by the tablet inspection with Ames' Clinitest for a period of time, the publication[4] and commercialization of a

glucose-specific test strip (Clinistix)[5] in the 1950s have triggered a renaissance of paper-based testing as a convenient diagnostic platform that requires only dipping of the paper strip into a specimen before the color change is visually read off. In 1964, the company Boehringer Mannheim (currently taken over by Roche Diagnostics) launched the Combur-Test strip with expanded inspection items offered. In spite of minor changes in appearance, colorimetric detection-based urine test strips have remained successful paper-based analytical devices thanks to their ability to inspect a number of urine constituents through simple user operation (dip-and-read) in a short time (~ 120 sec). Although precise determination of target analytes is not achievable, their simplicity and rapidity make them a valuable technique for high-throughput screening of kidney, urogenital tract, metabolic and liver diseases, as well as hemolytic disorders.[6]

Another representative diagnostic device made of "paper" substrates is the lateral flow immunoassay (LFIA). Considering the importance of LFIAs, the "paper" term is interpreted in a broad sense in this Thesis to include nitrocellulose membranes. Albeit not being as long-established as urine dipsticks, it has been already three decades since the concept of LFIAs appeared in US Patents.[7-8] Thanks to the use of antibodies conjugated with labelling agents (*e.g.* gold nanoparticles and dye-loaded particles), LFIAs allow visual detection of specific target antigens. Commercially-available paper-based analytical devices relying on this technique are represented by the pregnancy testing kits for detecting human chorionic gonadotropin (hCG), and influenza testing kits for detecting the nucleoprotein of the influenza virus.

Since the emergence of LFIAs in the 1980s, there seems to be no landmark in the development of paper-based analytical devices. However, a growing number of colorimetry-based paper-made chemical assays have come into the market (*e.g.* the Merckoquant test strips[9]), reflecting a high demand for simple, portable, rapid, and disposable testing devices for various analytical targets. A decade ago, scientists reignited their passion for R&D of paper-based analytical devices after being inspired by the American chemist George Whitesides, who rediscovered microfluidically patterned paper as a valuable platform to construct simple yet functional chemical sensing devices in 2007.[10]

1.2. Basics of microfluidically patterned paper-based chemical analysis

1.2.1. Emergence

The first publication on the use of patterned filter paper in the analytical chemistry field dates back to the 20th century. In 1937, Yagoda has reported colorimetric detection of metal ions (Ni^{2+} and Cu^{2+}) in a "confined" filter paper area prepared by using a water-repellent paraffin barrier (Figure 1-1a).[11] He stated that impregnation of a fixed volume of reagent(s) into the patterned paper spot contributes to quantitative determination of the target analytes in the sample. As another example, chromatographic separation of dyes on a piece of patterned filter paper has been demonstrated by Müller and Clegg in 1949 (Figure 1-1b).[12] In that application, the convenience of patterning of a confined separation paper channel lead to acceleration of the diffusion process and reduction of the reagent consumption.

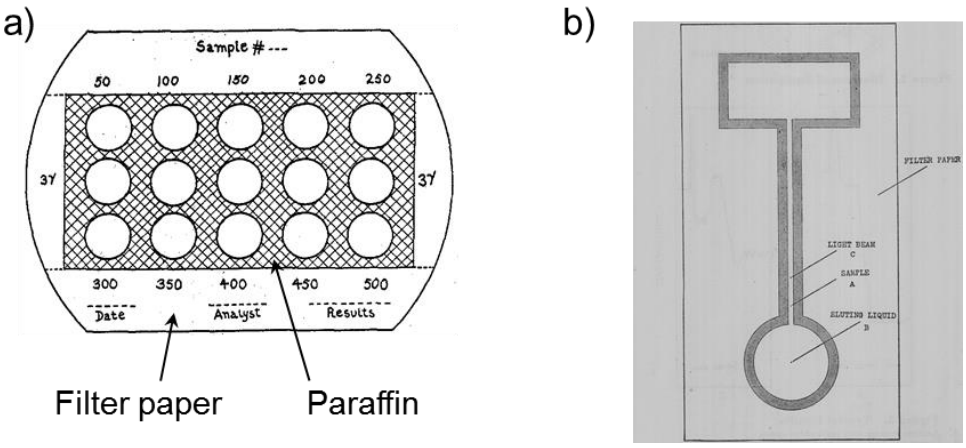

Figure 1-1. Early demonstrations of analytical application of patterned paper: a) confined paper spot for colorimetric metal ion detection. Adapted with permission from Ref 11. Copyright 1937 American Chemical Society; b) microfluidic paper channel for paper chromatography. Reprinted with permission from Ref 12. Copyright 1949 American Chemical Society.

In spite of the extra-values of a patterned paper substrate, there was no response of the scientific community to this research field at that time, with the exception of some follow-up research on paper chromatography.[13-14] It took more than half of a century since the report by Müller and Clegg until patterned paper was discovered as a valuable diagnostic platform. In 2007, the Whitesides group introduced a photolithographically patterned

filter paper targeting colorimetric analyses of urinary glucose and protein (Figure 1-2).[10] Therein they not only laid out some inherent advantages of using paper as a substrate material including its low-cost and safe disposability by incineration, but also demonstrated attractive functional capabilities as an analytical platform, such as multiplexing, capillary force-driven sample liquid transportation, and separation of solid contaminants. Additionally, the chemical composition of cellulosic paper and its high surface-to-volume ratio allows for the simple physical immobilization of reagents required in an analytical assay. As will be discussed in the following section, the external power-free sample driving particularly distinguishes paper-based platforms from conventional micro-total analysis systems (μTAS), of which market entry is hindered by the requirement of fluid handling with external pumping systems.[15]

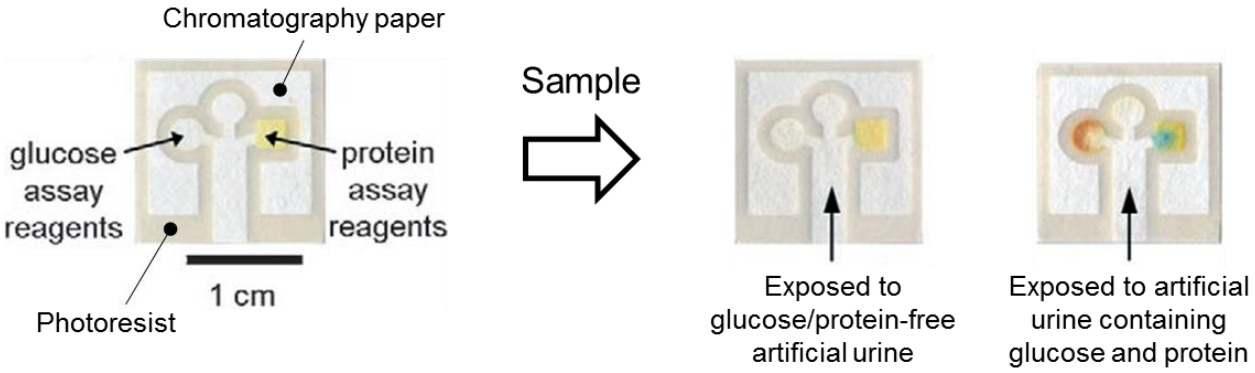

Figure 1-2. First μPAD reported in 2007 targeting simultaneous colorimetric detection of urinary glucose and protein. Adapted with permission from Ref 10. Copyright© 2007 WILEY-VCH Verlag GmbH & Co. KGaA, Weinheim.

In the subsequent decade, there has been an explosive growth of academic research in microfluidically patterned paper-based devices, which are nowadays commonly referred to in short as "μPADs", or as microfluidic paper-based analytical devices.[16] The significant number of relevant review papers indicates widespread interest in R&D of μPADs, and they describe the variety of application fields including medical diagnostics, environmental analysis and food safety monitoring, among others.[17-36] The most actively pursued practical application of μPADs remains probably in medical diagnostics, in line with the original purpose of μPADs.[10] Substantial efforts have been dedicated to expand the clinically-relevant targets (*e.g.* proteins,

metabolites, electrolytes) detectable by μPADs. They now cover a wide class of clinical purposes, ranging from personal daily health checks to biomedical diagnosis of serious conditions.

1.2.2. From microfluidic devices to μPADs: similarities and differences

Being driven by advancements of microfabrication technology in the semiconductor industry, the late 20th century witnessed a rapid growth of miniaturized analytical devices made of polymeric substrate materials (*e.g.* glass, plastics). Micro-total analysis system (μTAS) or lab-on-a-chip (LOC) has been an active research field since its concept was first introduced by Manz in 1990[37], integrating a series of steps for chemical analysis (sample processing, separation, detection, among others) in small channels typically with dimensions of μm.[38] The original intension of miniaturization was to enhance the analytical performance of chemical sensors, especially in terms of selectivity and rapidity profiting from minute diffusion distances.[39] Later on, reduced consumption of relevant components (*e.g.* sample, assay reagents, mobile phase in chromatography) has been recognized as a positive by-product of miniaturization.[39] Although the concept of μTAS has been envisioned as a revolutionary chemical analysis platform including medical diagnostics for its efficiency, rapidity, and economical use of components, the current state is still far from the situation where everyone checks his/her own health condition outside of hospitals using microfluidics.[40] The reason is primarily attributed to the 1) complexity of liquid handling systems requiring difficult start-up processes and operational expertise, and 2) the necessity of sophisticated optical detectors for signal acquisition. The most traditional research approaches in this field are devoted to fluidic control relying on external equipment, and hence, microfluidics have not evolved as the versatile “lab-on-a-chip” system, but partially remained a sophisticated “chip-in-a-lab” system.[41]

Very simply stated, μPADs can be regarded as a paper version of conventional microfluidics. Fluidic channels on typical μPADs are regarded as a bundle of numerous capillaries formed by interwoven cellulosic fibers, whereas μTAS possess a hollow flow path in a polymeric substrate. Despite their different configurations, the capability of sequential chemical reactions and multiplexed assays with small consumption of samples and reagents are common advantages. In addition, the liquid transportation in μPADs also exhibits laminar

flow[42-43] due to the μm-sized pore radius in the paper medium, making the Reynolds number (*Re*) less than 1, as expressed by the following equation:

$$Re = \frac{\rho V L}{\mu} < 1 \quad \ldots \ (1)$$

, where ρ is the fluid density (kg m^{-3}), V is the fluid velocity (m s^{-1}), L is the pore diameter, and μ is the fluid dynamic viscosity (kg m^{-1} s^{-1} = N s m^{-2}).

A clear difference lies in the fact that the fluidic channels are "fully closed" in conventional μTAS, whereas μPADs possess "open-air" flow paths, unless covered by lamination films. Since detection on conventional μTAS is carried out in a sealed channel, the detection signal relies on an equilibrium between the sample phase and a second interface hosting a receptor for the analytical target (*e.g.* adjacent laminar flow, channel surface, droplet interface). As is clear from this mechanism, the signal reflects the "concentration" of the analyte in the sample fluid. On the other hand, open-air flow paths on μPADs are prone to sample evaporation. Consequently, the detection mechanism on μPADs is often based on exhaustion of analyte molecules at the detection region, rather than an equilibrium state between a liquid sample phase and an immobile receptor, leading to "absolute analyte amount-based" signal generation, with the presumption that sufficient ligand/receptor is available.

1.2.3. Fabrication techniques

As schematically shown in Scheme 1-1, primary fabrication procedure of μPADs can be divided into 1) patterning of a microfluidic structure onto the substrate, 2) deposition of (bio)chemical assay components (including electrodes).

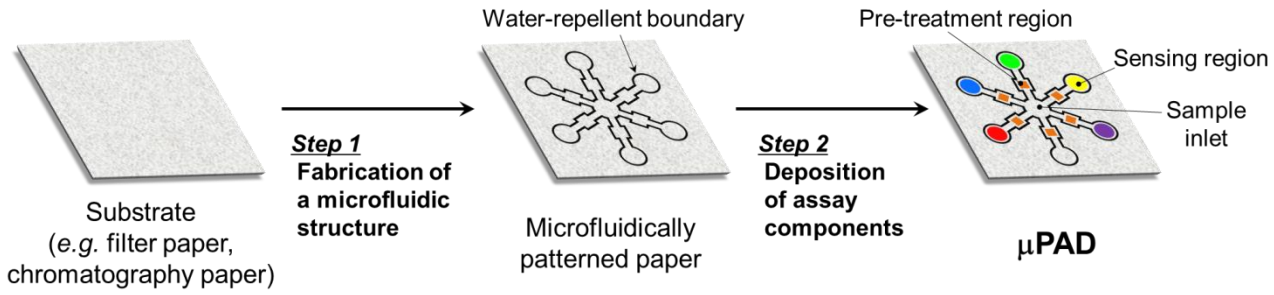

Scheme 1-1. Schematic illustration depicting a general μPAD fabrication procedure.

1.2.3.1. Microfluidic structure patterning

Patterning of microfluidic channels on paper is a manufacturing step exclusive to μPADs. This process is normally completed as a first step in order to avoid undesired exposure of chemical assay reagents to harsh manufacturing conditions (*e.g.* heating, exposure to UV). A wide array of patterning techniques has become available for laboratory-based R&D of μPADs, and features of representative patterning methods are summarized in Table 1-1. Although there are differences related to achievable resolution, pattern flexibility, speed, or simplicity of equipment, almost every patterning technique reported up to date is applicable to prototype development in laboratory experiments, as described in many relevant review articles.[23, 25, 32-33, 35] Currently, it might be a common perception that the wax printing approach (Figure 1-3) is the "best" patterning method. This fact is reflected by the largest number of original publications on wax-printed μPADs (Figure 1-4). The reasons for its wide acceptance lie in 1) the not very expensive cost of wax printers (~ $900), 2) the quick print speed (30 pages of A4-sized paper in 1 min (Ref [44])), 3) the simple post-printing treatment (heating for 30 s at 135°C (Ref [44])), and 4) the flexibility in print features (created on a graphic software). Wax patterning onto nitrocellulose substrates is also possible,[45] in spite of their flammable nature.

Table 1-1. Comparison of representative techniques for microfluidic structure patterning on paper.

Patterning method	Equipment	Advantage	Disadvantage	Ref.
Photolithography	UV light source, heating equipment	High-resolution of patterned features (186 ± 13 μm for channel; 248 ± 13 μm for barrier)	Uses volatile organic solvent; high-cost of photoresist; hydrophilic area exposed to polymers and solvents.	10, 16
Plotting	Modified plotter	Hydrophilic area not exposed to polymers and solvents.	Requires a customized plotter; uses volatile organic solvent.	46
Inkjet etching	Modified inkjet printer	Applicable to reagent dispensing	Requires a customized printer; uses volatile organic solvent; hydrophilic area exposed to polymers and solvents.	47-48
Inkjet printing	Inkjet printer, UV light source	Applicable to reagent dispensing; hydrophilic area not exposed to polymers and solvents.	Requires intense UV irradiation.	49
Wax printing	Wax printer, heating equipment	Rapid (< 5 min); hydrophilic area not exposed to polymers and solvents.	Requires heating equipment.	44, 50
Flexography	Flexographic press	High-throughput (60 m min^{-1}).	Requires two printing cycles; uses volatile organic solvent.	51

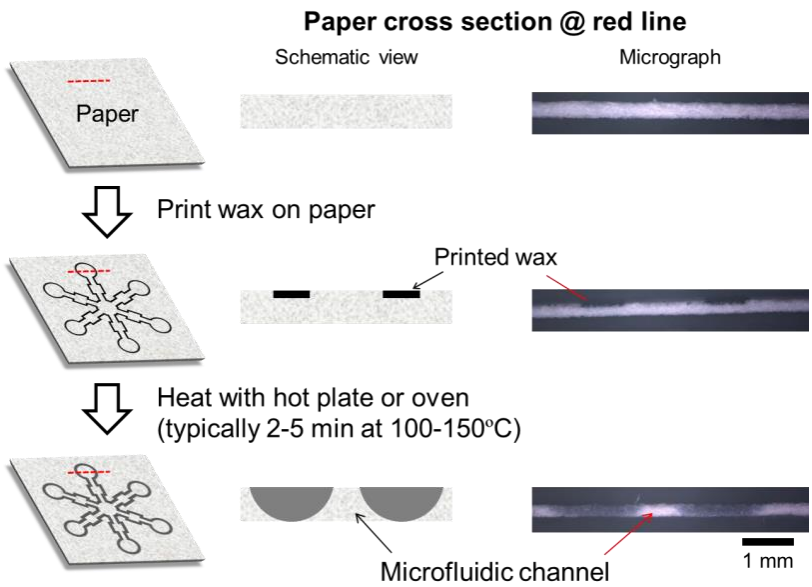

Figure 1-3. General procedure of microfluidic structure patterning by the wax printing method.

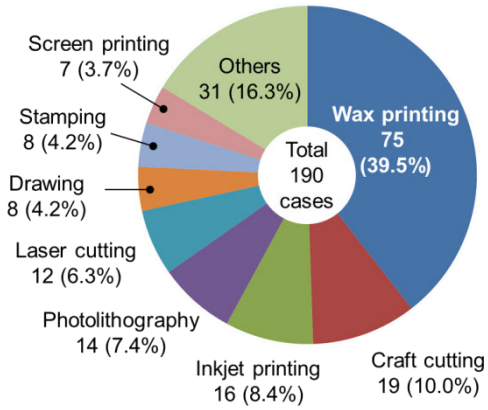

Figure 1-4. Classification of literature publications on μPADs according to the implemented patterning technique. The Web of Science™ (Thomson Reuters) was used as search engine. Scanned publications were limited based on the following criteria: 1) paper was published between January 2011 and December 2016, 2) paper is written in English, 3) paper is an original research article, and 4) the topic meets the conditions of "Title: paper-base*" OR "Title: patterned paper" OR "Title: paper device*" AND "microfluidic*". 199 results were found based on the above conditions. Of those publications, 14 were removed from the survey because of probably mistakenly-categorized review articles, missing relation to paper microfluidics, or the lack of access right to the original article.

Nevertheless, wax printing is not a universal patterning method. One first issue is the incompatibility of wax patterned microstructures with solutions of low surface tension, since the barrier function relies on the high surface energy of the wax-coated cellulosic fibers. This shortcoming is detrimental for example in handling poorly water-soluble indicators dissolved in organic solvents or blocking solutions containing high concentrations of surfactant. In those situations, inkjet printing will play an essential role. With the aid of inkjet printing, the Brennan group has demonstrated silica sol–gel-based patterning of channels that resist solutions with low surface tension (Figure 1-5a).[52] It is worth mentioning that mass production relying on inkjet printing technology is already routine in printed electronics,[53] patterning of polymers for light-emitting diodes and full-color high resolution displays,[54] and nucleic acids for DNA arrays.[55] As elaborated in recent reviews,[35-36] inkjet printing allows microfluidic structure patterning in several ways. In particular, methods relying on UV curable ink (Figure 1-5b)[49] or sizing agents including alkylketene dimer (Figure 1-5c)[56] and hexadecenyl succinic anhydride[57] will fit in mass production schemes, since those components are already in industrial use. Although inkjet printing technology will not be able to compete with flexography in terms of throughput, the capability of economical dispensing of chemical reagents is a significant feature.

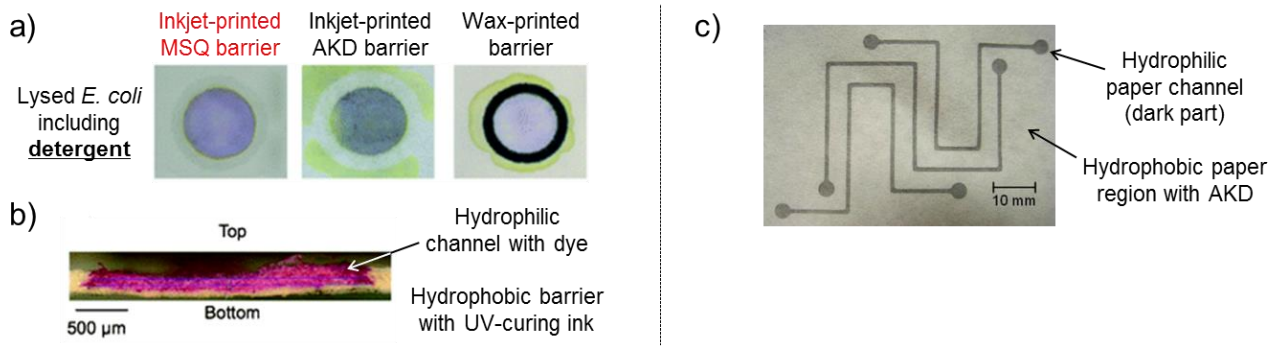

Figure 1-5. Examples of paper patterned by means of inkjet printing: a) inkjet-printed MSQ (methylsilsesquioxane)-based barrier (left) is not breached by a cell-lysing solution with low surface tension, whereas inkjet-printed AKD (alkylketene dimer)-based barrier (middle) and wax-printed barrier (right) were breached. Adapted from Ref 52 with permission of The Royal Society of Chemistry; b) a microscopic image of a cross section of filter paper patterned with an inkjet-printed UV-curable ink. Adapted from Ref 49 with permission of The Royal Society of Chemistry; c) microfluidic structure prepared by inkjet-printing of the AKD sizing reagent. Adapted from Ref 57, Copyright 2010, with permission from Elsevier.

1.2.3.2. Deposition of assay components

Following the microfluidic structure patterning, (bio)chemical assay components must be deposited to achieve ready-to-use diagnostic devices. For μPAD fabrication, most assay components need to be applied in a specific region along the fluid flow path. The simplest example is the deposition of different indicators onto independent sensing regions for the purpose of a multiplexed μPAD assay. Manual pipetting is commonly performed in laboratory-based proof-of-concept demonstration. However, a manual process is not an option for high volume manufacturing, due to issues of poor fabrication reproducibility and the high amount of labor. Additionally, manual handling limits the volume of production to several million tests per year.[58] Considering the production volume of glucose meter test strips and LFIA pregnancy tests (10^{10} per year, > 10^{7} per year, respectively[59]), the demand for μPADs targeting routine health checks will potentially be beyond the throughput achievable by manual fabrication.

For the purpose of reagent deposition on μPADs, inkjet printing has been known as a powerful instrumental approach. The main strengths of this technique lie in 1) a high degree of flexibility of pattern features based on digital image input, and 2) potential compatibility with custom inks. Since our research group first reported a microfluidic paper-based urine sensing device fabricated from a single inkjet dispensing system in 2008,[47]

this technique has remained the exclusive μPAD fabrication method allowing both assay reagent deposition and microfluidic structure patterning. Commonly used inkjet dispensing technology includes the thermal (Figure 1-6a) and piezoelectric (Figure 1-6b) actuation systems.

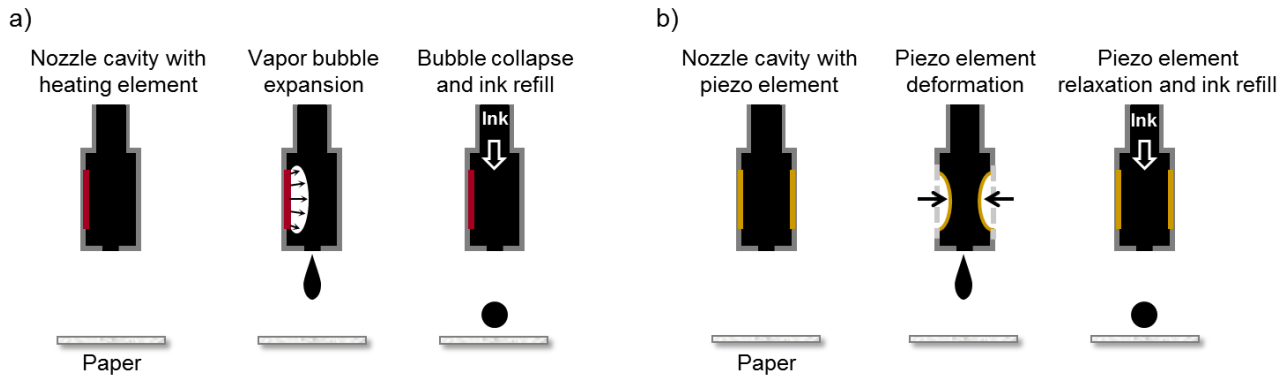

Figure 1-6. Schematics showing the working principle of drop-on-demand (DOD) inkjet printing; a) thermal actuation system; b) piezoelectric actuation system. Adapted with permission from Ref 35. Copyright© 2015 WILEY-VCH Verlag GmbH & Co. KGaA, Weinheim.

Under the drop-on-demand (DOD) inkjet technologies, the physical properties of a reagent solution to be dispensed as "ink" are crucial factors determining the success or failure of ejection. Printability is often evaluated by the Z value expressed by the following equation composed of the Ohnesorge (Oh), Reynolds (Re), and Weber (We) numbers[60-63]:

$$Z = Oh^{-1} = \frac{Re}{\sqrt{We}} = \frac{\sqrt{\gamma \rho a}}{\mu} \quad \ldots \ (2)$$

, where γ is the fluid surface tension, ρ is the fluid density, a is the nozzle diameter, and μ is the fluid dynamic viscosity. A number of studies tried to determine the range of the Z value for stable inkjet-printing. Although unique criteria are probably not available, Derby found that stable DOD inkjet dispensing is achievable in the range of $1 < Z < 10$.[60-61, 63] Another literature specifies a similar optimal range of $4 < Z < 14$.[62] Too low Z values lead to unsuccessful droplet ejection due to high viscosity, whereas inks with high Z values tend to be accompanied by a number of satellite drops, rather than resulting in clearly defined single droplets. Inkjet-printability plotted in the Re and We number coordinates can be summarized as in Figure 1-7.[60]

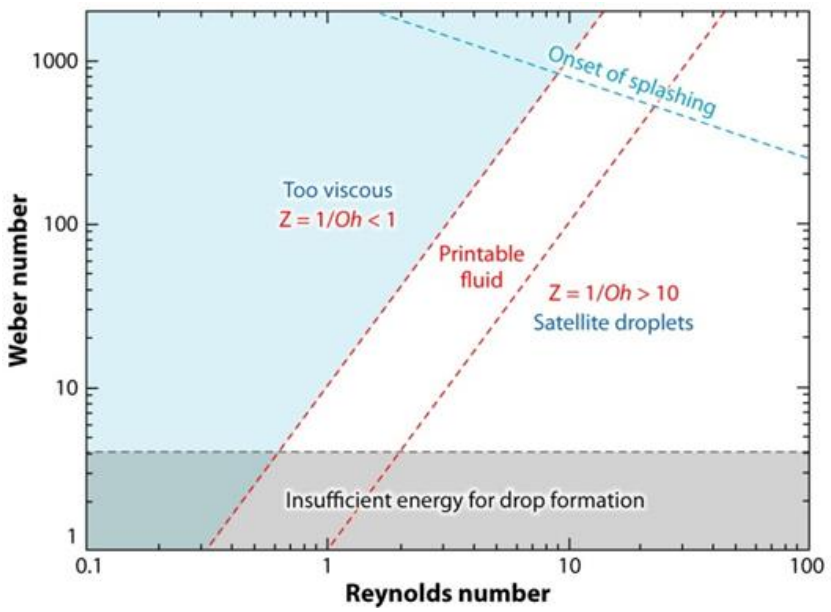

Figure 1-7. Requirements for stable inkjet printing plotted with the Reynolds and Weber number coordinates. Reproduced from Ref 60.

Aside from the *Z* value, the ink surface tension and viscosity have a certain working range for successful ejection. Typically, the suitable surface tension is reported to be 28−40 mN m^{-1} for both the thermal and piezoelectric systems.[64] The desirable ink viscosity differs depending on the actuation mechanism. A thermally-actuated inkjet printer is capable of dispensing liquids with viscosities of minimally 1−1.5 cP,[65] and typically < 5 cP,[66] and thus is compatible with simple aqueous solutions. On the other hand, a piezoelectrically-actuated system works at higher ink viscosities than thermal inkjet systems (minimally 5−10 cP (Ref [65]), typically < 20 cP (Ref [67]), and maximally ~ 50 cP (Ref [66])), mostly requiring addition of viscosity modifying agents, for instance glycerol or ethylene glycol. In handling an ink containing particulate materials, as a rule of thumb, the particle size should be less than one-hundredth part of the nozzle orifice diameter.[66]

Despite these limitations, various functional materials have been inkjet-printed for μPAD development (Table 1-2), and importantly, inkjet-printed μPADs cover a wide range of analytical application fields including not only medical diagnosis, but also environmental analysis, food quality monitoring and criminal investigation.[35] In this Thesis research, the utility of inkjet-printing is showcased in several applications of assay component dispensing onto μPADs (precise deposition of reagents into microfluidic structures, text-shaped printing of an indicator).

Table 1-2. Common analytical assays for inkjet-printed μPADs. Adapted with permission from Ref 35. Copyright© 2015 WILEY-VCH Verlag GmbH & Co. KGaA, Weinheim.

Type of assay	Printed functional material	Primary targeted analyte	Ink composition for inkjet printing	
			Thermal	Piezoelectric
Classical colorimetric indicator	Chromogenic dye	Metal ions, proteins	Water (buffer)	Water (buffer), viscosity modifier[a], surfactant[b]
Immunoassay	Antibody	Antigen	Buffer	Buffer, viscosity modifier, surfactant
Enzymatic assay	Enzyme	Metabolites	Buffer	Buffer, viscosity modifier, surfactant

[a] Glycerol and glycols are typical examples of viscosity modifiers. [b] Triton X-100 is an example of a surfactant (non-ionic) to adjust the ink surface tension..

1.3. User operation for μPADs targeting medical diagnosis

In contrast to well-established and sophisticated analytical techniques (*e.g.* mass spectrometry, high-performance liquid chromatography, nuclear magnetic resonance analysis, optical imaging), the philosophy of μPADs is to provide low-cost, user-friendly, and rapid testing. Although μPADs would not be able to compete with those sophisticated systems in terms of analytical performance (achievable limit of detection, accuracy, precision, among others), their simplicity removes barriers in on-site diagnosis, where trained personnel and laboratory settings are unavailable. According to the guidelines for "CLIA (Clinical Laboratory Improvement Amendments) waived tests", diagnostic devices for use outside of a laboratory should be readily operated by any user following instructions provided in 7th-grade level English.[68] Neither complicated user operation (*e.g.* sample processing, technique-dependent reagent manipulation, operator calibration/interpretation/calculation), nor high risk of operational errors (*e.g.* incorrect placement of specimen/reagent/device, order of reagent application, timing of procedures) is allowed for ideal μPADs.

User operation primarily involves the following two steps: 1) introduction of sample into the device and 2) interpretation of the resulting signal. Among those operational steps, this section focuses on the progress in simplification of 1) introduction of sample into the device.

1.3.1. Separation

In an idealized point-of-care diagnostic device, no user intervention except sample deposition is necessary to run assays.[59] Assumedly, the most commonly performed pretreatment of biological samples is the separation of blood cells from whole blood to remove the interfering red color and to prevent unwanted changes in target analyte or background concentrations caused by potential hemolysis. Conventionally used centrifugal separation methods have been eliminated either by incorporating a blood cell filter (Figure 1-8a),[69-74] by pre-depositing agglutination antibodies (Figure 1-8b)[75] or concentrated salt solution for blood cell deformation (Figure 1-8c)[76], or by filtering through paper pores via capillarity (Figure 1-8d).[77] Among those approaches, the integration of commercial cell filtering membranes is extensively investigated in the field of μPADs, because 1) expensive and chemically sensitive antibodies are not necessary, 2) the use of high salt

concentrations (adverse effects in some cases) is obsolete, and 3) the required blood volume is relatively small (around 30 μL). A crucial factor in membrane-based plasma separation is hemolysis. Pollock et al. observed a hemolysis rate of 9.5% in their ALT assay using a 3D-structured μPAD.[73] Interestingly, two different lots of blood cell filtering membranes brought significant differences in hemolysis rates of the resulting μPADs (21.1% versus 1.6%). This issue was later solved via anti-hemolytic coating of the membrane.[74]

Although most studies demonstrate real sample analysis using serum, those μPADs can in principle be adapted to whole blood analysis by attaching a filtering membrane without sacrificing simplicity of manipulation. One inevitable risk in using a blood cell filter is the uncertainty of analyte adsorption onto the membrane, which can be influenced by interaction between the membrane material and non-target blood components, of which the composition may vary from sample to sample.[59] Separation of small organic molecules has been also achieved mainly in the context of electrochemical analysis on μPADs. Therein, the paper substrate works as the stationary phase and organic molecules with different pKa values are separated depending on their distribution equilibrium between the paper/sample liquid phases. Examples of chromatographic separation on μPADs include ascorbic acid (pKa 4.1) and uric acid (pKa 5.4),[78] paracetamol (pKa 9.8 for the hydroxyl group) and 4-aminophenol (pKa 5.3 for the amino group),[79] as well as ascorbic acid and dopamine (pKa 8.9).[80] Separation of redox-active species such as ascorbic acid is efficient in amperometric measurements of analytes with similar redox potential. However, many parameters including separation pH, ionic strength and property of the paper substrate (porosity, cation exchange capacity) must be considered for achieving satisfactory separation resolution.

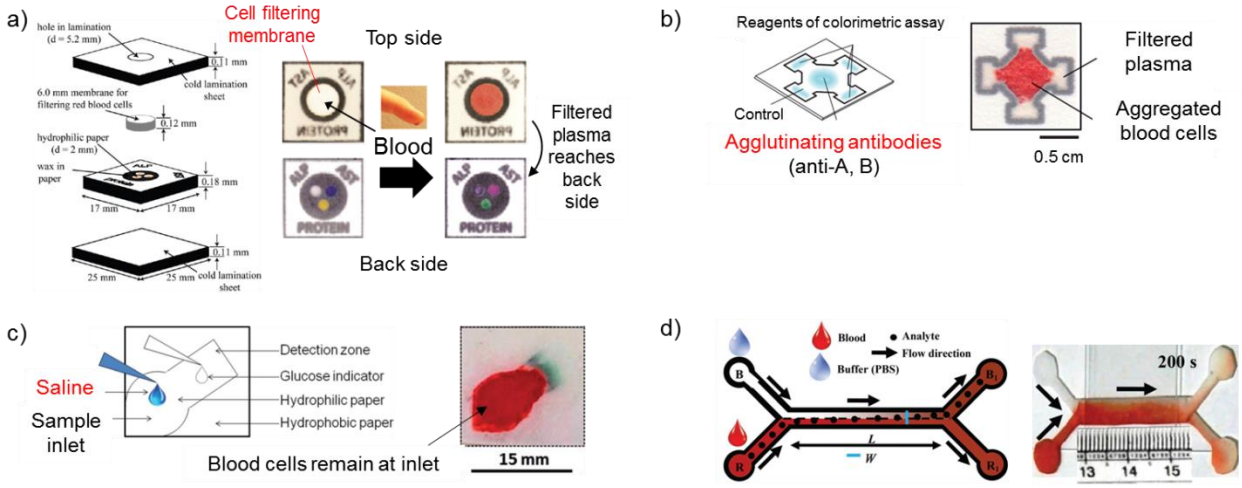

Figure 1-8. Proposed strategies for blood plasma separation on paperfluidic devices: a) integration of cell filtering membrane. Adapted with permission from Ref 71. Copyright 2012 American Chemical Society. b) Pre-deposition of agglutinating antibodies. Adapted from Ref 75 with permission from The Royal Society of Chemistry. c) Pre-deposition of high concentration salt solution. Adapted from Ref 76 with permission from The Royal Society of Chemistry. d) Capillarity-based cell filtering on cellulosic paper channel. Reproduced from Ref 77 with permission from The Royal Society of Chemistry.

1.3.2. Mixing and reagent addition

Aside from separation, mixing of reagent(s) is also an essential process to ensure that desired detection reactions occur. Automated mixing of assay components is possible by pre-depositing those reagents either onto the region where the detection reaction occurs or into mid-flow of paper channels if direct contact between multiple detection reagents is adverse. Sequential addition of multiple reagents contributes to highly sensitive and selective (bio)chemical assays, for example by adding signal amplifying agents or by washing away unbound substances. However, those operational steps cannot be achieved simply by pre-deposition of components. Immunoassays are a representative assay motif, which necessitates such multi-step procedure. Although single-step formats work properly as seen with commercial lateral flow immunoassay strips, an additional washing step with buffer and a signal enhancement step are desirable to improve detection limit and specificity of the assay, which will eventually contribute to eliminate false results. Based on the fact that the number of false negatives in rapid influenza diagnostic testing is reported to be as high as nearly 30%,[81] signal amplification is of utmost importance to detect trace amounts of disease markers. Primary signal enhancing

strategies include incorporation of enzymatic assays (*e.g.* combination of target-responsive oxidase, peroxidase and its chromogenic substrate[82]) and gold precipitation reaction on labelling particles.[83-86] The conventional format of microtiter plate-based methods can be straightforwardly transferred onto paper-based assay by preparing spots mimicking a 96-well plate (coined paper microzone plate).[87] Paper microzone plate-based immunoassays greatly reduce assay time, amount of reagents, and sample volume.[88] However, they still involve step-by-step addition of reagents and incubation, and thus are not suitable for untrained end users. As will be discussed later, handling of those systems remains limited to laboratory environment tests for biomedical diagnosis of tumors or other severe diseases.

The step-by-step reagent addition challenge has been cleared for μPADs by the manipulation of flow-channel geometry. The Yager group at the University of Washington pioneered programmed reagent delivery on a two-dimensional paper network (2DPN). Notably, they introduced a folding card platform, which allows to run the complete assay by simply 1) adding sample liquid and water onto predetermined pads from the beginning and 2) folding the card (Figure 1-9a).[85] Varying distances between the detection region and the reagent reservoirs result in sequential arrival of components. On this platform, they have performed a sandwich immunoassay of PfHRP2, a malaria marker protein, with integrated washing step and enhancement step of the labelling gold nanoparticles (reaction steps schematically shown in Figure 1-9a). The device showed 4-fold better limit of detection (2.9 ± 1.2 ng mL^{-1}) than the case without signal enhancement. Similarly, a “maze-like” flow path has been reported to be applicable for multi-step immunoassays (Figure 1-9b).[89] In this approach, users only have to immerse the device leg into a sample to run the assay. The authors have demonstrated the analytical application by the detection of urinary human chorionic gonadotropin (hCG) based on the ELISA mechanism. Despite the relatively large channel dimension, the achieved limit of detection (8.1 mIU mL^{-1}) was better than the one typically found with commercial pregnancy test kits (higher than 20 mIU mL^{-1}), possibly due to the signal amplification by the ALP-BCIP/NBT enzymatic reaction system. A shortcoming of this approach is the necessity of a relatively large sample volume (50 μL for 1.5 × 3.5 cm^2 device), which virtually limits the applicable clinical specimen to urine only. Accordingly, on-chip sample treatment is more challenging. For example, maintenance of assay pH is desired to ensure constant

enzymatic activity. However, there is a concern that simply pre-depositing pH buffer components is not efficient to maintain the desired pH for enlarged sample volumes. It is a general challenge to load large amounts of reagents onto μPADs to accommodate large sample volumes.

Later, Lutz and co-workers found that treatment of paper strip channels with sucrose solution is helpful to generate delayed flow on a 2DPN.[90] The higher the concentration of the treating sugar solution, the more delayed the fluid arrival in the detection zone (Figure 1-9c). Different impregnated sugar concentrations enable tuned delayed delivery (from minutes to nearly an hour[90]) without the need of manipulating channel geometry. The finalized device for malaria diagnosis is composed of quadruple legs treated with 0, 30, 54 and 65% of sucrose solution, a single detection channel with absorbent pad, and four sample/reagent source pads on the opposite side of the foldable card (Figure 1-9d, left).[90] The assay procedure is as simple as the previously developed 2DPN shown in Figure 1-9a. This strategy however, is accompanied by a viscous fingering effect, where locally sugar-free sample fluid randomly wicks faster due to interfacial instability between highly viscous and less viscous liquids. The authors have concluded that this effect does not diminish reproducibility in the delay time, but quantitative signal readout will be affected due to the heterogeneous color development as observed in Figure 1-9d (right).

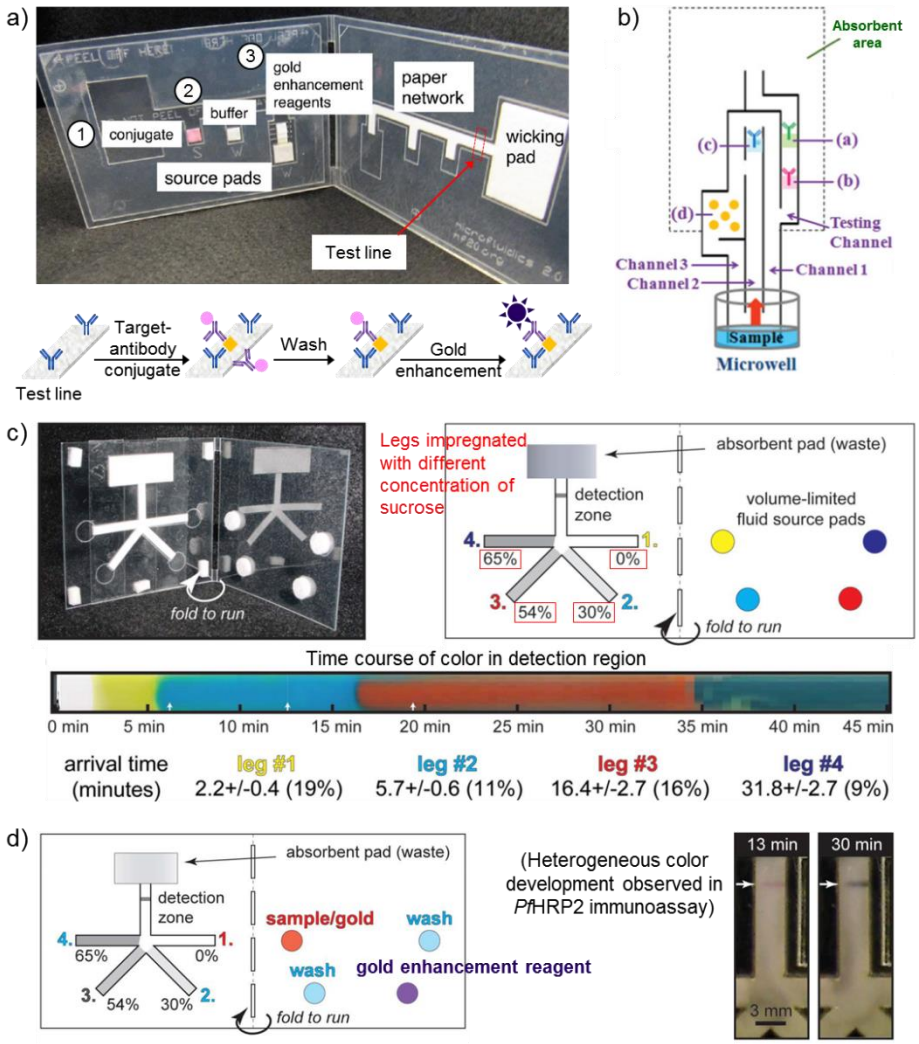

Figure 1-9. Representative approaches for automated sequential delivery of reagents on paper devices: a) gold enhancement-incorporated sandwich immunoassay for *Pf*HRP2 with the use of reagent source pads with different distances from the test line (top) and the reaction scheme of the relevant multistep immunoassay (bottom). Circled numbers in the top figure show the order of delivery at the test line. Adapted with permission from Ref 85. Copyright 2012 American Chemical Society. b) Automated enzyme-linked immunosorbent assay (ELISA) of human chorionic gonadotropin (hCG) on a nitrocellulose-based device with "mazelike" structured channel. Reproduced from Ref 89 with permission from The Royal Society of Chemistry. c) Device design of sucrose-treated nitrocellulosic channel for the demonstration of sequential transport of dye solution (top) and time-course of observed color delivery at the detection zone (bottom). Adapted from Ref 90 with permission from The Royal Society of Chemistry. d) Device design for *Pf*HRP2 sandwich immunoassay with gold enhancement mechanism (left) and images of the detection zone showing inhomogeneous color development after 13 and 30 min. Reproduced from Ref 90 with permission from The Royal Society of Chemistry.

All above approaches for automated multistep assays have own advantages and disadvantages. However, they inevitably entail enlargement of the device dimensions. In designing devices for practical use, it is of high importance to minimize the channel area to keep material cost, reagent consumption, and sample volume as low as possible. Though paper is valued as an economic substrate, it generally accounts for a large fraction of material costs of a paper-based device.[91-92] Additionally, decreased flow path areas will unsurprisingly contribute to better sensitivity by suppressing loss of target analyte molecules during sample transportation. One strategy not requiring an increase of device dimension has been reported for the purpose of a single step chemiluminescent LFIA.[93] The device consists of a reagent-loaded shunt pad in addition to a LFIA strip (Figure 1-10a). As schematically shown in Figure 1-10b, after sandwich immunoreaction activated by sample introduction, delayed release of enzyme substrate and signaling reagent (choline chloride and luminol) occurs from the shunt pad separated by a plasma separation membrane, enabling automatic timed delivery of the chemiluminescent agents. Analytical application has been demonstrated through C-reactive protein detection in serum. Although no washing step is achievable, operational simplicity (*i.e.* sample application only) of the conventional LFIAs is fully maintained.

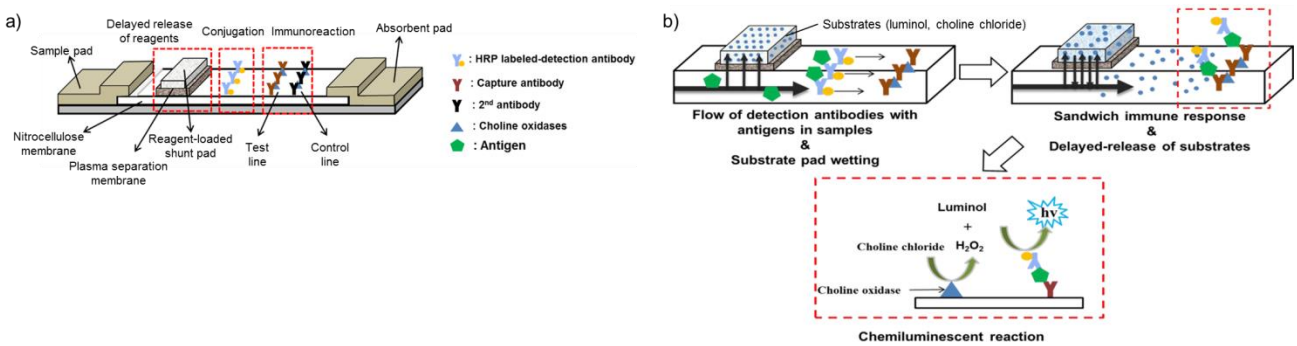

Figure 1-10. Single step enzymatic chemiluminescent lateral flow immunoassay without the need of substrate reagent addition: a) device design composed of a reagent-loaded shunt pad on a lateral flow immunoassay platform divided by a single layer of plasma separation membrane. b) Schematics of automatic enzyme-based chemiluminescent lateral flow immunoassay. Substrates for enzymatic chemiluminescence reaction are released from the shunt pad after sample passage. Adapted from Ref 93, Copyright 2014, with permission from Elsevier.

1.3.3. Control of sample volume

The deposited volume of sample is a dominant factor influencing the quantitative signal in analyses performed on μPADs. Conventional μTAS does not confront this issue since the detection is performed in a closed microfluidic channel. As described in section 1.2.2., open-air channels on μPADs are prone to liquid evaporation. Evaporation on the detection region drives continuous delivery of stationary sample solution in the inlet *via* capillary action, and therefore, the transported amount of analyte molecules strongly depends on the sample volume deposited. This phenomenon can be effectively used for analyte enrichment, for example by heating the detection area to promote evaporation.[94] However, it works adversely in most μPAD assays, as a fixed volume of sample must be deposited to reproducibly achieve quantitative measurements. Although micro-pipettors are used in most reports to guarantee a fixed sample volume, their necessity poses restrictions on practical application to home medical care and diagnostics in resource-limited regions, among others.

Lamination is a widely accepted technique to suppress sample evaporation, as well as to improve mechanical strength of paper-based devices.[95-97] Several concerns include prolonged assay times due to decreased flow rates of liquids in laminator-compressed paper channels, impact of direct contact of reagents with adhesives, and incompatibility with fluorescence-based measurement due to absorbance of excitation light by laminating films. Overprinting (e.g. toner,[98] UV curable ink[49]) has been reported as alternative solution to reduce evaporation, but incomplete physical coverage of the porous paper structure and interference of overprinted ink color with colorimetric assays remain issues.

There exist several attempts to achieve controlled sample delivery from unknown volumes deposited on paper-based microfluidics, mainly by using dissolvable polymeric materials. One of the early reports demonstrated fingertip blood collection targeting dried blood spot (DBS) sampling with the use of a dissolvable metering valve made from a polyvinyl alcohol (PVA) film (Figure 1-11a).[99] The device was able to transfer 0.87 ± 0.099 μL from 20–40 μL of total applied sample liquid. Later, a similar concept was extended to volume-controlled plasma separation in combination with a filtration membrane, which collects 4 μL of plasma from 30–60 μL of whole blood.[100] Another architecture utilizes a solid sugar block to serve as a dissolvable bridge, which shuts off the sample flow after the passage of a certain volume (Figure 1-11b).[101] Fu

et al. prepared several types of bridges by varying the sugar material (trehalose or mannose) and the dimension.[101] Depending on the bridge properties and sample source pad material, the transfer volume was tuned within the range of 10 to 80 µL. A practical application was demonstrated by embedding the sugar bridge in a lateral flow immunoassay format. The resulting device determined *Pf*HRP2 with an acceptable precision (coefficient of variation of 10%), indicating reasonable production reproducibility of the sugar bridge. One reported limitation is the prolonged assay time (45 min) assumedly due to the increased sample viscosity by dissolution of very high amounts of sugar. However, the use of sugars is expected to have a positive side effect in immunoassays, because of the stabilizing influence on encapsulated molecules.[102] Thus, inclusion of detection antibodies into a sugar bridge for example, might contribute to long-term stability of the device. A problem yet to be addressed in automatic sample volume metering systems on µPADs is their implementation into multiplexed assays or vertical flow-based three-dimensional devices.

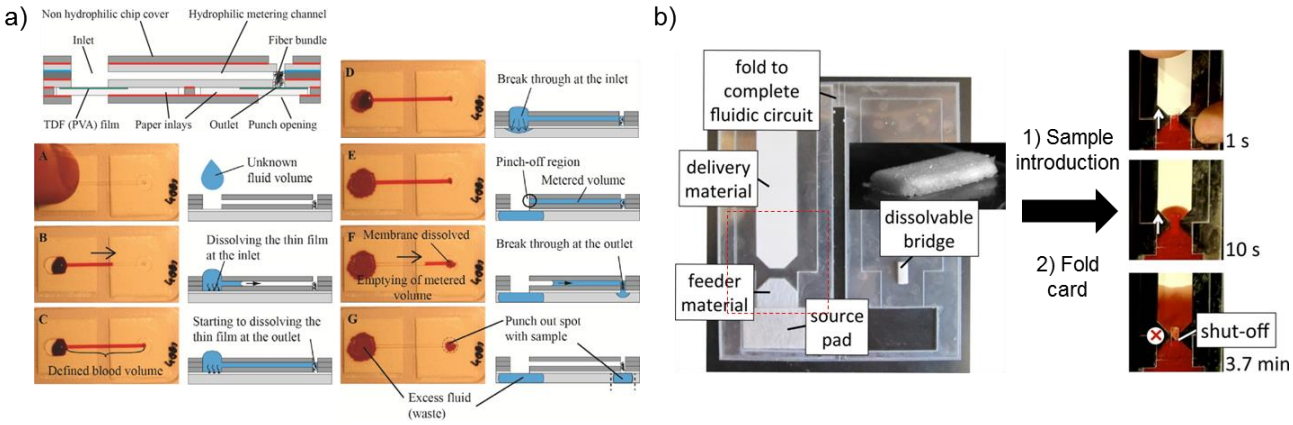

Figure 1-11. On-chip sample volume metering systems for paper-based devices: a) design and working principle of dried blood spot collection at fixed volume. Sample delivery to the outlet is ceased upon dissolution of the polyvinyl alcohol (PVA) film beneath the sample inlet. Reproduced from G. Lenk, A. Pohanka, G. Stemme, O. Beck, Proceedings of microTAS 2013, 281–283 (Ref 99). b) Overall view of lateral flow immunoassay device with a volume-metering solid sugar bridge and flow valving demonstrated with a model solution (expanded view of the dotted area in the left photograph). Adapted with permission from Ref 101. Copyright 2013 American Chemical Society.

1.4. Signal readout and result interpretation

Besides sample introduction into the device, interpretation of the resulting signal is another essential user-involved operation. Simplicity of result interpretation is also a crucial factor determining the broad acceptance of an analytical device. In many reports related to optical detection on μPADs, the target concentration-dependent response is evaluated in a quantitative manner by acquiring numerical color or luminescence intensity values from the paper substrate. Most generally, a device image taken with a camera or scanner undergoes digital color analysis using software (*e.g.* Image J, Adobe Photoshop), with the exception of some cases where more sophisticated instruments (*e.g.* gel documentation unit) are exploited.[82] Electrochemical measurements also represent the most mature detection technology along with colorimetry, and not surprisingly, electrochemical methods are most often described in publications related to μPADs. Acquisition of electrochemical signals (current, potential) is mostly performed on laboratory-type electrochemistry stations, which are incompatible with end users due to their cost (typically > $1000) and operational complexity. Such a precise quantitative evaluation is routinely shown in the literature for proof-of-concept, however, complexity of signal interpretation procedure and/or signal capturing equipment is detrimental to test throughput and acceptance by general users. This section introduces general issues of result interpretation in optical and electrochemical measurements on μPADs as well as some proposed approaches for simplification of signal readout.

1.4.1. Quantitative signal readout

If analysis of an analyte within a narrow concentration window is to be carried out, such instrument-based signal quantification is essential. Unfortunately, the standard procedure of quantitative optical signal detection on μPADs (Scheme 1-2) is too complicated and time-consuming for untrained end users. For practical use, the integration of self-calibrating systems is virtually indispensable.

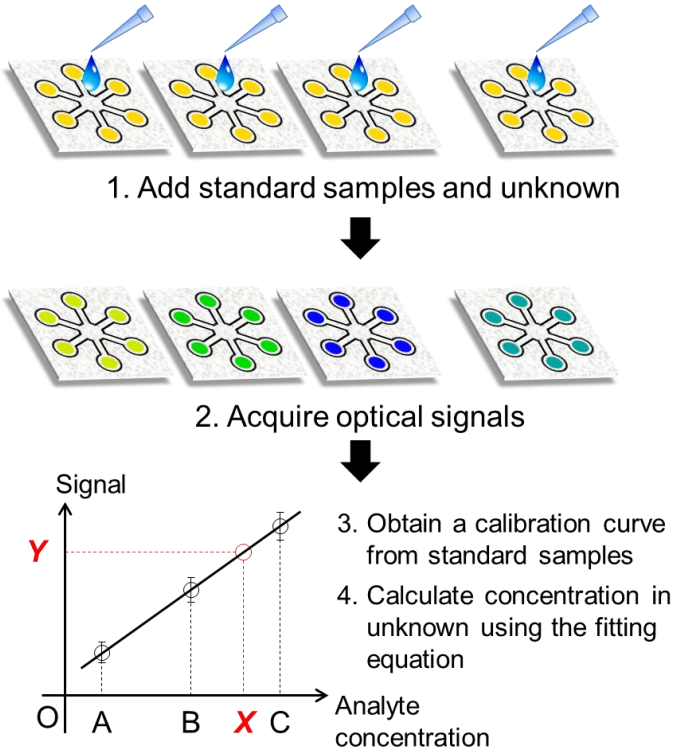

Scheme 1-2. Typical procedures for quantitative optical signal detection on μPADs.

The electrochemical personal glucose meter (PGM) used by millions of diabetic patients, although generally not based on paper substrates, is a representative example of a highly successfully commercialized diagnostic device. One reason is simply the fact that a PGM reports "sample glucose level" in place of "measured current" without the need of user calibration (except initial batch calibration) and data processing. In addition, other criteria of user-friendliness including fastness (result mostly available within 10 sec), single introduction of untreated whole blood sample (typically less than 1 μL) and disposability, are satisfied. One of the core issues hindering practical application of μPADs is that realization of such a fully integrated sample-to-answer device is still scarce. This holds for both electrochemical and optical detection-based μPADs. In electrochemical μPADs, Whitesides and co-workers diverted a PGM to detect cholesterol, lactate, and alcohol by using the respective oxidase enzymes specific for these analytes.[103] Non-PGM, but still fully integrated readout systems are found in other applications or platforms. One example shows the determination of salivary α-amylase based on a two-electrode system prepared on film substrates (Figure 1-12).[104] Signal interpretation is performed via a smartphone connected with a USB-based potentiometric reader. However, to the best of my

knowledge, non-PGM fully integrated readers have not been reported for electrochemical paper-based devices.

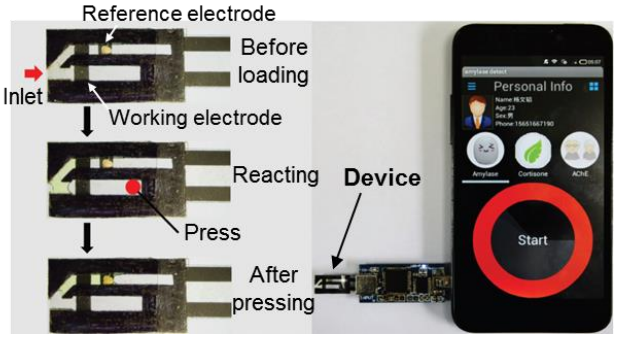

Figure 1-12. Electrochemical sample-to-answer smartphone device for α-amylase sensing. Adapted from Ref 104 with permission from The Royal Society of Chemistry.

In optical detection-based paper devices, there exist some examples of sample-to-answer system developments mainly relying on smartphones[105-106] or handheld readers.[107-108] Especially smartphone-based point-of-care testing has gained attention recently, because of their increasing accessibility, the possibility of software integration and the capability of data transmittance from the field to clinics (telemedicine).[23, 109-110] Smartphone subscriptions are predicted to be doubled between 2015 and 2021 (3.2 billion to 6.3 billion), with an expected enormous growth in the Middle East and Africa.[111] To meet the demand of smartphone-based signal acquisition systems, substantial efforts were made to adapt them not only to paper-based devices, but also to other microfluidic platforms, as described in a recent review article.[112] Typically, quantitative information on analyte amount is obtained by taking a device photograph with the built-in camera, followed by conversion of the optical signal based on a pre-loaded algorithm. For clinically-relevant targets, direct sample-to-answer paper-based devices with optical signal detection have been elaborated for urine analysis combined with a commercial colorimetric dipstick,[105, 107-108] colorimetric pH and nitrite sensing,[106] colorimetric cholesterol sensing,[113] and fluorescence-based pathogenic nucleic acid detection.[114] In practical use, the influence of ambient light conditions is a crucial factor in optical detection. This issue can be avoided either by integration of a cancelling algorithm (discussed in "**1.4.2. General issues in semi-quantitative**

colorimetric signal readout"), or by the use of an external light cutting housing (*e.g.* 3D-printed custom part,[115] readout inside handheld reader[107]). In the latter approach, the built-in light source of the smartphone (Figure 1-13a) or LEDs mounted in the handheld reader (Figure 1-13b) are used for controlled device illumination.

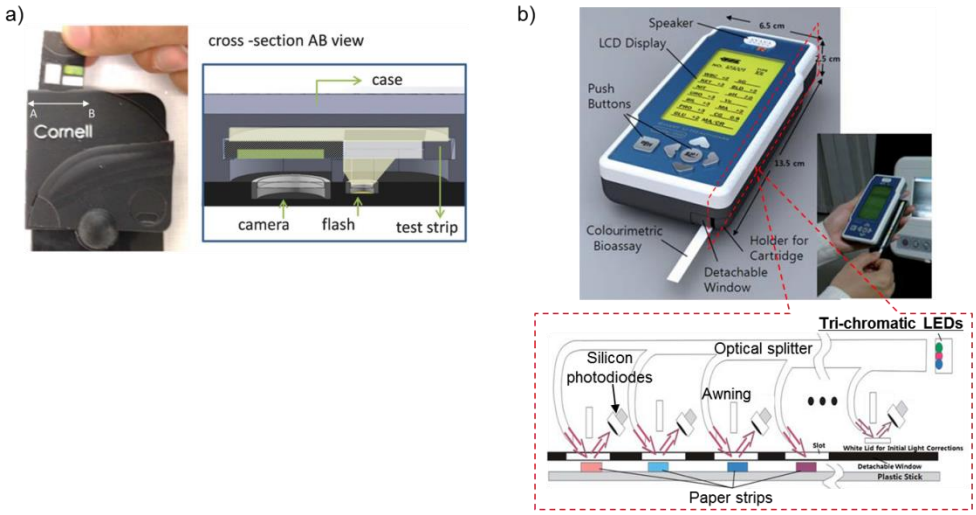

Figure 1-13. Examples of integrated signal reading systems with controlled illumination conditions: Colorimetric sensing of pH in sweat and saliva using a 3D-printed housing. Reproduced from Ref 115 with permission from The Royal Society of Chemistry. b) Quantitative urinary dipstick-based analysis using a custom-built handheld reader. Adapted from Ref 107 with permission from The Royal Society of Chemistry.

Again, the use of electronic readout systems provides high analyte concentration resolution without the need of signal interpretation by the user. Especially in colorimetric analysis, inaccurate diagnosis by color-blind observers can also be eliminated. In practical application, the following points are deemed to be critical: first, the system should be battery-powered with acceptable operating time. This issue is crucial in smartphone-based diagnostics, considering the enhanced power consumption during camera and light source use and the software running. Second, camera hardware and software compatibility differ from device to device, and adaptations to the readout software are required in accordance with smartphone device changes, as well as operating system updates. A specific example for the elimination of inter-model variations in smartphone-assisted readout of colorimetric assays has been described by Yetisen and coworkers.[116] Third, contamination of the device housing by biological samples should be considered. According to the WHO

biosafety guideline, it is forbidden to reuse (likely) contaminated components unless autoclaved.[117] Although customized part fabrication has been accelerated by recent advances of 3D printing technology,[118-120] the risk of biological contamination and their reusability must be evaluated for clinical diagnostics. In point-of-care tests, single-use of such auxiliary parts is generally not attractive for cost reasons.

1.4.2. General issues in semi-quantitative colorimetric signal readout

Colorimetry is a long-established assay technique where various detection chemistries are available including small-molecule organic indicators (*e.g.* acid-base indicator, metal indicator), nanoparticulate materials (*e.g.* gold, silver nanoparticles), chromogenic enzyme reactions (*e.g.* target-specific oxidases coupled with a colorimetric redox indicator), and the use of specific chemical reactions accompanied by a color change (*e.g.* coupling reaction of azo dyes). In addition, the easy-to-detect signal (*i.e.* observable by unaided eyes) is most suited in developing user-friendly analytical devices. Nevertheless, colorimetry suffers from several challenges to become a universal detection motif in practical diagnostic testing. Because of the vast number of reports on colorimetric detection-based paper devices, this section concentrates on critical issues of the present technology. Comprehensive reviewing of this topic is well provided elsewhere.[23, 25]

Heterogeneous color development affects accurate visual inspection as well as precise quantitative digital color analysis on μPADs. Commercial urine dipsticks, successful colorimetric paper-based devices for real world application, do not encounter this problem, as the sensing paper pad is dipped into a large amount of specimen, resulting in uniform color development in the entire area. In contrast, sample migration in paperfluidics frequently causes uneven color development, mainly because highly soluble signaling compounds are washed away towards the periphery of the detection region. Figure 1-14a shows the colorimetric sensing of protein (human serum albumin: HSA) on a lateral flow-based μPAD,[47] where the colorimetric indicators initially uniformly deposited on the sensing regions are swept away after sample application (Figure 1-14a, top). The authors figured out that deposition of the indicator within the microfluidic channel results in more homogeneous color distribution (Figure 1-14a, bottom), but at the cost of overall weaker developed color intensity (*i.e.* loss of sensitivity). Alternative use of a vertical flow-based μPAD

mitigates color heterogeneity thanks to the even entrance of sample liquid into the sensing area, as shown in the glucose and protein sensing spots on a multi-layered μPAD (Figure 1-14b).[121] Nevertheless, perfectly homogeneous color development is still challenging owing to insufficient inter-layer attachment and inherent heterogeneity of paper substrate materials.

To date, this issue has been addressed by "anchoring" the assay component onto the paper substrate either by covalent or non-covalent bonding. Covalent attachment strategies onto paper are well established for immobilizing biomolecules (detailed chemistries available in recent reviews[35, 122]). Though the robust linking is free of concerns about release of the anchored substances induced by the specimen flow, the difficulty of local paper surface modification and increased production costs are shortcomings.

Non-covalent approaches provide more spatially-flexible and faster immobilization of chromogenic substances. One of the earliest demonstrations is the fixation of the charged $[Fe(phenanthroline)_3]^{2+}$ metal-indicator complex via electrostatic attractive forces by depositing the oppositely charged poly(acrylic acid) polymer.[91] More recently, our research group has demonstrated immobilization of a water-soluble sulfonated colorimetric indicator for Zn^{2+} (Zincon) by using cationically-charged poly(diallyldimethylammonium chloride).[123] These strategies may be convenient for example to develop μPADs for detection of trace nutrient metals in blood. However, it should be noted that these immobilization methods were demonstrated in the context of airborne particulate metal detection and environmental water analysis, and thus, application to more complex biological samples would come with difficulty (*e.g.* weakened electrostatic attraction due to high ionic strength).

Aside from metal-ligand complexes, enzymes can be non-covalently fixed onto paper by means of nanoparticle materials. In a report by Garcia *et al.* in 2014,[124] the authors proposed amino-functionalized SiO_2 nanoparticles (SiNPs) to entrap relevant assay components. Therein, clinically important metabolites (lactate, glucose, and glutamate) were determined using established bi-enzymatic systems (analyte-specific oxidase combined with horseradish peroxidase) coupled with standard chromogenic agents (KI, TMB, and 4-AAP/DHBS). For all targets, significant improvement has been achieved in color homogeneity as well as in color intensity (Figure 1-14c). More recently, the choice of nanomaterials was further expanded to Fe_3O_4

magnetic nanoparticles (MNPs), multiwalled carbon nanotubes (MWCNTs), and graphene oxide (GO).[125] With these materials, similar improvement as with the above-mentioned SiNPs has been demonstrated for a glucose assay based on the GOx/HRP bi-enzymatic system with TMB as chromogen (Figure 1-14d). In all of these approaches,[124-125] the authors postulate that the modified nanomaterials interact with the involved enzymes (not the chromogenic substances) via electrostatic forces (SiNP, GO), hydrogen bonding (GO), π-π stacking and/or van der Waals forces (MWCNT, GO), as well as some reversible non-covalent interactions (MNP). As analytical applications, colorimetric target detection in artificial urine was demonstrated. It should be stressed that the results obtained showed some disagreement with those from simple aqueous standard solutions. In the SiNP-based system, all optical signals measured from artificial urine samples exhibited higher values than the standards.[124] Although the reason is not specified, different enzymatic activities in artificial urine and in simple phosphate buffered solution are possible. On the other hand, the detection sensitivity of MNP-modified μPADs was significantly lower for glucose in artificial urine in comparison with simple aqueous solutions.[125] The authors attribute this difference to interference of high urea levels with enzymatic activity.

These examples showcase the importance of evaluating the impact of complex biological sample matrices. Particularly, the influence of high protein concentrations should be investigated, so that the currently available techniques can be successfully transferred to blood sample analysis. Finally, color heterogeneity is often "overlooked" in publications on μPADs, but if observed, it should be eliminated in the interest of practical applications. Other possible strategies not further discussed include the mixing with water-soluble polymeric materials (*e.g.* polyvinyl alcohol, gelatin, carrageenan[126]) for encapsulation, which is also applicable to non-ionic chromogenic substances.

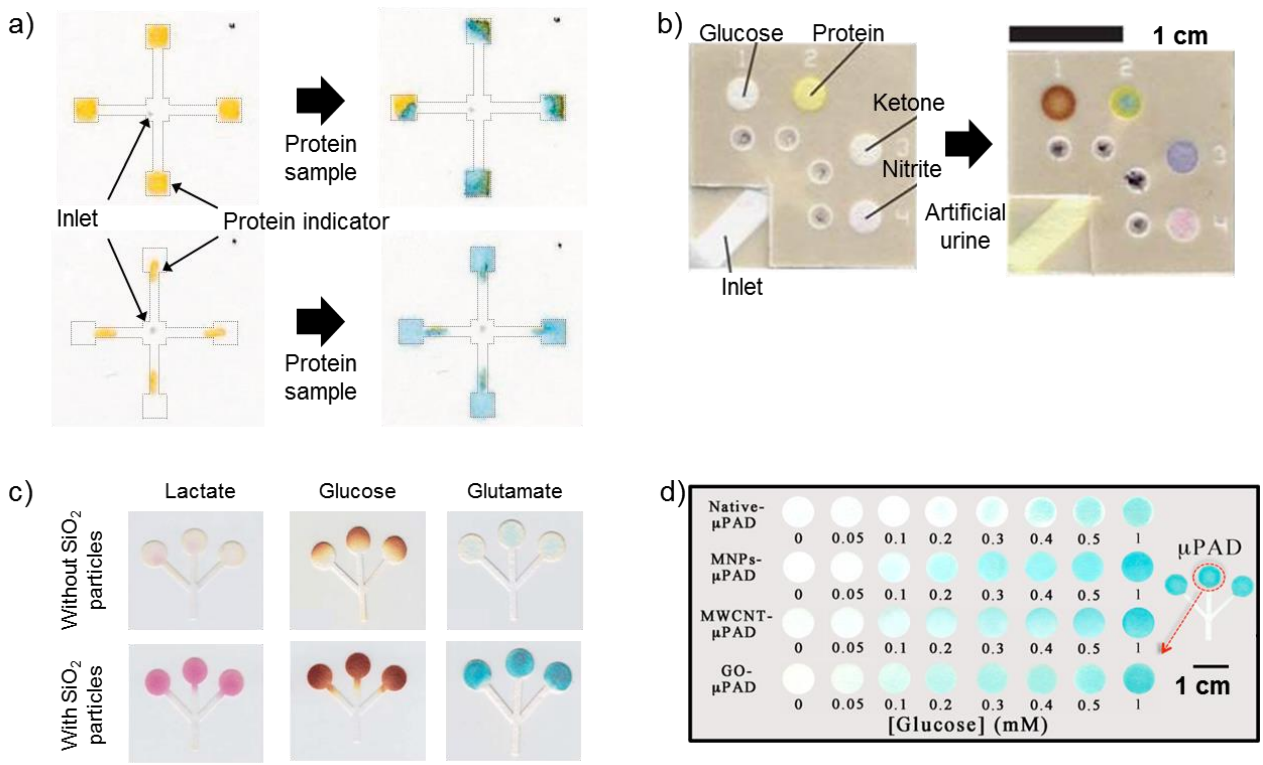

Figure 1-14. Examples of colorimetric assays addressing homogeneity of the developed signal: Heterogeneous color development on a lateral flow-based µPAD for protein with deposited colorimetric reagent on the sensing region (top) and improved color homogeneity by deposition of colorimetric reagent on the mid-flow of the microfluidic channel (bottom). The dotted grey outline shows the boundary of the microfluidic structure. Adapted with permission from Ref 47. Copyright 2008 American Chemical Society. b) Heterogeneous color development on a vertical flow-based µPAD for glucose, protein, ketone, and nitrite in artificial urine. Reproduced from Ref 121 with permission from The Royal Society of Chemistry. c) Enhanced color homogeneity and intensity on a lateral flow-based µPAD for lactate, glucose, and glutamate by paper surface treatment with amino-functionalized silica nanoparticles. Reproduced from Ref 124 with permission from The Royal Society of Chemistry. d) Enhanced color homogeneity and intensity on a lateral flow-based µPAD for glucose by paper surface treatment with Fe_3O_4 magnetic nanoparticles (MNPs), multiwalled carbon nanotubes (MWCNTs), and graphene oxide (GO). Reprinted with permission from Ref 125. Copyright 2016 American Chemical Society.

As another bottleneck of colorimetric detection, sensitivity to ambient illumination conditions is pointed out. The use of a scanner, which provides reproducible and even light illumination in imaging, is not desirable for practical use, especially at home or in electricity-limited settings. Alternatively used digital cameras and smartphone cameras are easily influenced by fluctuating ambient light conditions, but are less limited than scanners in terms of place of use. Digital cameras are advantageous over smartphone cameras, as undesirable automated correction of white balance, ISO settings and shutter speeds can be eliminated by fully manual control of exposure conditions, or by working with camera RAW files. Recently however, third party apps have become available, which offer similar control features for smartphone cameras. Digital cameras are not generally suited for sample-to-answer diagnosis, because of the difficulty to integrate image data processing software required to achieve self-standing analytical tools. In this context, smartphone cameras are more adequate as user-friendly signal interpreting platforms. In one of the earliest reports on smartphone-based colorimetry on a paper device,[127] the issue of automated white balance adjustment has been mitigated by capturing an image of a color reference chart together with the paper dipstick (Figure 1-15a). However, this method did not fully resolve the issues arising from fluctuating ambient light conditions.

Later, the influence of illumination conditions has been successfully eliminated for a commercial urine dipstick by utilizing the background color in the region of interest (ROI).[105] In that approach, the color intensity values of two areas with extreme brightness values (*i.e.* black and white) have been used to adjust the measured color value signals (Figure 1-15b). As shown in Figure 1-15c, reconstructed colors based on the corrected RGB values showed less discrepancy depending on the illumination light source. In addition, the authors of that study have demonstrated a fully automated, multiplexed semi-quantitative assay by coding a smartphone application in combination with open source computer vision (OpenCV) software. Although some deviations were observed near the boundaries of each threshold value, the clearly displayed assay result (Figure 1-15d) allows straightforward readout of multiple targets. Unlike urine dipsticks, μPADs with multiple detection regions often have radially-symmetrical outlines, making discrimination of each region difficult. This problem can be addressed by printing unique symbols onto the paper device to support detection region identification (Figure 1-15e).[106]

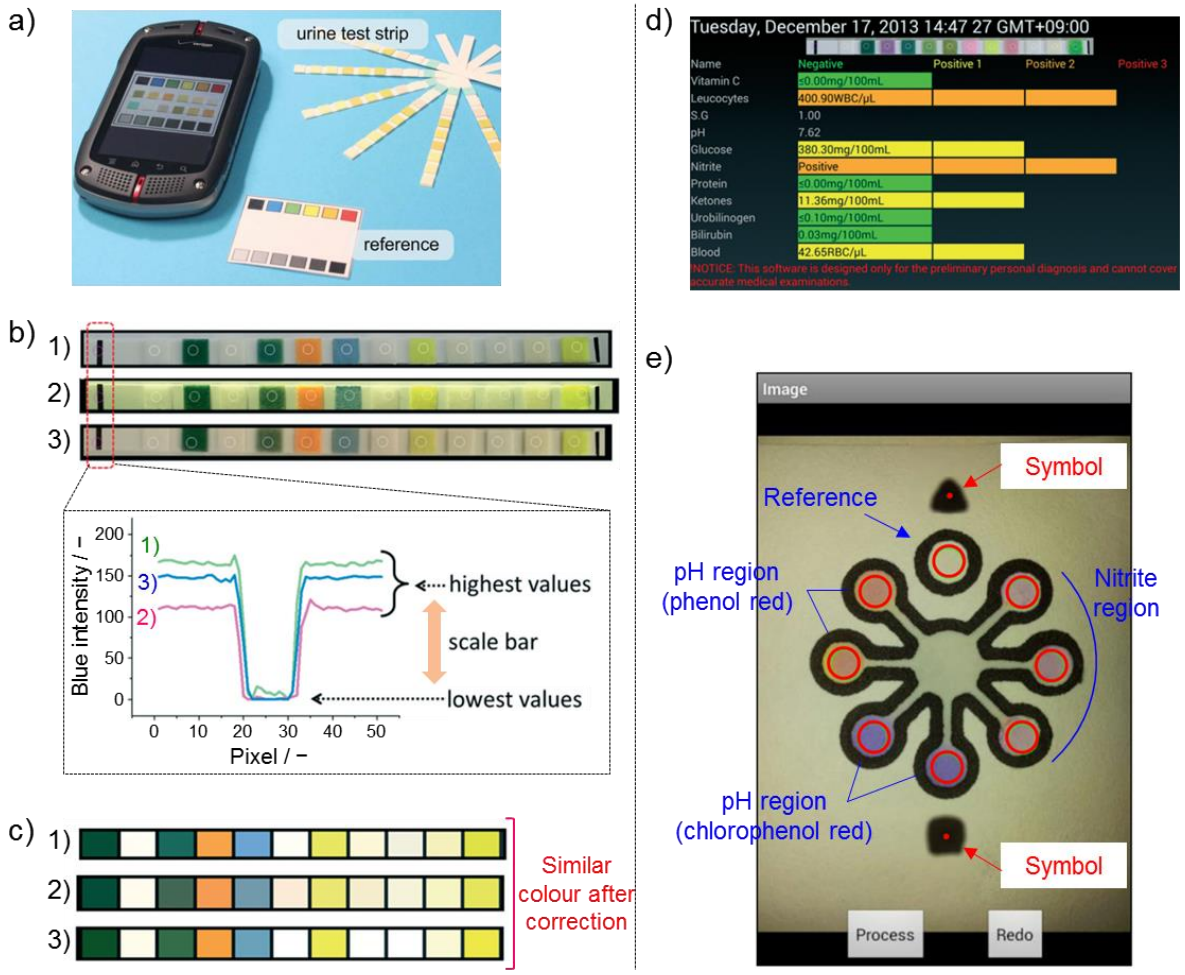

Figure 1-15. Paper-based analysis implementing smartphones: a) The use of a color reference chart targeting commercial urine dipsticks. Reproduced from Ref 127 with permission from The Royal Society of Chemistry. b) Images of urine dipstick after sample application (top) and color profiles of the background region in the dotted red rectangle (bottom) under different light conditions (1: indoor fluorescent light; 2: outdoor sunlight; 3: indoor low intensity light). The color profile shows the blue intensity value as an example. c) Reconstructed corrected colors based on images shown in Figure 1-15b. d) A screenshot of urinary analysis result by the smartphone software for colorimetric urine dipsticks. Figure 1-15b–d adapted from Ref 105 with permission from The Royal Society of Chemistry. e) The use of symbols for automated recognition of detection regions on a μPAD for pH and nitrite detection. Adapted with permission from Ref 106. Copyright 2014 American Chemical Society.

Elimination of interference caused by variations in illumination conditions has also been attempted by implementing a standard addition assay on a μPAD. Colorimetric detection of glucose without being influenced by ambient light condition (indoor vs outdoor) and imaging equipment (scanner vs digital camera) has been demonstrated using a single-point standard addition method.[128] The device consists of eight radially

arranged detection channels (for quadruple repetition of assay), with four of them pre-treated with a known amount of glucose to be hydrated upon sample application (Figure 1-16a). Data processing relies on a pre-determined fitting equation (calibration curve) and the net increase of the concentration in the glucose standard-spiked channels. Simultaneous capture of color changes from unknown and unknown plus standard-spiked samples prevents significant ambient light or imaging equipment-caused variation in determined glucose concentrations (Figure 1-16b). Although the current concept has also been demonstrated with yellow-colored artificial urine samples, there still remain various hurdles to be cleared before practical application: 1) large coefficient of variation (*e.g.* 2.7 % when using a scanner combined with conventional external calibration, in contrast to 21 % for the standard addition method using device images taken outdoor with a digital camera), 2) change of the calibration curve over time, 3) stable on-device storage of glucose standards, 4) sample matrix-dependent hydration of pre-deposited standard (fluctuation of net spiked concentration), 5) influence of channel direction in the paper fiber network.

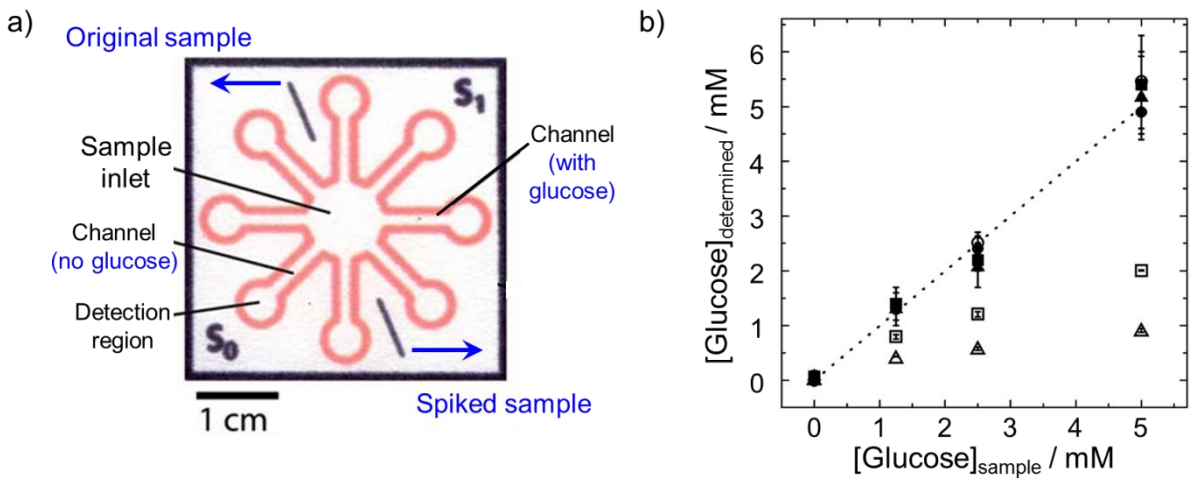

Figure 1-16. Glucose standard addition assay on a μPAD. a) Device design. b) Comparison between sample glucose concentration and determined glucose concentration under various light conditions: scanner (○, ●), camera outdoor (□, ■), and camera indoor (▲, Δ). Solid and open shapes represent results obtained by the standard addition assay and by external calibration, respectively. The dotted line indicates result agreement. Reproduced from Ref 128 with permission from The Royal Society of Chemistry.

1.4.3. Semi-quantitative signal readout with simplified result interpretation

In the case where an exact analyte concentration value is not essential, several elegant semi-quantitative detection motifs can be applied other than the classical readout chart-based method used for commercial urine dipsticks. In 2012, Phillips and co-workers invented a unique semi-quantitative detection mode for μPADs by either counting a number of colored paper regions at a fixed time (Figure 1-17, "Counting-based") or by measuring time until color appears on the device (Figure 1-17, "Timing-based").[129] Since the principle relies on the decomposition of a hydrophobic compound upon reaction with H_2O_2 in a 3D-structured μPAD, the current approach works for potentially H_2O_2-releasing clinical targets, such as substrates of oxidase enzymes (glucose, lactate, cholesterol, pyruvate, *etc.*). A derivative work by Yang *et al.* achieves similar functionality, but employs an aptamer-crosslinked DNA hydrogel that decomposes in the presence of the analyte,[130] which may largely expand the application of this detection format by overcoming the limitation of the H_2O_2 production requirement.

Among counting-based semi-quantitative assays, barcode-style lateral flow immunoassays, where the number of visible test line(s) reflects the analyte concentration,[131-134] have a longer history than μPADs. Although this assay format only provides semi-quantitative information, the ease of result interpretation and the relatively wide dynamic response range could be beneficial for inspection of clinical targets with a broad physiological concentration range, as for example C-reactive protein (CRP).[135] As a distinct approach to counting-based μPADs, titrations have been successfully performed on a paper device with branched channels (Figure 1-17, "Counting-based"). The flow channel of each branch of the device is pre-treated with a known varying amount of a target-consuming component (*e.g.* base in the case of an acid titration,[136] chelating agent for metal ion titrations[137]) and a target-responsive indicator is deposited on all of the terminal detection zones. Although the achievable concentration resolution is limited, an observer-dependent readout error is largely unlikely thanks to the off-on signaling in each detection zone. Although the authors of that study have shown the analytical application in the context of environmental monitoring, this signal reporting system has a great potential in clinical diagnostics, if a proper "target-scavenging" reagent is available. Urine screening tests might be one candidate clinical application, because 1) semi-quantitative evaluation is sufficient and 2) the

results of presently used color comparison with a reference guide are observer-dependent and challenging for color-blind users.

Classical analogue thermometers are among the simplest physical sensors, which do not require any knowledge to readout the result. Such a "distance-based" detection motif has already been introduced on paper-based devices (Figure 1-17, "Distance-based"). Yang et al. recently reviewed the history and development of distance-based microfluidic devices targeting quantitative point-of-care testing utilizing various substrate materials including paper, thread, glass, and PDMS.[138] In the design most preferable for practical use, scale marks directly interpreting the target concentration are already printed next to the detection channel, where a user can read out the analyte concentration in the same way as reading temperature from an analogue thermometer without the need of calibration. To achieve this goal, there still exist some hurdles to be cleared. Most straightforwardly, distance-based detection on μPADs is achieved by continuous consumption of analyte molecules within a paper channel with indicator(s), leading to an initial analyte amount-dependent length of the optical signal. Again, the applied sample volume should be kept constant to determine analyte concentrations. Secondly, it is of primary importance to immobilize the signaling compounds, for example by using a precipitation reaction,[139-140] applying a material with limited mobility on paper (*e.g.* nanoparticulate probes),[139] or paper surface treatment to enhance interfacial interaction between the paper substrate and the signaling compounds.[141] Third, it should be stressed that the complexity of a real sample matrix might have significant influence on the outcome of distance-based signaling. For example, the higher viscosity of human serum (plasma) compared to standard aqueous solutions will decrease the sample flow rate, resulting in inferior sensitivity. In addition, fluctuations in sample composition (*e.g.* ionic strength) might vary the solubility and intermolecular interactions of relevant components (detection reagent, analyte molecule, signaling compound) in the sample liquid, which eventually affects the subsequent length-based signal. Fourth, the generally poor precision should be addressed. Unfortunately, reported relative standard deviation values in recent distance-based μPAD assays[140-141] are larger than those of other detection motifs. This issue is not limited to clinical application in complex matrices, as concluded from the fact that the mean of the relative standard deviations are 27.2% and 23.5% in biological tear protein detection[141] and metal detection in welding

fumes,[140] respectively. In addition, particular attention should be paid to batch-to-batch fabrication reproducibility including the detection channel width and depth, the amount of deposited assay components, and the arrangement of the detection channel (*i.e.* angle between the flow channel direction and the cellulosic fiber orientation[97, 142]).

The probably most explicit signaling configuration is text describing the assay result. There exist two examples of text-reporting devices for 1) blood type determination[143] and 2) a multiplexed immunoassay.[144] In the first example developed by Shen *et al.*,[143] the device reports the ABO and Rh blood groups after introduction of a whole blood sample and washing with saline (Figure 1-17, "Text-based", top). The working principle relies on blood type-specific coagulation in each alphabetic character- or symbol-shaped hydrophilic region with pre-deposited anti-A, B, or D antibodies. In the current study, Kleenex paper towel has been selected as the optimum paper substrate, rather than standardly-used filter paper. The authors report that the finer porous structure of filter paper hampers thorough removal of non-agglutinated red blood cells during the saline washing step.[143] This paper-based device has been commercially launched under the name of "Group Legible Immunohematology Format (GLIF)" by an Australian company, Haemokinesis.[145] In the second example reported more recently,[144] a "seven-segment number display" has been proposed to interpret the results of multiplexed yes/no answering immunoassays (Figure 1-17, "Text-based", bottom). In this work, the presence of each specific target analyte turns on a corresponding color spot representing each segment, which finally indicates the combination of targets present in the sample in the form of a number. This approach enables multiplexed immunoassays (up to 17 targets in a hexadecimal display). Difficulties in device development lie in eliminating cross-reactions, and in optimizing the arrangement and amount of each deposited primary antibody to ensure sensitivity in all "segments". Unfortunately, to the best of the author's knowledge, this straightforward signaling system is yet to be converted to other types of targets.

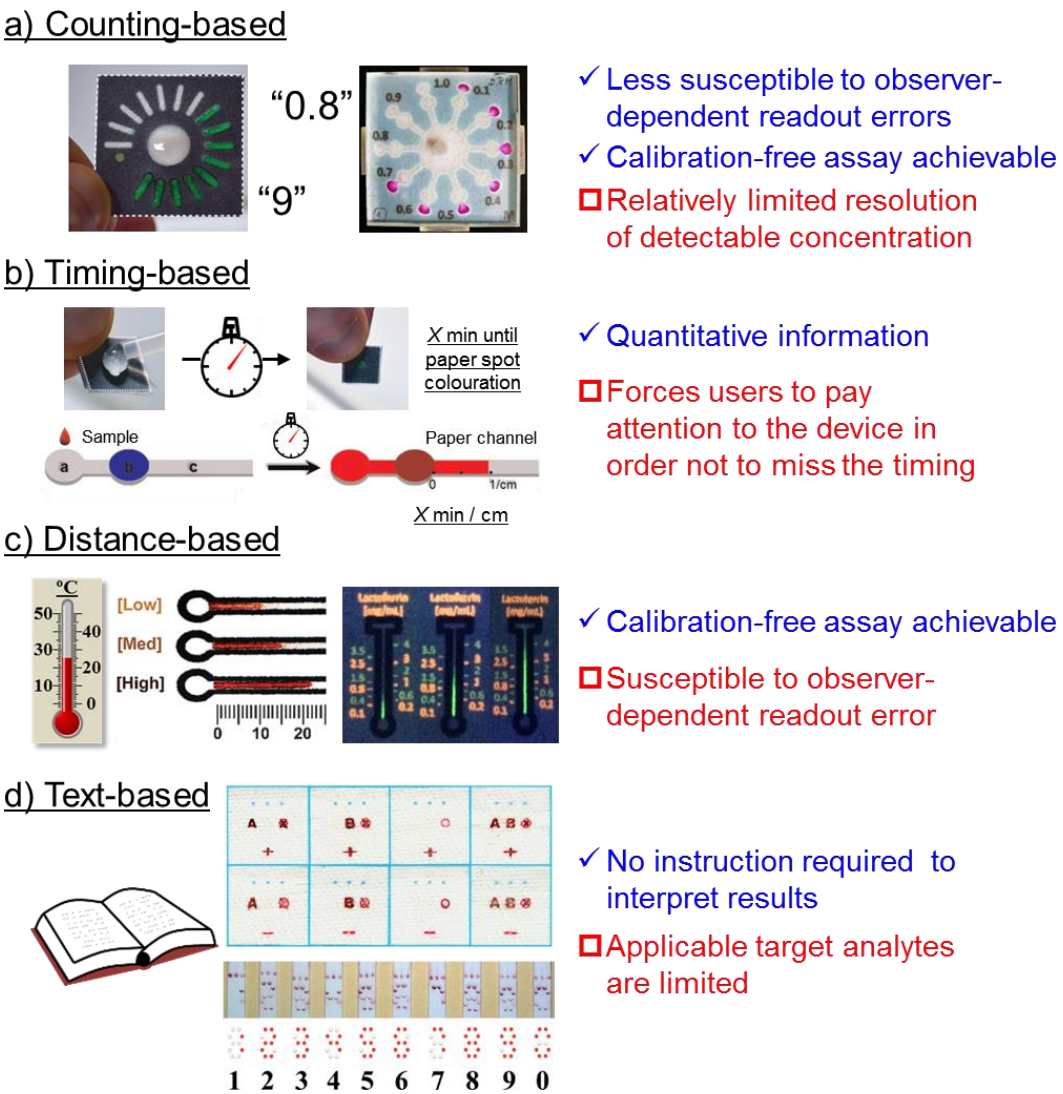

Figure 1-17. Summary of user-friendly signal reporting systems on paper-based devices. Advantages and challenges of each system are specified in blue and red text, respectively: a) Counting of colored regions. Reproduced with permission from Ref 129. Copyright© 2012 WILEY-VCH Verlag GmbH & Co. KGaA, Weinheim. Reprinted with permission from Ref 136. Copyright 2014 American Chemical Society. b) Time measurement until occurrence of appointed phenomena. Reproduced with permission from Ref 129. Copyright© 2012 WILEY-VCH Verlag GmbH & Co. KGaA, Weinheim. Adapted from Ref 146, Copyright 2015, with permission from Elsevier. c) Length of optical signal in a straight detection channel. Reproduced from Ref 139 with permission from The Royal Society of Chemistry. Reprinted with permission from Ref 141. Copyright 2015 American Chemical Society. d) Text-displayed tests of blood type determination and multiplexed immunoassay. Reproduced with permission from Ref 143. Copyright© 2012 WILEY-VCH Verlag GmbH & Co. KGaA, Weinheim. Reproduced from Ref 144 with permission from The Royal Society of Chemistry.

1.4.4. Conversion of electrochemical signal to visual signal

To achieve easy-to-use electrochemical paper-based analytical devices (ePADs), approaches are not limited to the development of external user interfaces. Several publications report elegant ideas to convert an electric signal into an optical output on paper-based devices with the aid of thermochromism or electrochromism. One of the earliest examples was proposed in 2009, where "a paper display" relying on thermochromism has been invented.[147] The device consists of a spray-deposited thermochromic dye and a conductive tin wire patterned by e-beam evaporation on the opposite side of the photo paper substrate (Figure 1-18a). Photo paper has been chosen as the substrate material due to its high surface smoothness, facilitating the preparation of electrically conductive wires. Upon application of electrical current, the conductive wire on the back side warms the paper substrate (Figure 1-18b) and the black thermochromic leucodye turns to translucent (Figure 1-18c). Based on this mechanism, proof-of-concept paper displays presenting assay results in text, number, or graphic have been designed (Figure 1-18d). Especially graphic-reporting paper-based analytical devices are deemed to be the most versatile format, since they are perfectly adapted to literacy-poor end users and to multilanguage environments. Surprisingly, despite the combined use of multiple functional materials (photo paper, 100 % Sn wire, thermochromic leucodye), material costs are estimated to be as low as < \$0.10 m^{-2} after optimization of production methods.[147] Nevertheless, to the best of my knowledge, an analytical application based on this signaling technology is yet to be demonstrated. The most straightforward approach would be the integration into an electrochemical sensing device involving electrical current generation (*e.g.* amperometric sensing). However, the thermochromic paper display typically requires > 25 mA of current to bring along an observable change in the leucodye transparency, which is much higher than that produced in normal redox reaction-based glucose detection on ePADs (typically < 100 μA). Additionally, the dependence of the required display switching current on ambient temperature is another thorny issue on the way to real world application.

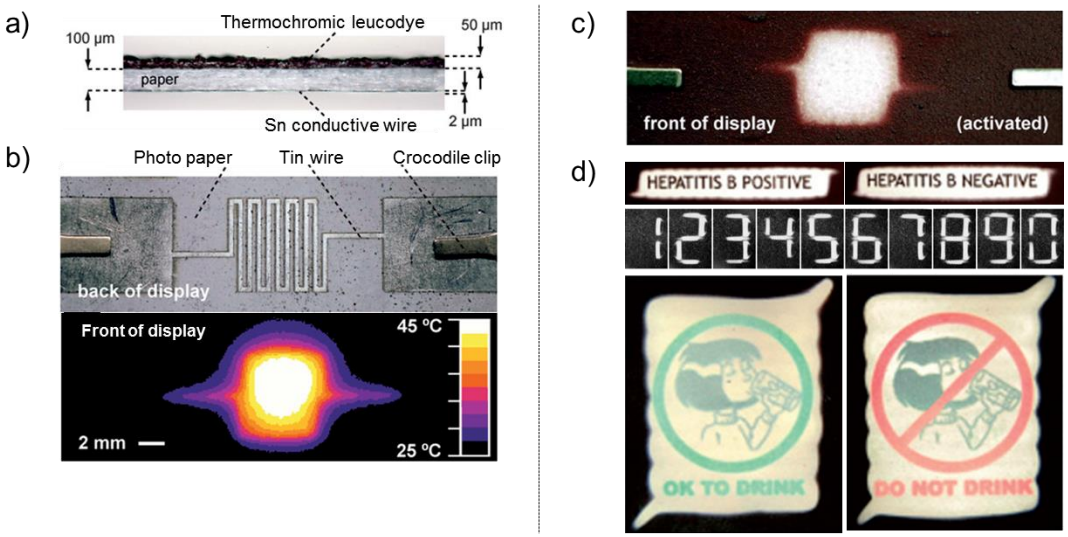

Figure 1-18. Paper-based display using thermochromism. a) Cross-sectional image of the photo paper-based thermochromic display. b) Conductive Sn wire patterned on the back side of the display (top) and infrared image (wavelength range: 3400−5000 nm) showing the temperature distribution on the front side of the display activated by applying 50 mA of current (bottom). c) Actual image of translucent thermochromic leucodye on the front side after activation (current: 50 mA). d) Examples of result display formats based on text (top), numbers (middle), and graphic (bottom). Reproduced from Ref 147 with permission from The Royal Society of Chemistry.

Electrochromism is the second approach used to convert an electric signal into an optical signal. In 2012, the Crooks group introduced an ePAD combining an electrochromic Prussian blue spot with an integrated metal/air battery and ITO film (Figure 1-19a).[148] The authors have demonstrated yes/no glucose sensing for proof-of-concept. The electrochromic sensing proceeds in three steps: 1) the glucose-dependent $Fe(CN)_6^{4-/3-}$ redox reaction on the sensing region, 2) transmission of electrical current to the metal(Al)/air battery region, and 3) electrochromic reaction of Prussian blue to colorless Prussian white (Figure 1-19b). The presence of glucose in artificial urine activates the oxidation of $Fe(CN)_6^{3-}$ by the GOx/HRP enzymatic reaction. Although the tested glucose concentrations were limited to 0.10 mM (spot turn-off) and 0 mM (spot remains visible), the lowest detectable concentration is variable depending on the Prussian blue spot diameter. Multiplexed Prussian blue spots with different features would enable semi-quantitative analysis for example according to the “counting-based” readout system. An issue remains the relatively high material cost ($ 0.95 for battery including ITO film).[148]

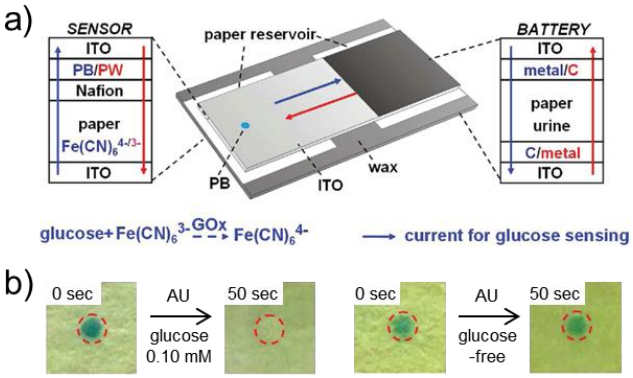

Figure 1-19. Metal/air battery-integrated μPAD for glucose detection relying on electrochromism of Prussian blue. a) Schematic illustration and working principle of the device. b) Images of Prussian blue spots before and after introduction of 40 μL of artificial urine (AU). The Prussian blue spot turns to colorless Prussian white only in the presence of glucose. Adapted with permission from Ref 148. Copyright 2012 American Chemical Society.

More recently, electrochromic detection using the Prussian blue indicator has been expanded to the "distance-based" readout system. In 2015, Chow and co-workers have demonstrated visualization of applied voltage or resistance in an electrical circuit by the length of a color-changing zone on an ePAD.[149] The distance-based principle is achieved by means of a Prussian blue/polyaniline layer deposited on a rectangular film made from sintered gold nanoparticles (Figure 1-20a). Co-doping with polyaniline (PANI) enables enhanced visibility according to the following reaction:

$$\underset{\text{Polyaniline (emeraldine salt)}}{(PANI^{2+})(ClO_4^-)_2} + \underset{\text{Prussian blue}}{Fe^{3+}{}_4[Fe^{2+}(CN)_6]_3} \underset{Ox}{\overset{Red}{\rightleftharpoons}} \underset{\text{Polyaniline (leucoemeraldine)}}{PANI} + 2ClO_4^- + \underset{\text{Prussian white}}{Li_4Fe^{2+}{}_4[Fe^{2+}(CN)_6]_3}$$

Upon application of voltage, the Prussian blue/PANI composite film turns to transparent at the position along the application direction where the local potential exceeds the reduction voltage of the electrochromic materials. The use of a completely sintered gold nanoparticle film with uniform resistance enables a distance-based readout system (Figure 1-20b). On the other hand, a "counting-based" readout system has also been demonstrated by preparing a segmented gold nanoparticle film divided by lines of unsintered gold (Figure 1-20c). The system allows semi-quantitative evaluation of potential or resistance produced in the electrical circuit. Achieved detectable ranges are −0.6 to −2.5 V (distance-based), −0.5 to −2.0 V

(counting-base) for voltage, and 6 to 160 Ω (distance-based) and 30 to 1100 Ω (counting-based) for resistance.[149] Future analytical applications should be considered taking into account the limited detectable resolution.

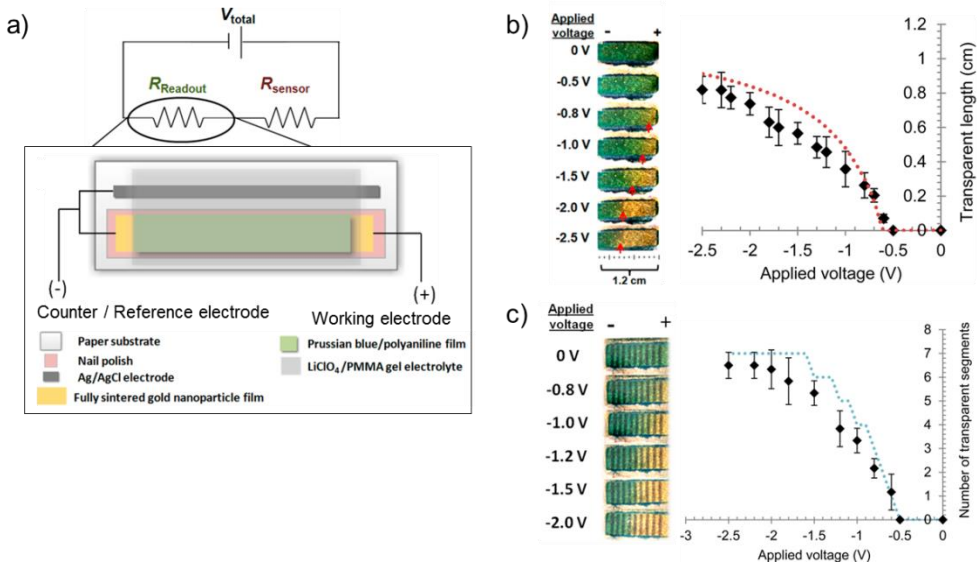

Figure 1-20. Electrochromism-based semi-quantitative readout system on a paper substrate. a) The system consists of voltage source, resistive sensor, and readout part. The electrochromic Prussian blue/polyaniline composite film is patterned on a sintered gold nanoparticle film in the readout part. Upon application of voltage (V_{total}), the Prussian blue/PANI composite film turns to transparent at the position along the application direction where the local potential exceeds the reduction voltage. b) Demonstration of distance-based voltage readout system using a fully sintered gold nanoparticle film. c) Demonstration of counting-based voltage readout system using a partially unsintered gold nanoparticle film. Adapted with permission from Ref 149. Copyright 2015 American Chemical Society.

1.5. Summary of the research motivation

1.5.1. General state-of-the-art of μPADs

As overviewed in the previous sections, the last decade has witnessed an explosive growth of academic research in (microfluidic) paper-based analytical devices. Figure 1-21 shows the growing number of publications citing the first paper on μPADs from the Whitesides group published in 2007,[10] depicting increasing interest in paper-based analytical devices. The use of paper provides a device substrate material being low-cost, portable, and safely disposable by incineration. In addition, the inherent availability of capillary action allows pump-free sample liquid transportation, making μPADs independent of any external drive system. Not surprisingly, the original purpose of μPAD development in 2007 was mainly devoted to point-of-care tests in resource-poor regions.[10] Currently, applications targeted by μPADs analysis also cover near-patient disease screening and early diagnosis of serious illnesses such as cancers.

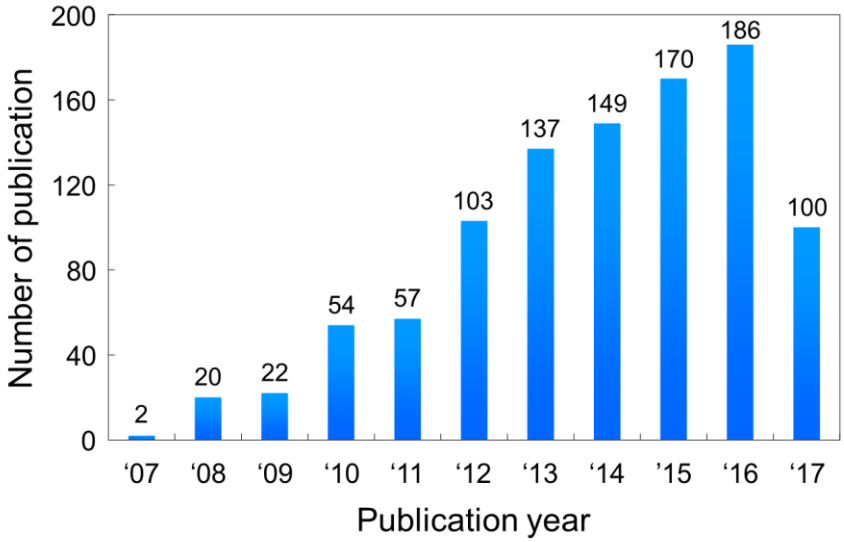

Figure 1-21. Number of publications citing the paper by Whitesides and co-workers,[10] which firstly introduced the μPAD concept in 2007 (searched on the Web of Science™ on June 29th, 2017).

Representative works performed on μPADs with the demonstration of clinical sample analysis are provided in Tables A-1 and A-2 of the Appendix. Despite extensive search with Google Scholar, SciFinder, and the Web of Science, the author has undoubtedly overlooked many relevant papers, and apologizes to the authors of those

unintentionally omitted contributions to the field. Table A-1 covers medical analytical targets that are inspected in routine urine checks or blood tests for the purpose of health monitoring. On the other hand, Table A-2 deals with a wide array of biomarkers not being routinely inspected, but potentially useful for screening or early diagnosis of diseases. The number of works listed in Tables A-1 and A-2 is obviously limited in contrast to the thriving research on μPADs indicated in Figure 1-21. These tables exclude a large fraction of μPAD research for medical applications, due to the absence of demonstration of real sample analysis. Most studies cast anchor at the successful demonstration of the analytical performance using impractical sample matrices (simple aqueous solution of analyte or artificial sample with reduced uncertainty in composition). The complexity of body fluids can cause discrepancy between the assay results obtained from real samples and standard samples,[71] and can eventually require major modification of device design.[141] In this context, the validation of devices using clinical samples is deemed to be essential, and hence, in my opinion, most μPADs are still far from real world application, because of insufficient examination of their compatibility with practical sample matrices.

Nevertheless, it is worth mentioning that not a few clinically-important biomarkers for routine health checks and for clinical diagnosis of more severe diseases have become measurable by μPAD analyses even in practical sample matrices. Translation of those newly developed devices into practical use calls for definite advantages in any aspect (*e.g.* cost, analytical performance, operational simplicity, assay time, sample volume) for overcoming the reluctance to replace established techniques. Importantly, the priority is variable depending on the intended medical application (routine health monitoring or screening of severe diseases) or intended users (general person or medical staff). For instance, μPADs for cancer screening must ensure accuracy and precision in detecting trace amounts of a tumor marker. Because of their potential usage in a central laboratory, the use of sophisticated equipment (*e.g.* chemiluminescence detector) would not be a serious issue. On the other hand, the routine monitoring of lifestyle-related metabolite biomarkers in a private home should avoid high device cost and complexity in device operations (sample application, result interpretation) and associated user interfaces. Infectious disease tests for developing countries further require robustness against harsh ambient conditions (extreme humidity and temperature).[150]

One of the primary motivations to use paper as the device substrate is its low material cost. Therefore, (bio)chemical assays involving an expensive detection system (*e.g.* spectrophotometer, photomultiplier tube-equipped luminescence analyzer, Raman spectrometer, laboratory-type potentiostat) would not be the "best" application of paper-based analysis. In this context, μPADs are deemed to be especially valuable for routine health checks at private homes and rapid screening of diseases for initial diagnosis, where relatively high concentration (mM−M or mg−g mL^{-1}) of clinical targets are potentially detectable on paper substrates relying on optical signals including color change and luminescence emission. In spite of the signal visibility, optical detection on μPADs has been generally reliant on cumbersome software-assisted color analysis (Scheme 1-2), with some exceptions of instrument-free approaches using a color read guide in the same manner as pH test papers. As reviewed in section 1.4.3 and summarized in Figure 1-17, alternative optical signaling approaches have been pursued in the last several years. In particular, semi-quantitative detection motifs relying on distance, counting, and text allow self-standing signaling (*i.e.* no reliance on external read guide or detector) and are exclusive to paper-based assays. Although those "simplified" signaling approaches may largely enhance convenience of medical screening tests, types of detectable clinical targets are still scarce.

1.5.2. Research objective of this thesis

This thesis describes the development of paper-based assays with simplified signaling approaches. For this purpose, detection of two clinically relevant biological proteins (tear fluid lactoferrin, urinary albumin) has been attempted. Measurement of tear fluid lactoferrin concentration contributes to screening of dry eye and related systemic autoimmune diseases (*e.g.* Sjögren's syndrome). Urinary albumin is also a clinically significant inspection item in urine screening tests for early diagnosis of nephropathia. In line with high demand of low-cost and rapid, yet reliable analytical techniques, paper-based assays with simplified signal detection systems have been elaborated for those two biological proteins. The outline of this thesis is summarized in Scheme 1-3.

In chapter 1, the current status and issues of μPADs for medical screening applications have been discussed by reviewing the recent literature on μPADs development.

Chapter 2 describes a μPAD for the antibody-free detection of tear lactoferrin. Immunoassays, the conventional analytical technique for quantifying lactoferrin, involve several challenges for routine disease screening: they require time-consuming (hours) multi-step operations and the use of costly and environment-sensitive antibodies for the specific recognition of lactoferrin. To eliminate the use of monoclonal antibodies, a lactoferrin assay principle relying on fluorescence sensitization of Tb^{3+} has been introduced by paying attention to the metal binding properties of lactoferrin. The specificity of this newly developed detection principle has been evaluated in an interference study by using primary human tear fluid constituents. The elaborated paper device has been applied to the quantification of lactoferrin in human tear samples and has been validated based on a method comparison with the established analytical technique (the enzyme-linked immunosorbent assay; ELISA).

Chapter 3 describes a method to further enhance the ease of lactoferrin quantification on a μPAD. A "fluorescence distance"-based quantitative signaling method mimicking a classical analog thermometer has eliminated the necessity of a camera and software-assisted digital color analysis, which was requisite in the fluorescence intensity-based approach described in Chapter 2. The distance-based signaling is realized by continuous consumption of sample lactoferrin in a paper channel. To achieve this goal, the behavior of the involved assay and analytical target components at the interface between the cellulosic substrate material and the liquid sample phase has been elaborated. The fluidic mobilities along the paper-liquid interface, dependent on electrostatic interactions between lactoferrin, the filter paper surface and Tb^{3+} deposited on the paper substrate as signaling reagent, have been studied by chromatographic experiments. The successful entrapment of Tb^{3+} and lactoferrin molecules after modification of the cellulose surface by sulfonated anionic polysaccharides is demonstrated even in the presence of electrolytes and proteins. The analytical reliability of the distance detection-based μPAD was confirmed in a direct comparison with the standard ELISA method using clinical human tear samples.

Chapter 4 describes a paper-based assay of urinary albumin that allows direct semi-quantitative result interpretation in the form of "text". Until present, a "text-displaying" paper device has been only achieved for qualitative assays (blood typing,[143] multiplexed lateral flow immunoassay[144]), which rely on antigen-antibody reaction. This research attempted for the first time at the conversion of a color change of an organic colorimetric indicator into "text"-based semi-quantitative signal. Text-displaying semi-quantitative assay has been achieved by combining a normal colorimetric assay with color printing. A colorimetric paper device was overlaid with a laser toner-printed transparent film in such a way that the printed color ink works as a screening color, which screens the text-shaped indicator color with smaller absorbance on the paper surface. Modulation of the screening color intensity allowed adjustment of the "threshold" for displaying the indicator color (*i.e.* detectable analyte range). The resulting device exhibited better analytical accuracy in urinary albumin sensing than a commercial colorimetric urine dipstick.

Chapter 5 summarizes the result of this thesis research and a future outlook of μPADs.

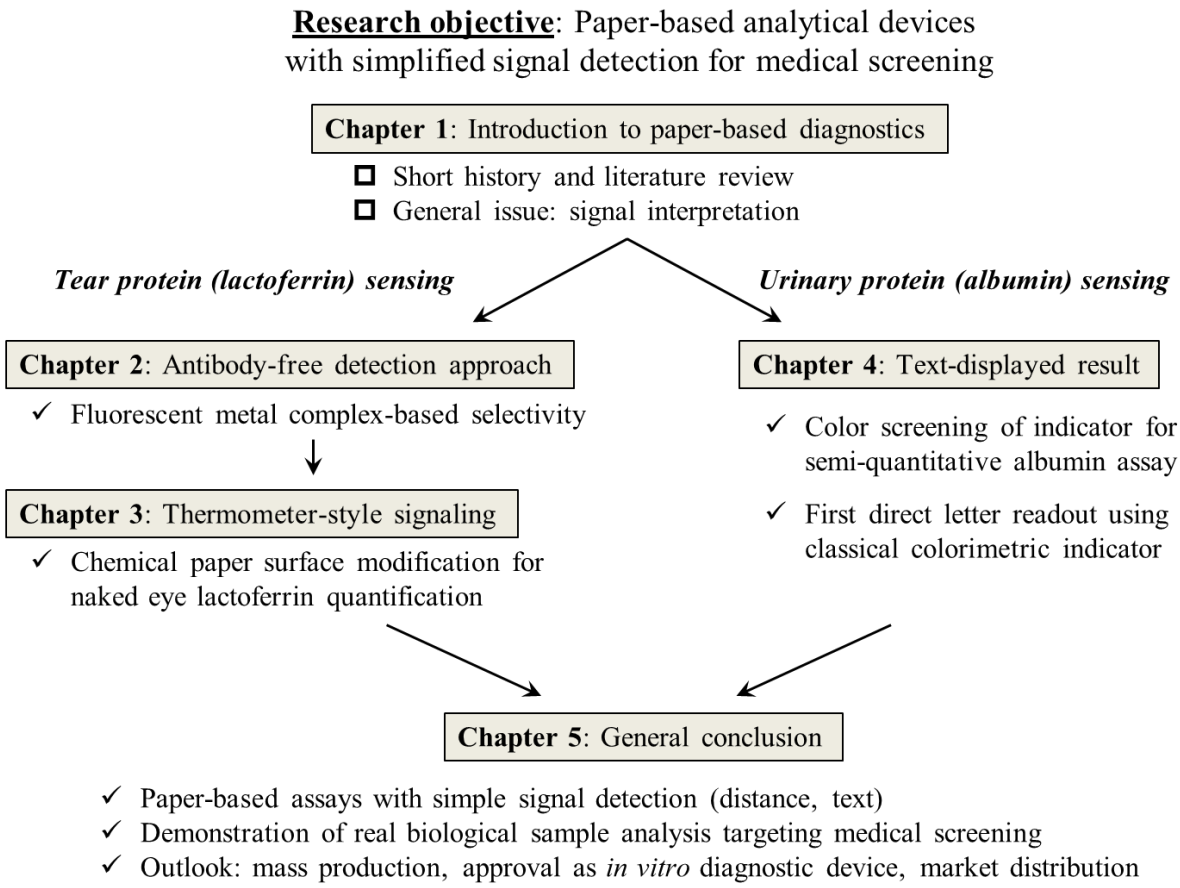

Scheme 1-3. Outline of the current thesis.

References

1. Rodney, C., Scientific American Inventions and Discoveries. John Wiley & Sons, Inc., Hoboken, New Jersey, **2004**.
2. Maumené, M., On a new reagent for ascertaining the presence of sugar in certain liquids. *Philos. Mag. Ser. 3* **1850,** *36*, 482.
3. Oliver, G., On Bedside Urinary Tests. *Lancet* **1883,** *121*, 139−140.
4. Comer, J. P., Semiquantitative Specific Test Paper for Glucose in Urine. *Anal. Chem.* **1956,** *28*, 1748−1750.
5. Free, A. H.; Adams, E. C.; Kercher, M. L.; Free, H. M.; Cook, M. H., Simple Specific Test for Urine Glucose. *Clin. Chem.* **1957,** *3*, 163−168.
6. Roche Diagnostics, Compendium of urinalysis - Urine test strips and microscopy. http://www.roche-diagnostics.ch/content/dam/corporate/roche-dia_ch/documents/broschueren/professional_diagnostics/urindiagnostik/12254620001_EN_EA_Compendium-of-urinanalysis_Brosch%C3%BCre_EN.pdf (accessed June 27, 2017).
7. Campbell, R. L.; Wagner, D. B.; O'Connell, J. P., Solid phase assay with visual readout. *US Pat.*, 4703017, October 27, **1987**.
8. Rosenstein, R. W.; Bloomster, T. G., Solid phase assay employing capillary flow. *US Pat.*, 4855240, August 8, **1989**.
9. Mills, C. K.; Afable, C.; Candanoza, C.; Ferreria, V.; Landon, S.; Repaske, A.; Scully, J.; Gherna, R., Comparison of the merckoquant 10007 nitrite test strip with conventional reagents in the detection of nitrate reduction by bacteria. *J. Microbiol. Methods* **1989,** *9*, 233−237.
10. Martinez, A. W.; Phillips, S. T.; Butte, M. J.; Whitesides, G. M., Patterned paper as a platform for inexpensive, low-volume, portable bioassays. *Angew. Chem. Int. Ed.* **2007,** *46*, 1318−1320.
11. Yagoda, H., Applications of Confined Spot Tests in Analytical Chemistry: Preliminary Paper. *Ind. Eng. Chem.* **1937,** *9*, 79−82.

12. Müller, R. H.; Clegg, D. L., Automatic Paper Chromatography. *Anal. Chem.* **1949,** *21*, 1123−1125.
13. Vaeck, S. V., Quantitative inorganic paper chromatography direct determination of nickel in microgram quantities. *Anal. Chim. Acta* **1954,** *10*, 48−67.
14. Vaeck, S. V., Quantitative inorganic paper chromatography direct determination of cobalt by a scanning method. *Anal. Chim. Acta* **1955,** *12*, 443−454.
15. Volpatti, L. R.; Yetisen, A. K., Commercialization of microfluidic devices. *Trends Biotechnol.* **2014,** *32*, 347−350.
16. Martinez, A. W.; Phillips, S. T.; Wiley, B. J.; Gupta, M.; Whitesides, G. M., FLASH: A rapid method for prototyping paper-based microfluidic devices. *Lab Chip* **2008,** *8*, 2146−2150.
17. Pelton, R., Bioactive paper provides a low-cost platform for diagnostics. *Trends Anal. Chem.* **2009,** *28*, 925−942.
18. Coltro, W. K.; de Jesus, D. P.; da Silva, J. A.; do Lago, C. L.; Carrilho, E., Toner and paper-based fabrication techniques for microfluidic applications. *Electrophoresis* **2010,** *31*, 2487−2498.
19. Ballerini, D. R.; Li, X.; Shen, W., Patterned paper and alternative materials as substrates for low-cost microfluidic diagnostics. *Microfluid. Nanofluidics* **2012,** *13*, 769−787.
20. Li, X.; Ballerini, D. R.; Shen, W., A perspective on paper-based microfluidics: Current status and future trends. *Biomicrofluidics* **2012,** *6*, 11301−1130113.
21. Liana, D. D.; Raguse, B.; Gooding, J. J.; Chow, E., Recent advances in paper-based sensors. *Sensors* **2012,** *12*, 11505−11526.
22. Nery, E. W.; Kubota, L. T., Sensing approaches on paper-based devices: a review. *Anal. Bioanal. Chem.* **2013,** *405*, 7573−7595.
23. Yetisen, A. K.; Akram, M. S.; Lowe, C. R., Paper-based microfluidic point-of-care diagnostic devices. *Lab Chip* **2013,** *13*, 2210−2251.
24. Hu, J.; Wang, S.; Wang, L.; Li, F.; Pingguan-Murphy, B.; Lu, T. J.; Xu, F., Advances in paper-based point-of-care diagnostics. *Biosens. Bioelectron.* **2014,** *54*, 585−597.

25. Cate, D. M.; Adkins, J. A.; Mettakoonpitak, J.; Henry, C. S., Recent developments in paper-based microfluidic devices. *Anal. Chem.* **2015,** *87*, 19−41.
26. Martinez, A. W.; Phillips, S. T.; Whitesides, G. M.; Carrilho, E., Diagnostics for the Developing World: Microfluidic Paper-Based Analytical Devices. *Anal. Chem.* **2010,** *82*, 3−10.
27. Chen, Y. H.; Kuo, Z. K.; Cheng, C. M., Paper - a potential platform in pharmaceutical development. *Trends Biotechnol.* **2015,** *33*, 4−9.
28. Choi, J. R.; Tang, R.; Wang, S.; Wan Abas, W. A.; Pingguan-Murphy, B.; Xu, F., Paper-based sample-to-answer molecular diagnostic platform for point-of-care diagnostics. *Biosens. Bioelectron.* **2015,** *74*, 427−439.
29. Lopez-Marzo, A. M.; Merkoci, A., Paper-based sensors and assays: a success of the engineering design and the convergence of knowledge areas. *Lab Chip* **2016,** *16*, 3150−3176.
30. Mettakoonpitak, J.; Boehle, K.; Nantaphol, S.; Teengam, P.; Adkins, J. A.; Srisa-Art, M.; Henry, C. S., Electrochemistry on Paper-based Analytical Devices: A Review. *Electroanalysis* **2016,** *28*, 1420−1436.
31. Nilghaz, A.; Guan, L.; Tan, W.; Shen, W., Advancement of Paper-based Microfluidics for Diagnostics – the Original Motivation and Current status. *ACS Sens.* **2016,** *1*, 1382−1393.
32. Xia, Y.; Si, J.; Li, Z., Fabrication techniques for microfluidic paper-based analytical devices and their applications for biological testing: A review. *Biosens. Bioelectron.* **2016,** *77*, 774−789.
33. Xu, Y.; Liu, M.; Kong, N.; Liu, J., Lab-on-paper micro- and nano-analytical devices: Fabrication, modification, detection and emerging applications. *Microchim. Acta* **2016,** *183*, 1521−1542.
34. Yang, Y.; Noviana, E.; Nguyen, M. P.; Geiss, B. J.; Dandy, D. S.; Henry, C. S., Paper-Based Microfluidic Devices: Emerging Themes and Applications. *Anal. Chem.* **2017,** *89*, 71−91.
35. Yamada, K.; Henares, T. G.; Suzuki, K.; Citterio, D., Paper-based inkjet-printed microfluidic analytical devices. *Angew. Chem. Int. Ed.* **2015,** *54*, 5294−5310.
36. Li, J.; Rossignol, F.; Macdonald, J., Inkjet printing for biosensor fabrication: combining chemistry and technology for advanced manufacturing. *Lab Chip* **2015,** *15*, 2538−2558.

37. Manz, A.; Graber, N.; Widmer, H. M., Miniaturized total chemical analysis systems: A novel concept for chemical sensing. *Sens. Actuat. B: Chem.* **1990,** *1*, 244−248.
38. Lisowski, P.; Zarzycki, P. K., Microfluidic Paper-Based Analytical Devices (μPADs) and Micro Total Analysis Systems (μTAS): Development, Applications and Future Trends. *Chromatographia* **2013,** *76*, 1201−1214.
39. Reyes, D. R.; Iossifidis, D.; Auroux, P.-A.; Manz, A., Micro Total Analysis Systems. 1. Introduction, Theory, and Technology. *Anal. Chem.* **2002,** *74*, 2623−2636.
40. Whitesides, G. M., The origins and the future of microfluidics. *Nature* **2006,** *442*, 368−373.
41. Mao, X.; Huang, T. J., Microfluidic diagnostics for the developing world. *Lab Chip* **2012,** *12*, 1412−1416.
42. Osborn, J. L.; Lutz, B.; Fu, E.; Kauffman, P.; Stevens, D. Y.; Yager, P., Microfluidics without pumps: reinventing the T-sensor and H-filter in paper networks. *Lab Chip* **2010,** *10*, 2659−2665.
43. Ahmed, S.; Bui, M.-P. N.; Abbas, A., Paper-based chemical and biological sensors: Engineering aspects. *Biosens. Bioelectron.* **2016,** *77*, 249−263.
44. Lu, Y.; Shi, W.; Jiang, L.; Qin, J.; Lin, B., Rapid prototyping of paper-based microfluidics with wax for low-cost, portable bioassay. *Electrophoresis* **2009,** *30*, 1497−1500.
45. Lu, Y.; Shi, W.; Qin, J.; Lin, B., Fabrication and Characterization of Paper-Based Microfluidics Prepared in Nitrocellulose Membrane By Wax Printing. *Anal. Chem.* **2010,** *82*, 329−335.
46. Bruzewicz, D. A.; Reches, M.; Whitesides, G. M., Low-Cost Printing of Poly(dimethylsiloxane) Barriers To Define Microchannels in Paper. *Anal. Chem.* **2008,** *80*, 3387−3392.
47. Abe, K.; Suzuki, K.; Citterio, D., Inkjet-Printed Microfluidic Multianalyte Chemical Sensing Paper. *Anal. Chem.* **2008,** *80*, 6928−6934.
48. Abe, K.; Kotera, K.; Suzuki, K.; Citterio, D., Inkjet-printed paperfluidic immuno-chemical sensing device. *Anal. Bioanal. Chem.* **2010,** *398*, 885−893.
49. Maejima, K.; Tomikawa, S.; Suzuki, K.; Citterio, D., Inkjet printing: an integrated and green chemical approach to microfluidic paper-based analytical devices. *RSC Adv.* **2013,** *3*, 9258−9263.

50. Carrilho, E.; Martinez, A. W.; Whitesides, G. M., Understanding Wax Printing: A Simple Micropatterning Process for Paper-Based Microfluidics. *Anal. Chem.* **2009,** *81*, 7091−7095.
51. Olkkonen, J.; Lehtinen, K.; Erho, T., Flexographically Printed Fluidic Structures in Paper. *Anal. Chem.* **2010,** *82*, 10246−10250.
52. Wang, J.; Monton, M. R.; Zhang, X.; Filipe, C. D.; Pelton, R.; Brennan, J. D., Hydrophobic sol-gel channel patterning strategies for paper-based microfluidics. *Lab Chip* **2014,** *14*, 691−695.
53. Teichler, A.; Perelaer, J.; Schubert, U. S., Inkjet printing of organic electronics – comparison of deposition techniques and state-of-the-art developments. *J. Mater. Chem. C* **2013,** *1*, 1910−1925.
54. Shimoda, T.; Kanbe, S.; Kobayashi, H.; Seki, S.; Kiguchi, H.; Yudasaka, I.; Kimura, M.; Miyashita, S.; Friend, R. H.; Burroughes, J. H.; Towns, C. R., Multicolor Pixel Patterning of Light-Emitting Polymers by Ink-Jet Printing. *SID Symposium Digest of Technical Papers* **1999,** *30*, 376−379.
55. Okamoto, T.; Suzuki, T.; Yamamoto, N., Microarray fabrication with covalent attachment of DNA using Bubble Jet technology. *Nat. Biotechnol.* **2000,** *18*, 438−441.
56. Li, X.; Tian, J.; Garnier, G.; Shen, W., Fabrication of paper-based microfluidic sensors by printing. *Colloids Surf., B* **2010,** *76*, 564−570.
57. Yu, W. W.; White, I. M., Inkjet Printed Surface Enhanced Raman Spectroscopy Array on Cellulose Paper. *Anal. Chem.* **2010,** *82*, 9626−9630.
58. Tisone, T. C.; O'Farrell, B., Manufacturing the Next Generation of Highly Sensitive and Reproducible Lateral Flow Immunoassay. Humana Press, Totowa, NJ, **2009**, 1−26.
59. Gubala, V.; Harris, L. F.; Ricco, A. J.; Tan, M. X.; Williams, D. E., Point of care diagnostics: status and future. *Anal. Chem.* **2012,** *84*, 487−515.
60. Derby, B., Inkjet Printing of Functional and Structural Materials: Fluid Property Requirements, Feature Stability, and Resolution. *Annu. Rev. Mater. Res.* **2010,** *40*, 395−414.
61. Derby, B., Inkjet printing ceramics: From drops to solid. *J. Eur. Ceram. Soc.* **2011,** *31*, 2543−2550.
62. Jang, D.; Kim, D.; Moon, J., Influence of Fluid Physical Properties on Ink-Jet Printability. *Langmuir* **2009,** *25*, 2629−2635.

63. Tekin, E.; Smith, P. J.; Schubert, U. S., Inkjet printing as a deposition and patterning tool for polymers and inorganic particles. *Soft Matter* **2008,** *4*, 703−713.

64. Monton, M. R. N.; Forsberg, E. M.; Brennan, J. D., Tailoring Sol–Gel-Derived Silica Materials for Optical Biosensing. *Chem. Mater.* **2012,** *24*, 796−811.

65. Di Risio, S.; Yan, N., Piezoelectric Ink-Jet Printing of Horseradish Peroxidase: Effect of Ink Viscosity Modifiers on Activity. *Macromol. Rapid Commun.* **2007,** *28*, 1934−1940.

66. Magdassi, S., Ink Requirements and Formulations Guidelines in *The Chemistry of Inkjet Inks*, ed. Magdassi, S. World Scientific, Singapore, **2010**, 19−41.

67. de Gans, B. J.; Duineveld, P. C.; Schubert, U. S., Inkjet Printing of Polymers: State of the Art and Future Developments. *Adv. Mater.* **2004,** *16*, 203−213.

68. Recommendations for Clinical Laboratory Improvement Amendments of 1988 (CLIA) Waiver Applications for Manufacturers of In Vitro Diagnostic Devices. http://www.fda.gov/MedicalDevices/DeviceRegulationandGuidance/GuidanceDocuments/ucm079632.htm (accessed June 27, 2017).

69. Pollock, N. R.; Rolland, J. P.; Kumar, S.; Beattie, P. D.; Jain, S.; Noubary, F.; Wong, V. L.; Pohlmann, R. A.; Ryan, U. S.; Whitesides, G. M., A Paper-Based Multiplexed Transaminase Test for Low-Cost, Point-of-Care Liver Function Testing. *Sci. Transl. Med.* **2012,** *4*, 152ra129.

70. Songjaroen, T.; Dungchai, W.; Chailapakul, O.; Henry, C. S.; Laiwattanapaisal, W., Blood separation on microfluidic paper-based analytical devices. *Lab Chip* **2012,** *12*, 3392−3398.

71. Vella, S. J.; Beattie, P.; Cademartiri, R.; Laromaine, A.; Martinez, A. W.; Phillips, S. T.; Mirica, K. A.; Whitesides, G. M., Measuring markers of liver function using a micropatterned paper device designed for blood from a fingerstick. *Anal. Chem.* **2012,** *84*, 2883−2891.

72. Noiphung, J.; Songjaroen, T.; Dungchai, W.; Henry, C. S.; Chailapakul, O.; Laiwattanapaisal, W., Electrochemical detection of glucose from whole blood using paper-based microfluidic devices. *Anal. Chim. Acta* **2013,** *788*, 39−45.

73. Pollock, N. R.; McGray, S.; Colby, D. J.; Noubary, F.; Nguyen, H.; Nguyen, T. A.; Khormaee, S.; Jain, S.; Hawkins, K.; Kumar, S.; Rolland, J. P.; Beattie, P. D.; Chau, N. V.; Quang, V. M.; Barfield, C.; Tietje, K.; Steele, M.; Weigl, B. H., Field evaluation of a prototype paper-based point-of-care fingerstick transaminase test. *PLoS One* **2013,** *8*, e75616.

74. Jain, S.; Rajasingham, R.; Noubary, F.; Coonahan, E.; Schoeplein, R.; Baden, R.; Curry, M.; Afdhal, N.; Kumar, S.; Pollock, N. R., Performance of an Optimized Paper-Based Test for Rapid Visual Measurement of Alanine Aminotransferase (ALT) in Fingerstick and Venipuncture Samples. *PLoS One* **2015,** *10*, e0128118.

75. Yang, X.; Forouzan, O.; Brown, T. P.; Shevkoplyas, S. S., Integrated separation of blood plasma from whole blood for microfluidic paper-based analytical devices. *Lab Chip* **2012,** *12*, 274−280.

76. Nilghaz, A.; Shen, W., Low-cost blood plasma separation method using salt functionalized paper. *RSC Adv.* **2015,** *5*, 53172−53179.

77. Kar, S.; Maiti, T. K.; Chakraborty, S., Capillarity-driven blood plasma separation on paper-based devices. *Analyst* **2015,** *140*, 6473−6476.

78. Carvalhal, R. F.; Simão Kfouri, M.; de Oliveira Piazetta, M. H.; Gobbi, A. L.; Kubota, L. T., Electrochemical Detection in a Paper-Based Separation Device. *Anal. Chem.* **2010,** *82*, 1162−1165.

79. Shiroma, L. Y.; Santhiago, M.; Gobbi, A. L.; Kubota, L. T., Separation and electrochemical detection of paracetamol and 4-aminophenol in a paper-based microfluidic device. *Anal. Chim. Acta* **2012,** *725*, 44−50.

80. Murphy, A.; Gorey, B.; de Guzman, K.; Kelly, N.; Nesterenko, E. P.; Morrin, A., Microfluidic paper analytical device for the chromatographic separation of ascorbic acid and dopamine. *RSC Adv.* **2015,** *5*, 93162−93169.

81. Yager, P.; Domingo, G. J.; Gerdes, J., Point-of-Care Diagnostics for Global Health. *Annu. Rev. Biomed. Eng.* **2008,** *10*, 107−144.

82. Chen, X.; Chen, J.; Wang, F.; Xiang, X.; Luo, M.; Ji, X.; He, Z., Determination of glucose and uric acid with bienzyme colorimetry on microfluidic paper-based analysis devices. *Biosens. Bioelectron.* **2012,** *35*, 363−368.

83. Fu, E.; Kauffman, P.; Lutz, B.; Yager, P., Chemical signal amplification in two-dimensional paper networks. *Sens. Actuat. B: Chem* **2010,** *149*, 325−328.

84. Fu, E.; Liang, T.; Houghtaling, J.; Ramachandran, S.; Ramsey, S. A.; Lutz, B.; Yager, P., Enhanced sensitivity of lateral flow tests using a two-dimensional paper network format. *Anal. Chem.* **2011,** *83*, 7941−7946.

85. Fu, E.; Liang, T.; Spicar-Mihalic, P.; Houghtaling, J.; Ramachandran, S.; Yager, P., Two-dimensional paper network format that enables simple multistep assays for use in low-resource settings in the context of malaria antigen detection. *Anal. Chem.* **2012,** *84*, 4574−4579.

86. Fridley, G. E.; Le, H.; Yager, P., Highly sensitive immunoassay based on controlled rehydration of patterned reagents in a 2-dimensional paper network. *Anal. Chem.* **2014,** *86*, 6447−6453.

87. Carrilho, E.; Phillips, S. T.; Vella, S. J.; Martinez, A. W.; Whitesides, G. M., Paper microzone plates. *Anal. Chem.* **2009,** *81*, 5990−5998.

88. Cheng, C.-M.; Martinez, A. W.; Gong, J.; Mace, C. R.; Phillips, S. T.; Carrilho, E.; Mirica, K. A.; Whitesides, G. M., Paper-Based ELISA. *Angew. Chem. Int. Ed.* **2010,** *49*, 4771−4774.

89. Apilux, A.; Ukita, Y.; Chikae, M.; Chailapakul, O.; Takamura, Y., Development of automated paper-based devices for sequential multistep sandwich enzyme-linked immunosorbent assays using inkjet printing. *Lab Chip* **2013,** *13*, 126−135.

90. Lutz, B.; Liang, T.; Fu, E.; Ramachandran, S.; Kauffman, P.; Yager, P., Dissolvable fluidic time delays for programming multi-step assays in instrument-free paper diagnostics. *Lab Chip* **2013,** *13*, 2840−2847.

91. Mentele, M. M.; Cunningham, J.; Koehler, K.; Volckens, J.; Henry, C. S., Microfluidic paper-based analytical device for particulate metals. *Anal. Chem.* **2012,** *84*, 4474−4480.

92. Yamada, K.; Takaki, S.; Komuro, N.; Suzuki, K.; Citterio, D., An antibody-free microfluidic paper-based analytical device for the determination of tear fluid lactoferrin by fluorescence sensitization of Tb^{3+}. *Analyst* **2014,** *139*, 1637−1643.

93. Joung, H. A.; Oh, Y. K.; Kim, M. G., An automatic enzyme immunoassay based on a chemiluminescent lateral flow immunosensor. *Biosens. Bioelectron.* **2014,** *53*, 330−335.

94. Wong, S. Y.; Cabodi, M.; Rolland, J.; Klapperich, C. M., Evaporative concentration on a paper-based device to concentrate analytes in a biological fluid. *Anal. Chem.* **2014,** *86*, 11981−11985.

95. Cassano, C. L.; Fan, Z. H., Laminated paper-based analytical devices (LPAD): fabrication, characterization, and assays. *Microfluid. Nanofluidics* **2013,** *15*, 173−181.

96. Liu, W.; Cassano, C. L.; Xu, X.; Fan, Z. H., Laminated paper-based analytical devices (LPAD) with origami-enabled chemiluminescence immunoassay for cotinine detection in mouse serum. *Anal. Chem.* **2013,** *85*, 10270−10276.

97. Tenda, K.; Ota, R.; Yamada, K.; Henares, T.; Suzuki, K.; Citterio, D., High-Resolution Microfluidic Paper-Based Analytical Devices for Sub-Microliter Sample Analysis. *Micromachines* **2016,** *7*, 80.

98. Schilling, K. M.; Lepore, A. L.; Kurian, J. A.; Martinez, A. W., Fully enclosed microfluidic paper-based analytical devices. *Anal. Chem.* **2012,** *84*, 1579−1585.

99. Lenk, G.; Pohanka, A.; Stemme, G.; Beck, O.; Roxhed, N., *Proc. MicroTAS 2013*, Freiburg, Germany, **2013,** 281−283.

100. Lenk, G.; Hansson, J.; W. van der Wijngaart, W.; Stemme, G.; Roxhed, N., *Proc. Transducers 2015*, Anchorage, Alaska, USA, **2015,** 335−338.

101. Houghtaling, J.; Liang, T.; Thiessen, G.; Fu, E., Dissolvable bridges for manipulating fluid volumes in paper networks. *Anal. Chem.* **2013,** *85*, 11201−11204.

102. Whitesides, G. M., Viewpoint on "Dissolvable fluidic time delays for programming multi-step assays in instrument-free paper diagnostics". *Lab Chip* **2013,** *13*, 4004−4005.

103. Nie, Z.; Deiss, F.; Liu, X.; Akbulut, O.; Whitesides, G. M., Integration of paper-based microfluidic devices with commercial electrochemical readers. *Lab Chip* **2010,** *10*, 3163−3169.

104. Zhang, L.; Yang, W.; Yang, Y.; Liu, H.; Gu, Z., Smartphone-based point-of-care testing of salivary alpha-amylase for personal psychological measurement. *Analyst* **2015,** *140*, 7399−7406.

105. Hong, J. I.; Chang, B. Y., Development of the smartphone-based colorimetry for multi-analyte sensing arrays. *Lab Chip* **2014,** *14*, 1725−1732.

106. Lopez-Ruiz, N.; Curto, V. F.; Erenas, M. M.; Benito-Lopez, F.; Diamond, D.; Palma, A. J.; Capitan-Vallvey, L. F., Smartphone-based simultaneous pH and nitrite colorimetric determination for paper microfluidic devices. *Anal. Chem.* **2014,** *86*, 9554−9562.

107. Lee, D. S.; Jeon, B. G.; Ihm, C.; Park, J. K.; Jung, M. Y., A simple and smart telemedicine device for developing regions: a pocket-sized colorimetric reader. *Lab Chip* **2011,** *11*, 120−126.

108. Smith, G. T.; Dwork, N.; Khan, S. A.; Millet, M.; Magar, K.; Javanmard, M.; Ellerbee Bowden, A. K., Robust dipstick urinalysis using a low-cost, micro-volume slipping manifold and mobile phone platform. *Lab Chip* **2016,** *16*, 2069−2078.

109. Martinez, A. W.; Phillips, S. T.; Carrilho, E.; Thomas, S. W.; Sindi, H.; Whitesides, G. M., Simple Telemedicine for Developing Regions: Camera Phones and Paper-Based Microfluidic Devices for Real-Time, Off-Site Diagnosis. *Anal. Chem.* **2008,** *80*, 3699−3707.

110. Zhu, H.; Isikman, S. O.; Mudanyali, O.; Greenbaum, A.; Ozcan, A., Optical imaging techniques for point-of-care diagnostics. *Lab Chip* **2013,** *13*, 51−67.

111. Ericsson, *Ericsson Mobility Report*; Report June 2016, **2016**.

112. Yang, K.; Peretz-Soroka, H.; Liu, Y.; Lin, F., Novel developments in mobile sensing based on the integration of microfluidic devices and smartphones. *Lab Chip* **2016,** *16*, 943−958.

113. Oncescu, V.; Mancuso, M.; Erickson, D., Cholesterol testing on a smartphone. *Lab Chip* **2014,** *14*, 759−763.

114. Fronczek, C. F.; Park, T. S.; Harshman, D. K.; Nicolini, A. M.; Yoon, J.-Y., Paper microfluidic extraction and direct smartphone-based identification of pathogenic nucleic acids from field and clinical samples. *RSC Adv.* **2014,** *4*, 11103−11110.

115. Oncescu, V.; O'Dell, D.; Erickson, D., Smartphone based health accessory for colorimetric detection of biomarkers in sweat and saliva. *Lab Chip* **2013,** *13*, 3232−3238.

116. Yetisen, A. K.; Martinez-Hurtado, J. L.; Garcia-Melendrez, A.; da Cruz Vasconcellos, F.; Lowe, C. R., A smartphone algorithm with inter-phone repeatability for the analysis of colorimetric tests. *Sens. Actuat. B: Chem.* **2014,** *196*, 156−160.

117. WHO, *Laboratory Biosafety Manual - Third Edition*.

118. Gross, B. C.; Erkal, J. L.; Lockwood, S. Y.; Chen, C.; Spence, D. M., Evaluation of 3D Printing and Its Potential Impact on Biotechnology and the Chemical Sciences. *Anal. Chem.* **2014,** *86*, 3240−3253.

119. Ho, C. M.; Ng, S. H.; Li, K. H.; Yoon, Y. J., 3D printed microfluidics for biological applications. *Lab Chip* **2015,** *15*, 3627−3637.

120. Gross, B.; Lockwood, S. Y.; Spence, D. M., Recent Advances in Analytical Chemistry by 3D Printing. *Anal. Chem.* **2017,** *89*, 57−70.

121. Martinez, A. W.; Phillips, S. T.; Nie, Z.; Cheng, C.-M.; Carrilho, E.; Wiley, B. J.; Whitesides, G. M., Programmable diagnostic devices made from paper and tape. *Lab Chip* **2010,** *10*, 2499−2504.

122. Credou, J.; Berthelot, T., Cellulose: from biocompatible to bioactive material. *J. Mater. Chem. B* **2014,** *2*, 4767−4788.

123. Kudo, H.; Yamada, K.; Watanabe, D.; Suzuki, K.; Citterio, D., Paper-Based Analytical Device for Zinc Ion Quantification in Water Samples with Power-Free Analyte Concentration. *Micromachines* **2017,** *8,* 127.

124. Evans, E.; Gabriel, E. F.; Benavidez, T. E.; Tomazelli Coltro, W. K.; Garcia, C. D., Modification of microfluidic paper-based devices with silica nanoparticles. *Analyst* **2014,** *139*, 5560−5567.

125. Figueredo, F.; Garcia, P. T.; Corton, E.; Coltro, W. K., Enhanced Analytical Performance of Paper Microfluidic Devices by Using Fe_3O_4 Nanoparticles, MWCNT, and Graphene Oxide. *ACS Appl. Mater. Interfaces* **2016,** *8*, 11−15.

126. Bauer, R. Composition for the semiquantitative determination of specific gravity of a test sample. *US Pat.*, 5302531, April 12, **1994**.

127. Shen, L.; Hagen, J. A.; Papautsky, I., Point-of-care colorimetric detection with a smartphone. *Lab Chip* **2012,** *12*, 4240−4243.

128. Chaplan, C. A.; Mitchell, H. T.; Martinez, A. W., Paper-based standard addition assays. *Anal. Methods* **2014,** *6*, 1296−1300.

129. Lewis, G. G.; DiTucci, M. J.; Phillips, S. T., Quantifying Analytes in Paper-Based Microfluidic Devices Without Using External Electronic Readers. *Angew. Chem. Int. Ed.* **2012,** *51*, 12707−12710.

130. Wei, X.; Tian, T.; Jia, S.; Zhu, Z.; Ma, Y.; Sun, J.; Lin, Z.; Yang, C. J., Target-Responsive DNA Hydrogel Mediated "Stop-Flow" Microfluidic Paper-Based Analytic Device for Rapid, Portable and Visual Detection of Multiple Targets. *Anal. Chem.* **2015,** *87*, 4275−4282.

131. Lou, S. C.; Patel, C.; Ching, S.; Gordon, J., One-step competitive immunochromatographic assay for semiquantitative determination of lipoprotein(a) in plasma. *Clin. Chem.* **1993,** *39*, 619−624.

132. Leung, W.; Chan, C. P.; Rainer, T. H.; Ip, M.; Cautherley, G. W.; Renneberg, R., InfectCheck CRP barcode-style lateral flow assay for semi-quantitative detection of C-reactive protein in distinguishing between bacterial and viral infections. *J. Immunol. Methods* **2008,** *336*, 30−36.

133. Fung, K.-K.; Chan, C. P.-Y.; Renneberg, R., Development of a creatinine enzyme-based bar-code-style lateral-flow assay. *Anal. Bioanal. Chem.* **2009,** *393*, 1281−1287.

134. Cho, J.-H.; Paek, S.-H., Semiquantitative, bar code version of immunochromatographic assay system for human serum albumin as model analyte. *Biotechnol. Bioeng.* **2001,** *75*, 725−732.

135. Lathwal, S.; Sikes, H. D., A Method for Designing Instrument-Free Quantitative Immunoassays. *Anal. Chem.* **2016,** *88*, 3194−3202.

136. Karita, S.; Kaneta, T., Acid-base titrations using microfluidic paper-based analytical devices. *Anal. Chem.* **2014,** *86*, 12108−12114.

137. Karita, S.; Kaneta, T., Chelate titrations of Ca^{2+} and Mg^{2+} using microfluidic paper-based analytical devices. *Anal. Chim. Acta* **2016,** *924*, 60−67.

138. Tian, T.; Li, J.; Song, Y.; Zhou, L.; Zhu, Z.; Yang, C. J., Distance-based microfluidic quantitative detection methods for point-of-care testing. *Lab Chip* **2016,** *16*, 1139−1151.

139. Cate, D. M.; Dungchai, W.; Cunningham, J. C.; Volckens, J.; Henry, C. S., Simple, distance-based measurement for paper analytical devices. *Lab Chip* **2013,** *13*, 2397−2404.

140. Cate, D. M.; Noblitt, S. D.; Volckens, J.; Henry, C. S., Multiplexed paper analytical device for quantification of metals using distance-based detection. *Lab Chip* **2015,** *15*, 2808−2818.

141. Yamada, K.; Henares, T. G.; Suzuki, K.; Citterio, D., Distance-Based Tear Lactoferrin Assay on Microfluidic Paper Device Using Interfacial Interactions on Surface-Modified Cellulose. *ACS Appl. Mater. Interfaces* **2015,** *7*, 24864−24875.

142. Walji, N.; MacDonald, D. B., Influence of Geometry and Surrounding Conditions on Fluid Flow in Paper-Based Devices. *Micromachines* **2016,** *7,* 73.

143. Li, M.; Tian, J.; Al-Tamimi, M.; Shen, W., Paper-based blood typing device that reports patient's blood type "in writing". *Angew. Chem. Int. Ed.* **2012,** *51*, 5497−5501.

144. Li, J.; Macdonald, J., Multiplex lateral flow detection and binary encoding enables a molecular colorimetric 7-segment display. *Lab Chip* **2016,** *16*, 242−245.

145. Haemokinesis, http://www.haemokinesis.com/products/bio-active-paper-tests (accessed June 27, 2017).

146. Zhang, Y.; Fan, J.; Nie, J.; Le, S.; Zhu, W.; Gao, D.; Yang, J.; Zhang, S.; Li, J., Timing readout in paper device for quantitative point-of-use hemin/G-quadruplex DNAzyme-based bioassays. *Biosens. Bioelectron.* **2015,** *73*, 13−18.

147. Siegel, A. C.; Phillips, S. T.; Wiley, B. J.; Whitesides, G. M., Thin, lightweight, foldable thermochromic displays on paper. *Lab Chip* **2009,** *9*, 2775−2781.

148. Liu, H.; Crooks, R. M., Paper-based electrochemical sensing platform with integral battery and electrochromic read-out. *Anal. Chem.* **2012,** *84*, 2528−2532.

149. Liana, D. D.; Raguse, B.; Gooding, J. J.; Chow, E., Toward Paper-Based Sensors: Turning Electrical Signals into an Optical Readout System. *ACS Appl. Mater. Interfaces* **2015,** *7*, 19201−19209.

150. Yamada, K.; Shibata, H.; Suzuki, K.; Citterio, D., Toward practical application of paper-based microfluidics for medical diagnostics: state-of-the-art and challenges. *Lab Chip* **2017,** *17*, 1206−1249.

Chapter 2 Colorimetric tear lactoferrin assay on μPAD based on fluorescence emission from terbium

This chapter is based on
"An antibody-free microfluidic paper-based analytical device for the determination of tear fluid lactoferrin by fluorescence sensitization of Tb^{3+}",
Kentaro Yamada; Shunsuke Takaki; Nobutoshi Komuro; Koji Suzuki; Daniel Citterio,
Analyst, **2014**, 139, 1637–1643.

Summary

An inkjet-printed microfluidic paper-based analytical device (μPAD) for the detection of lactoferrin has been developed. The analyte concentration dependent fluorescence emission, caused by the sensitization of pre-deposited terbium (Tb^{3+}) upon complexation with lactoferrin on the paper device, is captured using a digital camera. The dynamic response range (0.5–3 mg mL^{-1}) and the limit of detection (0.30 mg mL^{-1}) of the μPAD are suitable for the analysis of normal human tears and the detection of eye disorders. Finally, lactoferrin concentrations in human tear samples were analyzed by the μPADs and the assay results corresponded within 6% error to those obtained by an immunoassay (ELISA). The μPADs provide a simple, rapid and accurate method for lactoferrin detection in tear fluid. Results are obtained within 15 min of a single application of 2.5 μL of sample. To the best of my knowledge, this is the first report of a device for lactoferrin quantification relying neither on an immunoassay nor on high cost analytical instrumentation.

2.1. Introduction

Since their introduction by the Whitesides group in 2007, microfluidic paper-based analytical devices (μPADs) have gained significant attention as an analytical platform.[1] Owing to the intrinsic properties of paper, μPADs feature several advantageous characteristics relevant to simple and low-cost analytical devices: (1) they are fabricated from low-cost materials. (2) They are lightweight, making them easy to transport and to distribute. (3) They are safely disposable by incineration. Compared to plastic microplates contaminated with biological substances in laboratory tests, incineration of used μPADs enables sanitary disposal, which eliminates hazardous biological substances. (4) Assays performed on μPADs require only low sample volumes, which is important for samples with limited availability such as tears, saliva, urine from newborn infants, and blood from fingerstick.[2] (5) μPADs do generally not depend on external power sources. The need for pumps is eliminated, since capillary forces in the microporous cellulose fiber network of paper drive sample transport. In sum, μPADs are easy-to-handle and user-friendly analytical tools suitable for volume-limited samples, as has already been shown in various applications (*e.g.* blood test, food safety, and metal analysis).[3-7]

In 2008, our group had demonstrated μPADs for (bio)chemical sensing fabricated by inkjet printing technology for the first time.[8] Among the various reported printing technologies for the microfluidic patterning of paper substrates (plotting,[9] wax printing,[10-11] flexographic printing,[12] wax screen printing[13]), inkjet printing is so far the only industrially applied technology that allows performing all processing steps required for the fabrication of complete μPADs.[14-16]

Human tear fluid is a mixture of various components such as water, proteins, enzymes, electrolytes and lipids. The proteomics of tear fluid has recently become an active area of research.[17-18] Proteins in tears play a key role in the preservation of the ocular surface and in the adjustment of tear components. Therefore, disorders in tear protein secretion can be a cause of several diseases. It has been reported that analysis of the tear protein concentration enables their diagnosis.[19] In particular, the down-regulation of lactoferrin, a glycoprotein existing in human tear fluid at relatively high concentrations, is strongly linked to disorders of the corneal epithelium,[20] and the determination of its concentration is expected to facilitate the diagnosis of systemic autoimmune diseases. So far, most methods for lactoferrin quantification reported in the literature are based

on immunoassays. Examples include a conventional enzyme linked immunosorbent assay (ELISA),[21] a radial immunodiffusion assay (Lactoplate),[22] and a colorimetric solid phase immunoassay (Lactocard).[23] Although they are highly selective and sensitive, these assays have the drawbacks of being time-consuming and requiring multiple operational steps. To overcome these disadvantages, Karns and Herr have recently developed a homogeneous electrophoretic immunoassay on a microfluidic glass chip, which enables the quantification of lactoferrin in < 1 μL of human tear fluid within 5 sec.[18] However, costs associated with the use of monoclonal anti-lactoferrin antibodies for lactoferrin capture remain an issue. In addition, the requirement for sophisticated high-tech instruments for signal detection (*e.g.* fluorescence microscope and cooled CCD camera) makes it difficult to realize a more simple and low-cost assay. Although iTRAQ (isobaric tag for relative and absolute quantitation) technology combined with 2D-nanoLC-nanoESIMS/MS[24] and SELDI-TOF-MS[25] have been reported as analytical methods for lactoferrin quantification without employing antibodies, they require relatively large sample volumes and rely on high cost instrumentation not commonly found in small or medium sized clinical laboratories.

This work demonstrates a simple, low-cost, and rapid lactoferrin determination in human tear fluid using inkjet-printed μPADs based on fluorescence detection. Inkjet printing is used for both the patterning of microchannels and the deposition of the reagents required for sensing. The assay relies on the fluorescence emission from complexes formed between human lactoferrin in the sample solution and Tb^{3+} cations printed on the sensing area of μPADs. The concentration of lactoferrin in the sample is quantified by observing the color intensity of the fluorescence emitted from the complexes formed on the μPAD. This method allows for rapid analysis (15 min) of lactoferrin, based on a simple fluorometric assay without using costly antibodies. The achieved detection limit is sufficiently low for the detection of deviating lactoferrin levels in human tear fluid. To the best of the author's knowledge, this is the first report of a lactoferrin determination method relying neither on an immunoassay nor on high cost analytical instrumentation.

2.2. Experimental section

2.2.1. Reagents and instruments

All reagents were used as received. Terbium chloride hexahydrate ($TbCl_3 \cdot 6H_2O$) and human lactoferrin were purchased from Sigma-Aldrich (St. Louis, MO). 1,10- Decanediol diacrylate was purchased from TCI (Tokyo, Japan). *N*-(2-Hydroxyethyl)-1-piperazine ethanesulfonic acid (HEPES) was purchased from Dojindo Laboratories (Kumamoto, Japan). Sodium hydroxide and poly(vinyl alcohol) were purchased from Kanto Chemical (Tokyo, Japan). The human lactoferrin ELISA kit was purchased from EMD Chemicals, Inc. (San Diego, USA). All other reagents were purchased from Wako Pure Chemical Industries Ltd. (Osaka, Japan). All solutions were prepared in 18 MΩ cm Milli-Q water. Circular filter paper sheets of 185 mm diameter (Advantec No. 5C) were obtained from Toyo Roshi Co., Ltd. (Tokyo, Japan).

Fluorescence spectra in solution were recorded on a SPEX Fluorolog-NIR spectrophotometer (HORIBA, Kyoto, Japan). Patterning of the microfluidic structures was performed on an unmodified piezoelectric EPSON PX-105 inkjet printer (Epson, Suwa, Japan), whereas the reagents for lactoferrin detection were deposited with a piezoelectric Dimatix DMP 2831 (Dimatix-Fujifilm Inc., Santa Clara, USA) material printer with 10 pL nominal droplet volume cartridges (DMC-11610). Photopolymerization of printed structures was performed under irradiation from a Hg–Xe lamp (Lightingcure LC-6, Hamamatsu Photonics, Hamamatsu, Japan) at a power of 4 mW cm^{-2} (measured at 365 nm). For fluorescence emission signal detection from μPADs, UV hand lamps (Funakoshi, Tokyo, Japan) were used as excitation light sources inside a Mini UV viewing cabinet (UVP, Upland, CA, USA), and the emission was captured with a DMC-FZ50 digital camera (Panasonic, Osaka, Japan) through a 520 nm longpass filter (Sigma Koki Co., Ltd, Tokyo, Japan).

2.2.2. Fluorescence emission measurement

Fluorescence emission spectra were collected from HEPES buffered solutions (pH 7.4, 50 mM) containing 0 to 1 mg mL^{-1} lactoferrin in the presence of 100 μM $TbCl_3$ and 3.75 mM $NaHCO_3$. The excitation wavelength was set to 290 nm and the emission spectra were recorded between 480 nm and 640 nm through a 440 nm longpass filter (Sigma Koki Co., Ltd, Tokyo, Japan).

2.2.3. Device fabrication

The microfluidic patterns on μPADs were fabricated with the inkjet printer and a UV-curable ink by a method similar to the one earlier reported by our group.[15] Briefly, filter paper taped onto a sheet of A4 copy paper with a circular cut-out area in the center was fed into the EPSON inkjet printer. The attachment of the filter paper to a sheet of copy paper is necessary, because the paper feeder of the inkjet printer used in this work is unable to handle round shapes. By the circular cut-out in the copy paper, both surfaces of the attached filter paper are accessible for printing. The ink cartridges were loaded with the UV-curable ink based on octadecyl acrylate and 1,10-decanediol diacrylate. On the topside of the paper, microfluidic patterns designed with PowerPoint (Microsoft) were printed. After the paper was ejected from the printer, it was placed on a cooling plate at 10ºC, while being exposed to the UV light source for 15 min. On the backside of the paper, the UV-curable ink was deposited covering the entire area patterned on the topside, followed by cooling and UV light exposure for 10 min. With this method, 72 microfluidic patterns were printed onto a 9 × 9 cm^2 area of filter paper in a single batch. The design of a single pattern consists of two square areas for sampling and sensing connected by a straight channel, as shown in Figure 2-1.

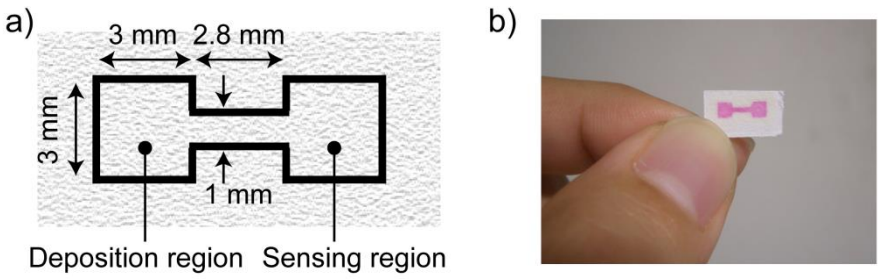

Figure 2-1. a) Outline and dimensions of a single microfluidic pattern. The black line indicates the hydrophobic barrier composed of photo-polymerized UV curable ink patterned by inkjet printing. b) Photograph of a pattern (red food colorant has been applied to visualize the patterned structure).

Before cutting into single devices, all reagents required for lactoferrin detection were deposited onto the patterned paper substrates. First, 8 printing cycles of 1 mM $TbCl_3$ solution with 15vol% ethylene glycol were deposited onto the sensing areas. To prevent the adsorption of lactoferrin to the paper surface, the entire paper was then soaked in 50 mL of 0.5wt% poly(vinyl alcohol) during 5 min, followed by drying for 20 min at 37ºC. The soaking solution was replaced after every use. Next, 12 printing cycles of 25 mM $NaHCO_3$ solution were deposited onto the sampling areas. In all cases HEPES buffered solutions (pH 7.4, 50 mM) were used. In the last step, the completely processed substrate was cut into single μPADs. A schematic illustration of the reagent deposition procedure for fabricating the final μPADs is shown in Figure 2-2.

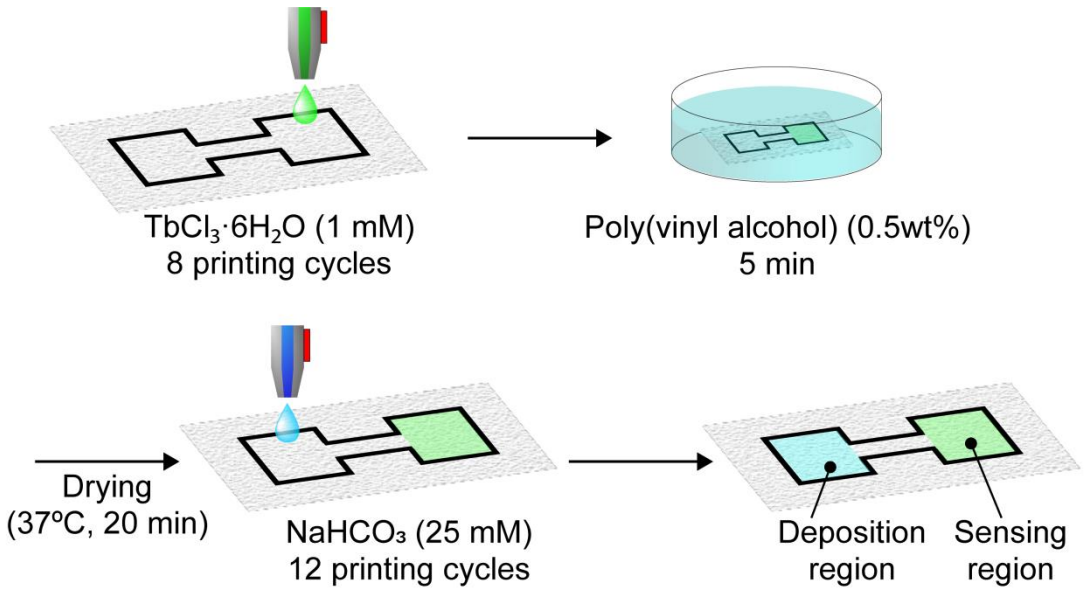

Figure 2-2. Schematic illustration of the reagent deposition process during final μPAD fabrication: $TbCl_3$ and $NaHCO_3$ solutions were printed by using an inkjet printer, while surface treatment of the paper substrate was performed by soaking in poly(vinyl alcohol) solution. All reagents were dissolved in HEPES buffered solution (pH 7.4, 50 mM).

2.2.4. Device calibration and quantitative data processing

For calibration and quantification of human lactoferrin levels in real samples, 2.5 μL of calibration solution (human lactoferrin in 50 mM HEPES pH 7.4 buffer) or tear sample (see below) was pipetted onto the sampling area of a μPAD. After complete drying at room temperature (10−12 min after sample application), the μPAD was placed between two UV hand lamps (λ_{ex} = 254 nm) in a darkened UV viewing cabinet, and the

emitted green fluorescence was imaged using the digital camera through the longpass filter to eliminate the influence of excitation light reflected from the paper substrate. The captured images were stored in JPEG format at 240 dpi and the green (G) intensity (RGB scale) in the sensing area was measured using the image processing software ImageJ (National Institutes of Health). All signals are reported as ΔG values ($G_{sample} - G_{blank}$). The setup for fluorescence signal capture is shown in Figure 2-3.

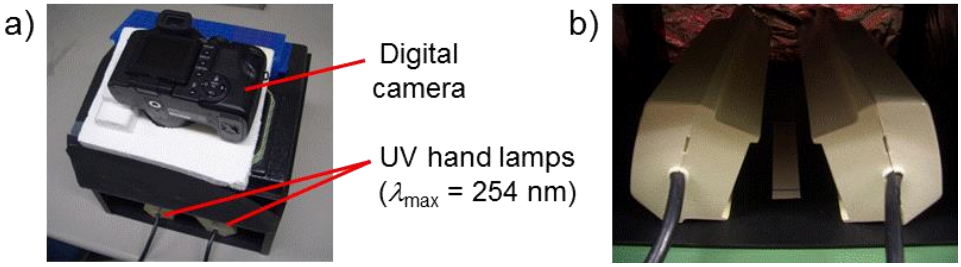

Figure 2-3. a) Photograph of the experimental setup used for obtaining images of fluorescence emitted from the μPAD. The μPAD is placed between two UV hand lamps (λ_{ex} = 254 nm) inside a darkened cabinet. The fluorescence signal is captured through the window on the topside of the cabinet by a standard digital camera with a 520 nm longpass filter attached to the lens. Shutter speed and aperture of the camera have been set to fixed values in the manual mode, to avoid uncontrolled automatic camera adjustments. b) The inside of the cabinet is covered with aluminum foil and ambient light is completely blocked by a black-out curtain.

2.2.5. Human tear fluid analysis

Human tear samples were collected from five volunteers with disposable polyethylene pipettes (AS ONE, Osaka, Japan) and stored in autoclaved Protein LoBind tubes (Eppendorf) at 4ºC until use and no longer than 3 days. For μPAD analysis of lactoferrin concentrations, undiluted human tear fluid was deposited into the sampling area. For ELISA analysis, human tear samples were 10^5-fold diluted in autoclaved Protein LoBind tubes with the sample diluting buffer provided in the kit. This step was necessary to adjust the lactoferrin concentrations to the dynamic response range of the kit (5−50 ng mL^{-1}).

2.3. Results and discussion

2.3.1. Assay principle

The glycoprotein lactoferrin is known for its capacity to reversibly bind two iron ions in their trivalent Fe^{3+} state. In this process, a bicarbonate ion acts as a synergistic anion by neutralizing a positive charge in the binding site of the protein.[26] It has also been reported that various other metal ions can be substituted for iron, including lanthanides.[27] On the other hand, the fluorescence emission of terbium ions is efficiently sensitized upon binding to certain peptides or proteins.[28-29] More recently, it has been shown that Tb^{3+} ions bound to the metal ion binding site of lactoferrin emit pH-dependent fluorescence (λ_{max} = 548 nm).[30] The fluorescence intensity shows a sharp increase between pH 6 and 7 and flattens out at around pH 7.2. Therefore, observing the intensity of the green fluorescence from lactoferrin-terbium complexes at a constant pH value was expected to be applicable to the quantification of lactoferrin. While the pH-dependence of the fluorescence emission from lactoferrin–Tb^{3+} complexes has been reported, the dependence on the lactoferrin concentration has not been investigated so far. In a proof-of-concept experiment, the fluorescence emission spectra of aqueous $TbCl_3$ solutions (100 mM) in the presence of increasing concentrations of human lactoferrin (0–1 mg mL^{-1}) were recorded at a fixed pH of 7.4 (50 mM HEPES buffer) and a background of 3.75 mM $NaHCO_3$. In analogy to the binding of Fe^{3+} to lactoferrin,[26] it was assumed that the presence of the bicarbonate anion would also strengthen the binding of Tb^{3+} to the protein. In that way, $NaHCO_3$ acts as an indirect fluorescence signal enhancer. The spectra shown in Figure 2-4a clearly demonstrate that the intensity of the main Tb^{3+} emission peak at 548 nm is strongly enhanced by the presence of lactoferrin. While a protein-free solution of Tb^{3+} is non-fluorescent, fluorescence turns on upon protein binding due to an energy transfer process. This results in the characteristic emission peaks of Tb^{3+}, which are observed as a green colored emission by the naked eye. The lactoferrin concentration-dependent emission at 548 nm is shown in Figure 2-4b.

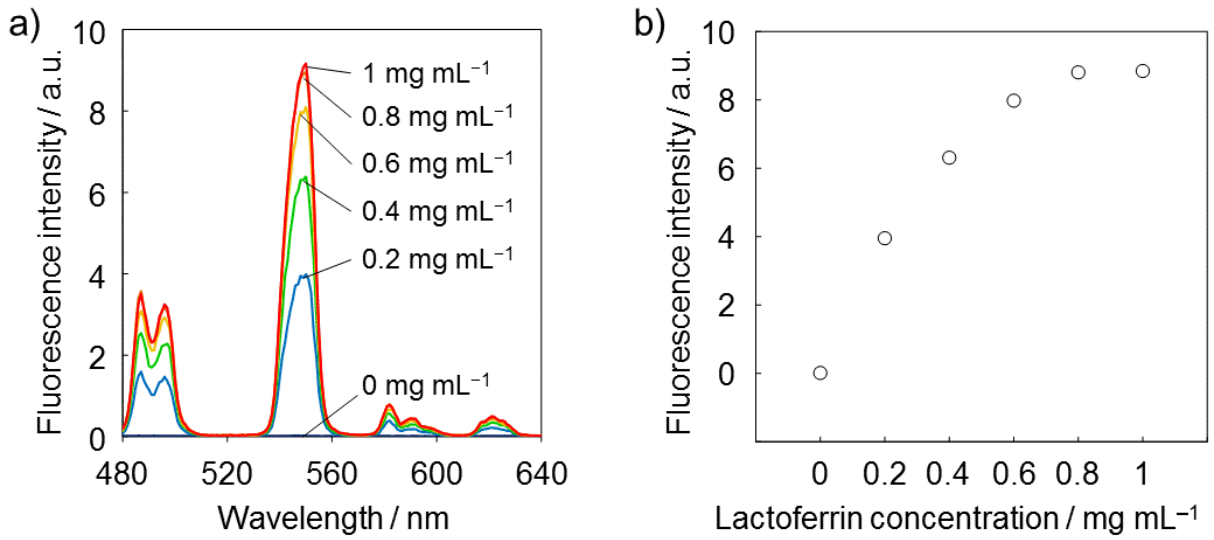

Figure 2-4. a) Fluorescence emission spectra of 100 mM $TbCl_3$ solutions (50 mM HEPES, 3.75 mM $NaHCO_3$, pH 7.4) in the absence and presence of human lactoferrin at various concentrations; λ_{ex} = 290 nm. b) Lactoferrin concentration dependent fluorescence emission of Tb^{3+} (100 µM) in solution (50 mM HEPES, 3.75 mM $NaHCO_3$, pH 7.4).

This newly developed fluorescence-based assay allows the quantification of lactoferrin without depending on antibodies or on labor-intensive and time-consuming analytical methods. However, the assay performed in solution, for example in a microtiter plate, requires sample volumes that are not readily available in the case of tear fluid. In addition, a costly fluorescence microplate reader is not a standard instrument for an ophthalmologist's clinic. The elaboration of an alternative format of the Tb^{3+}-based assay was regarded as an essential step towards simpler and more convenient lactoferrin determination. Therefore, a µPAD for the quantification of lactoferrin concentrations, based on the green fluorescence emission (λ_{max} = 548 nm) from lactoferrin–terbium complexes formed on the paper device, was developed.

2.3.2. µPAD design

The simple µPAD used throughout this work consists of two identical square areas connected by a single straight channel (Figure 2-1a). One of the square areas serves as the sample deposition area (sampling area), while the second one acts as the fluorescence response area (sensing area). Inkjet patterning of the paper substrate with hydrophobic barriers using a UV curable ink composition was performed by a slightly modified

version of our previously reported method.[15] In order to enable the fabrication of a larger number of μPADs in a single photocuring cycle, the UV irradiated area has been enlarged by increasing the distance between the light source and the paper substrate. To compensate for the weaker irradiation power per unit area caused by the larger distance from the light source, the UV irradiation time was extended from the previously reported 1 min to 15 min. This irradiation time was experimentally confirmed to be sufficient for the formation of hydrophobic barriers. To prevent the spreading of the liquid ink, which would lead to loss of structural resolution during the prolonged photocuring process, the filter paper was placed on a cooling plate at 10ºC, while being exposed to the UV light source. By this modified method, 72 μPADs were produced simultaneously in every batch. A single inkjet-printed microfluidic pattern visualized by a red food colorant is shown in Figure 2-1b.

To implement the fluorescence-based assay on the μPAD, three essential components were pre-deposited on the patterned paper substrate: (1) a Tb^{3+}–salt, (2) a bicarbonate salt, and (3) a pH-buffer system. The storage of all required reagents in dry form on the paper device enabled lactoferrin analysis by simply applying the sample without any pretreatment. A schematic illustration of the reagent deposition process is shown in Figure 2-2. Since all reagents for printing and surface treatment were dissolved in HEPES buffered solution (pH 7.4, 50 mM), the components remaining on the μPAD in dry form guarantee a constant pH value for the entire device, eliminating the requirement to adjust the pH of biological samples.

In the first printing step, 8 printing cycles of $TbCl_3$ solution were deposited into the sensing area. To reduce adsorption of lactoferrin to the paper surface during migration from the sampling area to the sensing area, μPADs were soaked in a solution of poly(vinyl alcohol) (PVA) after terbium deposition. Among five tested reagents (bovine serum albumin, poly(vinyl pyrrolidone), PVA, casein, and glycerol), PVA treated surfaces showed the best mobility of lactoferrin and little reduction of sample flow speed (see Figure 2-5 for the details). It was found to be essential to deposit the Tb^{3+} reagent before the surface treatment step. In the case of reversing the order, only weak signals were observed (data not shown). It is assumed that Tb^{3+} is immobilized to the paper by strong electrostatic interactions with negative surface charges of untreated cellulose fibers.[31] By modifying the paper surface with PVA before Tb^{3+} printing, the retention of the reagent

is assumed to decrease.

In the final printing step, 12 printing cycles of $NaHCO_3$ solution were deposited into the sampling area. The concentrations of $TbCl_3$ and $NaHCO_3$ in the printing inks are kept relatively low to guarantee a stable ejection of liquids. Therefore, multiple printing cycles are required for reagent deposition. The optimal number of printing repetitions for $TbCl_3$ and $NaHCO_3$ was empirically investigated and the above-mentioned numbers were found to be the most suitable (tested number of printing cycles: 4–12 cycles for terbium, 11–15 cycles for $NaHCO_3$, data not shown).

Due to the insolubility of terbium carbonate in water, $TbCl_3$ and $NaHCO_3$ cannot be inkjet deposited in the form of a mixed solution. Furthermore, considering the synergistic role of the bicarbonate anion during metal cation binding to lactoferrin, it was assumed to be advantageous to have the bicarbonate anion and the terbium cation deposited into different areas of the μPAD. By doing so, the positive charge in the metal binding site of lactoferrin would be neutralized by bicarbonate before the protein interacts with Tb^{3+} cations. This resulted in the present design of a μPAD with separate sampling and sensing areas.

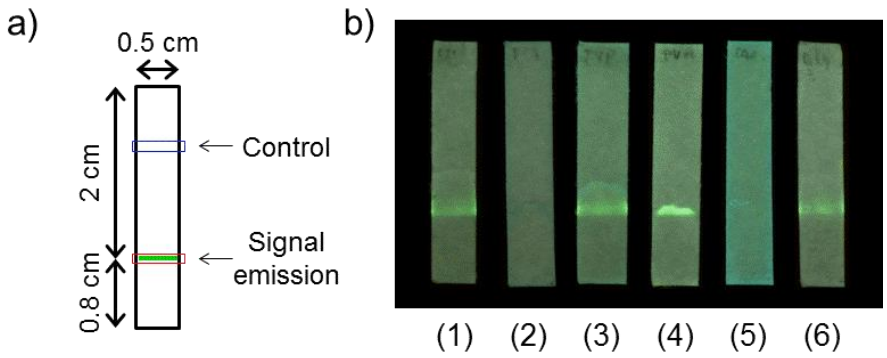

Figure 2-5. Optimization study of the surface treatment reagent. Performance was evaluated as follows: (i) 4 printing cycles of $TbCl_3$ solution (1 mM in pH 7.4 HEPES buffer) printed in a linear fashion onto No. 5C filter paper; (ii) cut into 0.5 × 2.8 cm^2 strips; (iii) soaked in surface treatment solution for 5 min and dried for 20 min at 37˚C; (iv) elution of lactoferrin by placing the bottom of the strip into a lactoferrin solution (2 mg mL^{-1} in pH 7.4 HEPES buffer). a) Dimensions of the strip. The position of printed $TbCl_3$ is indicated as a green line. b) Images of strips under UV light (λ_{ex} = 254 nm) after surface treatment with various substances: (1) control, (2) 0.5wt% bovine serum albumin, (3) 0.5wt% poly(vinyl pyrrolidone), (4) 0.5wt% poly(vinyl alcohol), (5) 0.5wt% casein, (6) 1wt% glycerol.

2.3.3. Fluorescence-based lactoferrin assay on μPADs

To confirm the fluorescence response of the developed μPADs, lactoferrin samples of various concentrations have been applied onto the sampling area of the devices. Because the normal tear fluid lactoferrin concentrations of humans are between 0.63 and 2.9 mg mL^{-1},[32] calibration solutions were prepared in the 0.1–4 mg mL^{-1} range. After application by a micropipette, the sample solution reached the sensing area within less than 1 min by capillary force driven flow through the connecting channel. μPADs were allowed to completely dry for 10–12 min at room temperature, before images of the fluorescence signal emitted from the sensing area were captured under UV illumination. The calibration curve (Figure 2-6a) shows a good correlation between the lactoferrin concentration and the green color intensity (on the RGB scale) in the sensing area recorded by the digital camera. The lactoferrin concentration dependent increase of the fluorescence intensity was also readily observable by the naked eye (Figure 2-6b). It should be noted that the μPADs are single-use devices. For this reason, every data point in the calibration curve (Figure 2-6a) has been measured with a separate μPAD. The assay (from the application of the sample to the fluorescence signal capture) takes no longer than 15 min, which is significantly shorter than the ELISA method requiring several hours. The limit of detection (LOD), calculated to be 0.30 mg mL^{-1} based on a sigmoidal curve fit and three times the standard deviation (3σ) of the intensity of a blank sample, is below the lower limit of lactoferrin concentrations found in tear fluid of healthy humans (0.63 mg mL^{-1}). Additionally, the dynamic response range fully covers the normal lactoferrin concentration range of human tear fluid. A further strength of the μPAD is the possibility of performing quantitative lactoferrin analysis at very low cost. A simple material cost estimation is given in Table 2-1.

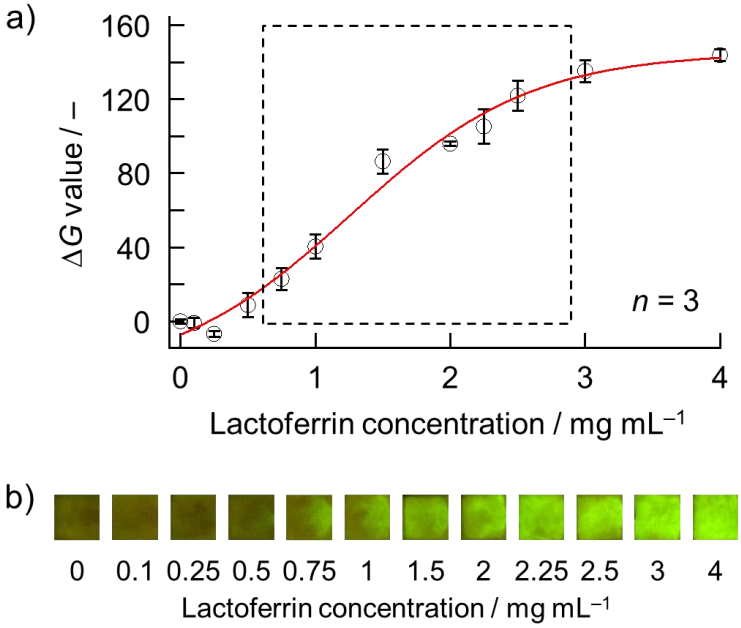

Figure 2-6. (a) μPAD calibration curve for human lactoferrin: the broken line indicates the limit of detection (LOD) of the μPAD, whereas the rectangular area represents the normal range of tear fluid lactoferrin (0.63–2.9 mg mL^{-1}). The markers and error bars reflect the average and standard deviations of three measurements. (b) Images of sensing areas after application of lactoferrin samples captured under UV light (λ = 254 nm).

Table 2-1. Material cost estimation in the case where 72 μPADs are printed per sheet.

Item	Cost per single μPAD
Filter paper	$0.0071
Copy paper	$0.0003
UV ink	$0.0012
Assay reagents	$0.0045
Total	**$0.0131**

2.3.4. Arrangement of pre-deposited reagents on μPADs

In a further series of experiments, the influence of the presence of $NaHCO_3$ as a signal-enhancing additive and the advantage of separate sampling and sensing areas connected by a flow channel compared to a simple spot test have been evaluated. By depositing $NaHCO_3$ solution onto the sampling area of the μPADs, lactoferrin interacts with the Tb^{3+} cations in the sensing area after being in contact with bicarbonate. It was experimentally confirmed that the presence of HCO_3^- in a distinct area from the sensing area improved the performance of the μPADs. For comparison purposes, simple spot tests with $NaHCO_3$ and $TbCl_3$ pre-deposited by inkjet-printing of separate solutions into a 3 × 3 mm^2 area surrounded by inkjet-printed hydrophobic barriers were fabricated. Similarly to the μPAD arrangement, these spot tests showed increasing Tb^{3+} fluorescence emission depending on the lactoferrin concentrations. However, as shown in Figure 2-7a, the observed sensitivity, expressed as the total green intensity signal change between a blank sample and a sample containing 4 mg mL^{-1} of lactoferrin, was lower (ΔG_{max} = 135) than in the case of μPADs with separate sampling and sensing areas connected by a flow channel (ΔG_{max} = 144) (Figure 2-6a). For a bicarbonate-free spot test arrangement with only the Tb^{3+} sensing reagent (Figure 2-7b), the sensitivity in terms of total signal change was further reduced (ΔG_{max} = 119). Figure 2-8 compares a set of calibration curves for lactoferrin obtained with μPADs with separate sampling and sensing areas in the presence (red line) and absence (blue line) of $NaHCO_3$ printed onto the sampling area. As in the case of the spot test, the measured ΔG signals are larger in the presence of the additive. Although the observed differences are not very large, the same trend was noted throughout all experiments performed with paper devices in this study. In all cases, the use of μPADs with separate sampling and sensing areas connected by a microfluidic channel, where $NaHCO_3$ had been pre-deposited onto the sampling area, showed the highest sensitivities.

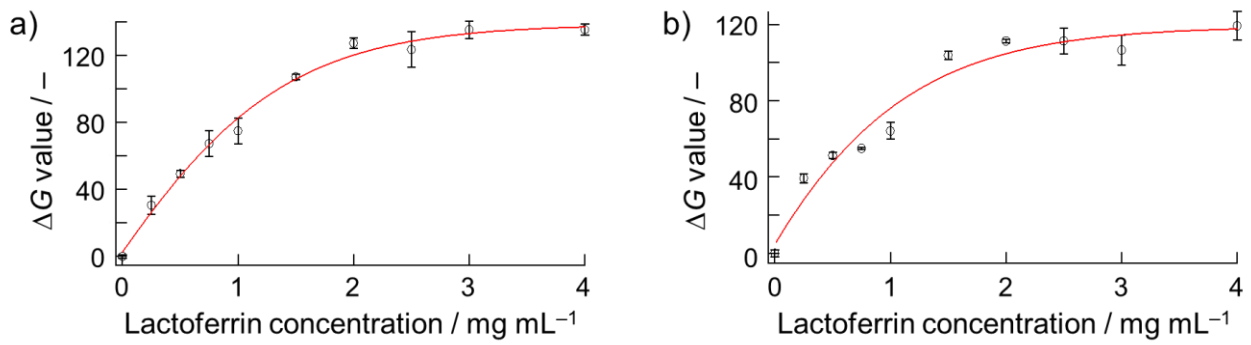

Figure 2-7. Evaluation of the advantage of separated sampling and sensing areas using a spot test (spot dimension: 3 × 3 mm^2 area surrounded by inkjet-printed hydrophobic barriers). a) Lactoferrin calibration curve in the case of both $TbCl_3$ and $NaHCO_3$ printed onto the spot. b) Lactoferrin calibration curve with only $TbCl_3$ printed onto the spot. Printing cycles of $TbCl_3$ and $NaHCO_3$ were 8 and 12, respectively. Blocking treatment was performed as described in the experimental section. The sample volume applied was 2.5 μL. The markers and error bars reflect the average and standard deviations of three measurements.

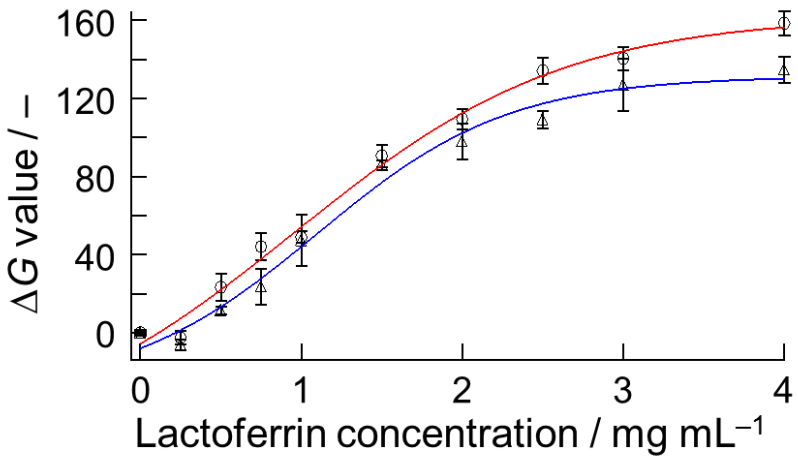

Figure 2-8. Experimental evaluation of the influence of $NaHCO_3$ on the lactoferrin calibration curve. Data was obtained with μPADs fabricated with (red curve) and without $NaHCO_3$ (blue curve) printed onto the sampling area. An enhanced response is observed in the presence of $NaHCO_3$ in the sampling area due to promoted complexation of lactoferrin and Tb^{3+}. Printing cycles of $TbCl_3$ and $NaHCO_3$ were 8 and 12, respectively. The sample volume applied was 2.5 μL. The markers and error bars reflect the average and standard deviations of three measurements. Every single measurement has been performed on a separate μPAD.

2.3.5. Shelf life of µPADs

The shelf life of the developed µPADs was investigated. For this purpose, devices were stored at room temperature (25ºC) wrapped in aluminum foil to protect against ambient light for up to 100 days after fabrication. Alternatively, they were kept in a dark climate control chamber at 35ºC and 50% relative humidity for 10 days. Calibration curves obtained by applying lactoferrin samples to the µPADs stored under various conditions are shown in Figure 2-9. Upon storing at room temperature, a reduction in sensitivity is observed after a period of 30 days (Figure 2-9a). In the case of storage at increased temperature (35ºC), the onset of decreasing sensitivity is observed after a 10-day period (Figure 2-9b). However, according to the calculated limits of detection (LOD) and limits of quantification (LOQ) shown in Table 2-2, the µPADs remain functional for at least 45 days when stored at room temperature, as long as proper calibration is performed at the time of use. After a storage period of 100 days, a significant change in the calibration curve accompanied by a general deterioration of LOD and LOQ was observed. As for the reasons of degradation, a reduction in sample flow speed after extended storage has been experimentally observed. This assumedly results in a lower amount of lactoferrin reaching the sensing area, leading to a sensitivity decrease. The causes for the reduction in sample flow speed are so far not known. However, the fact that µPADs can be stored at room temperature is a clear advantage over the currently commercially available ELISA kits for lactoferrin detection, which require constant refrigeration to preserve the functionality of the used antibodies.

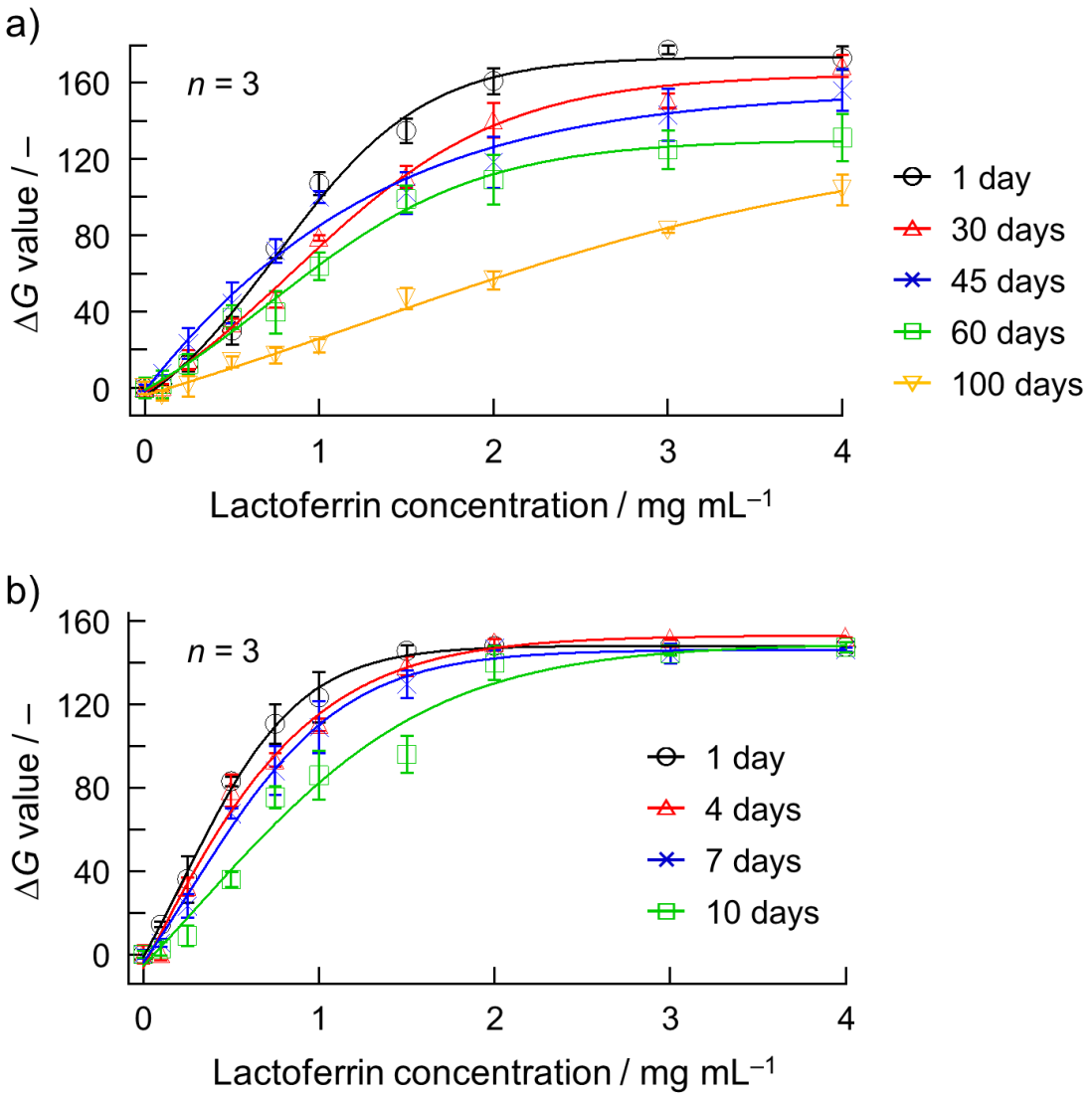

Figure 2-9. Investigation of the storage stability of µPADs. Calibration curves for lactoferrin were obtained by applying 3 µL samples onto µPADs stored in the dark at a) room temperature (25ºC); and b) in a climate control chamber at 35ºC and 50% relative humidity. The markers and error bars reflect the average and standard deviations of three measurements.

Table 2-2. Limits of detection (LOD; 3σ) and limits of quantification (LOQ; 10σ) for lactoferrin measured with μPADs stored in the dark at a) room temperature (25ºC); and b) in a climate control chamber at 35ºC and 50% relative humidity.

a)

Storage period / days	LOD / mg mL^{-1}	LOQ / mg mL^{-1}
1	0.20	0.46
30	0.12	0.28
45	0.06	0.16
60	0.30	0.84
100	0.49	1.20

b)

Storage period / days	LOD / mg mL^{-1}	LOQ / mg mL^{-1}
1	0.11	0.28
4	0.12	0.32
7	0.11	0.20
10	0.12	0.24

2.3.6. Selectivity evaluation

Human tear fluid consists of various substances including proteins and electrolytes. Primary constituents and their concentrations are shown in Table 2-3. Before applying the μPADs to the analysis of human tear fluid samples, possible interference of these components was investigated. Figure 2-10 summarizes the results of the interference study. None of the primary tear constituents except lactoferrin resulted in a significant fluorescence signal (indicated as ΔG) when applied as single components to the μPADs (Figure 2-10, blue bars) at concentrations indicated in Table 2-3. This demonstrates the high selectivity of the sensitizing interaction between Tb^{3+} and lactoferrin. In addition, the major tear fluid constituents did not interfere with the terbium sensitization by lactoferrin. This was confirmed by the identical fluorescence signals observed in mixed solutions of Tb^{3+} and other tear fluid constituents (Figure 2-10, orange bars). Thus, it has been clearly demonstrated that the μPADs respond to none of the major tear fluid constituents except lactoferrin, and that the presence of other constituents does not block the binding of lactoferrin to Tb^{3+}.

Table 2-3. Concentrations of primary constituents in human tear fluid.

Constituent	Concentration[a]	Reference
Lactoferrin	0.63–2.9[b] mg mL^{-1}	32
Sodium	80–**170** mM	33
Potassium	6–**42** mM	33
Calcium	0.3–**2.0** mM	33
Magnesium	0.3–**1.1** mM	33
Lysozyme	2.5–**3.4** mg mL^{-1}	34
Albumin	6.0–15.2 μg mL^{-1} (normal) 67–**150** μg mL^{-1} (ocular diseases)	35
Glucose	1.0–6.2 mg per 100 mL (normal) 7.2–**26** mg per 100 mL (diabetes)	36

[a] The underlined bold print values (the upper limit of the range) were used for selectivity evaluation. [b] A mean concentration of 1.84 mg mL^{-1} lactoferrin was used for selectivity evaluation.

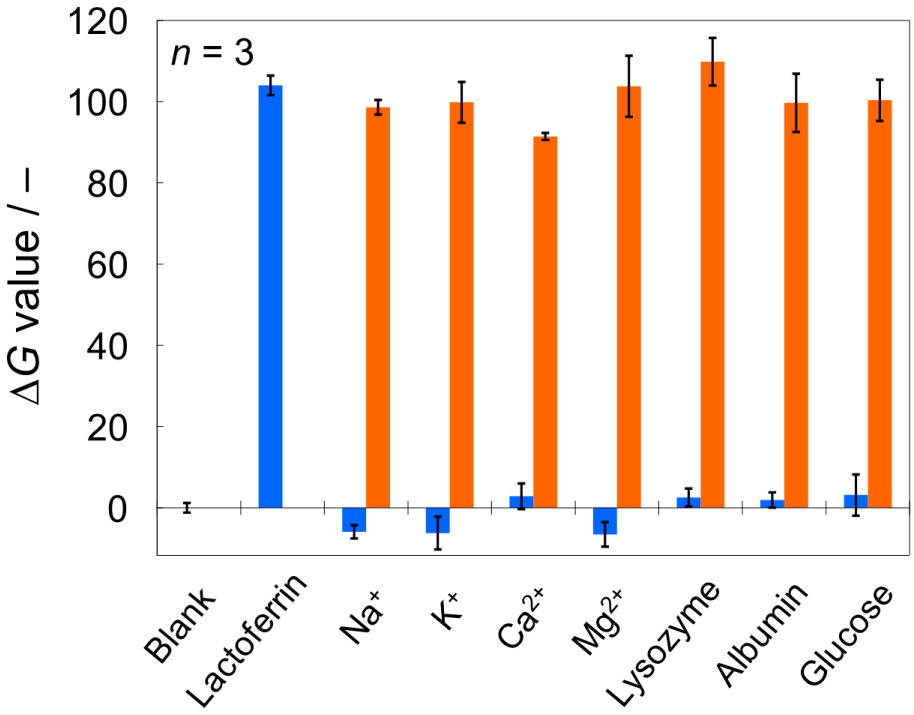

Figure 2-10. Selectivity of μPADs for lactoferrin: the graph shows the fluorescence response of μPADs to the application of single human tear fluid constituents (blue bars) or to mixtures of lactoferrin with the corresponding tear fluid constituent (orange bars). All concentrations are as shown in Table 2-3. The data reflect the average and standard deviations of three measurements.

2.3.7. Quantitative measurements of lactoferrin concentrations in human tear fluid

Quantitative lactoferrin analysis in human tear fluid from several volunteers was performed. The concentrations of lactoferrin in tear fluids were determined by using the developed μPADs. For validation purposes, the assay results were compared to those obtained by the ELISA method. Human tear samples were collected from the inferior *cul-de-sac* of five volunteers. The results of human tear analysis shown in Table 2-4 indicate that all samples were correctly analyzed with the developed μPADs within 6% error of the ELISA method. The direct comparison of the two different methods (Figure 2-11) shows a linear correlation coefficient R^2 of 0.991, with a slope close to unity (0.976) and a *y*-axis intercept close to zero (0.0725). A major conceptual difference between the μPAD assay and the ELISA method is the fact that the immunoassay detects the total concentration of lactoferrin, independent of its iron saturation state, while complex formation between lactoferrin and terbium on the μPAD occurs only with the iron free apo-lactoferrin. However, in the case of tear fluid, it is known that lactoferrin is essentially present only in its apo-form.[37] This is confirmed by the identical results within 6% error of lactoferrin concentrations measured by μPADs and by the ELISA method.

In the case of lactoferrin analysis with μPADs, small standard deviations were observed, with the exception of sample 5, which showed a relatively large value owing to its concentration being at the upper limit of the dynamic response range of the μPAD. Upon two-fold dilution of this sample with HEPES buffered solution, the analysis resulted in a value of 1.74 ± 0.11 mg mL^{-1} with a significantly lower standard deviation.

The developed μPAD demonstrates several advantages over the ELISA method for tear fluid lactoferrin determination (Table 2-5). The detectable range of the μPAD (0.3–4 mg mL^{-1}) allows tear lactoferrin quantification by single pipetting of 2.5 μL of undiluted tear samples. On the other hand, the ELISA method requires > 10 μL of diluted tear sample because of its much lower detectable lactoferrin concentration range (1–50 ng mL^{-1}). In addition, the estimated material costs for single sample analysis were significantly reduced in the μPAD (~ 1% in comparison with the ELISA) thanks to the antibody and enzyme-free detection approach. Finally, the shortened total assay time of the μPAD provides rapid quantification of tear lactoferrin in 15 min.

Table 2-4. Comparison of the assay results for lactoferrin in human tear samples obtained by the developed μPAD and a commercially available ELISA kit.

Sample no.	Method; concentration [mean ± 1 σ, mg mL^{-1}]		
	μPAD[a]	ELISA[b]	Error[c] (%)
1	1.82 ± 0.05	1.91 ± 0.28	–4.8
2	1.78 ± 0.01	1.87 ± 0.05	–4.8
3	2.13 ± 0.06	2.15 ± 0.18	–0.9
4	1.79 ± 0.06	1.70 ± 0.09	+5.2
5	3.58 ± 0.21	3.57 ± 0.10	+0.4

[a] Measured values were calculated from a calibration curve and the green intensity in the sensing area obtained by applying 2.5 μL of tear samples. The data reflect the average values and standard deviations of three measurements. [b] Tear samples were diluted 10^5-fold before use with the sample diluting buffer provided in the kit. The data reflect the average values and standard deviations of four measurements. [c] Error (%) calculated as 100 × (μPAD – ELISA)/ELISA.

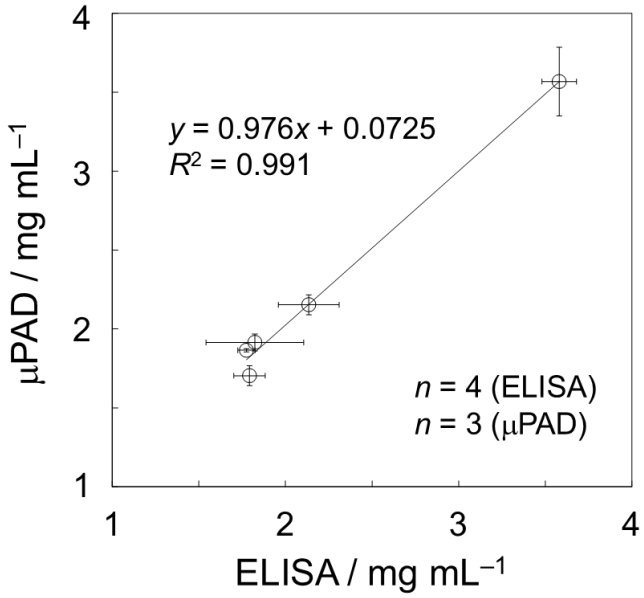

Figure 2-11. Correlation between lactoferrin concentrations in human tear fluid measured by the ELISA and the μPAD methods; the markers and error bars reflect the average and standard deviations of four (ELISA) and three (μPAD) measurements, respectively.

Table 2-5. Performance comparison with a commercial lactoferrin ELISA kit.

Item	ELISA kit	μPAD
Detection range	1–50 ng mL^{-1}	0.3–4 mg mL^{-1}
Sample volume	> 10 μL[a]	2.5 μL
Material cost	> $1.3 per sample[b]	$0.0131[c]
Assay time	Hours	15 min

[a] 10^4–10^5-fold dilution of human tear sample is required. [b] Approximate calculation result includes primary antibodies, HRP-labelled secondary antibodies, microtiter plate, and the *o*-phenylenediamine chromogenic substrate. Other reagents (sample dilution buffer, reagent dilution buffer, washing solution, stop solution) are not included because their compositions are unknown. [c] 72 μPADs are fabricated per sheet.

2.4. Conclusions

A rapid, user-friendly and low-cost sensing device for analysis of lactoferrin in human tear fluid was successfully developed. Lactoferrin detection was achieved by measuring the fluorescence emitted from lactoferrin–terbium complexes formed on the paper devices. This is to the best of my knowledge the first report of a quantitative lactoferrin assay without the requirement of using antibodies or high cost analytical instrumentation. It has been confirmed that the fluorescence emission intensity increases in proportion to the lactoferrin levels in the sample, which even allows detection by the naked eye. By applying filter paper as the sensing platform, a low-cost, light-weight, and easily and safely disposable device has been realized.

Although the achieved limit of detection was much higher compared to the one reported for the ELISA kit (1 ng mL^{-1}), the developed μPAD is a prospective alternative method for simple lactoferrin determination at concentrations encountered in human tear fluid usable by non-trained personnel. Assay results can be obtained within 15 min by simply pipetting a freshly collected tear sample to the sampling area. In contrast to the ELISA method requiring hours of multiple pipetting, incubation, and washing procedures, the simplicity of the μPAD makes it a widely applicable sensing tool for rapid diagnosis. Finally, the detection system proposed here is expected to be adaptable to the sensing of other metal binding proteins by changing the probe deposited on the sensing area.

References

1. Martinez, A. W.; Phillips, S. T.; Butte, M. J.; Whitesides, G. M., Patterned paper as a platform for inexpensive, low-volume, portable bioassays. *Angew. Chem. Int. Ed.* **2007,** 46, 1318–1320.
2. Yetisen, A. K.; Akram, M. S.; Lowe, C. R., Paper-based microfluidic point-of-care diagnostic devices. *Lab Chip* **2013,** 13, 2210–2251.
3. Hossain, S. M. Z.; Brennan, J. D., β-Galactosidase-Based Colorimetric Paper Sensor for Determination of Heavy Metals. *Anal. Chem.* **2011,** 83, 8772–8778.
4. Hossain, S. M. Z.; Ozimok, C.; Sicard, C.; Aguirre, S. D.; Ali, M. M.; Li, Y.; Brennan, J. D., Multiplexed paper test strip for quantitative bacterial detection. *Anal. Bioanal. Chem.* **2012,** 403, 1567–1576.
5. Jokerst, J. C.; Adkins, J. A.; Bisha, B.; Mentele, M. M.; Goodridge, L. D.; Henry, C. S., Development of a paper-based analytical device for colorimetric detection of select foodborne pathogens. *Anal. Chem.* **2012,** 84, 2900–2907.
6. Mentele, M. M.; Cunningham, J.; Koehler, K.; Volckens, J.; Henry, C. S., Microfluidic paper-based analytical device for particulate metals. *Anal. Chem.* **2012,** 84, 4474–4480.
7. Vella, S. J.; Beattie, P.; Cademartiri, R.; Laromaine, A.; Martinez, A. W.; Phillips, S. T.; Mirica, K. A.; Whitesides, G. M., Measuring markers of liver function using a micropatterned paper device designed for blood from a fingerstick. *Anal. Chem.* **2012,** 84, 2883–2891.
8. Abe, K.; Suzuki, K.; Citterio, D., Inkjet-Printed Microfluidic Multianalyte Chemical Sensing Paper. *Anal. Chem.* **2008,** 80, 6928–6934.
9. Bruzewicz, D. A.; Reches, M.; Whitesides, G. M., Low-Cost Printing of Poly(dimethylsiloxane) Barriers To Define Microchannels in Paper. *Anal. Chem.* **2008,** 80, 3387–3392.
10. Carrilho, E.; Martinez, A. W.; Whitesides, G. M., Understanding Wax Printing: A Simple Micropatterning Process for Paper-Based Microfluidics. *Anal. Chem.* **2009,** 81, 7091–7095.
11. Lu, Y.; Shi, W.; Jiang, L.; Qin, J.; Lin, B., Rapid prototyping of paper-based microfluidics with wax for low-cost, portable bioassay. *Electrophoresis* **2009,** 30, 1497–1500.

12. Olkkonen, J.; Lehtinen, K.; Erho, T., Flexographically Printed Fluidic Structures in Paper. *Anal. Chem.* **2010,** 82, 10246–10250.
13. Dungchai, W.; Chailapakul, O.; Henry, C. S., A low-cost, simple, and rapid fabrication method for paper-based microfluidics using wax screen-printing. *Analyst* **2011,** 136, 77–82.
14. Li, X.; Tian, J.; Garnier, G.; Shen, W., Fabrication of paper-based microfluidic sensors by printing. *Colloids Surf., B, Biointerfaces* **2010,** 76, 564–570.
15. Maejima, K.; Tomikawa, S.; Suzuki, K.; Citterio, D., Inkjet printing: an integrated and green chemical approach to microfluidic paper-based analytical devices. *RSC Adv.* **2013,** 3, 9258–9263.
16. Yamada, K.; Henares, T. G.; Suzuki, K.; Citterio, D., Paper-based inkjet-printed microfluidic analytical devices. *Angew. Chem. Int. Ed.* **2015,** 54, 5294–5310.
17. Li, N.; Wang, N.; Zheng, J.; Liu, X. M.; Lever, O. W.; Erickson, P. M.; Li, L., Characterization of Human Tear Proteome Using Multiple Proteomic Analysis Techniques. *J. Proteome Res.* **2005,** 4, 2052–2061.
18. Karns, K.; Herr, A. E., Human Tear Protein Analysis Enabled by an Alkaline Microfluidic Homogeneous Immunoassay. *Anal. Chem.* **2011,** 83, 8115–8122.
19. Grus, F. H.; Sabuncuo, P.; Augustin, A. J., Analysis of tear protein patterns of dry-eye patients using fluorescent staining dyes and two-dimensional quantification algorithms. *Electrophoresis* **2001,** 22, 1845–1850.
20. Danjo, Y.; Lee, M.; Horimoto, K.; Hamano, T., Ocular surface damage and tear lactoferrin in dry eye syndrome. *Acta Ophthalmol.* **1994,** 72, 433–437.
21. Hetherington, S. V.; Spitznagel, J. K.; Quie, P. G., An enzyme-linked immunoassay (ELISA) for measurement of lactoferrin. *J. Immunol. Methods* **1983,** 65, 183–190.
22. Abe, T.; Nakajima, A.; Matsunaga, M.; Sakuragi, S.; Komatsu, M., Decreased tear lactoferrin concentration in patients with chronic hepatitis C. *Br. J. Ophthalmol.* **1999,** 83, 684–687.
23. Sridhar, U.; Gupta, A. K., in *Clinical Ophthalmology*: *Contemporary Perspectives*. ed. Gupta, A. K.; Krishna, V., Elsevier Health Sciences 9th edn. **2009**.

24. Zhou, L.; Beuerman, R. W.; Chan, C. M.; Zhao, S. Z.; Li, X. R.; Yang, H.; Tong, L.; Liu, S.; Stern, M. E.; Tan, D., Identification of Tear Fluid Biomarkers in Dry Eye Syndrome Using iTRAQ Quantitative Proteomics. *J. Proteome Res.* **2009,** 8, 4889–4905.
25. Tomosugi, N.; Kitagawa, K.; Takahashi, N.; Sugai, S.; Ishikawa, I., Diagnostic Potential of Tear Proteomic Patterns in Sjögren's Syndrome. *J. Proteome Res.* **2005,** 4, 820–825.
26. Levay, P.; Viljoen, M., Lactoferrin: a general review. *Haematologica* **1995,** 80, 252–267.
27. Baker, E. N.; Anderson, B. F.; Baker, H. M.; Haridas, M.; Norris, G. E.; Rumball, S. V.; Smith, C. A., Metal and anion binding sites in lactoferrin and related proteins. *Pure Appl. Chem.* **1990,** 62, 1067–1070.
28. Sueda, S.; Tanaka, S.; Inoue, S.; Komatsu, H., A luminescent affinity tag for proteins based on the terbium(III)-binding peptide. *Anal. Biochem.* **2012,** 422, 52–54.
29. Lipchik, A. M.; Parker, L. L., Time-Resolved Luminescence Detection of Spleen Tyrosine Kinase Activity through Terbium Sensitization. *Anal. Chem.* **2013,** 85, 2582–2588.
30. Kataoka, Y.; Shinoda, S.; Tsukube, H., Transferrin-Terbium Complexes as Luminescent pH Sensing Devices. *J. Nanosci. Nanotechnol.* **2009,** 9, 655–657.
31. Alila, S.; Boufi, S.; Belgacem, M. N.; Beneventi, D., Adsorption of a Cationic Surfactant onto Cellulosic Fibers I. Surface Charge Effects. *Langmuir* **2005,** 21, 8106–8113.
32. Flanagan, J. L.; Willcox, M. D. P., Role of lactoferrin in the tear film. *Biochimie* **2009,** 91, 35–43.
33. Sariri, R.; Ghafoori, H., Tear proteins in health, disease, and contact lens wear. *Biochemistry* **2008,** 73, 381–392.
34. Meillet, D.; Hoang, P. L.; Unanue, F.; Kapel, N.; Diemert, M.-C.; Rousselie, F.; Galli, A.; Galli, J., Filtration and Local Synthesis of Lacrimal Proteins in Acquired Immunodeficiency Syndrome. *Eur. J. Clin. Chem. Clin. Biochem.* **1992,** 30, 319–322.
35. Prause, J. U., Serum Albumin, Serum Antiproteases and Polymorphonuclear Leucocyte Neutral Collagenolytic Protease in the Tear Fluid of Patients with Corneal Ulcers. *Acta Ophthalmol.* **1983,** 61, 272–282.

36. Sen, D. K.; Sarin, G. S., Tear glucose levels in normal people and in diabetic patients. *Br. J. Ophthalmol*. **1980,** 64, 693−695.

37. Weinberg, E. D., Human lactoferrin: a novel therapeutic with broad spectrum potential. *J. Pharm. Pharmacol*. **2001,** 53, 1303−1310.

Chapter 3 Tear lactoferrin assay on μPAD relying on distance as quantification signal

This chapter is based on
"Distance-Based Tear Lactoferrin Assay on Microfluidic Paper Device Using Interfacial Interactions on Surface-Modified Cellulose",
Kentaro Yamada; Terence G. Henares; Koji Suzuki; Daniel Citterio,
ACS Applied Materials & Interfaces, **2015**, 7, 24864–24875.

Summary

"Distance-based" detection motifs on microfluidic paper-based analytical devices (μPADs) allow quantitative analysis without using signal readout instruments in a similar manner to classical analogue thermometers. To realize a cost-effective and calibration-free distance-based assay of lactoferrin in human tear fluid on a μPAD not relying on antibodies or enzymes, we investigated the fluidic mobilities of the target protein and Tb^{3+} cations used as the fluorescent detection reagent on surface-modified cellulosic filter papers. Chromatographic elution experiments in a tear-like sample matrix containing electrolytes and proteins revealed a collapse of attractive electrostatic interactions between lactoferrin or Tb^{3+} and the cellulosic substrate, which was overcome by the modification of the paper surface with the sulfated polysaccharide *ι*-carrageenan. The resulting μPAD based on the fluorescence emission distance successfully analyzed 0−4 mg mL^{-1} of lactoferrin in complex human tear matrix with a lower limit of detection of 0.1 mg mL^{-1} by simple visual inspection. Assay results of 18 human tear samples including ocular disease patients and healthy volunteers showed good correlation to the reference ELISA method with a slope of 0.997 and a regression coefficient of 0.948. The distance-based quantitative signal and the good batch-to-batch fabrication reproducibility relying on printing methods enable quantitative analysis by simply reading out "concentration scale marks" printed on the μPAD without performing any calibration and using any signal readout instrument.

3.1. Introduction

Paper has long been one of the valuable platforms for chemical analysis. There are several early reports on paper-based analytical devices, represented for example by paper chromatography in the 1940s,[1-3] bioactive paper devices in the 1950s,[4-5] and immunoassays on nitrocellulose in 1982.[6] Since then, a number of assays reliant on "paper" substrates are marketed, targeting mainly clinical diagnosis (e.g., dipstick tests for urine analysis, lateral flow immunoassays for pregnancy testing). Following these developments, substantial efforts are nowadays devoted to the advancement of analytical devices based on patterned paper substrates. Six decades after the invention of paper chromatography in a restricted channel by Müller and Clegg,[3] Whitesides and co-workers first proposed a low-cost and user-friendly platform for simultaneous multiple bioassays[7] by introducing the concept of microfluidically patterned paper, later coined microfluidic paper-based analytical device (μPAD).[8] Advantages of μPADs over conventional micro total analysis systems (μTAS), such as (1) low-cost, (2) ease of fabrication, (3) pump-free fluid handling, and (4) disposability, have promoted the expansion of their application fields, which currently cover not only medical diagnosis but also environmental analysis and food quality monitoring.[9-16]

There exist several types of signaling methods for quantitative analysis on μPADs.[13-14, 17] Probably the most general approach is colorimetry, where an image of the paper substrate after sample application is recorded with a camera or a scanner, followed by conversion to numerical color intensity values (typically grayscale or RGB) by means of computer software. Albeit this method is straightforward, the requirements of signal readout and analysis equipment as well as considerable influence of ambient light condition on assay results remain issues in achieving facile and accurate quantitative assays.[18-19] Solutions to this problem have been worked out by alternative ideas such as utilizing colored distance,[20-22] displaying letters of the test result,[23-25] judging the number or the position of colored regions,[26-27] or measuring the time from sample introduction until occurrence of an appointed phenomenon.[28-30] Among them, the distance-based signaling system seems to have less restriction in terms of expandability to a wider range of analytes, since established detection chemistries (e.g., combination of an indicator and its specific analyte) can be straightforwardly transferred.

The applicability of distance-based μPADs has been demonstrated for several classes of clinically or

environmentally relevant analytes. Examples reported so far include the determination of serum glucose and glutathione,[20] aerosol oxidative activity,[21] and airborne metals (Ni, Cu, Fe) in welding fumes.[22] In these works, the detection motifs are based on the generation of colored insoluble products derived from the reaction between the target analyte in the sample and chromogenic substance(s) placed along a straight flow channel. During sample transportation in the paper channel, the analyte is sequentially consumed by the reactive chromogenic substance, leading to instantly formed visible precipitates. This precipitation reaction ceases upon exhaustion of the analyte, resulting in various colored distances depending on the initial analyte content of the sample. Recently, a distinct approach has been reported for the detection of several amphiphilic compounds, where a colored solution containing such compounds (surfactants, proteins, DNAs) travels over a concentration-dependent distance.[31] In this system, the aqueous sample travels within a straight microfluidic channel surrounded by hydrophobic wax, confined in the channel by the low surface free energy of the wax boundary. The presence of amphiphilic compounds in the sample induces leakage from the channel by reducing the surface tension, resulting in a lower amount of liquid traveling along the channel. Thus, higher concentrations of target analytes result in shorter colored distance signals.

The author previously reported the quantification of lactoferrin in human tear fluid on a μPAD without using antibodies or enzymes as a way to low-cost, noninvasive, and objective ocular disease diagnosis.[32] The antibody-free detection mechanism is based on the fluorescence emission intensity derived from Tb^{3+}, sensitized upon complexation with lactoferrin. This method, however, suffers from issues similar to the general colorimetric assays described above: (1) the requirement of a signal quantification system (digital camera and color analysis software) and (2) the potential errors derived from variant conditions of the excitation light source (illumination angle, intensity). To overcome these drawbacks, we attempted to adapt the distance-based detection scheme to a μPAD for lactoferrin quantification, wherein the length of the fluorescent section originating from Tb^{3+}–lactoferrin complexes along a straight paper channel indicates the concentration of lactoferrin in the sample, targeting simple yet reliable ocular disease diagnosis by untrained medical personnel. To eliminate the requirement of any signal readout instrument and calibration procedure, scale marks indicating the target concentration were incorporated into the device. The luminescent

"concentration scale marks", prepared by printing hydrophobic wax with colorants next to the straight microfluidic channel, empower the direct interpretation of quantitative information by simply illuminating UV light with a hand-held lamp. The μPAD allows lactoferrin analysis in 2 μL of human tear samples by a simplified assay and detection procedure, *i.e.*, by a single pipetting of sample and readout of scale marks by the naked eye.

3.2. Experimental section

3.2.1. Reagents and instruments

All reagents were used without further purification. Terbium chloride hexahydrate ($TbCl_3 \cdot 6H_2O$), human lactoferrin, *ι*-carrageenan, pectin, and heparin sodium salt (from porcine intestinal mucosa) were purchased from Sigma-Aldrich (St. Louis, MO, USA). Carboxymethylcellulose sodium salt was purchased from TCI (Tokyo, Japan). *N*-(2-Hydroxyethyl)-1-piperazineethanesulfonic acid (HEPES) was purchased from Dojindo Laboratories (Kumamoto, Japan). Sodium hydroxide was purchased from Kanto Chemical (Tokyo, Japan). The human lactoferrin ELISA kit was purchased from EMD Millipore (Billerica, MA, USA). All other reagents were purchased from Wako Pure Chemical Industries Ltd. (Osaka, Japan). Ultrapure water (> 18 MΩ cm) was obtained from a PURELAB flex water purification system (ELGA, Veolia Water, Marlow, U.K.) and used for the preparation of all solutions. Filter paper (Whatman grade 1, GE Healthcare, Buckinghamshire, U.K.) was cut into A4 size before fabricating the devices.

Patterning of the microfluidic structures and the scale marks was performed on a ColorQube 8570 wax printer (Xerox, Norwalk, CT, USA). A thermal Canon iP2700 inkjet printer (Canon, Tokyo, Japan) was used for the deposition of assay reagents ($TbCl_3 \cdot 6H_2O$, $NaHCO_3$). For this purpose, the standard Canon printer cartridges were cut open and the sponges inside were removed. After washing with copious amounts of ultrapure water, 10 mM $TbCl_3 \cdot 6H_2O$ aqueous solution and 25 mM $NaHCO_3$ in HEPES buffered solution (50 mM, pH 7.4) passed through a syringe filter (0.45 μm) were fed into the black and magenta ink tanks, respectively. A UV handlamp (Funakoshi, Tokyo, Japan) was used for the observation of fluorescence emission from the paper

substrate. ζ-Potentials of paper surfaces were measured by an ELSZ-2KOP analyzer equipped with a solid-plate sample cell (Otsuka Electronics Co., Ltd., Osaka, Japan). The microfluidic channel widths were measured with a DVM2500 optical microscope (Leica, Wetzlar, Germany). A climate control chamber (model SH-221, ESPEC, Osaka, Japan) was used for the evaluation of humidity influence.

3.2.2. Device fabrication

An A4 sheet of filter paper was fed into a wax printer to fabricate the microfluidic patterns and the scale marks designed with PowerPoint (Microsoft). The outline and dimensions of a single pattern used for real tear sample analysis are shown in the Figure 3-1. Dimensions selected for experiments evaluating channel width and length are summarized in Table 3-1. The backside of the paper was printed entirely with wax in gray color (black-and-white printing mode with the *R*, *G*, *B* color value settings all at 190) to form a complete barrier in the paper thickness. After printing hydrophobic wax on both sides of the filter paper, $TbCl_3 \cdot 6H_2O$ and $NaHCO_3$ solutions were simultaneously inkjet-printed inside the straight microfluidic channel. After printing, the paper was pouched with a hot laminator (QHE325, Meikoshokai Co., Ltd., Tokyo, Japan) to let the wax diffuse into the thickness of the paper. The topside part of the hot lamination film (100 μm thickness) was partially cut out before the heating process, in order not to cover the device, because the film absorbs the UV light required for excitation. For the paper surface treatment with anionic polysaccharides, the entire device was finally immersed in an aqueous solution (0.3w/w%) of the respective compound for 3 min, followed by complete drying at 37ºC for 10 min.

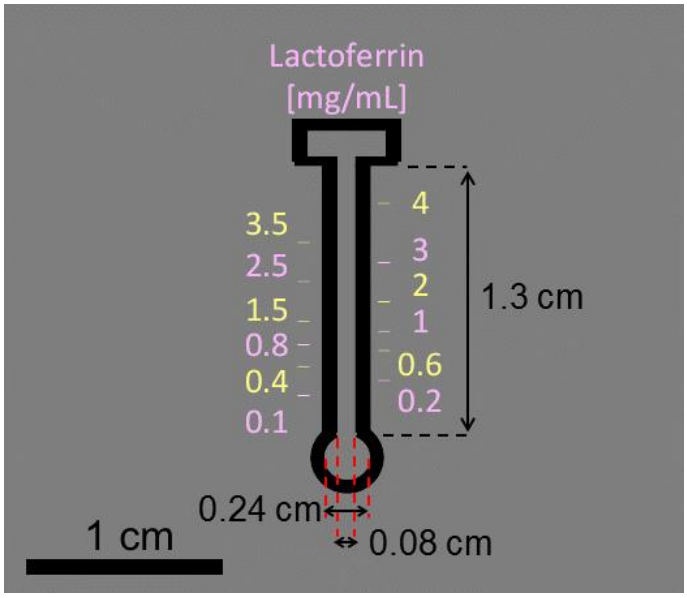

Figure 3-1. Outline of a single microfluidic pattern. The indicated dimensions represent the values set in the PowerPoint file used for wax printing. Colors of the concentration scale marks have been selected to be fluorescent under UV light illumination (the gray background has been added to improve visibility and is not part of the original design used for printing).

Table 3-1. Microfluidic channel widths and lengths.

Channel width		Channel length
Printed width	After lamination[a]	
800 μm	300 ± 14.6 μm	10 mm
900 μm	418 ± 19.0 μm	13 mm
1100 μm	627 ± 26.1 μm	16 mm

[a] The data represents the average values and standard deviations of 8 measurements with an optical microscope.

3.2.3. Evaluation of retention of Tb^{3+} on filter paper substrate

Filter paper strips were prepared by a procedure similar to the general device fabrication. Briefly, a hydrophobic wax boundary was printed on both sides of a sheet of filter paper (Whatman grade 1), and a spot (1 mm diameter) of 10 mM $TbCl_3 \cdot 6H_2O$ aqueous solution was inkjet-printed within the hydrophilic channel (28 mm length × 2.5 mm width). After passing through a hot laminator, the sheet was cut into single strips and used for the chromatographic experiment.

In the case of elution with pure water or the pseudo-tear matrix without lactoferrin, 1.5 mg mL^{-1} lactoferrin aqueous solution, and HEPES buffered solution (pH 7.4, 50 mM) were pipetted (0.5 μL) onto the position of the terbium spot after elution with the corresponding matrix. In the case of elution with the aqueous lactoferrin solution, the bottom of the original strip was first cut by 5 mm. This modification was necessary, because no fluorescence could be detected with strips of original length, since lactoferrin did not reach the position of the terbium spot due to strong non-specific adsorption on the paper surface. Prior to elution of lactoferrin solution prepared in pure water (1.5 mg mL^{-1}), 0.5 μL of HEPES buffered solution was pipetted on the terbium spot. For lactoferrin dissolved in the already pH-buffered pseudo-tear matrix, this step was not necessary. The control experiment was performed to visualize the original shape of the terbium spot by directly pipetting 0.5 μL of HEPES buffer (pH 7.4, 50 mM) and lactoferrin aqueous solution (1.5 mg mL^{-1}) on the spot. Addition of HEPES buffered solution was necessary in some cases, in order to ensure a slightly basic pH on the paper substrate, which is indispensable for the fluorescence emission of Tb^{3+}–lactoferrin complexes.[33]

3.2.4. Kinetics measurement of Tb^{3+}–lactoferrin complexation on paper substrate

Time-course fluorescence intensity derived from the complexation of Tb^{3+} and human lactoferrin was observed in a spot (8 mm diameter) prepared on filter paper. A circular wax pattern was printed on Whatman grade 1 filter paper. Backside wax printing and reagent ($TbCl_3 \cdot 6H_2O$ and $NaHCO_3$) deposition by an inkjet printer covering the entire spot, and hot lamination were performed in the same manner to the μPAD fabrication (described in the previous section).

Kinetic measurements were carried out in a dark room by recording a movie of the gradually developing

fluorescence with an iPhone5S camera under UV illumination (λ_{max} = 254 nm). For this purpose, 4 μL of lactoferrin dissolved in the pseudo-tear matrix (0.4, 1, 2, 3, 4 mg mL^{-1}) was dropped onto the center of the spot. The fluorescence emission intensity from the paper substrate was converted into the green intensity (*G* value on RGB scale). *G* values were extracted from still images at certain time intervals after sample introduction by using the ImageJ software (National Institutes of Health, Bethesda, MD, USA).

3.2.5. Lactoferrin quantification in human tear samples

Normal human tear fluids were collected from 16 healthy volunteers using disposable polyethylene pipettes (AS ONE, Osaka, Japan) and stored in Protein LoBind tubes (Eppendorf). Tear samples collected from two adult ocular disease patients were received from Keio University Hospital (Tokyo, Japan). The collection and use of patient samples were performed by approval of the bioethics committee of Keio University Hospital. All tear samples were stored at –30ºC until use. For μPAD analysis, 2 μL of human tear sample was applied without any pretreatment. For comparative ELISA analysis, all tear samples were 10^5-fold diluted in Protein LoBind tubes with the sample diluting buffer provided in the kit, in order to adjust the lactoferrin concentration (0–4 mg mL^{-1}) to the dynamic response range of the ELISA kit (5–50 ng mL^{-1}).

3.2.6. Spike test of lactoferrin in human tear fluid

Human tear fluid from a healthy adult was spiked with lactoferrin at concentrations of 1.0, 1.5, and 2.0 mg mL^{-1}. For this purpose, 1.0 mg of human lactoferrin powder was weighed in each of three Protein LoBind tubes and dissolved in 1000, 750, or 500 μL of human tear fluid, respectively. Lactoferrin concentrations in the original tear fluid and the spiked tear fluids were analyzed by the μPADs.

3.3. Results and discussion

3.3.1. Detection principle

Because of the antenna function of two tyrosine groups in the metal binding site of lactoferrin, trivalent terbium (Tb^{3+}) turns fluorescent in the presence of lactoferrin under neutral or basic pH condition.[32] Throughout this work, the green fluorescence emission from Tb^{3+}–lactoferrin complexes is used as the detection signal. For the quantification of lactoferrin based on the distance, $TbCl_3$ was deposited in a straight microfluidic channel on filter paper by means of an inkjet printer. As the sample travels along the channel, lactoferrin molecules are continuously consumed by formation of fluorescent Tb^{3+}–lactoferrin complexes until complete depletion of the analyte from the sample liquid. Consequently, a concentration-dependent length of a green fluorescent line is observed in the channel under UV illumination of the device. Although the basic strategy resembles that of the previously reported distance-based assays on μPADs,[20-22] what differs clearly is the fact that the distance-based response does not rely on precipitation of the signaling product. From the fact that $TbCl_3$ (assay reagent) and the Tb^{3+}–lactoferrin complex (signaling product) are soluble in aqueous systems (Figure 3-2), it is readily anticipated that these components travel all along the channel together with the sample flow, disabling an analyte concentration-dependent length-based signaling. When the emission "distance" is to be employed for signal quantification with non-precipitating reaction products, it is of high importance for these components to retain their position. Ideally, the analyte (lactoferrin) should instantly be adsorbed to the paper substrate or form a complex with fixed Tb^{3+} along the microfluidic channel and keep its position on the filter paper substrate (Scheme 3-1). In this context, understanding the behavior of terbium cations, lactoferrin, and the complex of the two compounds in a fluidic system at the interface of a liquid sample and a cellulosic paper substrate is crucial for the design of the intended μPAD. A systematic study was first carried out to clarify the relations of attractive interactions in the process of fluid transport within the cellulosic substrate. After confirmation of the appropriate conditions for successful entrapment of Tb^{3+} and lactoferrin during the flow of complex media, the acquisition of quantitative information on the lactoferrin concentration by using the fluorescence distance on a μPAD was attempted in practical sample matrix.

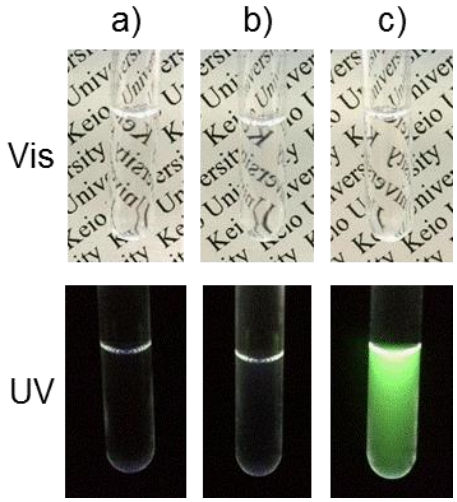

Figure 3-2. Solubility of assay-relevant components for distance-based lactoferrin measurements using fluorescence sensitization of Tb^{3+}. a) $TbCl_3 \cdot 6H_2O$ aqueous solution (10 mM); b) human lactoferrin (1.5 mg mL^{-1}) in HEPES buffered solution (pH 7.4, 50 mM); c) mixture of $TbCl_3 \cdot 6H_2O$ and human lactoferrin (final concentrations of 10 mM and 1.5 mg mL^{-1}, respectively) with small amount of HEPES buffered solution. Images were taken under visible light (top images) and under UV light (λ_{max} = 254 nm) (bottom images).

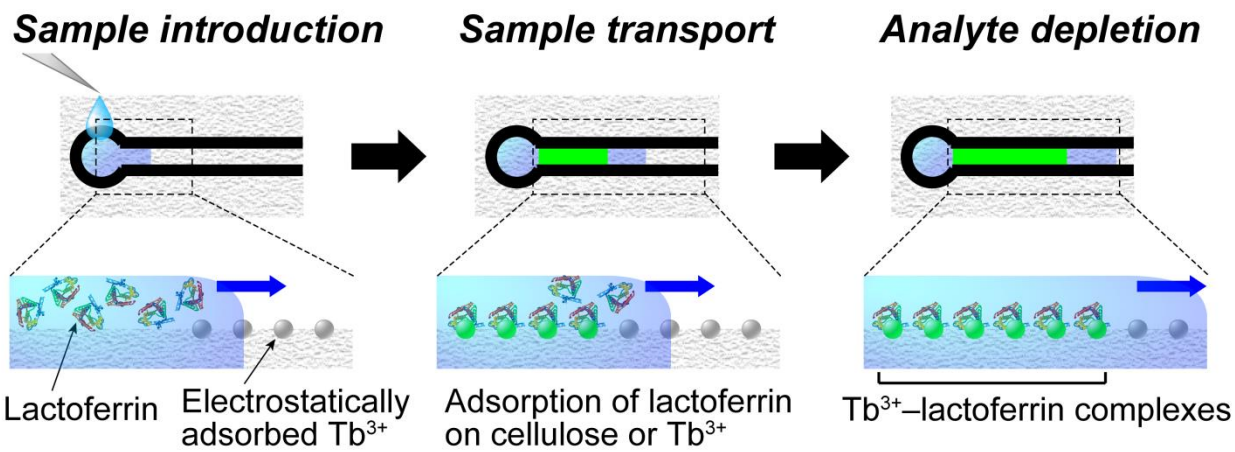

Scheme 3-1. Idealized detection principle for acquiring quantitative information on sample lactoferrin content based on the emission distance within a microfluidic paper channel.

3.3.2. Mobility of lactoferrin on filter paper

High-grade laboratory filter paper consists of pure cellulose with abundant hydroxyl groups in addition to a low amount of carboxyl groups derived from the oxidation of primary alcohol groups during papermaking.[34] Though some attractive interactions such as the nonspecific adsorption of lactoferrin onto untreated filter paper based on electrostatic forces are expected, their collapse due to the presence of electrolytes or other proteins in a real sample has to be considered. Therefore, the mobility of lactoferrin during the flow in several liquid matrices on filter paper was first investigated. A chromatographic study was carried out to evaluate the mobility of lactoferrin from the viewpoint of traveling distance within a filter paper strip (Figure 3-3a). A flow path of 28 mm length and 2.5 mm width, confined by barriers of hydrophobic wax, was prepared. The bottom edge was immersed in a lactoferrin containing solution (1.5 mg mL^{-1}) of varying matrix composition, allowing wicking along the flow path until the fluid front reached the top edge. After drying, terbium chloride solution was deposited on the whole area of the strip by inkjet printing, in order to visualize the location of the chromatographically eluted lactoferrin. In the case of lactoferrin dissolved in pure water, localized fluorescence was observed around the bottom of the strip (Figure 3-3b), indicating very little migration of the protein through the paper. On the contrary, the presence of an electrolyte (100 mM of NaCl) or another protein (3 mg mL^{-1} of lysozyme), as well as the case of lactoferrin being dissolved in a pseudo-tear matrix (pH 7.4, 300 mM HEPES buffered solution with primary components of human tear fluid; composition and concentrations listed in Table 3-2) induced extended migration of lactoferrin (Figure 3-3c,d,e, respectively). These matrix-dependent differences in the mobility behavior can be accounted for by changes of the adsorption property of lactoferrin onto the cellulosic substrate, as outlined in Scheme 3-2. Considering that the isoelectric point (pI) of lactoferrin is 8.0–8.5[35-36] and thus the protein carries a positive net charge at neutral pH condition, electrostatic interactions between the positively charged domains of lactoferrin and the weakly negatively charged filter paper surface with a few carboxylic groups are supposed. In the absence of any other matrix components in the aqueous lactoferrin sample, this attractive force is dominant and drives the nonspecific adsorption of lactoferrin onto the cellulosic paper substrate. The general presence of nonspecific adsorption was also confirmed in the case where the paper strip was modified by an aqueous lysozyme

solution (3 mg mL^{-1}) prior to elution of a lactoferrin containing liquid. As observed in Figure 3-3f, the travel distance of lactoferrin in pure water on the lysozyme-pretreated strip was significantly extended compared to the untreated filter paper (Figure 3-3b), owing to the surface blocking effect of the adsorbed lysozyme protein. It is interesting to note that the observed fluorescence emission from Tb^{3+}–lactoferrin complexes in Figure 3-3b indicates that the metal binding capacity of lactoferrin remains intact after nonspecific binding to the paper surface, which often induces conformational changes of proteins.[37] Meanwhile, when electrolytes or other proteins are present in the aqueous lactoferrin sample, the surface electrical charges of lactoferrin molecules are neutralized by the electrolyte ions or the surface charges of other proteins. These interactions attenuate the attractive forces adsorbing lactoferrin to the paper substrate surface and thus increase the mobility of lactoferrin molecules in the aqueous phase during sample transport. This tendency becomes remarkably strong when electrolytes and proteins are abundant in the eluent, as it is the case for the pseudo-tear matrix seen in Figure 3-3e. Intense fluorescence emission appears at the top edge of the paper strip, due to the high mobility of lactoferrin under these experimental conditions. The observation of slightly increased fluorescence emission along the wax barrier (Figure 3-3c–e) and its absence in the lysozyme pretreated paper (Figure 3-3f) can be attributed to hydrophobic interactions that are common between proteins and hydrophobic surfaces.[37]

The above results indicate that in the case of simple aqueous lactoferrin solutions a distance-based signaling motif relying on sequential exhaustive adsorption of lactoferrin along a microfluidic channel on filter paper can be realized. However, in the situation of a real sample matrix (*i.e.*, coexistence of numerous electrolytes, proteins, and lipids), this mechanism is not a viable approach to a distance-based signal detection scheme. Although lactoferrin in a practical sample matrix did not exhibit sequential exhaustive adsorption on filter paper, distance-based detection of lactoferrin is theoretically still possible, provided that terbium cations fixed on the paper substrate act not only as fluorescent reporters but as “trapping agents” for lactoferrin in the flowing sample matrix. The following section focuses on the feasibility of immobilizing Tb^{3+} on the paper substrate against the flow of various matrices.

Table 3-2. Composition of the pseudo-tear matrix prepared in HEPES buffered solution (pH 7.4, 300 mM).

Constituent	Concentration
Sodium	150 mM
Potassium	20 mM
Calcium	1.0 mM
Magnesium	0.6 mM
Lysozyme	2.36 mg mL^{-1}
Albumin	50 μg mL^{-1}
Glucose	0.14 mM

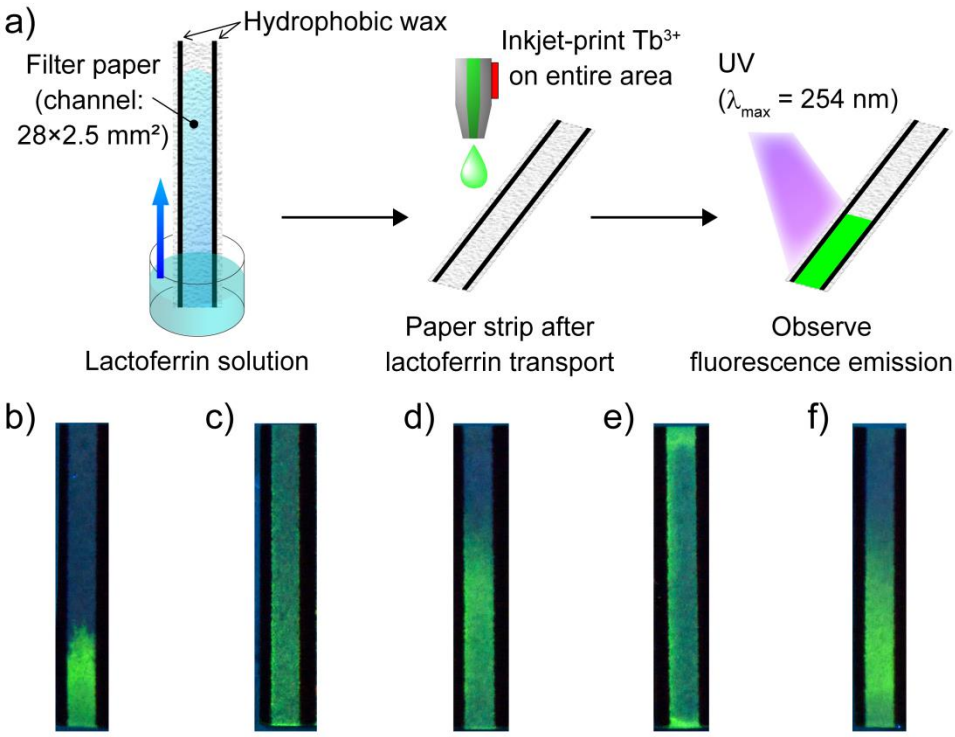

Figure 3-3. a) Schematic of the procedure for the investigation of lactoferrin mobility on filter paper strips. Visualization of transported lactoferrin in b) water, c) 100 mM NaCl aqueous solution, d) 3 mg mL^{-1} lysozyme aqueous solution, e) pseudo-tear matrix (composition shown in Table 3-1), and f) water on a strip treated with lysozyme (3 mg mL^{-1} aqueous solution) before elution. Photographs of the strips were taken under UV illumination (λ_{max} = 254 nm) with contrast and brightness modified for the sake of visibility of the fluorescent traces.

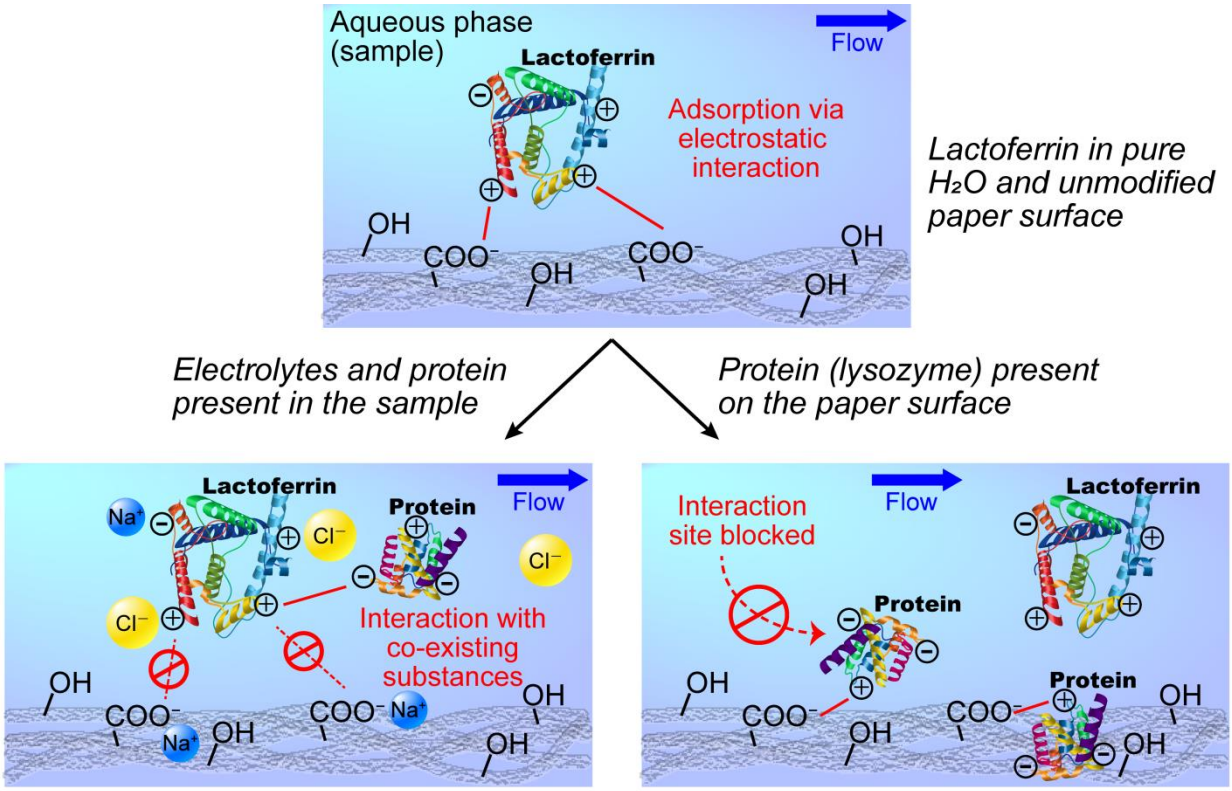

Scheme 3-2. Fluidic elution behavior of lactoferrin in aqueous samples within a cellulosic paper fiber network. (Top) Sample: lactoferrin in pure water. Paper substrate: no modification. (Left) Sample: aqueous lactoferrin solution containing electrolytes and proteins. Paper substrate: no modification. (Right) Sample: lactoferrin in pure water. Paper substrate: modified with protein prior to sample introduction.

3.3.3. Retention of Tb^{3+} on filter paper

Besides the mobility of lactoferrin, the retention of terbium cations to the paper substrate as signaling reagent is a key factor to achieve a distance-based fluorescence emission signal. The retention of Tb^{3+} on the filter paper surface was investigated by TLC-like elution experiments, similar to those described in the previous section. A spot of $TbCl_3$ solution (~1 mm diameter) was inkjet-printed on the filter paper strip, followed by elution with a lactoferrin containing matrix solution (Figure 3-4a). Although not relevant for practical application, a sample matrix without lactoferrin was also investigated in order to check the effect of the matrix itself. Parts b–e of Figure 3-4 depict the strips under UV light after elution with water or pseudo-tear matrix in the presence or absence of lactoferrin. After passing pure water (Figure 3-4b) or pseudo-tear matrix (Figure 3-4c) without lactoferrin, a small leaching from the original spot (Figure 3-4f) was observed. Even though

$TbCl_3$ is soluble in aqueous solution, the expected chelating effect of the cellulosic carboxyl groups contributes to the successful immobilization of the trivalent terbium cation. Despite the well-retained shape of the Tb^{3+} spot after eluting lactoferrin-containing water (Figure 3-4d), the presence of lactoferrin in the pseudo-tear matrix resulted in strong leaching of Tb^{3+} from the original deposition spot (Figure 3-4e), indicating unsuccessful entrapment of lactoferrin molecules during the fluid wicking. The latter result suggests that the terbium cation immobilized by the cellulosic carboxyl groups is being peeled off the paper surface by the traveling lactoferrin molecules. Lactoferrin is known for its high affinity for metal cations. The binding constant of Tb^{3+} with transferrin, a protein closely related to lactoferrin, has been reported to be as high as $\log K_1 \approx 11$ and $\log K_2 \approx 8$.[38] From the fact that the affinity of lactoferrin for metal cations (Fe^{3+}) is approximately 250-fold higher than that of transferrin,[39-40] the binding of lactoferrin to Tb^{3+} is assumed to be strong enough to break the chelation with cellulosic carboxyl groups. Leaching of Tb^{3+} from the original deposition spot does not occur when eluting lactoferrin in water, possibly because lactoferrin molecules continuously adsorb onto the paper surface via nonspecific binding, instead of traveling in the mobile matrix as discussed in the previous section. The assumed mechanism of Tb^{3+} retention on the paper substrate is schematically summarized in Scheme 3-3.

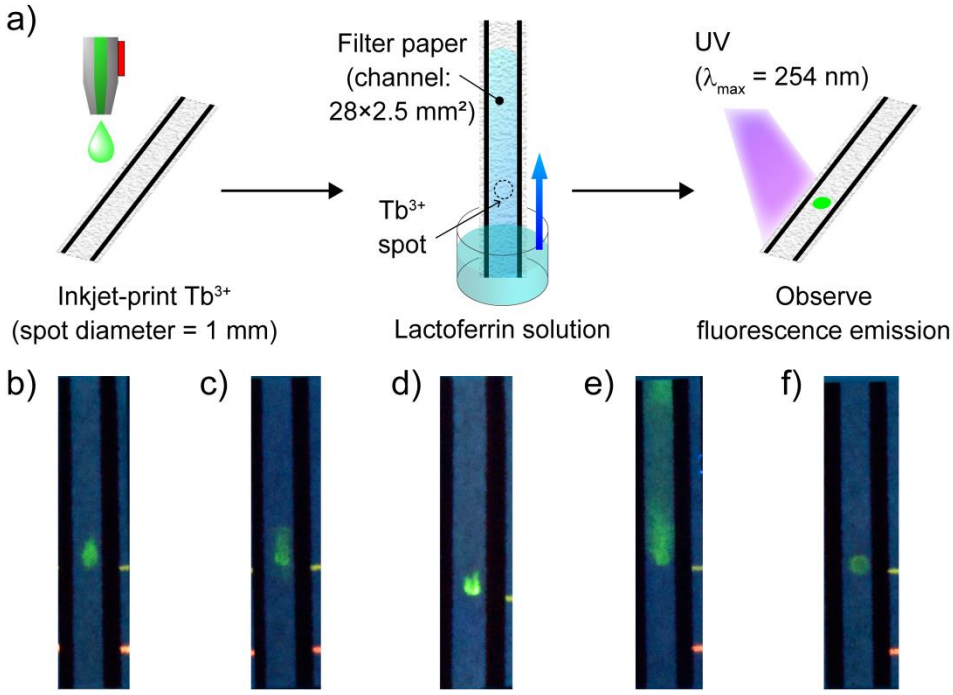

Figure 3-4. a) Schematic of the procedure for the investigation of Tb^{3+} retention on filter paper strips. b–e) Visualized Tb^{3+} spots after elution with b) pure water, c) pseudo-tear matrix, d) lactoferrin aqueous solution (1.5 mg mL^{-1}), and (e) lactoferrin solution in pseudo-tear matrix (1.5 mg mL^{-1}). (f) Direct pipetting of 0.5 μL of HEPES buffer (pH 7.4, 50 mM) and lactoferrin aqueous solution (1.5 mg mL^{-1}) as a control experiment with no fluidic elution. In b) and c), lactoferrin aqueous solution (1.5 mg mL^{-1}) was deposited (0.5 μL) after elution to visualize the position of Tb^{3+}. Photographs of the strips were taken under UV illumination (λ_{max} = 254 nm) with contrast and brightness modified for the sake of visibility of the fluorescent spots.

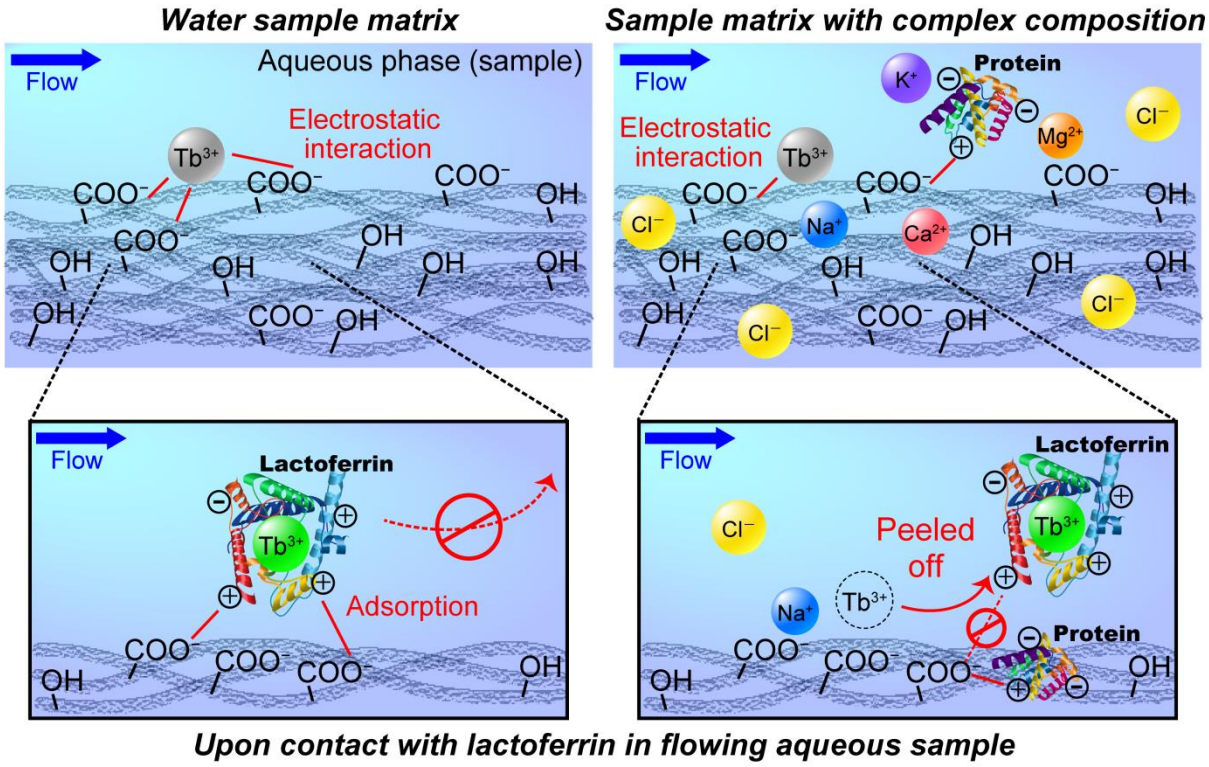

Scheme 3-3. Retention of terbium cation (Tb^{3+}) on unmodified filter paper substrate. (Left) Pure water. (Right) Pseudo-tear sample matrix containing electrolytes and proteins. (Lower row) Behavior of terbium cation (Tb^{3+}) upon contact with lactoferrin in the flowing sample with the corresponding composition (pure water or pseudo-tear matrix).

3.3.4. Effect of paper surface modification with anionic polysaccharides

The above-described experiments revealed that lactoferrin travels all along the microfluidic paper channel while removing Tb^{3+} off the paper substrate when the liquid sample phase contains electrolytes and proteins. Since the final goal is to measure lactoferrin in tear fluid by using the fluorescence emission distance as quantitative information, the sample should ideally be continuously depleted of lactoferrin during transportation within the cellulosic flow channel. Two strategies can be proposed to achieve this objective: (1) enhancing the affinity of the paper substrate toward lactoferrin to promote adsorption even in complex sample matrices; (2) more strongly anchoring Tb^{3+} cations to the paper surface to prevent their flush-out by lactoferrin in the complex sample matrix. In the former case, lactoferrin molecules are adsorbed to the paper substrate. In the latter one, the depletion of lactoferrin from the sample is reliant on terbium cations immobilized within the paper microfluidic channel. The former strategy was deemed to be more favorable because the second one

was expected to face several difficulties. First, a ligand with higher affinity for Tb^{3+} would be required for its immobilization to the paper substrate. However, the binding between this ligand and Tb^{3+} should not prevent the formation of the fluorescent Tb^{3+}–lactoferrin complex. Second, the kinetics of the Tb^{3+}–lactoferrin complexation would become an essential factor to be considered, since the depletion of lactoferrin from the sample would solely rely on this reaction. From the experimentally observed fact that it takes approximately 60 sec to get to full fluorescence emission intensity after mixing $TbCl_3$ and lactoferrin on paper, the complexation of lactoferrin to Tb^{3+} deposited on filter paper does not occur instantaneously, which makes this strategy unsuitable for a signaling system relying on distance measurements (detailed experimental procedures, results, and emission increase time-course are available in Figure 3-5. Therefore, enhancing the adsorption of lactoferrin to the filter paper substrate was chosen as the strategy for exhaustive lactoferrin depletion from the sample matrix during transportation.

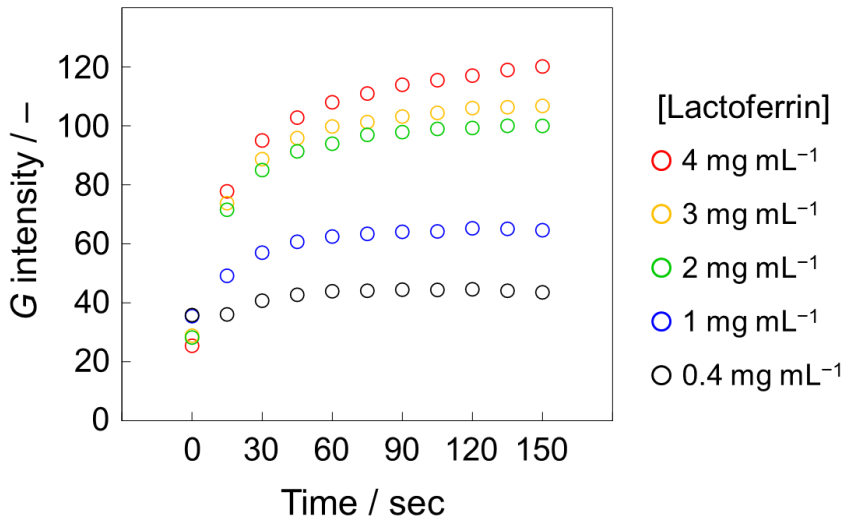

Figure 3-5. Kinetics of complexation between Tb^{3+} and lactoferrin on filter paper.

As candidate materials for reinforcing the adsorption of lactoferrin onto the paper substrate, anionic polysaccharides were selected based on the fact that they show high binding capacity toward milk proteins.[41-42] Herein, four types of anionic polysaccharides were tested: sodium alginate (Na-Alg), pectin, carboxymethylcellulose (CMC), and ι-carrageenan (ι-Cg) (structures available in Figure 3-6). The

chromatographic elution experiment evaluating the mobility of lactoferrin (described in Figure 3-3a) was carried out for paper strips after surface modification by the respective polysaccharide solutions (0.3w/w%). SEM images of the paper substrates shown in Figure 3-7 demonstrate that the modified cellulose network retains its porous structure with some swelling due to water retention of the polyanionic hydrogel nature of the polysaccharide. While treatment with Na-Alg, pectin, or CMC (Figure 3-8a–c in panel i) did not result in any significant improvement of lactoferrin adsorption from pseudo-tear fluid matrix onto the paper substrate compared to the bare filter paper (Figure 3-3e), the paper surface modification with *ι*-Cg showed a remarkable effect (Figure 3-8d in panel i). A simple increase in the total number of anionic sites by surface treatment of the paper substrate does not account for this different behavior, since the paper surface *ζ*-potential shifted to more negative values after coating with all anionic polysaccharides other than pectin (Table 3-3). The surface of bare filter paper has a weakly negative charge due to the presence of a small number of carboxyl groups.[43] The successful trapping of lactoferrin by *ι*-Cg only can be explained by the different chemical nature of the anionic functional groups in the polysaccharides (carboxylate group for Na-Alg, pectin, and CMC, and sulfate group for *ι*-Cg). Both types of anionic groups electrostatically interact with positively charged residues of the protein, predominantly present in the form of protonated amino groups ($-NH_3^+$). However, there are several reports stating that electrostatic attractive forces toward $-NH_3^+$ residues are significantly stronger in the case of sulfate groups than carboxylate groups.[41, 44] This is explained by the different water affinities of the anionic groups.[45] Due to its larger size, the $-SO_3^-$ group with the negative charge dispersed over three oxygens possesses a lower surface charge density compared to the $-COO^-$ group. This leads to weaker interaction with surrounding water molecules, making $-SO_3^-$ a weakly hydrated anion that is strongly interacting with weakly hydrated cationic groups such as $-NH_3^+$.[45] Thus, sulfated polysaccharides possess higher affinity to proteins,[42, 46-47] including lactoferrin, than carboxylated ones. This is further experimentally supported by the fact that λ- and κ-Cg treated paper substrates exhibited similar capacity of lactoferrin adsorption to that of *ι*-Cg (Figure 3-8e,f in panel i). However, the same behavior was not observed when treating the paper surface with heparin (Figure 3-8g of panel i), another well-known sulfated polysaccharide. This indicates that the existence of sulfate groups alone does not guarantee a distance-based signal in a microfluidic channel on paper. Further

clarification of the different lactoferrin retention behavior by the anionic polysaccharides was obtained by visual inspection of mixed aqueous solutions of polysaccharides and human lactoferrin (Figure 3-8, panel ii). In line with the chromatographic elution experiments (Figure 3-8, panel i), significant differences were observed between the three types of carrageenan (Figure 3-8d–f in panel ii) and the remaining anionic polysaccharides, including the sulfated polysaccharide heparin. The carrageenans resulting in strong lactoferrin retention (Figure 3-8d–f of panel i) showed either gel-like structures (*ι*-Cg and *κ*-Cg) or turbidity (*λ*-Cg), indicating the formation of products insoluble in aqueous solution. Although the strong binding capacity of heparin to lactoferrin is known,[48] the resulting complex is stably dispersed in the aqueous phase. Therefore, it can be concluded that both the capacity of the sulfated anionic polysaccharides to strongly interact with lactoferrin and the formation of insoluble polysaccharide–protein complexes upon interaction are a prerequisite for retention of lactoferrin on the surface-modified cellulose substrates.

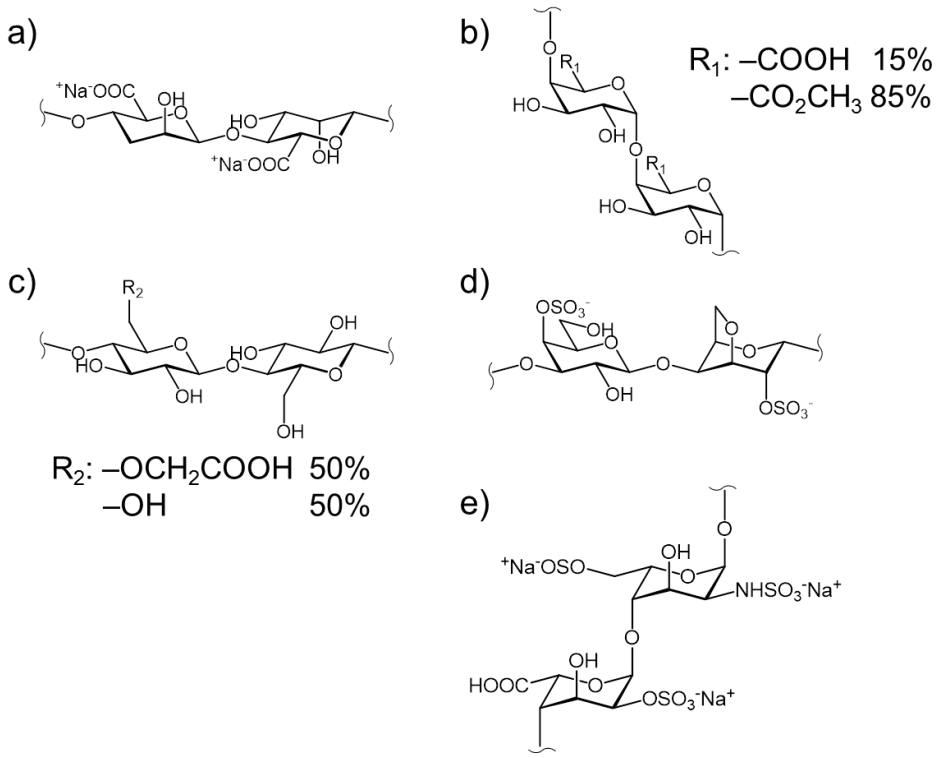

Figure 3-6. Chemical structures of anionic polysaccharides evaluated in this work: a) sodium alginate (Na-Alg); b) pectin; c) carboxymethyl cellulose (CMC); d) *ι*-carrageenan (*ι*-Cg); e) heparin.

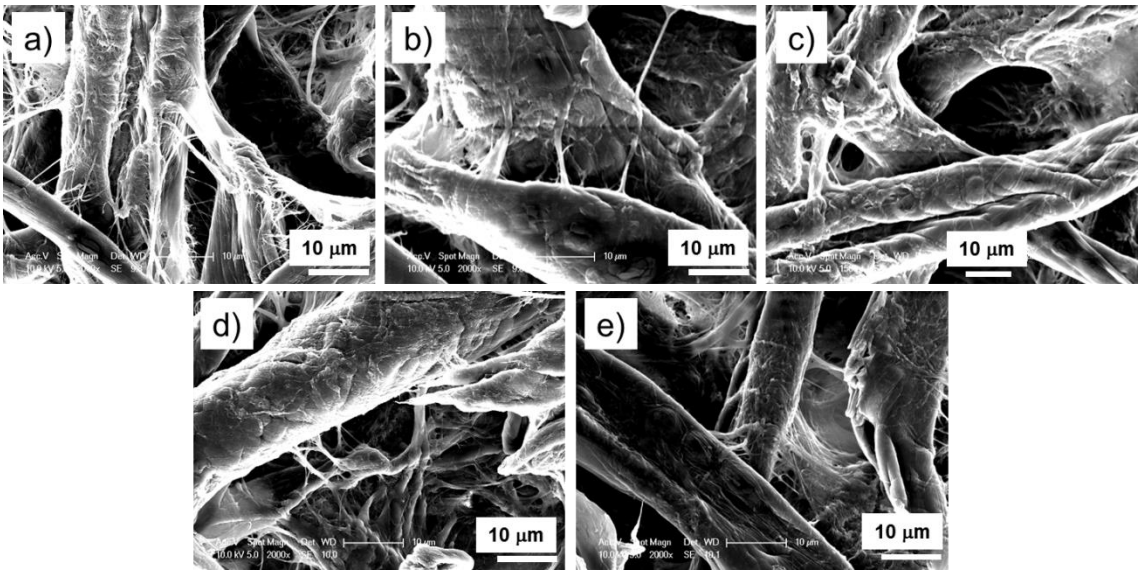

Figure 3-7. SEM images of filter paper substrates: a) plain Whatman grade 1 filter paper, b) coated with Na-Alg (sodium alginate), c) coated with pectin, d) coated with CMC (carboxymethyl cellulose), and e) coated with *ι*-Cg (*ι*-carrageenan). Paper surface coating was carried out by using 0.3w/w% aqueous solution of the respective anionic polysaccharide.

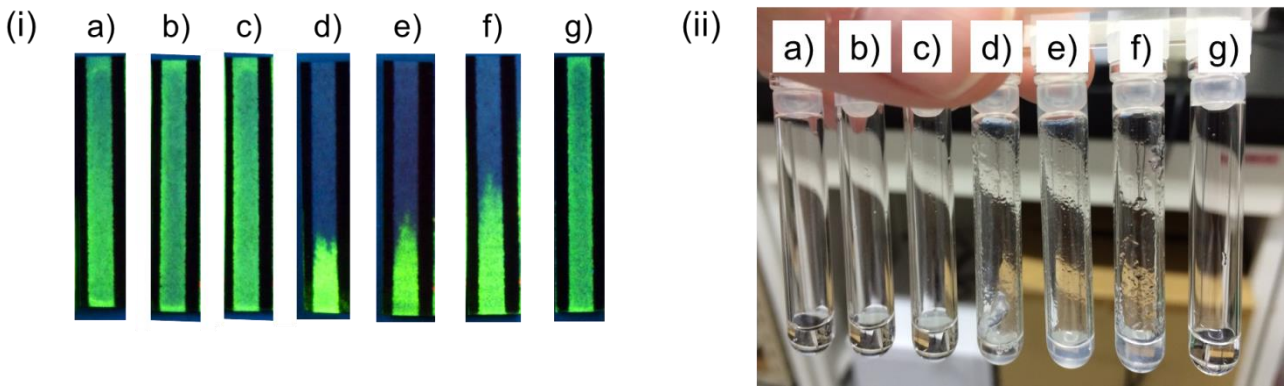

Figure 3-8. (i) Fluidic mobility of lactoferrin in pseudo-tear matrix on filter paper strips modified with 0.3w/w% aqueous solutions of various anionic polysaccharides. Photographs were taken under UV illumination (λ_{max} = 254 nm) with contrast and brightness modified for the sake of visibility of the fluorescent spots. (ii) 1:2 mixtures of aqueous solutions of anionic polysaccharides (0.3w/w%) and human lactoferrin (4 mg mL^{-1}) in pseudo-tear matrix: a) Na-Alg (sodium alginate), b) pectin, c) CMC (carboxymethylcellulose), d) *ι*-Cg (*ι*-carrageenan), e) *λ*-Cg, f) *κ*-Cg, and g) heparin.

Table 3-3. *ζ*-Potential values of filter paper surfaces after modification with anionic polysaccharides

Sample	*ζ*-Potential [mV][a]
No modification	−3.71 ± 1.09
Sodium alginate	−22.7 ± 8.59
Pectin	−2.94 ± 4.37
Carboxymethyl cellulose	−14.4 ± 6.30
ι-Carrageenan	−12.8 ± 1.01

[a] The data reflect the average values and standard deviations of three independent measurements.

The retention of Tb^{3+} on the modified paper substrate was also investigated by elution experiments. As observed in Figures 3-9a–d, all the tested anionic polysaccharides (Na-Alg, pectin, CMC, ι-Cg) showed improved Tb^{3+} retention efficiency against the flow of lactoferrin-containing pseudo-tear matrix compared to the unmodified filter paper (Figure 3-4e). This suggests the contribution of an electrostatic interaction of the sulfated polysaccharide (*ι*-Cg) with terbium cations and a chelating effect with the carboxylated polysaccharides (Na-Alg, pectin, CMC). However, small differences in Tb^{3+} retention efficiency between ι-carrageenan and the carboxylated polysaccharides could be observed by analyzing the longitudinal green intensity profile along the filter paper strip (Figure 3-9e), where the *ι*-Cg modified paper showed the lowest leaching of Tb^{3+} from the original deposition spot. This difference is assumed to be due to the lack of mobility of the water-soluble Tb^{3+}–lactoferrin complexes on the *ι*-Cg modified paper, which is favorable for application to a distance-based detection motif.

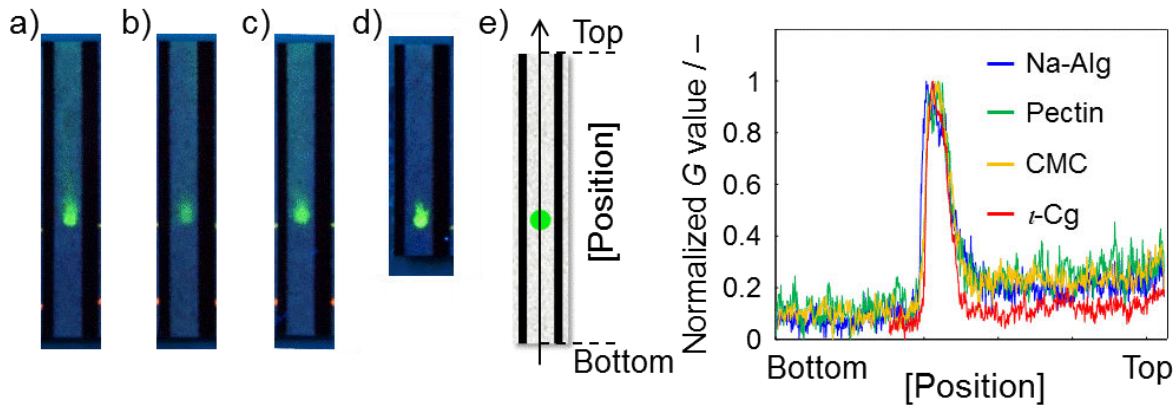

Figure 3-9. Retention of Tb^{3+} on filter paper strips modified with anionic polysaccharides after elution with pseudotear matrix: a) Na-Alg (sodium alginate), b) pectin, c) CMC (carboxymethylcellulose), and d) *ι*-Cg (*ι*-carrageenan); due to the strong adsorption of lactoferrin to the modified paper substrate, this strip had to be shortened for the protein to reach the spot with deposited Tb^{3+}. Photographs were taken under UV illumination (λ_{max} = 254 nm) with contrast and brightness modified for the sake of visibility of the fluorescent spots. e) Longitudinal profile of the green intensity (*G* value on RGB scale) on each paper strip.

3.3.5. Distance-based lactoferrin measurements on μPADs

In the sections above, the mobility behavior of the lactoferrin protein and the terbium cation on filter paper substrates depending on the sample matrix and paper surface conditions has been revealed. Most importantly, paper modification by *ι*-Cg solution led to the enhancement of lactoferrin adsorption and Tb^{3+} adhesion onto the filter paper substrate even in the presence of electrolytes and proteins found in tear sample matrix. These findings allow the realization of a μPAD for the determination of lactoferrin within a microfluidic paper channel using the length of the fluorescent channel section as the quantitative signal.

In a proof-of-concept experiment, samples consisting of lactoferrin dissolved in pure water were first applied onto the straight microfluidic channel of μPADs based on unmodified filter paper. The length of the green fluorescence emitting line increased with increasing lactoferrin concentrations (Figure 3-10). As expected, switching the sample matrix from pure water to the pseudo-tear matrix, a mixture of primary tear fluid components as mentioned above, made a major difference in the distance-based signal appearance. On unmodified paper, no longer the distance but the fluorescence emission intensity over the entire channel showed an analyte concentration-dependent increase (Figure 3-11a). This issue was not resolved by pretreatment of the filter paper substrate with any of the tested carboxylated anionic polysaccharides (Figures 3-11b–d). Only the coating with *ι*-Cg resulted in successful recovery of the distance-based response scheme for the series of lactoferrin samples in pseudo-tear matrix (Figure 3-12a). This difference in signal appearance, a change in emission intensity versus a change in length of the fluorescent section, emphasizes the importance of exhaustive analyte depletion from the sample while keeping the signaling agents in place. In the present case, *ι*-Cg contributes to the continuous and instantaneous adsorption of lactoferrin molecules onto the paper substrate during sample flow, despite the complex composition of the mobile matrix, resulting in changes of the distance-based signal depending on the amount of lactoferrin in the sample. The quantitative correlation between the lactoferrin sample concentration and the distance of fluorescence is shown in Figure 3-12b. The nonlinearity of this calibration curve can be explained by changes in the sample wicking speed in porous paper media.[49-50] The continuously decreasing flow speed of the aqueous sample with distance during transport in the paper-based microfluidic channel results in increasing interaction times between the analyte

and the paper substrate and/or deposited reagents.[22] For this reason, the lactoferrin depletion in the flowing sample liquid due to analyte adsorption to the modified paper surface is not linear over the flow distance but increases with length traveled along the channel. The optimal concentration of *ι*-Cg solution for paper surface modification was selected as 0.3w/w% among the tested 0.1, 0.2, 0.3, 0.4, 0.5, and 1w/w%. Lower concentrations resulted in a not clearly identifiable border of the emissive region because of too low capacity for lactoferrin adsorption. On the other hand, higher concentrations lead to a shortening of the overall distance and frequent clogging of the microchannel, possibly due to a loss of the cellulosic porous structure required for capillary flow driven sample transport (data not shown).

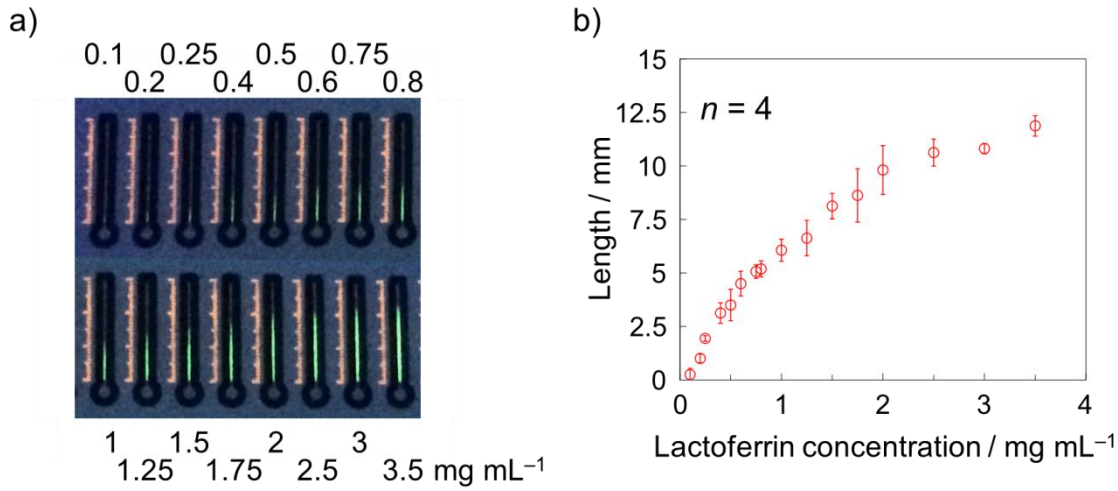

Figure 3-10. Measurement of lactoferrin (0.1–3.5 mg mL^{-1}) dissolved in pure water on unmodified μPADs in a proof-of-concept experiment: a) visual appearance of the distance-based fluorescence emission under UV illumination (λ_{max} = 254 nm); b) typical relationship between the sample lactoferrin concentration and the fluorescence emission distance (1 scale increment corresponds to 0.5 mm).

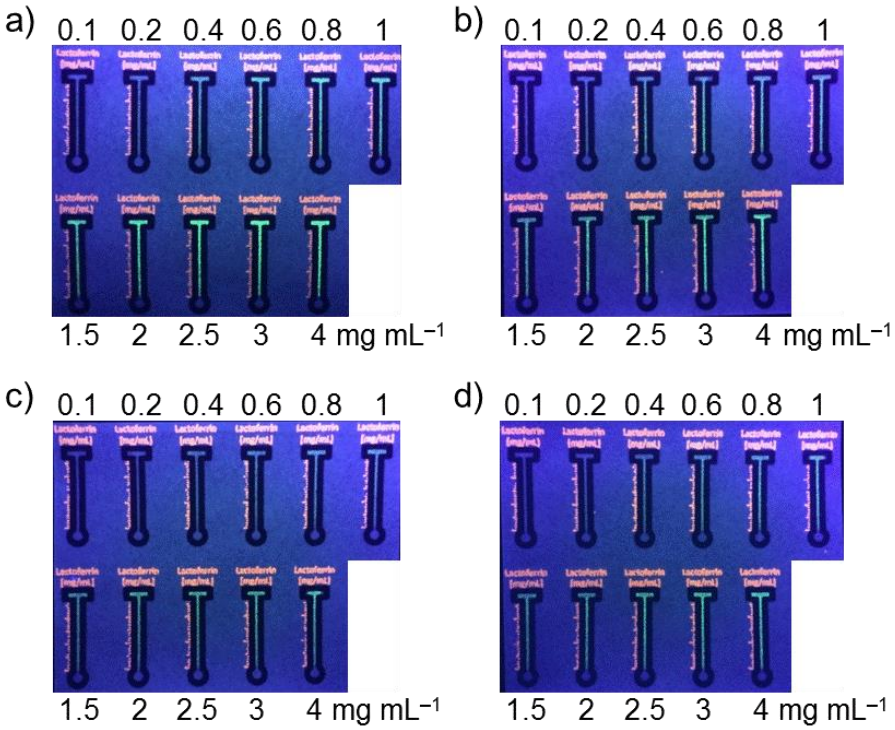

Figure 3-11. Appearance of the fluorescence emission after pipetting 2 μL of lactoferrin samples in pseudo-tear matrix (0.1–4 mg mL^{-1}) on μPADs with different paper surface treatments: a) unmodified filter paper, b) soaked in 0.3w/w% aqueous solution of Na-Alg, c) soaked in 0.3w/w% aqueous solution of pectin, and d) soaked in 0.3w/w% aqueous solution of CMC.

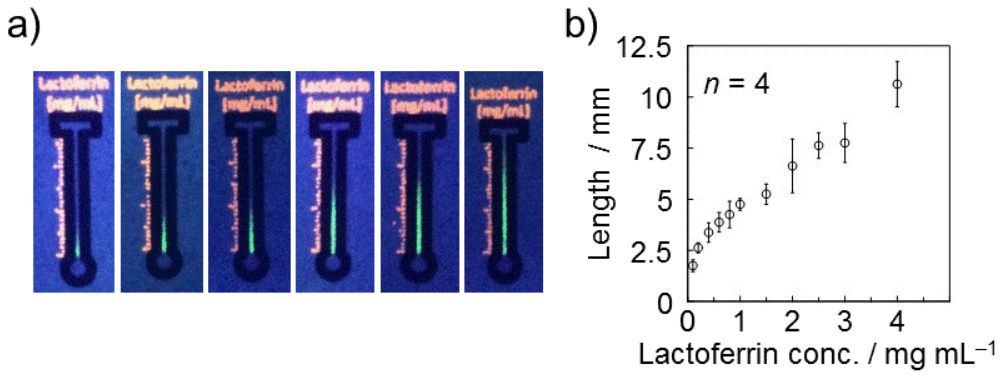

Figure 3-12. a) Images of *ι*-Cg-coated μPADs after pipetting of various concentrations of lactoferrin in pseudo-tear matrix (0.1, 0.6, 1, 2, 3, 4 mg mL^{-1} from left to right). b) Calibration curve representing the relationship between sample lactoferrin concentration and the length of the fluorescence emitting line (1 scale increment corresponds to 0.5 mm).

The distance-based signal is presumably influenced by the geometrical design of the straight microfluidic channel and the concentration of the assay components. In the present work, the effects of the width and length of the microfluidic channel as well as the number of printing cycles of the assay components were studied. Printed channel widths of 900 µm (medium) (used as standard throughout this work), 800 µm (narrow), and 1100 µm (wide) have been tested. The actual widths observed after wax diffusion by hot lamination and the experimental results are shown in Table 3-1 and Figure 3-13, respectively. As reported earlier by Cate *et al.*,[22] a wider channel resulted in a decreased distance signal, since larger amounts of lactoferrin are consumed per distance unit. On the other hand, narrowing of the channel did not result in significant differences, since the lower depletion of analyte per distance unit is compensated by reduced sample flow speed in the narrow channel with higher resistance caused by the hydrophobic wax barrier. The influence of channel length was studied at 10 mm (short), 13 mm (medium) (used as standard throughout the work), and 16 mm (long), with a constant amount of 2 µL of sample liquid applied. Although not significant, the sensitivity of the distance-based assay slightly decreased in the 10 mm short channel (Figure 3-14). After sample application, only the shortest channel is completely wetted by the sample solution. In the completely wetted state, capillary force driven liquid flow comes to a halt, and consequently, analyte is no longer actively transported. For the medium and long channel versions, this limitation does not apply, resulting in channel length independent signals. Finally, the number of inkjet printing cycles of the assay components was varied from 1 to 9 times in order to investigate the effect of the amount of Tb^{3+}. Interestingly, increasing the amount of Tb^{3+} deposited on the channel by repeated printing enhanced the sensitivity compared to a single printing cycle (Figure 3-15). This result suggests that adsorption onto the modified paper substrate is the primary cause of lactoferrin depletion during sample flow in the microfluidic channel rather than binding to Tb^{3+}. In the latter situation, an increased concentration of Tb^{3+} should lead to shorter fluorescent sections, which is not the case. The experimentally observed extended length with increasing deposition of Tb^{3+} can be attributed to the improved visibility of the fluorescence at the emission front, where the amount of lactoferrin becomes gradually scarce. However, it should be noted that increased numbers of printing cycles are time-consuming and bring along higher risks of error in device fabrication. As discussed in the following paragraph, the

batch-to-batch reproducibility is crucial for the current μPAD, and thus, it was decided to adopt a single printing cycle throughout this work.

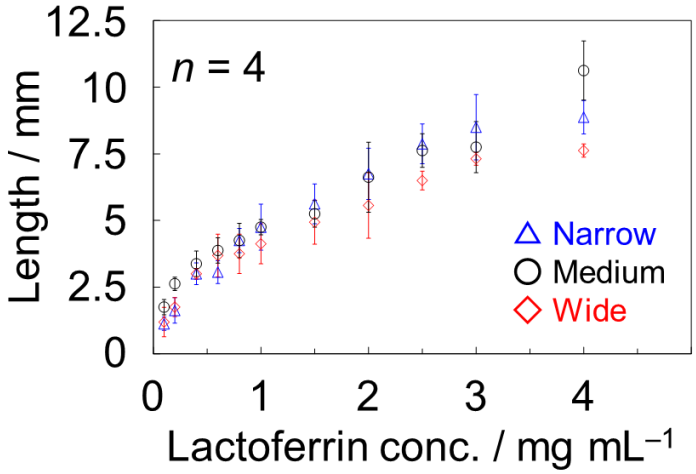

Figure 3-13. Relationship between the sample lactoferrin concentration and the fluorescence emission distance for three types of channel width (1 scale increment corresponds to 0.5 mm). The widths of the channels prior to hot lamination were 800 μm (narrow), 900 μm (medium), and 1100 μm (wide). After lamination, the wax diffused within the paper substrate and the channels narrowed down to 300 ± 14.6 μm, 418 ± 19.0 μm, 627 ± 26.1 μm, respectively (data reflect the average and standard deviation of 8 measurements with a microscope; see also Table 3-1).

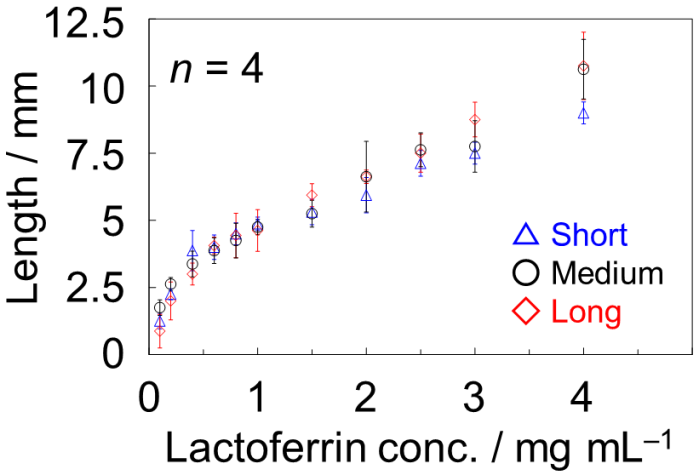

Figure 3-14. Relationship between the sample lactoferrin concentration and the fluorescence emission distance for three types of channel length (1 scale increment corresponds to 0.5 mm). The lengths of the channels were 10 mm (short), 13 mm (medium), and 16 mm (long).

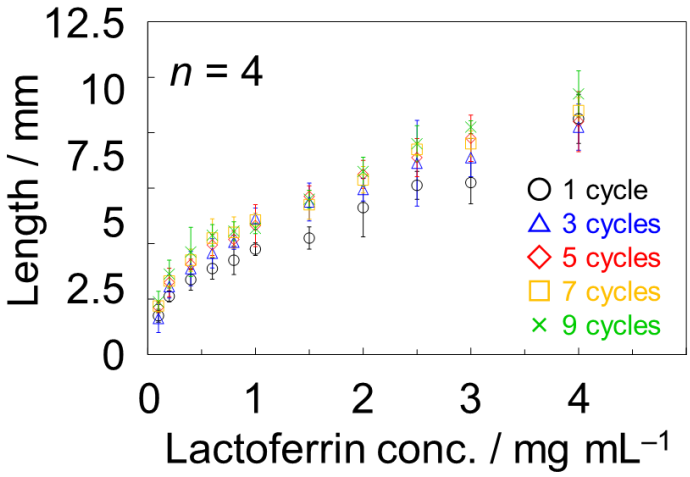

Figure 3-15. Relationship between the sample lactoferrin concentration and the fluorescence emission distance for various repetitions of inkjet-printing cycle(s) of the assay components.

On the basis of the calibration curve shown in Figure 3-12b, the ruler-like scale marks with constant increments (0.5 mm) were replaced by those directly indicating the analyte concentration (Figure 3-16a). These "concentration scale marks" allow the direct quantification of lactoferrin without the requirement of device calibration by the user, as long as the volume of the applied sample is kept constant. For the signal reader-free quantitative assay, the emission front was compared with the concentration scale marks under UV illumination from a handlamp (λ_{max} = 254 nm) after pipetting a series of lactoferrin standards (2 μL) in the tear fluid-like matrix. Figure 3-16b shows the correlation between the sample lactoferrin concentration and the values read off from the concentration scale marks. In order to achieve this calibration-free quantification, the batch-to-batch reproducibility is a critical factor to be guaranteed. The results obtained from the μPADs fabricated on different days showed slopes of 0.996, 0.973, 0.971, and 0.993 with regression coefficients of 0.991, 0.990, 0.996, and 0.995, denoting good reproducibility of the entire device fabrication procedure (wax printing, inkjet deposition of the assay reagents, hot lamination, and coating with the anionic polysaccharide). Furthermore, the usability of the developed μPAD by untrained personnel has been demonstrated by calibration curves individually drawn by various observers with no distinct deviance in unity and linearity (Figure 3-17 and Table 3-4). Finally, it has been experimentally demonstrated that the intensity of the UV light source as well as the ambient humidity (33%, 54%, 90% relative humidity) trivially affect the outcome of the

signal readout, reinforcing the simplicity and easy handling of the device (results and experimental conditions are shown in Figures 3-18 and 3-19 and their captions).

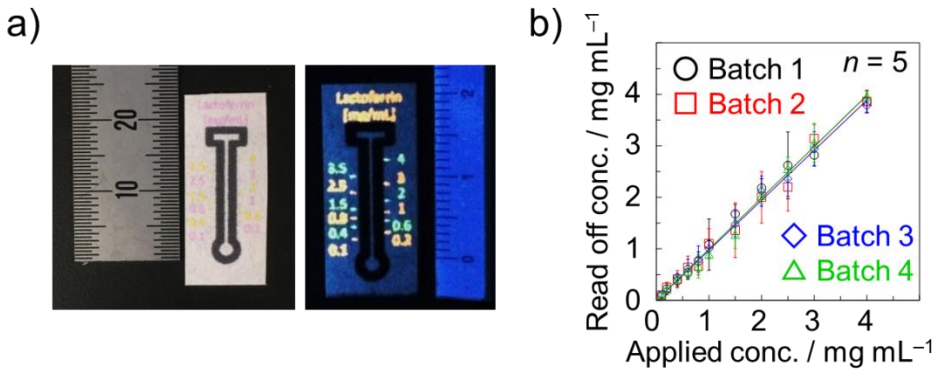

Figure 3-16. a) Photograph of the μPAD for calibration-free quantitative lactoferrin assay under ambient light (left) and UV (λ_{max} = 254 nm) (right). b) Correlation between lactoferrin concentrations in the applied sample and the concentrations read off the device by the naked eye. Four data sets represent the results from independent batches (fabricated on different days) of μPADs. The slopes (a) and regression coefficients (R^2) for the linear regression curves are as follows: $a = 0.996$, $R^2 = 0.991$ (batch 1); $a = 0.973$, $R^2 = 0.990$ (batch 2); $a = 0.971$, $R^2 = 0.996$ (batch 3); $a = 0.993$, $R^2 = 0.995$ (batch 4).

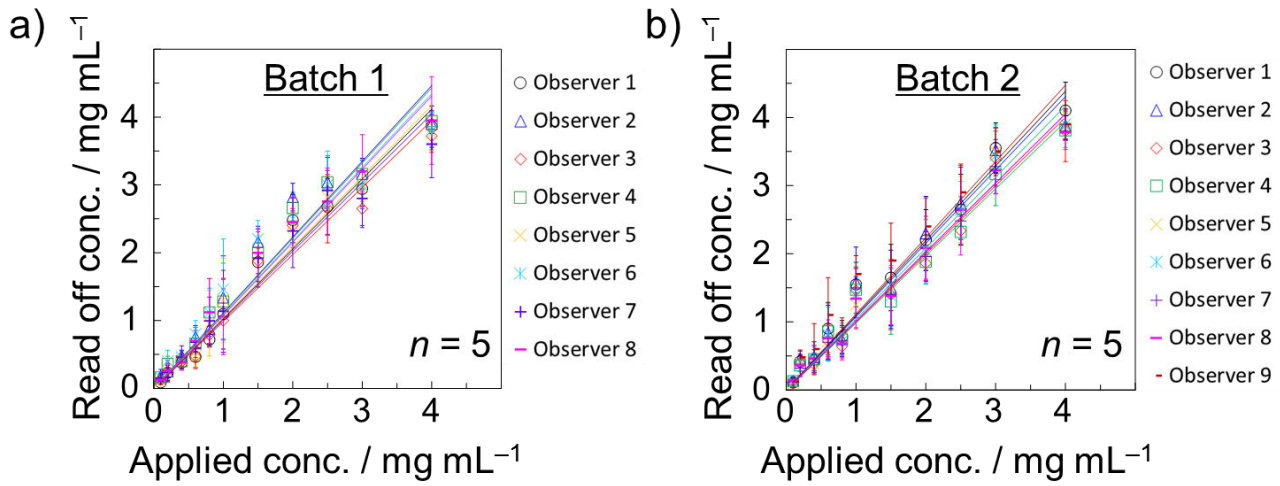

Figure 3-17. Lactoferrin concentrations read out by various independent observers. The μPADs used here are identical to those used in Figure 3-16b.

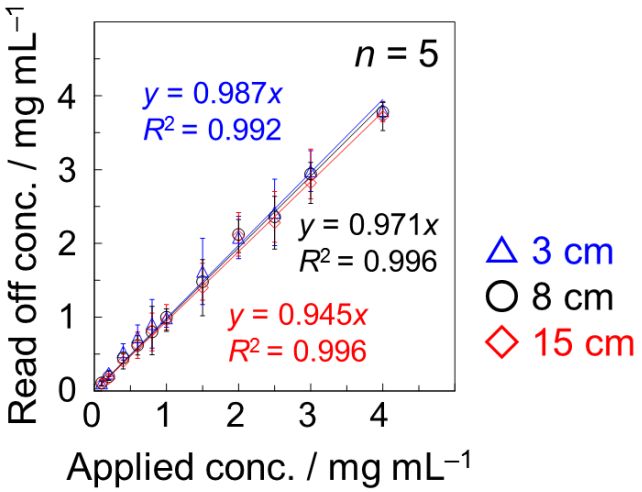

Figure 3-18. Dependency of direct concentration readout on the UV light source intensity: in order to modulate the excitation light intensity, the UV handlamp was placed at different distances from the μPADs (3 cm, 8 cm, and 15 cm). The power of the UV handlamp used in this experiment is 760 μW cm^{-2} (information provided by the manufacturer for a distance of 15 cm).

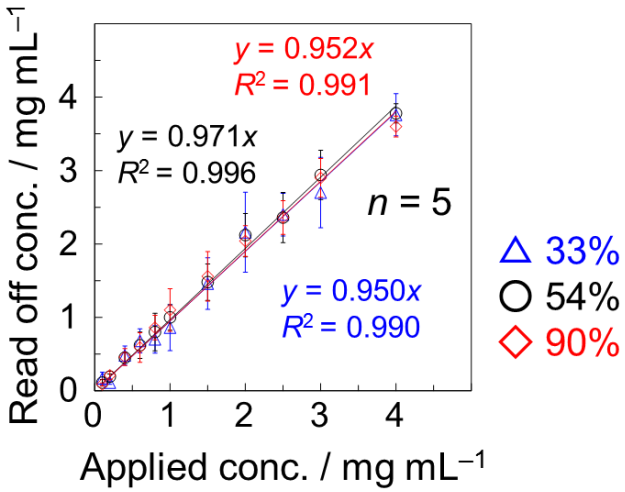

Figure 3-19. The effect of humidity on lactoferrin assay with direct concentration readout: the μPADs were incubated in a climate control chamber (25ºC, 90% RH) for 1 hour prior to introduction of lactoferrin standard samples (0.1–4 mg mL^{-1} dissolved in pseudo-tear matrix). The experiments under 33% and 54% humidity were conducted in a normal experimental laboratory (~ 25ºC) without environmental control (monitoring was performed to guarantee constant temperature and humidity).

Table 3-4. Slopes and regression coefficients (R^2 values) for the regression curves shown in Figure 3-17.

Batch 1			Batch 2		
Observer	Slope	R^2 value	Observer	Slope	R^2 value
1	1.03	0.975	1	1.10	0.973
2	1.12	0.940	2	1.08	0.960
3	0.987	0.964	3	1.00	0.965
4	1.11	0.956	4	0.985	0.968
5	1.04	0.963	5	1.04	0.979
6	1.09	0.926	6	1.04	0.975
7	1.01	0.951	7	1.01	0.985
8	1.08	0.974	8	1.01	0.979
			9	1.12	0.935

The lowest concentration of lactoferrin detectable with the current device was determined to be 0.05 mg mL^{-1} (see Table 3-5 for the result and the associated footnote for the detailed experimental method). In spite of the identical detection chemistry (*i.e.*, observation of the fluorescence emission from sensitized Tb^{3+} on the paper substrate), this value is lower than that of the μPAD previously developed by our group.[32] In the current approach, lactoferrin molecules are concentrated within the narrow space of the microfluidic channel in close proximity to the sample application area. In the previously developed μPAD, the analyte, after traveling through a 2.8 mm channel, is spread over a square detection region of 3×3 mm^2, preventing the detection of a visible fluorescence signal from the same low concentration.

Table 3-5. Determination of the lowest detectable lactoferrin concentration with the distance-based μPAD.

Concentration [mg mL^{-1}]	1	2	3	4	5	6	7	8	9	10	Success rate
0.09	✓	✓	✓	✓	✓	✓	✓	✓	✓	✓	10/10
0.08	✓	✓	✓	✓	✓	✓	✓	✓	✓	✓	10/10
0.07	✓	✓	✓	✓	✓	✓	✓	✓	✓	✓	10/10
0.06	✓	✓	✓	✓	✓	✓	✓	✓	✓	✓	10/10
0.05	✓	✓	✓	✓	✓	✓	✓	✓	✓	✓	10/10
0.04	×	✓	✓	✓	✓	×	✓	✓	✓	✓	8/10
0.03	×	✓	✓	✓	×	×	×	✓	×	×	4/10
0.02	×	×	×	×	×	×	×	×	✓	✓	2/10
0.01	×	×	×	×	×	×	×	×	×	×	0/10

A classical limit of detection according to the 3σ method cannot be estimated for the distance-based assay, because a blank sample does not produce any signal (*i.e.* blank signal is zero). Thus, the "lowest detectable lactoferrin concentration" was examined alternatively in this work. Lactoferrin samples with concentrations of 0.01–0.09 mg mL^{-1} were deposited on the μPAD (n = 10) and the fluorescence signal was observed under UV illumination (λ_{max} = 254 nm). A separation into "detectable" (tick mark) or "undetectable" (cross mark) was made according to whether any fluorescence emission was observed within the microfluidic channel. The concentration of 0.05 mg mL^{-1} was finally chosen, which was the lowest among those yielding a detectable signal in all 10 trials.

3.3.6. Lactoferrin assay using human tear samples

Quantification of lactoferrin in human tear fluid was performed by using the developed μPADs with the concentration scale marks. Human tear samples were collected from 16 healthy volunteers and 2 ocular disease patients. All the results obtained with the μPADs were compared with those of the conventional ELISA method for validation. As shown in Table 3-6, 16 out of 18 samples, including those collected from ocular disease patients, were analyzed by the μPAD within 15% error of the ELISA method. Due to the simplicity of the assay procedure of the distance-based device (signal quantification by the naked eye and elimination of the calibration step), the analytical performance in terms of accuracy and precision is lower compared to the previously developed conventional μPAD (details are provided in Table 3-7).[32] However, both accuracy and precision are comparable to the system reported by Cate *et al*. for an equally simple distance-based assay targeting metals in welding fumes.[22] It is noteworthy that the signal quantification process in the distance-based detection motif is not reliant on any signal translation instrument but simple visual inspection of the length. Considering its simplicity, the correlation of the distance-based μPAD to the established ELISA method is reasonably good. The direct method comparison (Figure 3-20) showed a regression coefficient of 0.946 and a slope close to unity (0.977). Although due to diffuse borders of the fluorescent front in some instances the standard deviations for results obtained with the developed μPADs are larger than those obtained with the ELISA method, the performance of the μPADs is sufficient to clearly distinguish the clinically relevant down-regulation of lactoferrin secretion in the tear samples of ocular disease patients (samples 17 and 18 in Table 3-6) from those of the healthy volunteers (samples 1−16).

Table 3-6. Assay results for lactoferrin in human tear samples obtained by the μPAD and a commercial ELISA kit.

	Method; concentration [mean ± 1σ, mg mL^{-1}]		
Sample no.	μPAD[a]	ELISA[b]	Error [%][c]
1	1.18 ± 0.37	1.35 ± 0.06	–12
2	2.38 ± 0.26	2.55 ± 0.07	–6.5
3	3.52 ± 0.36	3.54 ± 0.33	–0.75
4	2.00 ± 0.34	1.94 ± 0.54	+2.9
5	2.02 ± 0.46	1.94 ± 0.04	+3.7
6	1.22 ± 0.45	1.11 ± 0.03	+9.3
7	2.15 ± 0.29	2.23 ± 0.07	–3.7
8	1.18 ± 0.43	1.39 ± 0.07	–15
9	1.97 ± 0.29	1.46 ± 0.04	+34
10	2.58 ± 0.55	2.73 ± 0.20	–5.3
11	1.48 ± 0.45	1.65 ± 0.09	–10
12	1.48 ± 0.58	1.70 ± 0.08	–13
13	1.53 ± 0.34	1.37 ± 0.11	+12
14	1.02 ± 0.25	1.27 ± 0.09	–20
15	1.48 ± 0.45	1.62 ± 0.18	–8.7
16	1.38 ± 0.54	1.34 ± 0.19	+3.5
17	0.20 ± 0.13	0.21 ± 0.09	–5.7
18	0.45 ± 0.11	0.42 ± 0.17	+5.9

[a]Measurement values show the read-off concentration from the scale marks printed on the device after pipetting of human tear sample (2 μL). The data reflect the average values and standard deviations of six independent measurements. [b]Tear samples were diluted 10^5-fold prior to analysis by using the sample diluting buffer provided in the ELISA kit. The data reflect the average values and standard deviations of four measurements. [c]Error [%] calculated as 100 × (μPAD – ELISA)/ELISA.

Table 3-7. Comparison of accuracy and precision for human tear fluid assays.

	Method		
Parameter	ELISA	Intensity-based μPAD[a]	This work[b]
Accuracy[c]	–	3.20%	9.59%
Precision[d]	11.1%[e] / 13.9%[f]	3.22%	27.2%

[a] Based on the data of human tear fluid analysis from Ref. 32 (5 human tear fluid samples); [b] based on the μPAD data shown in Table 3-6 (18 human tear fluid samples); [c] expressed as the mean absolute percentage error of lactoferrin concentration determination regarding the ELISA values as the correct reference values; [d] expressed as the mean of the relative standard deviations; [e] based on the ELISA data shown in Table 3-6 (18 human tear fluid samples); [f] based on the ELISA data from Ref. 32 (5 human tear fluid samples).

For comparison purposes, the corresponding analytical parameters for an alternative distance-based μPAD assay reported by Cate *et al.*[22] for the determination of metals in welding fumes has been calculated accordingly (based on the data provided in Table 3 of Ref. 22): accuracy 8.00%; precision 23.5%.

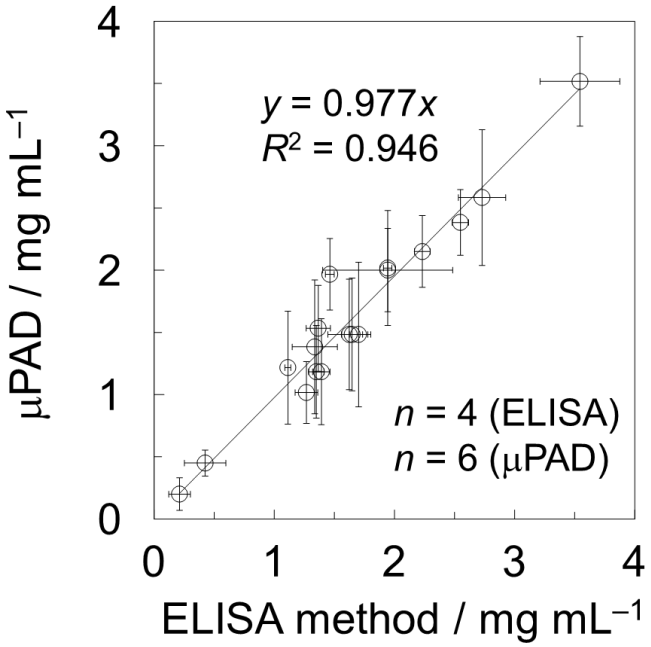

Figure 3-20. Correlation between lactoferrin measurements by ELISA and μPADs. The markers and error bars represent the average and standard deviations of four (ELISA) and six (μPAD) repetitions, respectively.

In a final confirmation experiment, concentrations of lactoferrin in spiked human tear fluid were measured with the direct-readout μPADs. As can be seen from the results in Table 3-8, the μPAD is able to reliably detect the added amounts of lactoferrin in the real sample matrix. Finally, the developed μPADs satisfy the criteria of low-cost (< $0.004/assay), rapidity (< 10 min), and simple analytical procedure (single pipetting of untreated tear sample) compared to the conventional ELISA method (calculation and detailed comparison are shown in Tables 3-9 and 3-10, respectively).

Table 3-8. μPAD measurement of lactoferrin spiked into human tear fluid.

Sample	Added [mg mL^{-1}]	Measured value[a] [mean ± 1σ, mg mL^{-1}]	Recovery [%]
Original	0	1.05 ± 0.30	–
Spiked tear 1	1	2.07 ± 0.31	101
Spiked tear 2	1.5	2.45 ± 0.27	93.3
Spiked tear 3	2	2.87 ± 0.24	90.7

[a] Measurement values show the read-off concentration from the scale marks printed on the device after pipetting of the sample (2 μL). The data reflect the average values and standard deviations of seven independent measurements.

Table 3-9. Cost estimation for the developed μPAD.

Material cost

Material	Market price per quantity	Quantity per μPAD	Cost per μPAD
$TbCl_3 \cdot 6H_2O$	\$90 per 5 g	0.5 μL (10 mM)	\$0.0000336
$NaHCO_3$	\$10 per 500 g	0.5 μL (25 mM)	\$0.00000002
HEPES	\$200 per 500 g	0.5 μL (50 mM)	\$0.00000238
ι-Carrageenan	\$520 per 1 kg	2 mL (0.3w/w%)	\$0.000312
Filter paper	\$120 per 46 × 57 cm^2 × 100 sheets	1.5 × 3 cm^2	\$0.00206
Laminate film	\$90 per A4 × 500 sheets	(160 μPADs/A4 sheet)	\$0.00113
Total			\$0.00353

Printer cost

Wax printer (ColorQube 8570): \$0.0000341

Inkjet printer (Canon iP2700): \$0.0000364

* Based on the printer lifetimes of 120,000 pages (wax printer) and 5,000 pages (inkjet printer), 160 μPADs per A4 page.

Total material cost of single μPAD = \$0.00353 + \$0.0000341 + \$0.0000364 = **\$0.0036**

Table 3-10. Comparison of assay performance between the μPAD and a commercial ELISA kit.

Items	ELISA	μPAD
Sample	> 10 μL (10^5-fold dilution required)	2 μL (no pretreatment required)
Procedure	Multiple steps of incubation, washing, pipetting	Single pipetting of sample
Assay time	Hours	5 min
Analytical instruments	Microplate reader	UV handlamp
Estimated cost	≈ \$1.2/assay	~ \$0.0036/assay

3.4. Conclusions

Simple, yet quantitative analysis of lactoferrin has been demonstrated on a μPAD by converting the analyte concentration into a distance-based signal without the requirement of user calibration and signal quantifying equipment. In contrast to previously reported distance-based detection approaches relying on aggregation or precipitation of analyte-indicator complexes, a highly water-soluble detection reagent ($TbCl_3$) and signaling product (fluorescent Tb^{3+}–lactoferrin complex) have been adapted to a distance-based detection scheme for the first time by specific modification of the interface between the solid cellulose substrate and the liquid sample matrix. To achieve a distance-based signal despite of a combination of a soluble assay component and soluble signaling product, fluidic mobilities of all involved components on a cellulosic filter paper substrate have been elaborated. The presence of electrolytes and proteins in the sample matrix was found to have a significant influence on their mobility on untreated cellulosic paper surfaces, which is primarily based on electrostatic interactions. It could be demonstrated that the modification of the paper surface with sulfated anionic polysaccharides of the carrageenan family allowed control of the assay component mobility in a way required for distance-based signaling by further enhancing the interfacial interactions between the inherently negatively charged paper surface and the positively charged target protein and assay component. Following paper surface modification with the sulfated anionic polysaccharide *ι*-carrageenan, successful distance-based lactoferrin quantification in real human tear samples has been achieved. The assay results from the developed μPAD showed a good correlation with those of the reference method, demonstrating the applicability to real-world samples. Furthermore, the μPAD provides a direct display of quantitative assay results, which can be accurately interpreted by untrained users. With its low-cost (< \$0.004/assay), short assay time (< 10 min), and simplicity of use, it is expected to become a promising alternative for ocular disease diagnosis by untrained medical staff.

References

1. Gordon, A. H.; Martin, A. J. P.; Synge, R. L. M., Partition Chromatography of Free Amino-Acids and Peptides. *Biochem. J.* **1943,** 37, xiii.
2. Consden, R.; Gordon, A. H.; Martin, A. J. P., Qualitative analysis of proteins: a partition chromatographic method using paper. *Biochem. J.* **1944,** 38, 224–232.
3. Müller, R. H.; Clegg, D. L., Automatic Paper Chromatography. *Anal. Chem.* **1949,** 21, 1123–1125.
4. Comer, J. P., Semiquantitative Specific Test Paper for Glucose in Urine. *Anal. Chem.* **1956,** 28, 1748–1750.
5. Free, A. H.; Adams, E. C.; Kercher, M. L.; Free, H. M.; Cook, M. H., Simple Specific Test for Urine Glucose. *Clin. Chem.* **1957,** 3, 163–168.
6. Hawkes, R., Identification of concanavalin A-binding proteins after sodium dodecyl sulfate-gel electrophoresis and protein blotting. *Anal. Biochem.* **1982,** 123, 143–146.
7. Martinez, A. W.; Phillips, S. T.; Butte, M. J.; Whitesides, G. M., Patterned paper as a platform for inexpensive, low-volume, portable bioassays. *Angew. Chem. Int. Ed.* **2007,** 46, 1318–1320.
8. Martinez, A. W.; Phillips, S. T.; Wiley, B. J.; Gupta, M.; Whitesides, G. M., FLASH: A rapid method for prototyping paper-based microfluidic devices. *Lab Chip* **2008,** 8, 2146–2150.
9. Ballerini, D. R.; Li, X.; Shen, W., Patterned paper and alternative materials as substrates for low-cost microfluidic diagnostics. *Microfluid. Nanofluidics* **2012,** 13, 769–787.
10. Li, X.; Ballerini, D. R.; Shen, W., A perspective on paper-based microfluidics: Current status and future trends. *Biomicrofluidics* **2012,** 6, 011301.
11. Liana, D. D.; Raguse, B.; Gooding, J. J.; Chow, E., Recent advances in paper-based sensors. *Sensors* **2012,** 12, 11505–11526.
12. Nery, E. W.; Kubota, L. T., Sensing approaches on paper-based devices: a review. *Anal. Bioanal. Chem.* **2013,** 405, 7573–7595.

13. Yetisen, A. K.; Akram, M. S.; Lowe, C. R., Paper-based microfluidic point-of-care diagnostic devices. *Lab Chip* **2013,** 13, 2210–2251.
14. Cate, D. M.; Adkins, J. A.; Mettakoonpitak, J.; Henry, C. S., Recent developments in paper-based microfluidic devices. *Anal. Chem.* **2015,** 87, 19–41.
15. Yamada, K.; Henares, T. G.; Suzuki, K.; Citterio, D., Paper-based inkjet-printed microfluidic analytical devices. *Angew. Chem. Int. Ed.* **2015,** 54, 5294–5310.
16. Meredith, N. A.; Quinn, C.; Cate, D. M.; Reilly, T. H.; Volckens, J.; Henry, C. S., Paper-based analytical devices for environmental analysis. *Analyst* **2016,** 141, 1874–1887.
17. Yamada, K.; Shibata, H.; Suzuki, K.; Citterio, D., Toward practical application of paper-based microfluidics for medical diagnostics: state-of-the-art and challenges. *Lab Chip* **2017,** 17, 1206–1249.
18. Martinez, A. W.; Phillips, S. T.; Carrilho, E.; Thomas, S. W.; Sindi, H.; Whitesides, G. M., Simple Telemedicine for Developing Regions: Camera Phones and Paper-Based Microfluidic Devices for Real-Time, Off-Site Diagnosis. *Anal. Chem.* **2008,** 80, 3699–3707.
19. Shen, L.; Hagen, J. A.; Papautsky, I., Point-of-care colorimetric detection with a smartphone. *Lab Chip* **2012,** 12, 4240–4243.
20. Cate, D. M.; Dungchai, W.; Cunningham, J. C.; Volckens, J.; Henry, C. S., Simple, distance-based measurement for paper analytical devices. *Lab Chip* **2013,** 13, 2397–2404.
21. Dungchai, W.; Sameenoi, Y.; Chailapakul, O.; Volckens, J.; Henry, C. S., Determination of aerosol oxidative activity using silver nanoparticle aggregation on paper-based analytical devices. *Analyst* **2013,** 138, 6766–6773.
22. Cate, D. M.; Noblitt, S. D.; Volckens, J.; Henry, C. S., Multiplexed paper analytical device for quantification of metals using distance-based detection. *Lab Chip* **2015,** 15, 2808–2818.
23. Li, M.; Tian, J.; Al-Tamimi, M.; Shen, W., Paper-based blood typing device that reports patient's blood type "in writing". *Angew. Chem. Int. Ed.* **2012,** 51, 5497–5501.
24. Carrasquilla, C.; Little, J. R. L.; Li, Y.; Brennan, J. D., Patterned Paper Sensors Printed with Long-Chain DNA Aptamers. *Chem. - Eur. J.* **2015,** 21, 7369–7373.

25. Li, M.; Cao, R.; Nilghaz, A.; Guan, L.; Zhang, X.; Shen, W., "Periodic-Table-Style" Paper Device for Monitoring Heavy Metals in Water. *Anal. Chem.* **2015,** 87, 2555–2559.
26. Lewis, G. G.; DiTucci, M. J.; Phillips, S. T., Quantifying Analytes in Paper-Based Microfluidic Devices Without Using External Electronic Readers. *Angew. Chem. Int. Ed.* **2012,** 51, 12707–12710.
27. Karita, S.; Kaneta, T., Acid-base titrations using microfluidic paper-based analytical devices. *Anal. Chem.* **2014,** 86, 12108–12114.
28. Lewis, G. G.; Robbins, J. S.; Phillips, S. T., Point-of-Care Assay Platform for Quantifying Active Enzymes to Femtomolar Levels Using Measurements of Time as the Readout. *Anal. Chem.* **2013,** 85, 10432–10439.
29. Lewis, G. G.; Robbins, J. S.; Phillips, S. T., A prototype point-of-use assay for measuring heavy metal contamination in water using time as a quantitative readout. *Chem. Commun.* **2014,** 50, 5352–5354.
30. Zhang, Y.; Fan, J.; Nie, J.; Le, S.; Zhu, W.; Gao, D.; Yang, J.; Zhang, S.; Li, J., Timing readout in paper device for quantitative point-of-use hemin/G-quadruplex DNAzyme-based bioassays. *Biosens. Bioelectron.* **2015,** 73, 13–18.
31. Chen, Y.-T.; Yang, J.-T., Detection of an amphiphilic biosample in a paper microchannel based on length. *Biomed. Microdevices* **2015,** 17, 52.
32. Yamada, K.; Takaki, S.; Komuro, N.; Suzuki, K.; Citterio, D., An antibody-free microfluidic paper-based analytical device for the determination of tear fluid lactoferrin by fluorescence sensitization of Tb^{3+}. *Analyst* **2014,** 139, 1637–1643.
33. Kataoka, Y.; Shinoda, S.; Tsukube, H., Transferrin-Terbium Complexes as Luminescent pH Sensing Devices. *J. Nanosci. Nanotechnol.* **2009,** 9, 655–657.
34. Pelton, R., Bioactive paper provides a low-cost platform for diagnostics. *Trends Anal. Chem.* **2009,** 28, 925–942.
35. González-Chávez, S. A.; Arévalo-Gallegos, S.; Rascón-Cruz, Q., Lactoferrin: structure, function and applications. *Int. J. Antimicrob. Agents* **2009,** 33, 301.e1–301.e8.

36. García-Montoya, I. A.; Cendón, T. S.; Arévalo-Gallegos, S.; Rascón-Cruz, Q., Lactoferrin a multiple bioactive protein: An overview. *Biochim. Biophys. Acta, Gen. Subj.* **2012,** 1820, 226–236.
37. Rabe, M.; Verdes, D.; Seeger, S., Understanding protein adsorption phenomena at solid surfaces. *Adv. Colloid Interface Sci.* **2011,** 162, 87–106.
38. Harris, W. R.; Yang, B.; Abdollahi, S.; Hamada, Y., Steric restrictions on the binding of large metal ions to serum transferrin. *J. Inorg. Biochem.* **1999,** 76, 231–242.
39. Brock, J., Lactoferrin: a multifunctional immunoregulatory protein? *Immunol. Today* **1995,** 16, 417–419.
40. El-Loly, M. M.; Mahfouz, M. B., Lactoferrin in Relation to Biological Functions and Applications: A Review. *Int. J. Dairy Sci.* **2011,** 6, 79–111.
41. Dickinson, E., Stability and rheological implications of electrostatic milk protein–polysaccharide interactions. *Trends Food Sci. Technol.* **1998,** 9, 347–354.
42. Ye, A., Complexation between milk proteins and polysaccharides via electrostatic interaction: principles and applications – a review. *Int. J. Food Sci. Technol.* **2008,** 43, 406–415.
43. Alila, S.; Boufi, S.; Belgacem, M. N.; Beneventi, D., Adsorption of a Cationic Surfactant onto Cellulosic Fibers I. Surface Charge Effects. *Langmuir* **2005,** 21, 8106–8113.
44. Dautzenberg, H., Polyelectrolyte Complex Formation in Highly Aggregating Systems. 1. Effect of Salt: Polyelectrolyte Complex Formation in the Presence of NaCl. *Macromolecules* **1997,** 30, 7810–7815.
45. Crouzier, T.; Picart, C., Ion Pairing and Hydration in Polyelectrolyte Multilayer Films Containing Polysaccharides. *Biomacromolecules* **2009,** 10, 433–442.
46. Teramoto, A.; Takagi, Y.; Hachimori, A.; Abe, K., Interaction of albumin with polysaccharides containing ionic groups. *Polym. Adv. Technol.* **1999,** 10, 681–686.
47. Doublier, J. L.; Garnier, C.; Renard, D.; Sanchez, C., Protein–polysaccharide interactions. *Curr. Opin. Colloid Interface Sci.* **2000,** 5, 202–214.
48. Zou, S.; Magura, C. E.; Hurley, W. L., Heparin-binding properties of lactoferrin and lysozyme. *Comp. Biochem. Physiol. B* **1992,** 103, 889–895.

49. Masoodi, R.; Pillai, K. M., Darcy's law-based model for wicking in paper-like swelling porous media. *AIChE J*. **2010,** 56, 2257–2267.

50. Masoodi, R.; Tan, H.; Pillai, K. M., Numerical simulation of liquid absorption in paper-like swelling porous media. *AIChE J*. **2012,** 58, 2536–2544.

Chapter 4 Urinary protein sensing paper device relying on text as semi-quantification signal

This chapter is based on
"Text-displaying colorimetric paper-based analytical device",
Kentaro Yamada; Koji Suzuki; Daniel Citterio,
ACS Sensors, 2017, in press (DOI: 10.1021/acssensors.7b00464).

Summary

This work describes a paper-based analytical device allowing the direct semi-quantitative interpretation of the result of a chemical assay in the form of "text". The combined use of a classical colorimetric indicator system and an additional inert colorant enables a versatile text-displaying detection mechanism on a paper device. For proof-of-concept, urinary protein has been selected as a model analytical target. The whole text-displaying paper device has been developed based on printing techniques including wax printing, inkjet printing, and 3D printing. The results of user tests performed with protein (human serum albumin) samples in aqueous standard solutions and human urine demonstrated that the accuracy was comparable for the elaborated paper device (74.7% for standard samples and 66.7% for urine) and a conventional colorimetric urine dipstick (67.2% for standard samples and 65.3% for urine). Storage stability as long as at least 117 days has been confirmed based on software-assisted quantitative color analysis. The developed text-displaying approach is proposed as an alternative simple detection motif for paper-based analytical devices.

4.1. Introduction

The last decade has witnessed an explosive growth of devices for point-of-care testing (POCT) made from paper. Although diagnostic devices relying on paper substrates have been known from much earlier, for example urinary glucose testing paper from the 1950s[1-2] and lateral flow immunochromatographic assays from the 1980s,[3-4] the application of paper-based analytical devices has greatly expanded since Whitesides and co-workers have introduced a microfluidically patterned paper platform in 2007.[5] A variety of attractive features of patterned paper (*e.g.* low-cost, disposability, multiplexation of assays, automation of chemical assay procedures) accelerated research and development of so-called microfluidic paper-based analytical devices (μPADs) targeting a wide array of application fields including medical diagnosis,[6-12] environmental monitoring,[8-9, 13-14] and food quality monitoring,[8-9] among others.

Since paper devices were rediscovered as a promising (bio)chemical analysis tool a decade ago, their practical application has gained significant interest. However, their real-world application is still scarce, despite the originally high expectation of rapid success. On the basis of conclusions drawn in recently published review articles on paper-based devices, the signal readout and interpretation method is one of the most crucial factors determining the chances of practical use of paper devices for POCT.[10, 15-16] Colorimetric detection is the simplest signaling motif of which the result is ideally observable by the naked eyes. Despite the signal being visible, paper-based colorimetric assays are generally reliant on software-assisted digital color analysis[17]. Besides commercial paper-based tests (*e.g.* urine dipsticks, pregnancy test kits), there are only few examples of instrument-free detection approaches, including the use of a color reference guide for semi-quantitative detection of liver function marker enzymes[18-20] and the appearance of colored circles on a paper surface providing a simple qualitative yes/no output for pregnancy testing[21] or the detection of malaria and dengue fever biomarkers[22]. With the purpose of achieving simpler colorimetric detection requiring no analysis equipment, several alternative approaches of signal interpretation have been elaborated. In 2012, Lewis *et al.* have achieved semi-quantitative detection of H_2O_2, either by counting the number of colored paper regions or by measuring the time until the appearance of a colored spot on a paper device.[23] Similarly, pH titration targeting environmental water analysis[24] and lateral flow tests for nucleic acids targeting infectious disease

diagnosis[25-26] have been demonstrated relying on counting-based quantification. Another simplified colorimetry-based signaling motif includes analog thermometer-style quantitative analysis, where the length of a colored section in a straight paper channel reflects the amount of analytical target in the sample (distance-based approach).[27-28] However, despite the very simple nature of these readout motifs, the risk of result misinterpretation, although relatively low, cannot be excluded for non-trained users, for example in situations of fatigue or stress.

Besides the aforementioned simple detection approaches for paper devices (counting,[23-26, 29] timing,[23, 30-32] distance measurement[27-28, 33-35]), a "text"-based signal allows the most straightforward result interpretation. In 2012, the Shen group has reported a paper device that reports the ABO and Rh blood groups in the form of letters (A, B, O) and symbols (+, −) directly appearing on the device.[36] Similarly, aptamer-based ATP (adenosine triphosphate) and PDGF (platelet-derived growth factor) detection has been successfully performed by Brennan and co-workers relying on the "A" and "P" letters displayed in fluorescence mode on a paper device.[37] More recently, multiplexed antigen detection on a single lateral flow immunoassay device has been demonstrated mimicking a seven-segment display.[38] Despite the simplicity of result interpretation, reports on text-displaying assays on paper devices remain scarce as compared to other simple signaling methodologies. More specifically, they have been limited to "off-on" type of colorimetric signaling, where text or text segments appear in the presence of target analyte, but a quantitative readout is not required. A text-based colorimetric signaling approach providing (semi-)quantitative results has to the best of our knowledge never been reported.

The current work describes a new approach to realize semi-quantitative text-based analyte detection on a paper device using a classical colorimetric indicator system undergoing an analyte concentration-dependent color change. The target-responsive colorimetric indicator is deposited onto the paper substrate in the form of "text" (*e.g.* numbers, symbols) indicating all possible assay results. For this purpose, inkjet-printing technique has been adopted, because reproducible deposition of various reagent solutions is performable with flexible arrangements.[9, 39-41] The text-displaying assay is achieved with the aid of an additional transparent colored layer to "hide" ("screen") a part of the text-shaped colorimetric indicators. This transparent colored layer

(referred to as "screening color") can be prepared by means of color laser printing on a transparent film. Since the mechanism is reliant on a colorimetric indicator and a laser-printed screening color, the current system of text-display-based detection on paper devices is compatible with a wide class of analytes, as long as a classical colorimetric indicator system is available.

For proof-of-concept, urinary protein has been selected as a model analytical target. In routine urine tests, the concentration of protein is inspected by using a colorimetric dipstick, where a user compares the sample to the reference color guide, followed by evaluation in a semi-quantitative manner relying on symbols (typically in 6 levels; −, Trace (Tr.), 1+, 2+, 3+, and 4+ from the lowest). The developed text-displaying paper device allows users to semi-quantitatively determine the sample protein concentration by reading out the highest recognizable concentration symbol. Result comparison of observer-dependent readout tests using the text-displaying paper device and a commercial colorimetric dipstick, as well as a storage stability study have been performed for analytical performance evaluation. The elaborated urinary protein sensing device exhibited a comparable accuracy to the conventional colorimetric urine dipstick and shelf life of at least approximately 4 months at room temperature under dry and dark conditions.

4.2. Experimental section

4.2.1. Reagents and instruments

All reagents were used without further purification. Tetrabromophenol blue (TBPB), γ-globulin was purchased from Sigma-Aldrich (St. Louis, MO). Ethanol, citric acid, trisodium citrate dehydrate, sodium hydroxide, human serum albumin (HSA), and lysozyme were purchased from Wako Pure Chemical Industries Ltd. (Osaka, Japan). Urine dipsticks (Uropaper III 7S) were purchased from Eiken Chemical Co., Ltd. (Tokyo, Japan). Ultrapure water (> 18 MΩ cm) was obtained from a PURELAB flex water purification system (ELGA, Veolia Water, Marlow, UK). Whatman grade 1 filter paper was purchased from GE Healthcare (Buckinghamshire, UK) and was cut into A4 size before fabricating the devices. Reflectance spectra of the paper surface were acquired with an R200-7-VIS-NIR reflection probe combined with a USB2000+ miniature

spectrometer (Ocean Optics, Dunedin, FL).

A ColorQube 8570 printer (Xerox, Norwalk, CT, USA) was used to pattern wax on filter paper. A thermally-actuated Canon iP2700 inkjet printer (Canon, Tokyo, Japan) was used to deposit the TBPB colorimetric reagent. For this purpose, the standard color cartridge of the Canon printer was cut open and the sponge inside was removed, followed by washing with copious amounts of ultrapure water.

4.2.2. Paper device fabrication

An A4 sheet of filter paper was fed into the wax printer to pattern the hydrophobic frame defining the sensing region and the "–" symbol designed with PowerPoint (Microsoft). The printed wax was melted into the entire thickness of the filter paper by heating with a NHS-450ND hot plate (Nissinrika, Tokyo, Japan) for 3 min at 150°C. Citrate buffer (pH 3.0, 250 mM) was manually pipetted onto the entire sensing region (70 μL per sensing region). After complete drying at room temperature, 1 mM TBPB solution in 1:2 (v/v) ethanol/water was inkjet-printed in 8 printing cycles (for the "Tr., 1+, 2+, 3+" symbols) or 15 printing cycles (for the "4+" symbol).

An A4 size lamination sheet (150 μm thickness) obtained from JOINTEX (Tokyo, Japan) was cut with a Silhouette Cameo electronic knife blade cutting machine (Silhouette, Lindon, UT, USA) to prepare a sample introduction area on the top sheet layer. Lamination was performed on a QHE325 hot laminator (Meikoshokai, Tokyo, Japan). The instrument settings for substrate thickness and feeding speed were "150 μm" and "fast", respectively. The detailed design and dimensions of the paper device are shown in Figure 4-1.

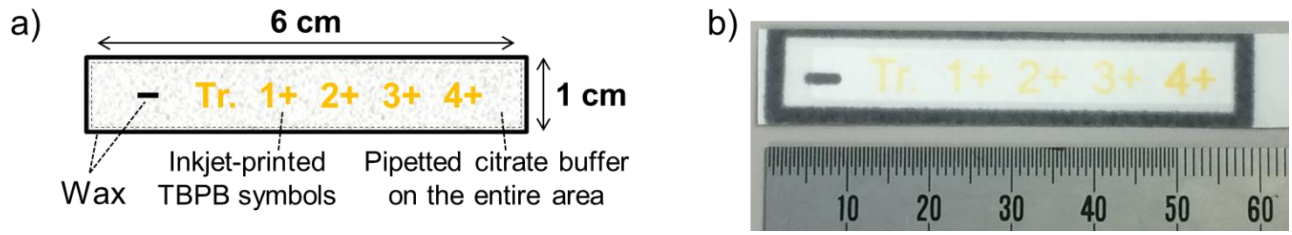

Figure 4-1. a) Schematic illustration and b) photograph of the paper device for text-displaying semi-quantitative protein detection.

4.2.3. Integration of screening color

To achieve a text-displaying assay, the screening color was overlaid with the colorimetric paper device. The screening color was printed on a laser transparency film (3M, Maplewood, MN, USA) with a DocuCentre-IV C2263 laser printer (Fuji Xerox, Tokyo, Japan). A 3D-printed housing for the paper device and the screening color-printed film was designed with 123D Design (Autodesk, San Rafael, CA, USA). An Objet30 Prime (Stratasys, Eden Prairie, MN, USA) was used to fabricate the 3D printed housing (detailed design is described in Figure 4-2). To prepare the screening color unit, the transparency film was inserted into the slit of the 3D-printed housing.

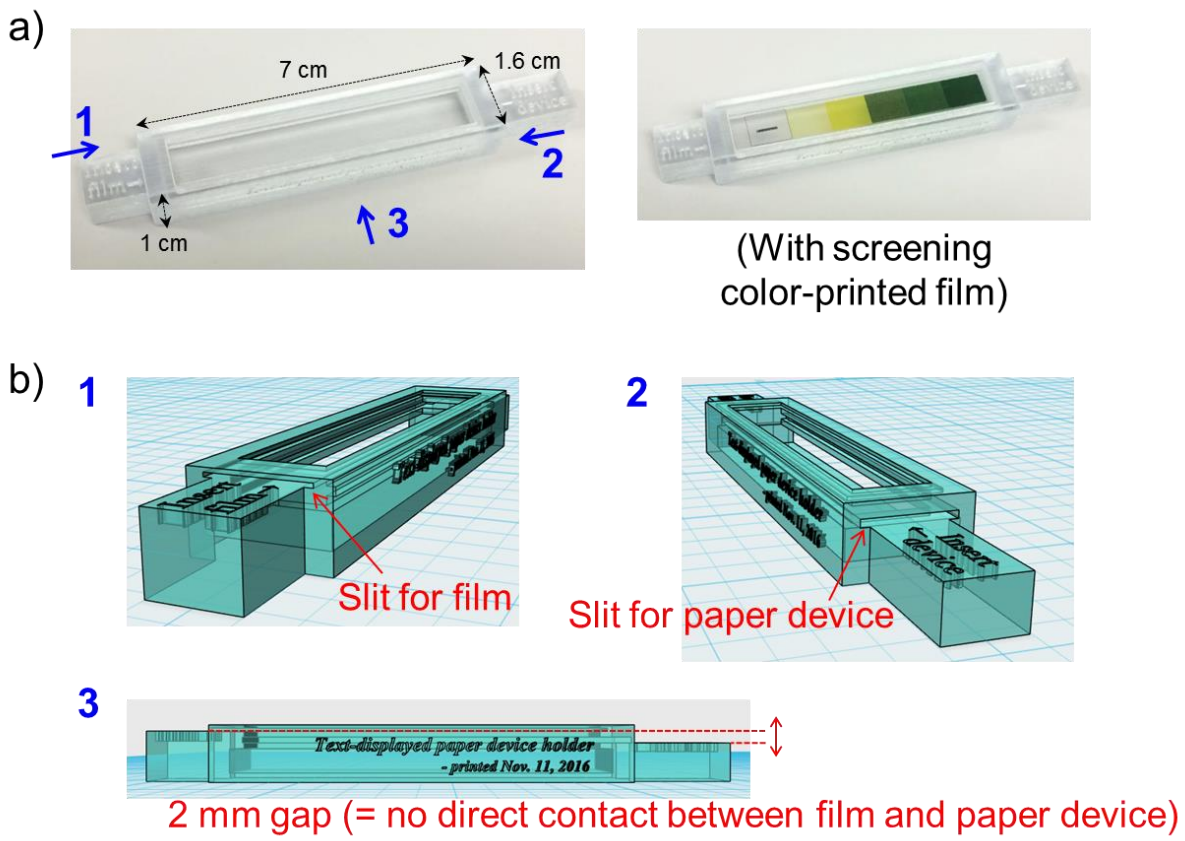

Figure 4-2. Design of the 3D-printed unit for text-displaying protein sensing on a paper device. a) Photograph of the 3D-printed unit before (left) and after (right) inserting the screening color-printed film. b) CAD software-based design showing the structure of the 3D-printed unit from three viewpoints as indicated by arrows accompanied by numbers in a).

4.2.4. Text-displaying protein assay

Aqueous solutions of HSA were prepared as protein standard samples. Spiked real urine samples were prepared by dissolving HSA powder in a urine sample collected from a healthy adult. Operational procedure of the text-displaying semi-quantitative protein assay is shown in Scheme 4-1. Briefly, the entire paper device was first dipped in approximately 15 mL of protein sample prepared in a centrifuge tube and removed quickly. Immediately after, the paper device was inserted into the slit of the 3D-printed screening color unit to observe the displayed symbol(s). The semi-quantitative result was recorded by reading the highest protein concentration symbol displayed on the resulting paper device against a white background.

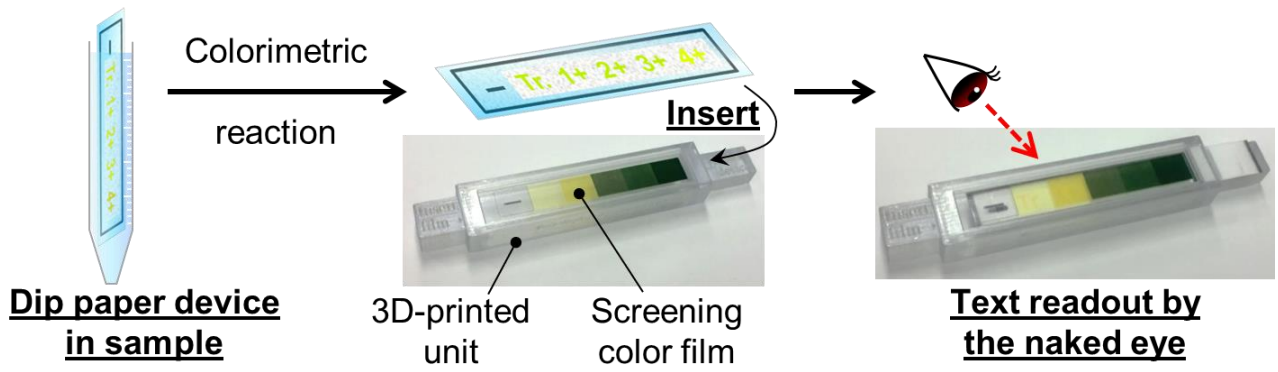

Scheme 4-1. Operational process of the text-displaying protein assay.

4.2.5. Storage stability evaluation

For the storage stability evaluation, the symbols on the text-displaying paper device have been replaced by circular spots with 6 mm diameter. Except for the shape of TBPB deposition, the design is identical to that of the text-displaying paper device. The device was wrapped with aluminum foil and stored in a desiccator at room temperature for various time spans (8, 20, 27, 41, 72, 117 days). After sample application, a color image of the device was acquired with a CanoScan 9000F Mark II scanner (Canon, Tokyo, Japan). Numerical color intensity values of the scanned TBPB spots were analyzed using the ImageJ software (NIH, Bethesda, MD, USA).

4.3. Results and discussion

4.3.1. Principle of text-displaying colorimetric assay

The text-displaying colorimetric assay motif proposed in this work involves two components: (1) a paper-based device with the colorimetric indicator (TBPB) undergoing protein concentration-dependent color changes inkjet-deposited in the form of symbols indicating the assay result, and (2) an additional transparent colored layer to screen the symbol-shaped colorimetric indicator deposited on the paper device (screening color). A schematic illustration depicting the working principle is shown in Figure 4-3. The symbol-shaped TBPB shows protein concentration-dependent colorimetric response (Figure 4-3a). After the colorimetric response, a series of screening colors is overlaid to shield the TBPB symbols with weaker color intensity than that of the respective screening color, making the symbols invisible to the human eye (Figure 4-3b). The current mechanism allows users to semi-quantitatively determine the concentration of protein by reading out the recognizable symbol interpreting the maximum protein concentration.

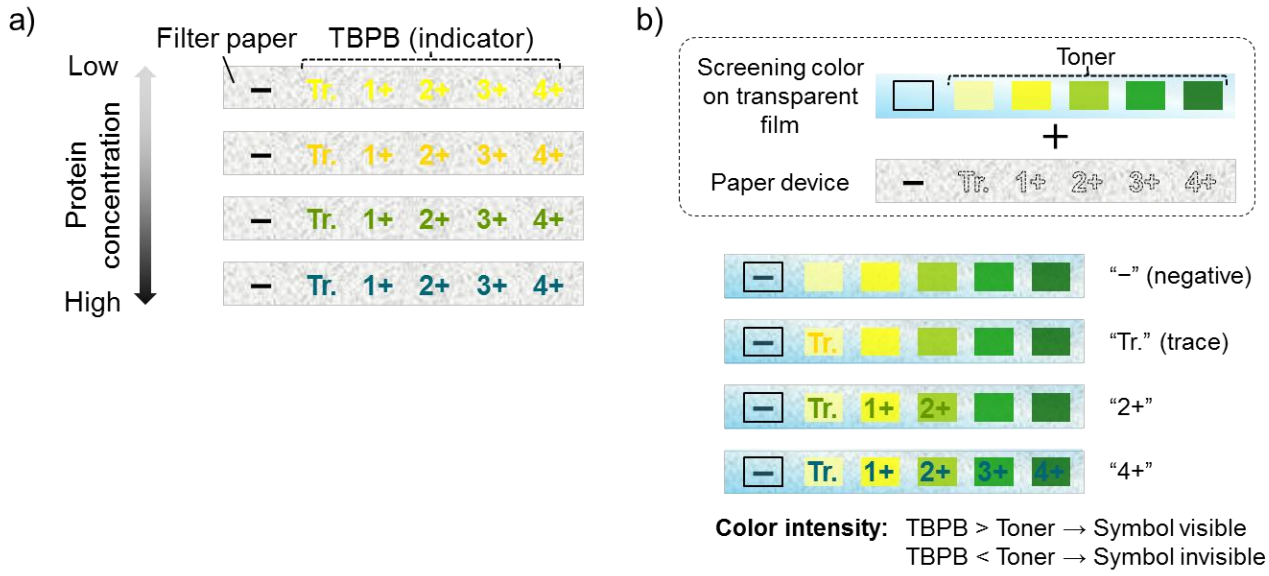

Figure 4-3. Schematic illustration explaining the working principle of the text-displaying paper device for protein assay utilizing a TBPB-based colorimetric indicator system: a) all inkjet-deposited TBPB symbols on the paper device exhibit identical colorimetric response depending on the sample protein concentration; b) after the colorimetric reaction, the paper device is overlaid with a toner-printed transparent film with the screening color. Since the resulting recognizable symbol is dependent on the color change of TBPB symbols, sample protein concentration can be semi-quantitatively determined by reading the highest visible symbol on the device.

Figure 4-4a shows the reflectance spectral changes upon the colorimetric response of the TBPB indicator to protein on the paper substrate, which manifest themselves in the form of wavelength-dependent decreasing reflectance of the paper surface. The reflectance was converted to "pseudo-absorbance" of the paper using the following equation:

$$Abs' = Ref_{\text{paper}} - Ref_{\text{sample}} \quad (1)$$

where Abs' is the pseudo-absorbance within a TBPB spot on the paper surface after exposure to sample, Ref_{paper} is the reflectance of bare filter paper, and Ref_{sample} is the reflectance of a TBPB spot after exposure to sample. The spectra in Figure 4-4b depict increasing pseudo-absorbance of the paper surface around 620 nm with increasing sample protein concentration. In the case of protein detection by the TBPB indicator, the screening colors need therefore to be designed in such a way that their intensity gets more intense along with the increase of the protein concentration expressed by the TBPB symbol. It should be noted that the screening colors selected here are specific for the indicator system used for protein detection. If applied to other analytical targets, the colors on the transparent film need to be tailored depending on the color change pattern of the selected indicator.

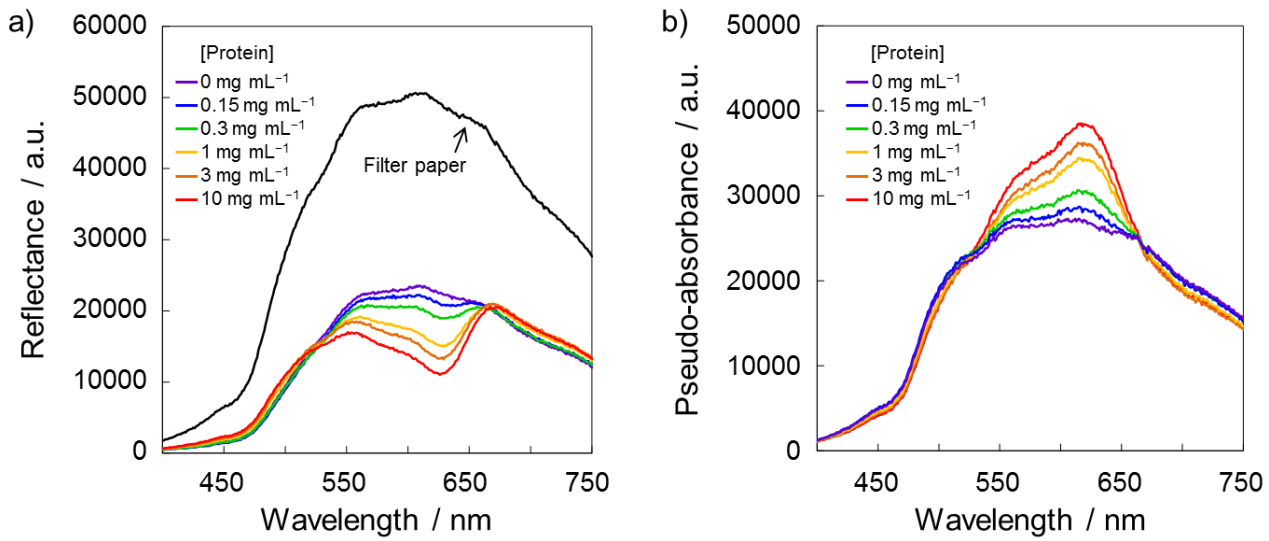

Figure 4-4. Measurement of optical properties of the paper surface: a) reflectance spectra of bare filter paper (black line) and TBPB spots on paper at 8 inkjet-printing cycles after exposure to protein samples of different concentration (colored lines); b) spectra showing the pseudo-absorbance of the TBPB paper spots calculated based on eq. (1).

4.3.2. Optimization of the text-displaying assay

Table 4-1 summarizes the required visibility of each TBPB symbol depending on the protein concentration in the sample. For the sake of accuracy, all TBPB symbols in combination with the overlaid screening color should exhibit a particularly clear color transition at their "off-on" (corresponding to "invisible-visible") switching concentration. Since the color transition behavior of the colorimetric detection of protein assay was strongly dependent on the amount of deposited TBPB, an optimization study on inkjet-printing cycles of TBPB solution has been carried out.

Table 4-1. Required visibility of TBPB symbols at each sample protein concentration.

Protein /mg mL^{-1}	Symbol[a]	TBPB symbols on paper device[b]				
		Tr.	1+	2+	3+	4+
0	–	Off	Off	Off	Off	Off
0.15	Trace	On	Off	Off	Off	Off
0.3	1+	On	On	Off	Off	Off
1	2+	On	On	On	Off	Off
3	3+	On	On	On	On	Off
10	4+	On	On	On	On	On

[a] The relationship between protein concentration in urine samples and the semi-quantitative readout results represented by the selected symbols reflect the categories used in the commercial colorimetric dipstick applied as reference method in this work. [b] "Off" and "on" states indicate that the TBPB symbol is "invisible" or "visible" after overlaying the screening color, respectively. The "–" symbol patterned with black wax remains always visible.

Figure 4-5a shows the colorimetric response of TBPB spots to the presence of protein depending on the number of inkjet-printing cycles (2−20) of the indicator. Not surprisingly, increased cycles of inkjet deposition of TBPB resulted in stronger overall color intensities. The result of the red color intensity values, which exhibited the largest sensitivity among the RGB color coordinates, is shown in Figure 4-5b as a representative example. Interestingly, a clearly different sensitivity pattern of the colorimetric response was observed in the hue signal-based calibration curves (Figure 4-5c). Larger amounts of deposited TBPB resulted in an onset of

sensitive hue value response only at higher protein concentration, whereas signal increase was low in the lower concentration range. Because the hue parameter virtually reflects the color regardless of its intensity[30], the results of Figure 4-5c indicate that the reaction efficiency between TBPB and protein changes depending on the amount of TBPB indicator present on the paper substrate. This observation is mainly attributed to the increased hydrophobicity of the paper surface modified with larger amounts of TBPB, which is insoluble in aqueous systems in its protonated form (before reaction with protein). It is postulated that the reduced accessibility of protein present in the aqueous sample to the TBPB-rich paper surface led to a hue value response only at higher protein concentration.

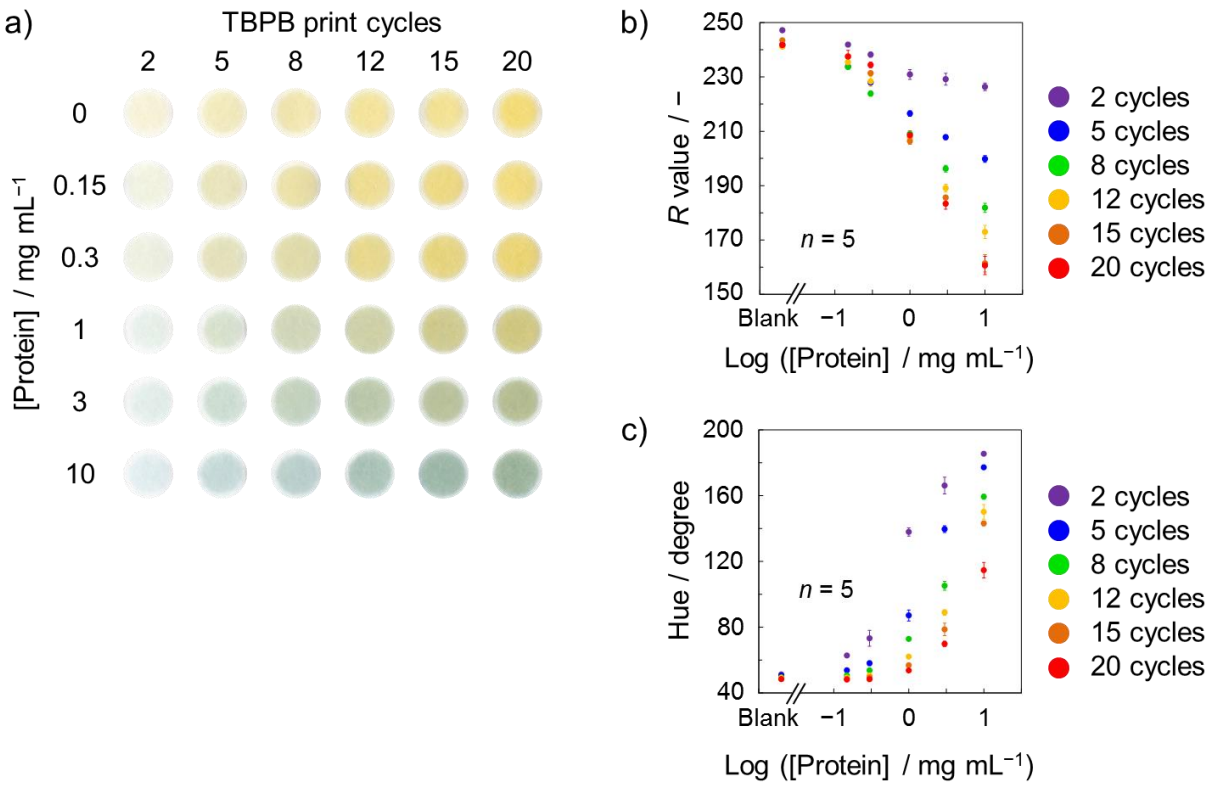

Figure 4-5. Relationship between the number of TBPB inkjet-printing cycles and colorimetric response to protein: a) scanned images of TBPB spots after contact with aqueous protein samples at various concentrations; b) protein concentration-dependent calibration curves based on the red color intensity value; c) protein concentration-dependent calibration curves based on the hue parameter.

As is clear from the above discussion, the selection of the number of inkjet-printing cycles of the indicator solution allows adjusting the color change of the TBPB symbols to each desired protein concentration range. The optimal deposition amounts have been selected as 8 printing cycles for the "Tr., 1+, 2+, 3+" symbols, whereas 15 printing cycles have been chosen for the "4+" symbol. These decisions were made solely based on subjective visual inspection of the color changes, rather than the data from numerical color intensity value analysis shown in Figures 4-5b and 4-5c, because visual information perceived by the naked human eye plays the most crucial role in the current text-displaying assay approach.

4.3.3. Standard sample analysis

Following assay optimization, text-displaying assays have been carried out using aqueous solutions of HSA. Figure 4-6a shows the original color change of paper devices after dipping into protein solutions, with TBPB symbols turning from yellow to greenish blue with increasing protein concentration. The combination of the paper device and the 3D-printed unit with inserted screening color film enables semi-quantitative protein sensing by reading out the highest symbol visible to the naked eye (Figure 4-6b). It should be noted that the photographs taken are unfortunately unable to reproduce the original quality of the visibility of the displayed symbols perceived by the naked human eye, despite all efforts to modify the brightness, sharpness, and contrast. The use of a 3D-printed unit is helpful to avoid direct contact between the screening color-printed film and the underlying paper device, and it guarantees a constant distance between the two layers. Avoiding contact of the film and the paper device eliminates film contamination with sample, as well as blurring of the TBPB symbols. A constant distance between the film and the paper device is crucial for the reproducible readout of the symbols. Nevertheless, the readout result is inherently observer-dependent because of individually different perception of the text. Ambiguity of assay results however, is also an issue when using a commercial colorimetric dipstick (Figure 4-6c), where significant discrepancy between the color reference (Figure 4-6c, left) and the actual sample pad color (Figure 4-6c, right) is observable, making the assignment of an observed color to a specific color reference strongly user dependent.

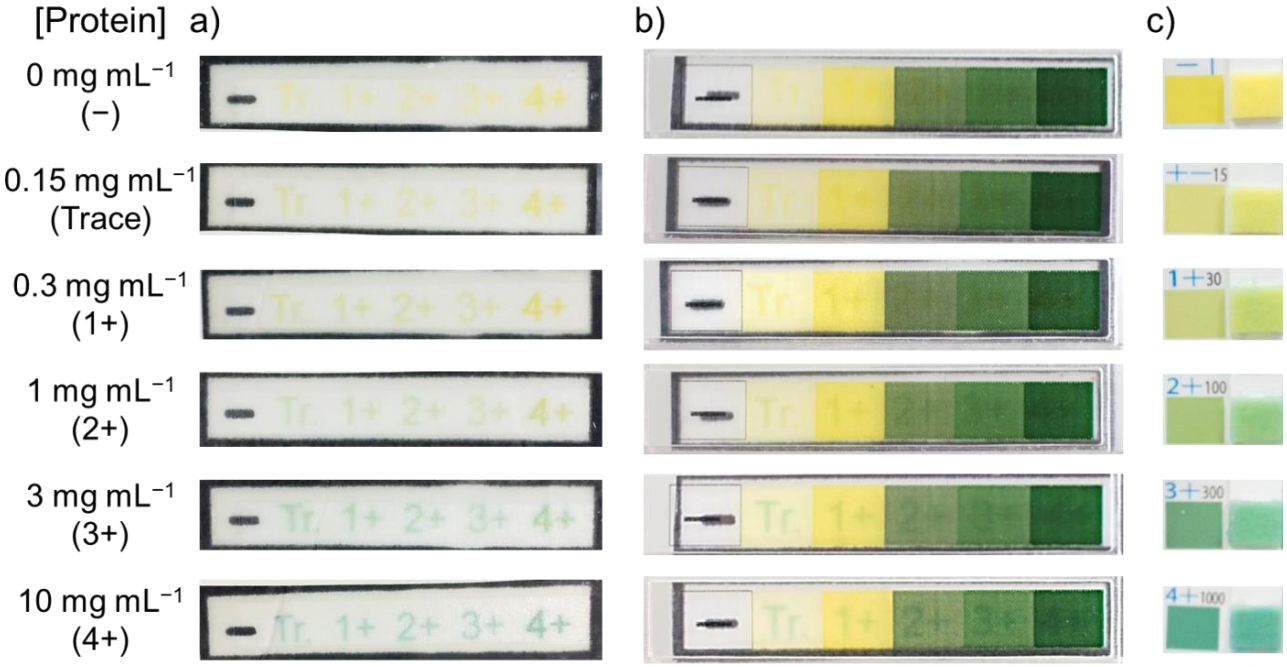

Figure 4-6. Protein concentration-dependent response of a) the original paper device; b) the text-displaying device composed of the paper layer with printed indicator, the 3D-printed unit, and the screening color-printed transparent film; c) the commercial colorimetric dipstick (left: color reference shown on package; right: actual color of test pad). Brightness, sharpness, and contrast have been modified for the sake of visibility in Figures 4-6a and 4-6b.

In this context, the analytical performances of the text-displaying protein detection and commercial colorimetric dipstick has been evaluated on the basis of user tests. Randomly ordered protein samples of various concentrations (0, 0.15, 0.225, 0.3, 0.6, 1, 3, 6, 10 mg mL^{-1}) have been blind tested by multiple observers using text-displaying devices and commercial colorimetric dipsticks. The results obtained by 40 users with the text-displaying device and the dipstick are summarized in Tables 4-2 and 4-3, respectively. To interpret the semi-quantitative user test results, three evaluation criteria as defined below, have been applied:

1) Accuracy: exact match between the readout result and the concentration of the prepared sample. In the case of intermediate concentrations located between two adjacent symbols, both the upper and the lower symbol results are regarded as accurate answers. However, the readout result of 1+ obtained from samples with a concentration of 0.225 mg mL^{-1} (intermediate between Tr. and 1+) has been exceptionally categorized as “inaccurate”, since this case falls under the false-positive criterion defined below.

2) False-positive: 1+ (corresponding to 0.3 mg mL^{-1}) or higher readout results obtained from samples with concentrations lower than 0.3 mg mL^{-1} (*i.e.* 0, 0.15, 0.225 mg mL^{-1}).

3) False-negative: − and Tr. (corresponding to 0 and 0.15 mg mL^{-1}, respectively) readout results obtained from samples with concentrations of 0.3 mg mL^{-1} or higher.

In defining the false-positive and false-negative results, 0.3 mg mL^{-1} has been adopted as the critical cutoff value, based on the generally-accepted reference value of urinary protein (< 0.3 mg mL^{-1})[43]. In Tables 4-2 and 4-3, accurate, false-positive and false-negative results are highlighted with green, orange and pink colors, respectively. On the other hand, results with no highlight identify inaccurate readouts not belonging to false-positive or false-negative results. One of the 40 test observers produced a particularly high number of readout mistakes when working with the text-displaying system (*e.g.* user number 13 failed with 6 out of 9 samples). In general however, there is a larger number of readouts within only one single mistake (16 users out of 40), compared to assays performed with dipsticks (6 users out of 40). In addition, user number 6, diagnosed with color vision anomaly, performed better in the text-displaying approach than with the colorimetric dipstick (results summarized in Table 4-4), where direct color comparison with a reference color guide is essential. Since the text-displaying detection relies on the contrast between the underlying text symbol and the screening color, the proposed approach might be an advantageous alternative to simple colorimetry for color vision-impaired users.

Table 4-2. Results obtained from user tests of aqueous HSA samples with text-displaying paper devices.

Protein / mg mL^{-1}	User number																			
	1	2	3	4	5	6	7	8	9	10	11	12	13	14	15	16	17	18	19	20
0	—	—	—	—	—	—	Tr.	Tr.	—	Tr.	—	—	—	—	—	Tr.	—	—	—	—
0.15	Tr.	—	Tr.	Tr.	Tr.	—	Tr.	—	—	Tr.	1+	1+	Tr.	—	—	1+	Tr.	Tr.	Tr.	Tr.
0.225	1+	1+	1+	1+	Tr.	Tr.	—	1+	Tr.	1+	1+	Tr.	1+	Tr.	Tr.	1+	1+	1+	Tr.	1+
0.3	1+	Tr.	1+	1+	1+	1+	1+	1+	1+	1+	1+	1+	Tr.	1+	Tr.	1+	2+	2+	Tr.	1+
0.6	2+	1+	2+	1+	2+	2+	1+	2+	1+	2+	1+	2+	1+	Tr.	1+	2+	2+	2+	1+	2+
1	2+	2+	2+	2+	2+	2+	2+	2+	1+	2+	2+	2+	1+	2+	1+	3+	3+	2+	1+	2+
3	3+	3+	2+	3+	3+	3+	3+	3+	3+	3+	3+	3+	2+	1+	2+	3+	3+	4+	2+	4+
6	3+	3+	3+	4+	3+	4+	4+	3+	2+	4+	4+	4+	2+	3+	3+	4+	3+	4+	3+	4+
10	3+	4+	3+	4+	4+	4+	4+	4+	4+	4+	4+	4+	3+	3+	3+	4+	4+	4+	4+	4+

Table 4-2. *(continued)*

Protein / mg mL^{-1}	User number																			
	21	22	23	24	25	26	27	28	29	30	31	32	33	34	35	36	37	38	39	40
0	—	—	—	—	—	—	—	—	—	—	—	Tr.	—	—	—	—	Tr.	—	—	—
0.15	—	Tr.	—	Tr.	—	Tr.	Tr.	—	1+	Tr.	Tr.	Tr.	Tr.	Tr.	Tr.	Tr.	Tr.	—	—	Tr.
0.225	Tr.	1+	1+	1+	Tr.	1+	1+	Tr.	1+	1+	1+	1+	Tr.	1+	Tr.	1+	Tr.	Tr.	Tr.	1+
0.3	1+	Tr.	1+	1+	1+	1+	2+	1+	1+	1+	1+	1+	1+	1+	1+	1+	1+	1+	1+	2+
0.6	1+	1+	2+	2+	2+	2+	2+	1+	2+	2+	2+	2+	2+	2+	2+	2+	2+	2+	2+	2+
1	1+	1+	1+	3+	3+	2+	2+	2+	3+	2+	2+	2+	2+	2+	2+	2+	2+	2+	2+	2+
3	3+	3+	4+	3+	3+	3+	3+	2+	3+	3+	3+	4+	4+	3+	3+	3+	3+	3+	3+	4+
6	3+	3+	4+	3+	3+	4+	3+	3+	4+	3+	3+	3+	4+	4+	4+	4+	4+	3+	4+	4+
10	3+	4+	4+	4+	3+	4+	4+	3+	4+	4+	4+	4+	4+	4+	4+	4+	4+	4+	4+	4+

Green highlights identify accurate readout results. Orange and pink highlights identify the samples determined as false-positive and false-negative, respectively. Results with no highlight identify inaccurately determined samples neither being false-positive nor false-negative.

Table 4-3. Results obtained from user tests of aqueous HSA samples with commercial colorimetric dipsticks.

Protein / mg mL^{-1}	User number																			
	1	2	3	4	5	6	7	8	9	10	11	12	13	14	15	16	17	18	19	20
0	–	–	–	–	–	–	–	–	–	–	–	–	–	–	–	Tr.	–	–	–	–
0.15	1+	Tr.	1+	Tr.	1+	2+	2+	1+	1+	1+	–	1+	1+	1+	Tr.	1+	1+	1+	1+	Tr.
0.225	1+	1+	1+	Tr.	1+	Tr.	1+	1+	1+	1+	1+	1+	1+	1+	Tr.	1+	1+	1+	1+	1+
0.3	2+	1+	1+	1+	1+	Tr.	2+	1+	1+	2+	2+	2+	1+	2+	1+	1+	2+	2+	2+	2+
0.6	2+	2+	2+	2+	2+	2+	2+	2+	2+	2+	2+	2+	2+	2+	2+	2+	2+	2+	2+	2+
1	3+	2+	2+	2+	2+	2+	Tr.	2+	2+	3+	3+	2+	2+	2+	2+	3+	3+	3+	3+	3+
3	3+	3+	3+	3+	3+	1+	3+	3+	4+	3+	3+	3+	4+	3+	3+	3+	3+	3+	4+	4+
6	3+	4+	3+	4+	4+	3+	4+	3+	4+	4+	4+	3+	4+	4+	4+	4+	4+	4+	4+	4+
10	4+	4+	3+	3+	4+	4+	4+	4+	4+	4+	4+	4+	4+	4+	4+	4+	4+	4+	4+	4+

Table 4-3. *(continued)*

Protein / mg mL^{-1}	User number																			
	1	2	3	4	5	6	7	8	9	10	11	12	13	14	15	16	17	18	19	20
0	–	–	–	–	–	–	–	–	–	–	–	–	–	–	–	–	–	–	–	–
0.15	1+	1+	1+	Tr.	1+	1+	2+	1+	1+	1+	Tr.	Tr.	Tr.	1+	Tr.	–	–	–	–	–
0.225	1+	1+	1+	Tr.	1+	1+	1+	1+	1+	Tr.	1+	1+	1+	Tr.	1+	1+	Tr.	Tr.	1+	Tr.
0.3	2+	1+	2+	1+	1+	2+	2+	2+	1+	2+	2+	2+	1+	1+	2+	1+	1+	1+	1+	1+
0.6	2+	2+	2+	2+	2+	2+	2+	2+	2+	1+	2+	2+	2+	2+	2+	2+	2+	2+	2+	2+
1	3+	2+	3+	2+	2+	2+	2+	3+	2+	3+	3+	2+	2+	2+	3+	2+	2+	2+	2+	3+
3	4+	3+	3+	3+	4+	3+	3+	4+	3+	4+	4+	4+	4+	3+	4+	3+	4+	3+	3+	4+
6	4+	3+	4+	4+	4+	3+	4+	4+	3+	3+	4+	4+	3+	4+	4+	4+	3+	3+	3+	3+
10	4+	3+	4+	4+	4+	4+	4+	4+	3+	4+	4+	4+	4+	4+	4+	4+	4+	4+	4+	4+

Green highlights identify accurate readout results. Orange and pink highlights identify the samples determined as false-positive and false-negative, respectively. Results with no highlight identify inaccurately determined samples neither being false-positive nor false-negative.

Table 4-4. Result of user number 6 (diagnosed as having a color vision anomaly) for aqueous HSA samples with a) text-displaying paper devices and b) commercial colorimetric dipsticks. Grids surrounded by black lines identify accurate readout results.

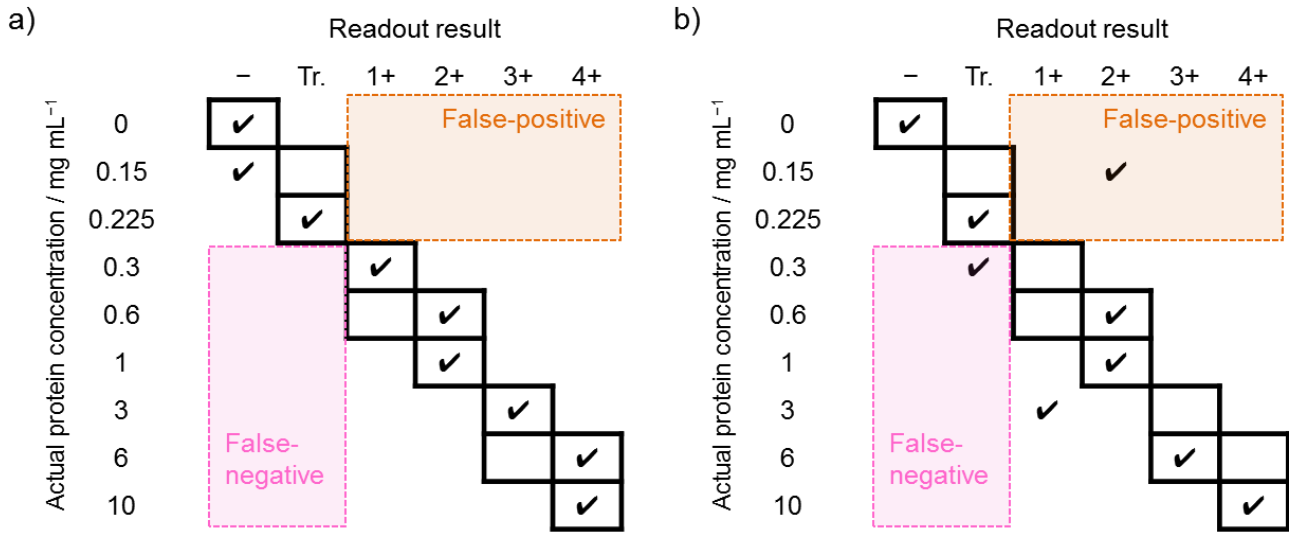

Heat maps of Figure 4-7 and Table 4-5 summarizes the comparison of the analytical performance of the text-displaying device and the colorimetric dipstick regarding all three evaluation criteria applied in this study. Notable difference was obtained in the accuracy rate and the number of false-positive results (highlighted in green and orange in Tables 4-2 and 4-3, respectively). While the dipstick showed better performance in identifying samples with absence of protein (1/40 compared to 6/40 misinterpretations of 0 mg mL^{-1} samples), a truly "protein positive" status (≥0.3 mg mL^{-1}) was more accurately identified when using the text-displaying device. This improvement of the text-displaying approach mainly contributes to the better accurate rate than the colorimetric dipstick. Finally, the chance of reading out a false-negative result was slightly increased in the current text-displaying device in comparison with the dipstick. It is possible to reduce false-negative results in the text-displaying approach by dampening the intensity of the screening color for the "1+" symbol. However, this would be accompanied by an increased frequency of false-positive results.

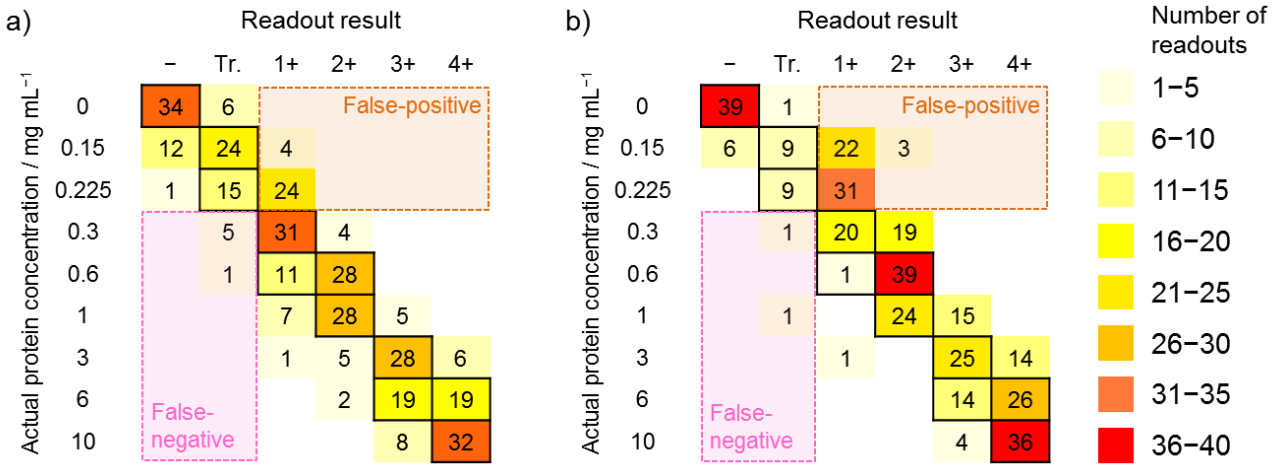

Figure 4-7. Heat maps showing the distribution of readout results obtained from aqueous standards of HSA by using a) the text-displaying device; b) the commercial colorimetric dipstick. The data show the number of semi-quantitative readout results of 40 observers at each sample HSA concentration. Grids surrounded by black lines identify accurate readout results.

Table 4-5. Overall comparison of the analytical performance of the text-displaying device and the commercial colorimetric dipstick based on user tests with aqueous standard samples.

Method	Evaluation criteria[a]		
	Accuracy	False-positive	False-negative
Text	269/360 (74.7%)	28/360 (7.8%)	6/360 (1.7%)
Dipstick	242/360 (67.2%)	56/360 (15.6%)	2/360 (0.6%)

[a] Results are given as counts out of 360 tests (9 types of sample protein concentrations evaluated by 40 users) as well as the percentage.

4.3.4. Application to spiked urine samples

To evaluate the analytical performance under practical sample matrix conditions, a similar user test has been performed using urine samples spiked with HSA at various concentrations (0, 0.15, 0.225, 0.3, 0.6, 1, 3, 6, 10 mg mL^{-1}). A protein-free urine sample was collected from an adult regarded as healthy in a routine medical checkup. The results from 8 users are summarized in Tables 4-6 and 4-7 for the text-displaying device and the dipstick, respectively. Green and orange highlights identify accurate and false-positive results, respectively. It should be noted that pink highlight has not been made since no false-negative result was obtained in HSA-spiked urine samples. For the sake of clearer result interpretation, heat maps summarizing the result of

Tables 4-6 and 4-7 are provided in Figures 4-8a and 4-8b, respectively.

The results summarized in Table 4-8 demonstrate that the overall readout accuracy of the text-displaying approach declined compared to the analysis of aqueous samples and was similar for the two detection approaches. Decreased accuracy rate of the developed system is closely related to the fact that inaccurate elevated concentration readouts occurred more frequently in detecting low protein concentrations (especially between 0 and 0.225 mg mL^{-1}) with the text-displaying device applied in urine samples compared to the analysis of simple aqueous solutions. This difference has been attributed to changes in pH to values higher than pH 3.0 required for optimal protein assays, due to the limited buffering capacity of the citrate buffer pre-deposited on the paper device. Human urine (normal pH 4.5-8.0)[43] has some natural pH-buffering capacity derived from its constituents such as ammonia, phosphate, and organic solutes[44], inducing a colorimetric pH response of TBPB symbols. For the same reason, an increased number of false-positive result read outs was obtained from the paper device applied to urine samples (15.2%) in contrast to aqueous samples (7.8%). This hypothesis is also supported by the fact that no false-negative results have been obtained.

Table 4-6. User test of HSA-spiked urine samples with text-displaying paper devices.

Protein / mg mL^{-1}	User number							
	1	2	3	4	5	6	7	8
0	Tr.	Tr.	–	Tr.	Tr.	Tr.	Tr.	–
0.15	Tr.	1+	Tr.	1+	Tr.	Tr.	1+	1+
0.225	1+	1+	Tr.	1+	1+	1+	1+	1+
0.3	1+	1+	1+	1+	1+	1+	1+	2+
0.6	1+	2+	2+	2+	2+	2+	3+	2+
1	2+	2+	2+	2+	2+	2+	3+	3+
3	3+	3+	3+	3+	3+	3+	4+	4+
6	4+	4+	3+	3+	4+	3+	4+	4+
10	4+	4+	4+	4+	3+	4+	4+	4+

Green highlights identify accurate readout results. Orange highlights identify the samples determined as false-positive. Results with no highlight identify inaccurately determined samples being neither false-positive nor false-negative.

Table 4-7. User test of HSA-spiked urine samples with a commercial colorimetric dipstick.

Protein / mg mL^{-1}	User number							
	1	2	3	4	5	6	7	8
0	Tr.	—	Tr.	Tr.	—	Tr.	—	—
0.15	1+	Tr.	1+	1+	Tr.	1+	1+	1+
0.225	Tr.	1+	1+	1+	1+	1+	1+	1+
0.3	1+	1+	2+	2+	1+	1+	2+	2+
0.6	1+	1+	2+	2+	2+	2+	2+	2+
1	2+	2+	2+	2+	2+	2+	2+	2+
3	2+	3+	3+	4+	2+	3+	3+	3+
6	3+	3+	4+	4+	3+	4+	3+	4+
10	4+	4+	4+	4+	3+	4+	4+	4+

Green highlights identify accurate readout results. Orange highlights identify the samples determined as false-positive. Results with no highlight identify inaccurately determined samples being neither false-positive nor false-negative.

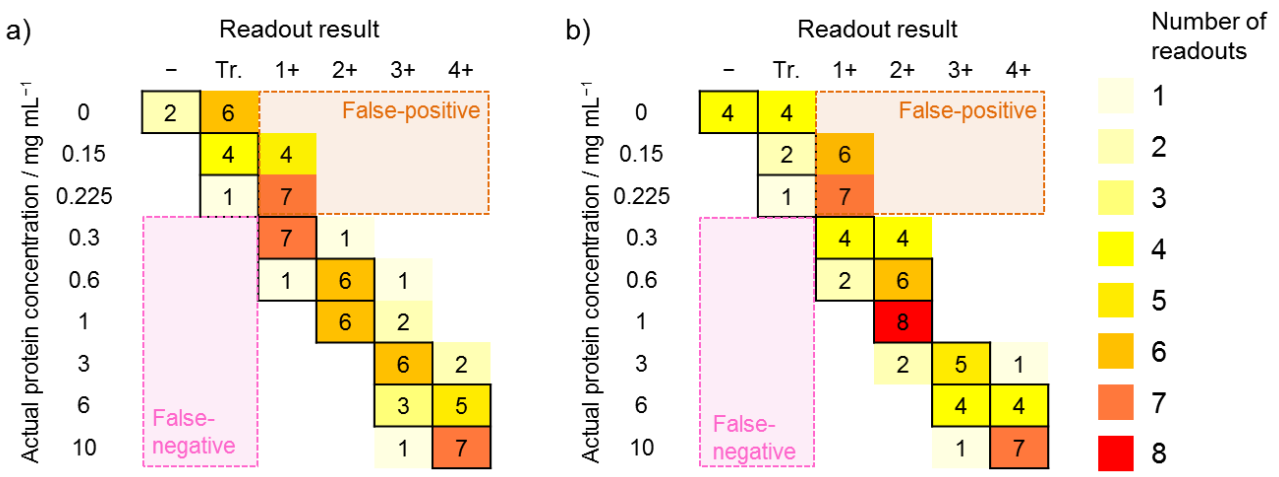

Figure 4-8. Heat maps showing the distribution of readout results obtained from HSA-spiked urine samples by using a) the text-displaying device; b) the commercial colorimetric dipstick. The data show the number of semi-quantitative readout results of 8 observers at each sample HSA concentration. Grids surrounded by bold black lines identify accurate readout results.

Table 4-8. Overall comparison of the analytical performance of the text-displaying device and the commercial colorimetric dipstick based on user tests with HSA-spiked urine samples.

Method	Evaluation criteria[a]		
	Accuracy	False-positive	False-negative
Text	48/72 (66.7%)	11/72 (15.2%)	0/72 (0%)
Dipstick	47/72 (65.3%)	13/72 (18.1%)	0/72 (0%)

[a] Results are given as counts out of 72 tests (9 types of sample protein concentrations evaluated by 8 users) as well as the percentage.

4.3.5. Specificity/sensitivity comparison with other proteins

TBPB-based protein detection is more sensitive to albumin than other proteins, because of the presence of a large number of amino groups in albumin molecules to accept the protons of the indicator[43]. Sensitivity to other urinary proteins (lysozyme and γ-globulin) was evaluated to investigate the specificity of the text-displaying approach. Aqueous solutions of lysozyme and γ-globulin were prepared at concentrations of 0.15, 0.3, 1, 3, and 10 mg mL^{-1}. To prepare the γ-globulin samples, aqueous NaOH solution (50 mM) was added until complete dissolution of the protein. For quantitative evaluation of the colorimetric response, circular TBPB spots with 6 mm diameter were first prepared in 8 inkjet-printing cycles and exposed to the lysozyme and γ-globulin samples. The spot images were acquired by scanning with the scanner and RGB color intensity values were analyzed with the ImageJ software. The result of the red color intensity values, which exhibited the largest sensitivity, is shown in Figure 4-9a as a representative example. These protein samples were also subject to the text-displaying assay. Images of the text-displaying detection using lysozyme and γ-globulin are shown in Figures 4-9b and 4-9c, respectively. Table 4-9 summarizes the relationship between the results of the quantitative specificity evaluation based on RGB color intensity values and the text-displaying readout.

Results in Figure 4-9a demonstrate the limited colorimetric response of TBPB to lysozyme and γ-globulin, in accordance with the literature[43]. The images of text-displaying devices in Figures 4-9b and 4-9c confirm the lower sensitivity of the device to lysozyme and γ-globulin samples as compared to the same concentration (mg mL^{-1}) of albumin (Figure 4-9d). As summarized in Table 4-9, positive results ("1+" or higher) of the

text-displaying assay were obtained only at high concentrations of the other two proteins (10 mg mL^{-1} for lysozyme, 3 mg mL^{-1} for γ-globulin). Although not all known urinary proteins can be tested, the text-displaying device demonstrates specificity to urinary albumin in the same manner as most commercial urine dipsticks, of which the detection chemistry is also based on the TBPB indicator.

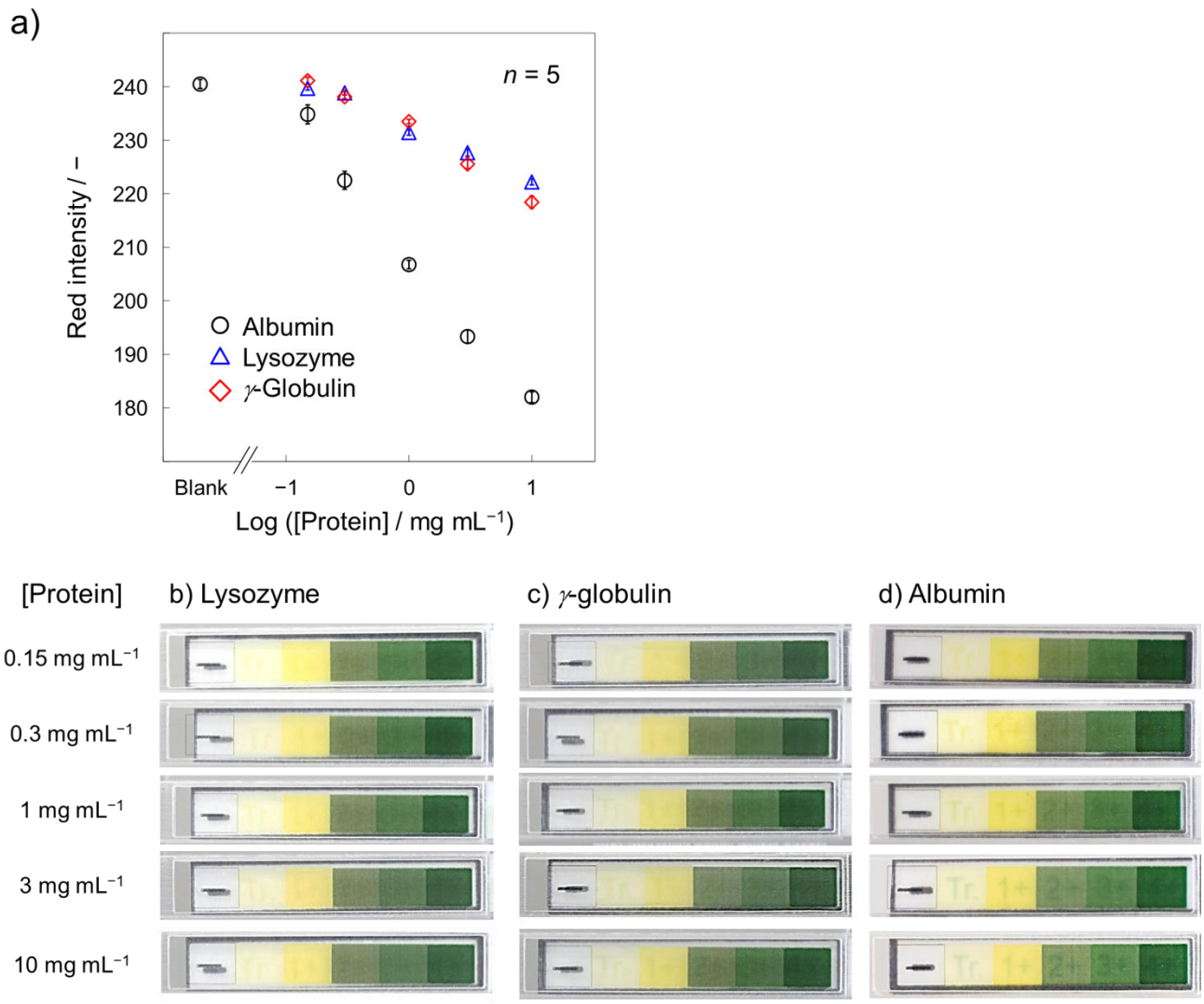

Figure 4-9. Result of specificity and sensitivity evaluation using lysozyme and γ-globulin: a) calibration curves based on the red color intensity value at various concentrations of HSA (black circles), lysozyme (blue triangles), and γ-globulin (red diamonds); b) images of the text-displaying paper device using lysozyme samples; c) images of the text-displaying paper device using γ-globulin samples; d) images of the text-displaying paper device using albumin samples for comparison purpose (identical to Figure 4-6b). Brightness, sharpness, and contrast have been modified for the sake of visibility.

Table 4-9. Relationship between the results of quantitative specificity/sensitivity evaluation based on RGB color intensity values and text-displaying readout for a) lysozyme and b) γ-globulin.

a)

Lysozyme concentration	Red	Green	Blue	Text-displayed result	
				Expected[a]	Readout[b]
0.15 mg mL^{-1}	239.7 ± 0.3	227.3 ± 0.4	168.7 ± 0.6	−	−
0.3 mg mL^{-1}	238.8 ± 0.4	226.9 ± 0.6	169.2 ± 0.8	− or Tr.	Tr.
1 mg mL^{-1}	231.4 ± 0.5	223.1 ± 0.8	169.9 ± 1.4	Tr. or 1+	Tr.
3 mg mL^{-1}	227.7 ± 0.7	221.3 ± 0.6	171.2 ± 1.4	Tr. or 1+	Tr.
10 mg mL^{-1}	222.2 ± 0.6	217.6 ± 0.7	168.3 ± 1.7	1+	1+

b)

γ-Globulin concentration	Red	Green	Blue	Text-displayed result	
				Expected[a]	Readout[b]
0.15 mg mL^{-1}	241.1 ± 0.6	228.7 ± 0.9	169.4 ± 1.0	−	−
0.3 mg mL^{-1}	238.1 ± 0.4	226.5 ± 0.3	168.2 ± 0.5	− or Tr.	Tr.
1 mg mL^{-1}	233.5 ± 0.4	224.7 ± 0.3	170.8 ± 0.3	Tr.	Tr.
3 mg mL^{-1}	225.5 ± 0.8	220.8 ± 0.7	171.2 ± 0.8	Tr. or 1+	1+
10 mg mL^{-1}	218.4 ± 1.1	219.9 ± 0.7	178.7 ± 1.2	1+ or 2+	1+

[a] The "expected" result was determined by comparing the red color intensity values obtained for lysozyme or γ-globulin samples with the calibration curve for HSA shown in Figure 4-9a (black circles). If the red color intensity value of lysozyme or γ-globulin samples lies between calibration plots without overlapping error bars, the two adjacent results are regarded as expected readout. [b] The "readout" result was obtained from the text-displaying device shown in Figures 4-9b and 4-9c.

4.3.6. Storage stability evaluation

Since the text-display assay method does not allow to evaluate the storage stability in a quantitative matter, digital color analysis has been performed with inkjet-deposited circular TBPB spots after dry storage at room temperature protected from light for various periods of time. Figures 4-10a and 4-10b show the time course of the colorimetric response of TBPB spots (8 and 15 printing cycles of TBPB, respectively) towards aqueous HSA solutions measured as red color intensity values. Data collected in the green and blue color signal coordinates is available in Figures 4-10c and 4-10d for the green intensity values at 8 and 15 printing cycles, and Figures 4-10e and 4-10f for the blue intensity values at 8 and 15 printing cycles. No significant changes in color intensity values have been observed over the testing period up to 117 days. With the long-term stability confirmed by the absence of colorimetric signal degradation, no loss of accuracy is expected in text-displaying assays relying on identical reagents for storage of at least 117 days at room temperature. Storage under dry and dark condition is readily achievable in practical use by keeping the devices in a bottle with a desiccant[10], as it is already routinely done for conventional urine dipsticks.

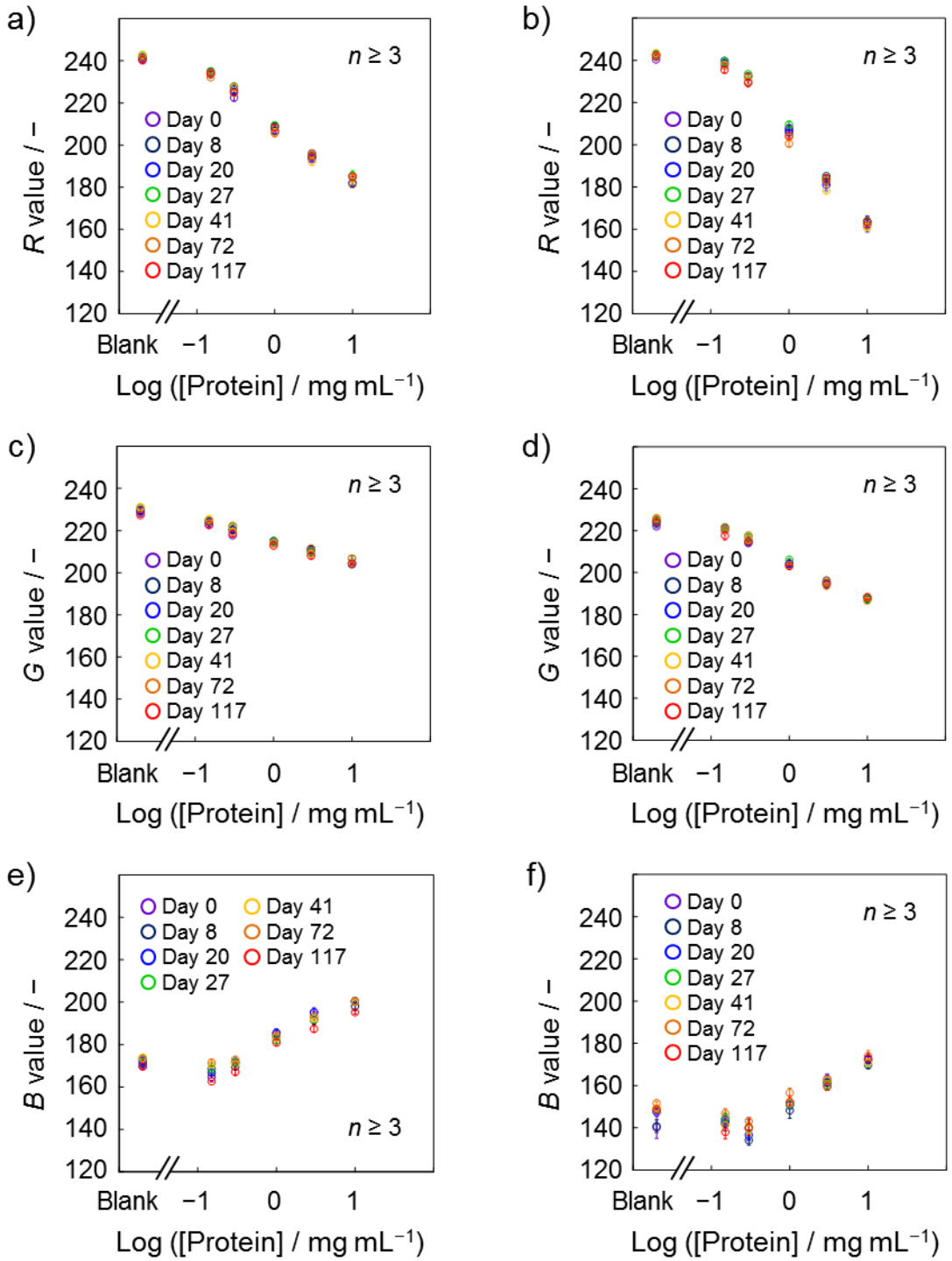

Figure 4-10. Storage stability evaluation of the TBPB-based colorimetric detection system for protein. Software-assisted color analysis after aqueous HSA solution application has been performed for TBPB spots stored for various periods. Each graph shows the colorimetric response of inkjet-deposited TBPB spots in the corresponding color coordinates: a) red intensity, 8 printing cycles; b) red intensity, 15 printing cycles; c) green intensity, 8 printing cycles; d) green intensity, 15 printing cycles; e) blue intensity, 8 printing cycles; f) blue intensity, 15 printing cycles.

4.4. Conclusions

This work describes to the best of my knowledge the first text-reporting semi-quantitative detection approach on a paper-based device relying on classical colorimetry. In the current study, urinary protein determination has been demonstrated as a proof-of-concept. The developed text-displaying paper device exhibited analytical performance comparable to the well-established colorimetric urine dipstick method. Although the achieved accuracy and the risk of reading out false-positive or false-negative results is not significantly differing from the conventional colorimetric technique, the elaborated detection system provides an alternative for users with specific color recognition capacities or for those with impaired color vision. Although impossible to evaluate with a limited number of test users, it is believed that the “direct” readout of a numerical value instead of a color needing to be matched with a reference chart, result misinterpretation might be reduced. In addition, the developed concept is expected to be expandable to a variety of analytical targets, simply by exchanging the combination of colorimetric indicator and the screening color film. In this way, this work brings paper-based analytical devices with advantageous features such as low-cost and simplicity one step closer to the more widespread real-world application by ordinary users.

References

1. Comer, J. P., Semiquantitative Specific Test Paper for Glucose in Urine. *Anal. Chem.* **1956,** *28*, 1748−1750.
2. Free, A. H.; Adams, E. C.; Kercher, M. L.; Free, H. M.; Cook, M. H., Simple Specific Test for Urine Glucose. *Clin. Chem.* **1957,** *3*, 163−168.
3. Campbell, R. L.; Wagner, D. B.; O'Connell, J. P., Solid phase assay with visual readout. *US Pat.*, 4703017, October 27, **1987**.
4. Rosenstein, R. W.; Bloomster, T. G., Solid phase assay employing capillary flow. *US Pat.*, 4855240, August 8, **1987**.
5. Martinez, A. W.; Phillips, S. T.; Butte, M. J.; Whitesides, G. M., Patterned paper as a platform for inexpensive, low-volume, portable bioassays. *Angew. Chem. Int. Ed.* **2007,** *46*, 1318−1320.
6. Martinez, A. W.; Phillips, S. T.; Whitesides, G. M.; Carrilho, E., Diagnostics for the Developing World: Microfluidic Paper-Based Analytical Devices. *Anal. Chem.* **2010,** *82*, 3−10.
7. Yetisen, A. K.; Akram, M. S.; Lowe, C. R., Paper-based microfluidic point-of-care diagnostic devices. *Lab Chip* **2013,** *13*, 2210−2251.
8. Cate, D. M.; Adkins, J. A.; Mettakoonpitak, J.; Henry, C. S., Recent developments in paper-based microfluidic devices. *Anal. Chem.* **2015,** *87*, 19−41.
9. Yamada, K.; Henares, T. G.; Suzuki, K.; Citterio, D., Paper-based inkjet-printed microfluidic analytical devices. *Angew. Chem. Int. Ed.* **2015,** *54*, 5294−5310.
10. Yamada, K.; Shibata, H.; Suzuki, K.; Citterio, D., Toward practical application of paper-based microfluidics for medical diagnostics: state-of-the-art and challenges. *Lab Chip* **2017,** *17*, 1206−1249.
11. Choi, J. R.; Tang, R.; Wang, S.; Wan Abas, W. A. B.; Pingguan-Murphy, B.; Xu, F., Paper-based sample-to-answer molecular diagnostic platform for point-of-care diagnostics. *Biosens. Bioelectron.* **2015,** *74*, 427−439.

12. Hu, J.; Cui, X.; Gong, Y.; Xu, X.; Gao, B.; Wen, T.; Lu, T. J.; Xu, F., Portable microfluidic and smartphone-based devices for monitoring of cardiovascular diseases at the point of care. *Biotechnol. Adv.* **2016,** *34*, 305−320.
13. Lin, Y.; Gritsenko, D.; Feng, S.; Teh, Y. C.; Lu, X.; Xu, J., Detection of heavy metal by paper-based microfluidics. *Biosens. Bioelectron.* **2016,** *83*, 256−266.
14. Meredith, N. A.; Quinn, C.; Cate, D. M.; Reilly, T. H.; Volckens, J.; Henry, C. S., Paper-based analytical devices for environmental analysis. *Analyst* **2016,** *141*, 1874−1887.
15. Fu, E., Enabling robust quantitative readout in an equipment-free model of device development. *Analyst* **2014,** *139*, 4750−4757.
16. Nilghaz, A.; Guan, L.; Tan, W.; Shen, W., Advancement of Paper-based Microfluidics for Diagnostics – the Original Motivation and Current status. *ACS Sens.* **2016,** *1*, 1382−1393.
17. Martinez, A. W.; Phillips, S. T.; Carrilho, E.; Thomas, S. W.; Sindi, H.; Whitesides, G. M., Simple Telemedicine for Developing Regions: Camera Phones and Paper-Based Microfluidic Devices for Real-Time, Off-Site Diagnosis. *Anal. Chem.* **2008,** *80*, 3699−3707.
18. Pollock, N. R.; Rolland, J. P.; Kumar, S.; Beattie, P. D.; Jain, S.; Noubary, F.; Wong, V. L.; Pohlmann, R. A.; Ryan, U. S.; Whitesides, G. M., A Paper-Based Multiplexed Transaminase Test for Low-Cost, Point-of-Care Liver Function Testing. *Sci. Transl. Med.* **2012,** *4*, 152ra129.
19. Pollock, N. R.; McGray, S.; Colby, D. J.; Noubary, F.; Nguyen, H.; Nguyen, T. A.; Khormaee, S.; Jain, S.; Hawkins, K.; Kumar, S.; Rolland, J. P.; Beattie, P. D.; Chau, N. V.; Quang, V. M.; Barfield, C.; Tietje, K.; Steele, M.; Weigl, B. H., Field evaluation of a prototype paper-based point-of-care fingerstick transaminase test. *PLoS One* **2013,** *8*, e75616.
20. Jain, S.; Rajasingham, R.; Noubary, F.; Coonahan, E.; Schoeplein, R.; Baden, R.; Curry, M.; Afdhal, N.; Kumar, S.; Pollock, N. R., Performance of an Optimized Paper-Based Test for Rapid Visual Measurement of Alanine Aminotransferase (ALT) in Fingerstick and Venipuncture Samples. *PLoS One* **2015,** *10*, e0128118.

21. Schonhorn, J. E.; Fernandes, S. C.; Rajaratnam, A.; Deraney, R. N.; Rolland, J. P.; Mace, C. R., A device architecture for three-dimensional, patterned paper immunoassays. *Lab Chip* **2014,** *14*, 4653−4658.
22. Deraney, R. N.; Mace, C. R.; Rolland, J. P.; Schonhorn, J. E., Multiplexed, Patterned-Paper Immunoassay for Detection of Malaria and Dengue Fever. *Anal. Chem.* **2016,** *88*, 6161−6165.
23. Lewis, G. G.; DiTucci, M. J.; Phillips, S. T., Quantifying Analytes in Paper-Based Microfluidic Devices Without Using External Electronic Readers. *Angew. Chem. Int. Ed.* **2012,** *51*, 12707−12710.
24. Karita, S.; Kaneta, T., Acid-base titrations using microfluidic paper-based analytical devices. *Anal. Chem.* **2014,** *86*, 12108−12114.
25. Choi, J. R.; Yong, K. W.; Tang, R.; Gong, Y.; Wen, T.; Yang, H.; Li, A.; Chia, Y. C.; Pingguan-Murphy, B.; Xu, F., Lateral Flow Assay Based on Paper–Hydrogel Hybrid Material for Sensitive Point-of-Care Detection of Dengue Virus. *Adv. Healthcare Mater.* **2017,** *6*, 1600920.
26. Hu, J.; Choi, J. R.; Wang, S.; Gong, Y.; Feng, S.; Pingguan-Murphy, B.; Lu, T. J.; Xu, F., Multiple test zones for improved detection performance in lateral flow assays. *Sens. Actuat. B: Chem.* **2017,** *243*, 484−488.
27. Cate, D. M.; Dungchai, W.; Cunningham, J. C.; Volckens, J.; Henry, C. S., Simple, distance-based measurement for paper analytical devices. *Lab Chip* **2013,** *13*, 2397−2404.
28. Cate, D. M.; Noblitt, S. D.; Volckens, J.; Henry, C. S., Multiplexed paper analytical device for quantification of metals using distance-based detection. *Lab Chip* **2015,** *15*, 2808−2818.
29. Karita, S.; Kaneta, T., Chelate titrations of Ca^{2+} and Mg^{2+} using microfluidic paper-based analytical devices. *Anal. Chim. Acta* **2016,** *924*, 60−67.
30. Lewis, G. G.; Robbins, J. S.; Phillips, S. T., Point-of-Care Assay Platform for Quantifying Active Enzymes to Femtomolar Levels Using Measurements of Time as the Readout. *Anal. Chem.* **2013,** *85*, 10432−10439.
31. Lewis, G. G.; Robbins, J. S.; Phillips, S. T., A prototype point-of-use assay for measuring heavy metal contamination in water using time as a quantitative readout. *Chem. Commun.* **2014,** *50*, 5352−5354.

32. Zhang, Y.; Fan, J.; Nie, J.; Le, S.; Zhu, W.; Gao, D.; Yang, J.; Zhang, S.; Li, J., Timing readout in paper device for quantitative point-of-use hemin/G-quadruplex DNAzyme-based bioassays. *Biosens. Bioelectron.* **2015,** *73*, 13−18.
33. Wei, X.; Tian, T.; Jia, S.; Zhu, Z.; Ma, Y.; Sun, J.; Lin, Z.; Yang, C. J., Target-Responsive DNA Hydrogel Mediated "Stop-Flow" Microfluidic Paper-Based Analytic Device for Rapid, Portable and Visual Detection of Multiple Targets. *Anal. Chem.* **2015,** *87*, 4275−4282.
34. Yamada, K.; Henares, T. G.; Suzuki, K.; Citterio, D., Distance-Based Tear Lactoferrin Assay on Microfluidic Paper Device Using Interfacial Interactions on Surface-Modified Cellulose. *ACS Appl. Mater. Interfaces* **2015,** *7*, 24864−24875.
35. Berry, S. B.; Fernandes, S. C.; Rajaratnam, A.; DeChiara, N. S.; Mace, C. R., Measurement of the hematocrit using paper-based microfluidic devices. *Lab Chip* **2016,** *16*, 3689−3694.
36. Li, M.; Tian, J.; Al-Tamimi, M.; Shen, W., Paper-based blood typing device that reports patient's blood type "in writing". *Angew. Chem. Int. Ed.* **2012,** *51*, 5497−5501.
37. Carrasquilla, C.; Little, J. R. L.; Li, Y.; Brennan, J. D., Patterned Paper Sensors Printed with Long-Chain DNA Aptamers. *Chem. - Eur. J.* **2015,** *21*, 7369−7373.
38. Li, J.; Macdonald, J., Multiplex lateral flow detection and binary encoding enables a molecular colorimetric 7-segment display. *Lab Chip* **2016,** *16*, 242−245.
39. Abe, K.; Suzuki, K.; Citterio, D., Inkjet-Printed Microfluidic Multianalyte Chemical Sensing Paper. *Anal. Chem.* **2008,** *80*, 6928−6934.
40. Komuro, N.; Takaki, S.; Suzuki, K.; Citterio, D., Inkjet printed (bio)chemical sensing devices. *Anal. Bioanal. Chem.* **2013,** *405*, 5785−5805.
41. Li, J.; Rossignol, F.; Macdonald, J., Inkjet printing for biosensor fabrication: combining chemistry and technology for advanced manufacturing. *Lab Chip* **2015,** *15*, 2538−2558.
42. Cantrell, K.; Erenas, M. M.; de Orbe-Payá, I.; Capitán-Vallvey, L. F., Use of the Hue Parameter of the Hue, Saturation, Value Color Space As a Quantitative Analytical Parameter for Bitonal Optical Sensors. *Anal. Chem.* **2010,** *82*, 531−542.

43. Strasinger, S. K.; Di Lorenzo, M. S., *Urinalysis & Body Fluids*. F. A. Davis Company, 2008.

44. Hamm, L. L.; Simon, E. E., Roles and mechanisms of urinary buffer excretion. *Am. J. Physiol. Renal Physiol.* **1987,** *253*, F595.

Chapter 5 General conclusions

5.1. Summary of the results

The most actively pursued practical application of μPADs remains probably in medical diagnostics. Substantial efforts have been dedicated to expand the clinically-relevant analytes detectable by paper-based analytical devices including proteins, metabolites, and electrolytes. Determination of their concentration in body fluids contributes to a wide class of clinical purposes ranging from personal daily health checks (*e.g.* blood glucose detection for diabetes diagnosis) to biomedical diagnosis of serious conditions (*e.g.* serum tumor marker protein detection for cancer diagnosis). However, translation of most μPADs reported in the literature into practical use has been hindered mainly because of 1) necessity of complicated user operations (sample processing, control of applied sample volume), 2) insufficient examination on long-term stability, and 3) reliance on detection equipment unfamiliar for general users (scanner, camera under controlled lighting, potentiostat). The current work mainly focused on simplification of result interpretation on (μ)PADs to eliminate the necessity of signal capturing equipment.

The second chapter described quantification of lactoferrin on a μPAD which utilizes fluorescence emission from the terbium cation (Tb^{3+})–lactoferrin complexes as a detection signal. Being free of expensive antibodies and enzymes, lactoferrin has been successfully detected on a microfluidic paper-based analytical device relying on the sensitized fluorescence emission from the Tb^{3+} cation. The second section described human tear lactoferrin quantification based on software-assisted fluorescence image analysis. Importantly, the application to a lactoferrin assay using 5 tear samples from healthy persons was validated against the conventional enzyme-linked immunosorbent assay (ELISA).

In the third chapter, the lactoferrin assay procedure has been further simplified by introducing distance as a quantification signal. Visual comparison of the fluorescence emission distance in a straight detection paper channel and adjacent printed scale marks allows calibration-free lactoferrin quantification without influence from the excitation source power and the need of signal capturing equipment. 18 real samples including 2

specimens collected from ocular disease patients were analyzed using the elaborated paper device and ELISA for the purpose of method validation. The coefficient of correlation of 0.97 demonstrated accuracy in real human tear sample analysis.

Aside from the distance-based detection, this thesis covered text-displaying detection as another user-friendly result interpretation approach on paper-based analytical devices. The fourth chapter described the development of a semi-quantitative urinary albumin assay where symbol(s) displayed on a paper device are used as a detection signal. A conventional colorimetric system has been converted to text-based detection with the aid of printing techniques including wax-, inkjet-, laser-, and 3D-printing. The resulting device exhibited comparable analytical accuracy to that of conventional colorimetric urine dipsticks in observer-dependent readout tests.

To summarize, this thesis demonstrated a series of user-friendly signal interpretation approaches on (μ)PADs, elaborated by choosing biological proteins, tear lactoferrin and urinary albumin, as clinically-relevant analytical targets. Considering the observer-dependent nature of those signal readout approaches, user tests have also been performed to confirm the compatibility of the elaborated (μ)PADs with various persons.

5.2. Future outlook

Figure 5-1 illustrates the author's view on the pathway towards real-world application of μPADs. For the development of μPADs with practical utility, unambiguous signaling systems being free of detection equipment are among the most essential needs. Particularly, semi-quantitative detection motifs based on counting, timing, distance, and text are most appealing for μPADs. Further expansion of analytical targets detectable by those approaches as well as the invention of other user-friendly interpretation methods will be of high importance to propel real-life applications of μPADs. Although unmet issues should be noted in the necessity of sample volume control for tear lactoferrin measurement and in-depth evaluation of long-term stability, the author believes that the current work brings significant insights in the development of end user paper devices with simplified result interpretation in practical biological sample matrices. In the future, collaborative action of academic institutes and industry will be increasingly desired to put μPAD prototypes into high volume production and market distribution.

Figure 5-1. Pathway towards real-world application of μPADs.

Appendix

The information in this section is mainly based on
"Toward practical application of paper-based microfluidics for medical diagnostics: state-of-the-art and challenges",
Kentaro Yamada; Hiroyuki Shibata; Koji Suzuki; Daniel Citterio,
Lab on a Chip, **2017**, *17*, 1206−1249.

In this appendix, representative works performed on μPADs with the demonstration of real sample analysis are provided. Despite extensive search with Google Scholar, SciFinder, and the Web of Science, the author has undoubtedly overlooked many relevant papers, and apologizes to the authors of those unintentionally omitted contributions to the field. Table A-1 covers medical analytical targets that are inspected in routine urine checks or blood tests for the purpose of health monitoring. On the other hand, Table A-2 deals with a wide array of biomarkers not being routinely inspected, but potentially useful for screening or early diagnosis of diseases. It should be noted that the number of works listed in Tables A-1 and A-2 (96 publications) is obviously limited in contrast to the thriving research on μPADs (approximately 1,000 publications). These tables exclude a large fraction of μPAD research for medical applications, due to the absence of demonstration of real sample analysis.

Table A-1. Examples of μPADs with demonstration of application to real sample analysis targeting routine health check. This table is based on Ref 1 – Reproduced by permission of The Royal Society of Chemistry.

Analyte	Sample body fluid	Detection type	Detectable range[a]	Detection limit[b]	Precision[c]	Storage stability	Ref.
Glucose	Human whole blood	Colorimetry (intensity)	2.8-11.1 mM	N. A.	5.25%	N. A.	2
			0.1−10 mM	2.5 μM	N. A.	> 90% of initial response after 1 week	3
		Electrochemical (amperometry)	0−28 mM	1.4 mM	9.1%	N. A.	4
		Electrochemical (amperometry)	1−12 mM	0.05 mM	1.5−6.6%	N. A.	5
		Electrochemical (chronoamperometry)	0−33.1 mM	N. A.	11%	N. A.	6
		Electrochemical (differential pulse voltammetry)	0.2−11.2 mM	0.1 mM	6.7%	N. A.	7
	Human serum	Colorimetry (intensity)	3.0×10^{-4}–1.0×10^{-3} M	2.13×10^{-4} M	2.55−7.51%	< 30 days at −20ºC	8
		Colorimetry (intensity)	0−28 mM	N. A.	8.36%	N. A.	9
		Colorimetry (distance)	0.6−15 mM	0.6 mM (lowest detectable level)	1.6−3.3%	N. A.	10
		Electrochemical (chronoamperometry)	0−100 mM	0.21 mM (0.70 mM)	< 14%	N. A.	11
		Electrochemical (chronoamperometry)	0−5 mM	N. A.	N. A.	N. A.	12
		Electrochemical (potentiometry)	0.1-3.2 mM	32 mM	3.4%	> 2 months under dry condition at 4ºC	13
	Human serum, urine	Colorimetry (intensity)	0.5−30 mM	N. A.	4.3%	N. A.	14
		Colorimetry (intensity)	0.5−20 mM	N. A.	N. A.	Stable for 8 days at 22ºC (signal decrease after 12 days at 22ºC and 40ºC)	15
	Human urine	Colorimetry (intensity)	0−110 mM	N. A.	N. A.	N. A.	16
		Electrochemical (amperometry)	0.8−26 mM	0.8 mM	4−15%	N. A.	17
		Electrochemical (chronoamperometry)	0−10 mM	0.35 mM	1.9−8.8%	N. A.	18
	Human tear	Colorimetry (intensity)	0.1−1.0 mM	50 μM	2.9−9.5%	N. A.	19

Table A-1. *(continued)*

Analyte	Sample body fluid	Detection type	Detectable range[a]	Detection limit[b]	Precision[c]	Storage stability	Ref.
Lactate	Human serum, urine	Colorimetry (intensity)	1−25 mM	N. A.	N. A.	Stable for 8 days at 22ºC (significant signal decrease after 12 days at 22 ºC and 40 ºC)	15
		Colorimetry (intensity)	2.5−35 mM	N. A.	4.3%	N. A.	14
	Human plasma	Electrochemical (amperometry)	1−11 mM	1.1 mM	N. A.	N. A.	4
	Human serum	Electrochemical (chronoamperometry)	0−50 mM	0.36 mM (1.19 mM)	< 14%	N. A.	11
Uric acid	Human serum, urine	Colorimetry (intensity)	0.1−7 mM	N. A.	N. A.	Stable for 8 days at 22ºC (significant signal decrease after 12 days at 22ºC and 40ºC)	15
		Colorimetry (intensity)	0.8−35 mM	N. A.	4.3%	N. A.	14
	Human serum	Colorimetry (intensity)	3.0×10^{-4}–1.0×10^{-3} M	2.87×10^{-4} M	4.97−8.57%	< 60 days at −20ºC	8
		Electrochemical (chronoamperometry)	0−35 mM	1.38 mM (4.60 mM)	< 14%	N. A.	11
	Human urine		0−2 mM	0.08 mM	4.5−14.4%	N. A.	18
Cholesterol	Human serum, urine	Colorimetry (intensity)	0.5−50 mM	N. A.	4.3%	N. A.	14
	Human serum	Electrochemical (amperometry)	0.05−10 mM	1 mM	1.06−9.37%	89.1% of initial response after 2 weeks	20
	Human plasma	Electrochemical (amperometry)	0.5−5.2 mM	0.34 mM	6.2%	N. A.	4
	Bovine serum	Electrochemical (amperometry)	1 µM−7 mM	1 nM (1 µM)	N. A.	N. A.	21
		Electrochemical (chronoamperometry)	0.01−7 mM	6.5 µM	< 3.5%	N. A.	22
Creatinine	Human urine	Colorimetry (intensity)	2.5−25 mg dL^{-1}	2.0 mg dL^{-1}	6.1−16.6%	N. A.	23
			0−6 mg dL^{-1}	0.42 mg dL^{-1}	< 3%	N. A.	24
C-reactive protein	Human whole blood	Transmittance	0−50 µg mL^{-1}	N. A.	3.9%	N. A.	25
	Human serum	Chemiluminescence	*1−10000 ng mL^{-1}*	1.05 ng mL^{-1}	N. A.	N. A.	26

Table A-1. *(continued)*

Analyte	Sample body fluid	Detection type	Detectable range[a]	Detection limit[b]	Precision[c]	Storage stability	Ref.
Ferritin	Human whole blood	Transimttance	5−350 ng mL^{-1}	N. A.	2.5%	N. A.	25
		Colorimetry (intensity)	0−250 ng mL^{-1}	N. A.	N. A.	N. A.	27
Retinol binding protein	Human whole blood	Transimttance	10−70 µg mL^{-1}	N. A.	10.8%	N. A.	25
β-hydroxybutyrate	Human whole blood	Electrochemical (amperometry)	0−6 mM	0.3 mM	<12%	N. A.	28
Potassium	Human serum	Colorimetry (timing)	0.5−200 µM	0.49 µM	~ 4.1%	> 1 month under dark condition at room temperature	29
		Electrochemical (potentiometry)	0.8−100 mM	0.8 mM	± 3.2 mM[d]	N. A.	30
Chloride	Human serum (10-fold diluted)	Electrochemical (potentiometry)	0.8−200 mM	0.8 mM	± 1.6 mM[d]	N. A.	30
Ammonium	Human sweat	Electrochemical (potentiometry)	0.1−100 mM	12.6 µM	5.21%	N. A.	31
Iron	Human whole blood	Fluorescence (intensity)	**1-1000 µM**	N. A.	5.5%	N. A.	27
	Human serum	Colorimetry (intensity)	0−200 µM	N. A.	< 17%	N. A.	12
Zinc Cadmium Lead	Human serum (mixed with 10-fold volume of acetate buffer)	Electrochemical (square-wave voltammetry)	1.0−300 µg L^{-1}	1.0 µg L^{-1} 0.1 µg L^{-1} 0.1 µg L^{-1}	9.2% 7.8% 4.8%	82 ± 2 % of initial response after 3 weeks at standard temperature and humidity	32
Protein (albumin)	Human whole blood	Colorimetry (intensity)	0−100 g L^{-1}	7 g L^{-1}	N. A.	N. A.	33
		Colorimetry (intensity)	1.6−5.3 g dL^{-1}	N. A.	5.48%	N. A.	34
	Human serum	Colorimetry (intensity)	0−6 g dL^{-1}	N. A.	12.5%	N. A.	9
	Human urine	Colorimetry (text)	0−10 mg mL^{-1}	0.15 mg mL^{-1} (visual inspection)	N.A.	> 117 days under dry, dark condition at room temperature	35
hCG	Human serum	Electrochemical (amperometry)	**2 mU L^{-1}–120 U L^{-1}**	0.7 mU L^{-1}	5.5%	91.3% of initial response after 30 days at 4ºC	36

Table A-1. *(continued)*

Analyte	Sample body fluid	Detection type	Detectable range[a]	Detection limit[b]	Precision[c]	Storage stability	Ref.
AST	Human whole blood	Colorimetry (intensity)	0−200 U L^{-1}	44 U L^{-1}	N. A.	> 1 month at room temperature, > 3 months at 4ºC	33
			40−200 U L^{-1}	84 U L^{-1}	2.64−8.01%	> 11 weeks under dry condition at 25ºC	37
	Human serum	Colorimetry (intensity)	5.4−91.2 U L^{-1}	N. A.	1.93−5.55%	Refrigeration necessary if not used immediately	38
ALT	Human whole blood	Colorimetry (intensity)	40−200 U L^{-1}	53 U L^{-1}	5.08−7.22%	> 11 weeks under dry condition at 25ºC	37
		Colorimetry (intensity)	0−400 U L^{-1}	40 U L^{-1} (lowest detectable level)	3.32−17.57%	18 months under dry condition at 18−30ºC	39
	Human serum	Colorimetry (intensity)	5.38−86.1 U L^{-1}	N. A.	2.53−3.25%	Refrigeration necessary if not used immediately	38
ALP	Human whole blood	Colorimetry (intensity)	0−1000 U L^{-1}	15 U L^{-1}	N. A.	> 3 months at room temperature	33
	Human serum (40−100 fold diluted)	Colorimetry (intensity)	1.5−20 U L^{-1}	0.78 U L^{-1}	3.44−13.4%	N. A.	40
	Human serum	Colorimetry (distance)	75−5000 U L^{-1}	75 U L^{-1}	5.5−6.6%	N. A.	41

hCG: human chorionic gonadotropin, AST: aspartate transaminase, ALT: alanine aminotransferase, ALP: alkaline phosphatase, N. A.: not available. [a] Underlined concentration shows linear range; underlined concentration written in bold shows logarithmically linear range; concentration written in italic shows dynamic response range. [b] Detection limit is specified as the limit of detection (LoD) calculated based on the 3σ method unless otherwise noted. Concentration in parenthesis indicates the limit of quantification (LoQ) calculated based on the 10σ method. [c] Expressed as relative standard deviation of repeated measurements. [d] Standard deviation of standard electrode potential.

Table A-2. Examples of μPADs with demonstration of application to real sample analysis targeting biomedical diagnosis. This table is based on Ref 1 – Reproduced by permission of The Royal Society of Chemistry.

Analyte	Sample body fluid	Detection type	Detectable range[a]	Detection limit[b]	Precision[c]	Storage stability	Ref.
AFP	Human whole blood (mixed with anti-D antibody)	Chemiluminescence	2.5−110 ng mL^{-1}	1.0 ng mL^{-1}	2.2−4.3%	> 90% of initial response after 40 days at r.t.	42
	Human serum	Electrochemical (differential pulse voltammetry)	**0.001−100 ng mL^{-1}**	0.80 pg mL^{-1}	3.8%	97.5% of initial response after 10 days at 4ºC	43
		Electrochemical (square-wave voltammetry)	**0.1 pg mL^{-1}−100 ng mL^{-1}**	0.08 pg mL^{-1}	2.25%	91.0% of initial response after 20 days at 4ºC	44
		Chemiluminescence	0.1−35.0 ng mL^{-1}	0.06 ng mL^{-1}	4.9−7.1%	> 5 weeks at 4ºC (sealed)	45
		ECL	*0.5−100 ng mL^{-1}*	0.15 ng mL^{-1}	N. A.	> 3 weeks under dry condition at 4ºC	46
			0.005−1 ng mL^{-1} **0.005−100 ng mL^{-1}**	1.2 pg mL^{-1}	3.2%	N. A.	47
			0.1−10 ng mL^{-1} **0.1−200 ng mL^{-1}**	0.02 ng mL^{-1}	3.03%	6 weeks under ambient condition, 8 weeks under dry condition at 4ºC	48
		PEC	0.01−65 ng mL^{-1}	2.3 pg mL^{-1}	N. A.	> 4 weeks at 4ºC	49
CEA	Human whole blood (mixed with anti-D antibody)	Chemiluminescence	0.1−130 ng mL^{-1}	0.02 ng mL^{-1}	4.1−5.2%	> 90% of initial response after 40 days at r.t.	42
	Human whole blood, serum	Fluorescence (intensity)	0−500 ng mL^{-1}	N. A.	< 10%	N. A.	50
	Human serum	Colorimetry (intensity)	0.1−20 ng mL^{-1}	0.03 ng mL^{-1}	3%	N. A.	51
		Electrochemical (amperometry)	**0.001−100 ng mL^{-1}**	0.33 pg mL^{-1}	5.3%	91.7% of initial response after 30 days at 4ºC	36
		Electrochemical (amperometry)	1−10 ng mL^{-1}	N. A.	0.7−9.3%	93% of initial response after 21 days	52

Table A-2. *(continued)*

Analyte	Sample body fluid	Detection type	Detectable range[a]	Detection limit[b]	Precision[c]	Storage stability	Ref.
CEA	Human serum	Electrochemical (differential pulse voltammetry)	**0.05–50.0 ng mL^{-1}**	0.01 ng mL^{-1}	4.21%	> 4 weeks at 4ºC (sealed)	53
			0.0001–50 ng mL^{-1}	0.08 pg mL^{-1}	0.4−1.6%	Full activity after 14 days, 96% of initial response after 30 days	54
			0.001–100 ng mL^{-1}	0.50 pg mL^{-1}	3.8%	97.5% of initial response after 10 days at 4ºC	43
		Electrochemical (square-wave voltammetry)	**0.1 pg mL^{-1}–100 ng mL^{-1}**	0.06 pg mL^{-1}	2.62%	91.0% of initial response after 20 days at 4ºC	44
		Chemiluminescence	0.1−70.0 ng mL^{-1}	0.05 ng mL^{-1}	4.6−8.3%	> 5 weeks at 4ºC (sealed)	45
			0.01−30.0 ng mL^{-1}	6.5 pg mL^{-1}	2.4−6.5%	3 weeks under ordinary condition, 4 weeks under dry condition at 4ºC	55
			0.1−80 ng mL^{-1}	0.03 ng mL^{-1}	4.7%	N.A.	56
			0.1−20.0 ng mL^{-1}	0.03 ng mL^{-1}	2.8−3.1%	N. A.	57
		ECL	**0.005–50 ng mL^{-1}**	0.001 ng mL^{-1} in standard sample, 0.008 ng mL^{-1} in human control serum sample	2.32%	> 3 weeks under dry condition at 4ºC	58
			0.001−1 ng mL^{-1} **0.001–10 ng mL^{-1}**	0.8 pg mL^{-1} (1.4 pg mL^{-1})	2.49%	100%, 90%, 85% of initial response after 3 days, 1 week, 1 month under dry condition at 4ºC	59
			1.0−100 ng mL^{-1}	0.5 ng mL^{-1}	N. A.	> 3 weeks under dry condition at 4ºC	46
			0.001−2 ng mL^{-1} **0.001−5 ng mL^{-1}**	0.7 pg mL^{-1}	4.7%	93% of initial response after 2 months at 4ºC	60
			0.05−5 ng mL^{-1} **0.05–100 ng mL^{-1}**	4.0 pg mL^{-1}	2.49%	6 weeks under ambient condition, 8 weeks under dry condition at 4ºC	48

Table A-2. *(continued)*

Analyte	Sample body fluid	Detection type	Detectable range[a]	Detection limit[b]	Precision[c]	Storage stability	Ref.
CEA	Human serum	PEC	**0.001−90 ng mL^{-1}**	0.33 pg mL^{-1}	4.8%	Gradual decrease of response after 1 week (90.1% of initial response after 4 weeks)	61
			0.01−50 ng mL^{-1}	2.1 pg mL^{-1}	2.76−3.24%	> 4 weeks at 4ºC	49
CA 125	Human serum	Chemiluminescence	0.5−80.0 U mL^{-1}	0.33 U mL^{-1}	6.2−9.4%	> 5 weeks at 4ºC (sealed)	45
			0.5−20.0 U mL^{-1}	0.2 U mL^{-1}	3.7−4.2%	N. A.	57
		Electrochemical (differential pulse voltammetry)	**0.001−75.0 U mL^{-1}**	0.2 mU mL^{-1}	N. A.	> 4 weeks at 4ºC (sealed)	53
			0.0001−50 U mL^{-1}	0.06 mU mL^{-1}	0.6−1.5%	Full activity after 14 days, 96% of initial response after 30 days	54
		Electrochemical (square-wave voltammetry)	**0.1−100 U mL^{-1}**	0.02 U mL^{-1}	2.45%	91.5 % of initial response after 21 days at 4ºC	62
		ECL	*1.0−100 U mL^{-1}*	0.6 U mL^{-1}	N. A.	> 3 weeks under dry condition at 4ºC	46
CA 15-3	Human whole blood (mixed with anti-D antibody)	Chemiluminescence	1.0−100 U mL^{-1}	0.4 U mL^{-1}	2.5−3.2%	> 90% of initial response after 40 days at r.t.	42
	Human serum	Electrochemical (amperometry)	0.01−50 U mL^{-1}	0.004 U mL^{-1}	6.8−8.3%	Slight decrease of response after 4 weeks at 4ºC	63
		ECL	*0.05−10 U mL^{-1}*	0.005 U mL^{-1}	2.41%	6 weeks under ambient condition, 8 weeks under dry condition at 4ºC	48
			0.05−200 U mL^{-1}				
		PEC	**0.02−70 U mL^{-1}**	7.1 mU mL^{-1}	N. A.	> 4 weeks at 4ºC	49
CA 19-9	Human whole blood (mixed with anti-D antibody)	Chemiluminescence	0.5−150 U mL^{-1}	0.06 U mL^{-1}	4.5−5.8%	> 90% of initial response after 40 days at r.t.	42

Table A-2. *(continued)*

Analyte	Sample body fluid	Detection type	Detectable range[a]	Detection limit[b]	Precision[c]	Storage stability	Ref.
CA 19-9	Human serum	Chemiluminescence	0.5−20 U mL^{-1}	0.2 U mL^{-1}	1.3−3.8%	N. A.	57
		Electrochemical (square-wave voltammetry)	**0.1−100 U mL^{-1}**	0.04 U mL^{-1}	2.21%	91.5% of initial response after 21 days at 4ºC	62
		ECL	*0.5−100 U mL^{-1}*	0.17 U mL^{-1}	N. A.	> 3 weeks under dry condition at 4ºC	46
			0.05−200 U mL^{-1}	0.006 mU mL^{-1}	2.27%	6 weeks under ambient condition, 8 weeks under dry condition at 4ºC	48
		PEC	**0.05−80 U mL^{-1}**	16.3 mU mL^{-1}	N. A.	> 4 weeks at 4ºC	49
PSA	Human serum	Colorimetry (intensity)	*0.5−50 μg L^{-1}*	360.2 ng L^{-1}	8.2−11.7%	N. A.	64
		Electrochemical (amperometry)	**0.001−110 ng mL^{-1}**	0.35 pg mL^{-1}	5.7%	92.2% of initial response after 30 days at 4ºC	36
		Electrochemical (amperometry)	**4.0−60 ng mL^{-1}**	1.5 pg mL^{-1}	7.2%	> 4 weeks under dark, moisturizing condition at 4ºC	65
		Electrochemical (differential pulse voltammetry)	*0.005−1 ng mL^{-1}* **0.005−100 ng mL^{-1}**	1.2 pg mL^{-1}	2.12−5.12%	97.58% of initial response after 4 weeks at 4ºC	66
		Electrochemical (differential pulse voltammetry)	31−250 pg mL^{-1}	6 pg mL^{-1}	N. A.	N. A.	67
		ECL	*0.003−1 ng mL^{-1}* **0.003−20 ng mL^{-1}**	1 pg mL^{-1} (2.5 pg mL^{-1})	2.82%	100, 90, 85% of initial response after 3 days, 1 week, 1 month under dry condition at 4ºC	59
MMP-2	Human whole blood (1000-fold diluted), serum	Fluorescence (intensity)	50−5000 pg mL^{-1}	8.3 pg mL-1	< 10%	N. A.	50
TFF3	Human urine	Electrochemical (anodic stripping voltammetry)	0.0125−3.0 μg mL^{-1}	0.0125 mg mL^{-1}	17.8%	N. A.	68

Table A-2. *(continued)*

Analyte	Sample body fluid	Detection type	Detectable range[a]	Detection limit[b]	Precision[c]	Storage stability	Ref.
*Pf*HRP2	Human serum	Electrochemical (square-wave voltammetry)	**10−1000 ng mL^{-1}**	4 ng mL^{-1}	2.9%	N. A.	69
Hepatitis C virus	Human serum	Chemiluminescence	80 ng mL^{-1}–8 µg mL^{-1} (mouse IgG as model)	80 ng mL^{-1} (mouse IgG as model)	N. A.	> several weeks under dry, dark condition at 4ºC	70
Escherichia coli malB cell	Human plasma	Fluorescemce	> 500 cells mL^{-1}	500 cells mL^{-1}	N. A.	N. A.	71
K-562 cell	Human serum	Electrochemical (differential pulse voltammetry)	*1.0 × 10^{2}–1.0 × 10^{6} cells mL^{-1}*	31 cells mL^{-1}	3.5−5.1%	95.8, 85.5% of initial response after 1, 2 month at r.t.	72
H1N1 (influenza A) RNA	Nasopharyngeal swab	Colorimetry (intensity)	10^{5}–10^{10} cp mL^{-1}	10^{6} cp mL^{-1}	N. A.	N. A.	73
DNA	Human serum	Electrochemical (differential pulse voltammetry)	**0.8 fM−0.5 nM**	0.2 fM	6.2%	90% of initial response after 30 days at 4ºC	74
		Chemiluminescence	**1 aM−10 fM**	0.856 aM	3.36−4.24%	> 6 weeks at 4ºC	75
		PEC	**50 fM−100 nM**	15 fM	3.2−4.7%	2 weeks at 4ºC	76
ATP	Human serum	PEC	1.0 pM−1.0 nM	0.2 pM	3.3−4.4%	> 4 weeks at 4ºC	77
Adenosine	Human serum	Colorimetry (number of colored detection regions)	1.5 µM−19.3 mM	1.5 µM	11.3%	Up to 91 days under vacuum and dark condition	78
Anionic species	Human sweat	Colorimetry (intensity)	0−140 mM (NaCl equivalent)	N. A.	< 15%	> 1 year below 30ºC	79
Dopamine	Human serum	Electrochemical (square-wave voltammetry)	1−100 µM	0.37 µM	4.32%	N. A.	80
Theophiline	Human plasma, whole blood	Colorimetry (distance)	0−40 mg L^{-1}	N. A.	5−8%	> 21 weeks (4−37ºC)	81
	Human whole blood	Colorimetry (distance)	0−40 mg L^{-1}	2.5 mg L^{-1}	5.4−9.4%	N. A.	82
Lithium	Human whole blood	Electrochemical (potentiometry)	3.6×10^{-5}–1×10^{-1} M	1.1×10^{-5} M	2−23%	N. A.	83
Nitrite	Human saliva	Colorimetry (intensity)	10−1000 µM	10 µM	N. A.	> 12 hours under nitrogen atmosphere	84

Table A-2. *(continued)*

Analyte	Sample body fluid	Detection type	Detectable range[a]	Detection limit[b]	Precision[c]	Storage stability	Ref.
Lactoferrin	Human tear	Fluorescence (color analysis)	0.1−4 mg mL^{-1}	0.30 mg mL^{-1}	0.6−5.9%	< 30 days at 25ºC < 10 days at 35ºC	85
		Fluorescence (distance)	0−4 mg mL^{-1}	0.05 mg mL^{-1}	27.2%	> 16 days at r.t.	86
VEGF	Human tear	Colorimetry (intensity)	10^{-14}–10^{-6} g mL^{-1}	33.7 fg mL^{-1}	< 10%	N. A.	87
pH	Human saliva	Colorimetry (intensity)	4.5−7.5	N. A.	N. A.	N. A.	88
Reductase	Human saliva	Colorimetry (intensity)	N. A.	N. A.	N. A.	N. A.	88
NC16A	Blister fluid Human serum	Colorimetry (intensity)	1−50 μg mL^{-1}	N. A.	N. A.	Refrigeration necessary if not used immediately	89
NPY	Human saliva	Colorimetry (intensity)	1 nM−5 μM	2.3 nM	N. A.	N. A.	90
Phenylalanine	Human whole blood	Colorimetry (intensity)	0−16 mg dL^{-1}	N. A.	N. A.	Vacuum or freeze-drying necessary for storage	91
S-nitrothiols	Human plasma (protein removal necessary)	Colorimetry (intensity)	10−100 μM (nitrite as a reference)	3 μM (nitrite as a reference)	N. A.	N. A.	92
Thiocyanate	Human saliva	Colorimetry (intensity)	**0.25−20 mM**	0.06 mM (0.21 mM)	3.0%	< 1 day at 25ºC, 2 days at 4ºC, < 5 days at −20ºC	93
ABO blood type	Human whole blood	Direct reporting in characters	A, B, O, AB Rh (+), Rh (−)	−	Accuracy rate: 100%	N. A.	94
		Colorimetry (distance)	A, B, O, AB Rh (+), Rh (−)	−	Accuracy rate:85−96%	21 days under refrigeration	95
Hemoglobin	Human whole blood	Spectrometry	2.4−16.1 g dL^{-1}	N. A.	4−6%	N. A.	96
Hematocrit	Human whole blood	Colorimetry (distance)	28−57%	N. A.	16%	N. A.	97

AFP: alpha-fetoprotein, CEA: carcinoembryonic antigen, CA 125: cancer antigen 125, CA 15-3: cancer antigen 15-3, CA 19-9: carbohydrate antigen 19-9, PSA: prostate specific antigen, MMP-2: matrix metalloproteinase-2, TFF3: trefoil factor 3, *Pf*HRP2: *Plasmodium falciparum* histidine-rich protein 2, ATP: adenosine triphosphate, VEGF: vascular endothelial growth factor, NC16A: noncollagenous 16A, NPY: neuropeptide Y, ECL: electrochemiluminescence, PEC: photoelectrochemical, N. A.: not available, r.t.: room temperature. [a] Underlined concentration shows linear range; concentration written in italic shows dynamic response range; underlined concentration written in bold shows logarithmically linear range. [b] Detection limit is specified as the limit of detection (LoD) calculated based on the 3σ method unless otherwise noted. Concentration in parenthesis indicates the limit of quantification (LoQ) calculated based on the 10σ method. [c] Expressed as relative standard deviation of repeated measurements.

References

1. Yamada, K.; Shibata, H.; Suzuki, K.; Citterio, D., Toward practical application of paper-based microfluidics for medical diagnostics: state-of-the-art and challenges. *Lab Chip* **2017,** *17*, 1206−1249.
2. Yang, X.; Forouzan, O.; Brown, T. P.; Shevkoplyas, S. S., Integrated separation of blood plasma from whole blood for microfluidic paper-based analytical devices. *Lab Chip* **2012,** *12*, 274−280.
3. Zhu, X.; Huang, J.; Liu, J.; Zhang, H.; Jiang, J.; Yu, R., A dual enzyme-inorganic hybrid nanoflower incorporated microfluidic paper-based analytic device (μPAD) biosensor for sensitive visualized detection of glucose. *Nanoscale* **2017,** *9*, 5658−5663.
4. Nie, Z.; Deiss, F.; Liu, X.; Akbulut, O.; Whitesides, G. M., Integration of paper-based microfluidic devices with commercial electrochemical readers. *Lab Chip* **2010,** *10*, 3163−3169.
5. Li, W.; Qian, D.; Wang, Q.; Li, Y.; Bao, N.; Gu, H.; Yu, C., Fully-drawn origami paper analytical device for electrochemical detection of glucose. *Sens. Actuat. B: Chem.* **2016,** *231*, 230−238.
6. Noiphung, J.; Songjaroen, T.; Dungchai, W.; Henry, C. S.; Chailapakul, O.; Laiwattanapaisal, W., Electrochemical detection of glucose from whole blood using paper-based microfluidic devices. *Anal. Chim. Acta* **2013,** *788*, 39−45.
7. Kong, F. Y.; Gu, S. X.; Li, W. W.; Chen, T. T.; Xu, Q.; Wang, W., A paper disk equipped with graphene/polyaniline/Au nanoparticles/glucose oxidase biocomposite modified screen-printed electrode: toward whole blood glucose determination. *Biosens. Bioelectron.* **2014,** *56*, 77−82.
8. Chen, X.; Chen, J.; Wang, F.; Xiang, X.; Luo, M.; Ji, X.; He, Z., Determination of glucose and uric acid with bienzyme colorimetry on microfluidic paper-based analysis devices. *Biosens. Bioelectron.* **2012,** *35*, 363−368.
9. Songjaroen, T.; Dungchai, W.; Chailapakul, O.; Laiwattanapaisal, W., Novel, simple and low-cost alternative method for fabrication of paper-based microfluidics by wax dipping. *Talanta* **2011,** *85*, 2587−2593.

10. Cate, D. M.; Dungchai, W.; Cunningham, J. C.; Volckens, J.; Henry, C. S., Simple, distance-based measurement for paper analytical devices. *Lab Chip* **2013,** *13*, 2397−2404.
11. Dungchai, W.; Chailapakul, O.; Henry, C. S., Electrochemical Detection for Paper-Based Microfluidics. *Anal. Chem.* **2009,** *81*, 5821−5826.
12. Dungchai, W.; Chailapakul, O.; Henry, C. S., A low-cost, simple, and rapid fabrication method for paper-based microfluidics using wax screen-printing. *Analyst* **2011,** *136*, 77−82.
13. Parrilla, M.; Canovas, R.; Andrade, F. J., Paper-based enzymatic electrode with enhanced potentiometric response for monitoring glucose in biological fluids. *Biosens. Bioelectron.* **2016,** *90*, 110−116.
14. Deng, L.; Chen, C.; Zhu, C.; Dong, S.; Lu, H., Multiplexed bioactive paper based on GO@SiO_2@CeO_2 nanosheets for a low-cost diagnostics platform. *Biosens. Bioelectron.* **2014,** *52*, 324−329.
15. Dungchai, W.; Chailapakul, O.; Henry, C. S., Use of multiple colorimetric indicators for paper-based microfluidic devices. *Anal. Chim. Acta* **2010,** *674*, 227−233.
16. Jia, M. Y.; Wu, Q. S.; Li, H.; Zhang, Y.; Guan, Y. F.; Feng, L., The calibration of cellphone camera-based colorimetric sensor array and its application in the determination of glucose in urine. *Biosens. Bioelectron.* **2015,** *74*, 1029−1037.
17. Lankelma, J.; Nie, Z.; Carrilho, E.; Whitesides, G. M., Paper-based analytical device for electrochemical flow-injection analysis of glucose in urine. *Anal. Chem.* **2012,** *84*, 4147−4152.
18. Yao, Y.; Zhang, C., A novel screen-printed microfluidic paper-based electrochemical device for detection of glucose and uric acid in urine. *Biomed. Microdevices* **2016,** *18*, 92.
19. Gabriel, F. E.; Garcia, T. P.; Lopes, M. F.; Coltro, K. W., Paper-Based Colorimetric Biosensor for Tear Glucose Measurements. *Micromachines* **2017,** *8*, 104.
20. Ruecha, N.; Rangkupan, R.; Rodthongkum, N.; Chailapakul, O., Novel paper-based cholesterol biosensor using graphene/polyvinylpyrrolidone/polyaniline nanocomposite. *Biosens. Bioelectron.* **2014,** *52*, 13−19.
21. Ruecha, N.; Siangproh, W.; Chailapakul, O., A fast and highly sensitive detection of cholesterol using polymer microfluidic devices and amperometric system. *Talanta* **2011,** *84*, 1323−1328.

22. Nantaphol, S.; Chailapakul, O.; Siangproh, W., A novel paper-based device coupled with a silver nanoparticle-modified boron-doped diamond electrode for cholesterol detection. *Anal. Chim. Acta* **2015,** *891*, 136−143.

23. Talalak, K.; Noiphung, J.; Songjaroen, T.; Chailapakul, O.; Laiwattanapaisal, W., A facile low-cost enzymatic paper-based assay for the determination of urine creatinine. *Talanta* **2015,** *144*, 915−921.

24. Sittiwong, J.; Unob, F., Paper-based Platform for Urinary Creatinine Detection. *Anal. Sci.* **2016,** *32*, 639−643.

25. Lee, S.; Aranyosi, A. J.; Wong, M. D.; Hong, J. H.; Lowe, J.; Chan, C.; Garlock, D.; Shaw, S.; Beattie, P. D.; Kratochvil, Z.; Kubasti, N.; Seagers, K.; Ghaffari, R.; Swanson, C. D., Flexible opto-electronics enabled microfluidics systems with cloud connectivity for point-of-care micronutrient analysis. *Biosens. Bioelectron.* **2016,** *78*, 290−299.

26. Joung, H. A.; Oh, Y. K.; Kim, M. G., An automatic enzyme immunoassay based on a chemiluminescent lateral flow immunosensor. *Biosens. Bioelectron.* **2014,** *53*, 330−335.

27. Hu, S.-W.; Qiao, S.; Xu, B.-Y.; Peng, X.; Xu, J.-J.; Chen, H.-Y., Dual-Functional Carbon Dots Pattern on Paper Chips for Fe^{3+} and Ferritin Analysis in Whole Blood. *Anal. Chem.* **2017,** *89*, 2131−2137.

28. Wang, C. C.; Hennek, J. W.; Ainla, A.; Kumar, A. A.; Lan, W. J.; Im, J.; Smith, B. S.; Zhao, M.; Whitesides, G. M., A Paper-Based "Pop-up" Electrochemical Device for Analysis of Beta-Hydroxybutyrate. *Anal. Chem.* **2016,** *88*, 6326−6333.

29. Zhang, Y.; Fan, J.; Nie, J.; Le, S.; Zhu, W.; Gao, D.; Yang, J.; Zhang, S.; Li, J., Timing readout in paper device for quantitative point-of-use hemin/G-quadruplex DNAzyme-based bioassays. *Biosens. Bioelectron.* **2015,** *73*, 13−18.

30. Hu, J.; Stein, A.; Bühlmann, P., A Disposable Planar Paper-Based Potentiometric Ion-Sensing Platform. *Angew. Chem. Int. Ed.* **2016,** *55*, 7544−7547.

31. Guinovart, T.; Bandodkar, A. J.; Windmiller, J. R.; Andrade, F. J.; Wang, J., A potentiometric tattoo sensor for monitoring ammonium in sweat. *Analyst* **2013,** *138*, 7031−7038.

32. Ruecha, N.; Rodthongkum, N.; Cate, D. M.; Volckens, J.; Chailapakul, O.; Henry, C. S., Sensitive electrochemical sensor using a graphene-polyaniline nanocomposite for simultaneous detection of Zn(II), Cd(II), and Pb(II). *Anal. Chim. Acta* **2015,** *874*, 40−48.
33. Vella, S. J.; Beattie, P.; Cademartiri, R.; Laromaine, A.; Martinez, A. W.; Phillips, S. T.; Mirica, K. A.; Whitesides, G. M., Measuring markers of liver function using a micropatterned paper device designed for blood from a fingerstick. *Anal. Chem.* **2012,** *84*, 2883−2891.
34. Songjaroen, T.; Dungchai, W.; Chailapakul, O.; Henry, C. S.; Laiwattanapaisal, W., Blood separation on microfluidic paper-based analytical devices. *Lab Chip* **2012,** *12*, 3392−3398.
35. Yamada, K.; Suzuki, K.; Citterio, D., Text-displaying colorimetric paper-based analytical device. *ACS Sens.* **2017,** in press (DOI: 10.1021/acssensors.7b00464).
36. Sun, G.; Zhang, L.; Zhang, Y.; Yang, H.; Ma, C.; Ge, S.; Yan, M.; Yu, J.; Song, X., Multiplexed enzyme-free electrochemical immunosensor based on ZnO nanorods modified reduced graphene oxide-paper electrode and silver deposition-induced signal amplification strategy. *Biosens. Bioelectron.* **2015,** *71*, 30−36.
37. Pollock, N. R.; Rolland, J. P.; Kumar, S.; Beattie, P. D.; Jain, S.; Noubary, F.; Wong, V. L.; Pohlmann, R. A.; Ryan, U. S.; Whitesides, G. M., A Paper-Based Multiplexed Transaminase Test for Low-Cost, Point-of-Care Liver Function Testing. *Sci. Transl. Med.* **2012,** *4*, 152ra129.
38. Wang, H.-L.; Chu, C.-H.; Tsai, S.-J.; Yang, R.-J., Aspartate Aminotransferase and Alanine Aminotransferase Detection on Paper-Based Analytical Devices with Inkjet Printer-Sprayed Reagents. *Micromachines* **2016,** *7*, 9.
39. Jain, S.; Rajasingham, R.; Noubary, F.; Coonahan, E.; Schoeplein, R.; Baden, R.; Curry, M.; Afdhal, N.; Kumar, S.; Pollock, N. R., Performance of an Optimized Paper-Based Test for Rapid Visual Measurement of Alanine Aminotransferase (ALT) in Fingerstick and Venipuncture Samples. *PLoS One* **2015,** *10*, e0128118.

40. Chen, X.; Chen, J.; Zhang, H.-Y.; Wang, F.-B.; Wang, F.-F.; Ji, X.-H.; He, Z.-K., Colorimetric Detection of Alkaline Phosphatase on Microfluidic Paper-based Analysis Devices. *Chin. J. Anal. Chem.* **2016,** *44*, 591−596.
41. Zhang, L.; Nie, J.; Wang, H.; Yang, J.; Wang, B.; Zhang, Y.; Li, J., Instrument-free quantitative detection of alkaline phosphatase using paper-based devices. *Anal. Methods* **2017,** *9*, 3375−3379.
42. Ge, L.; Wang, S.; Song, X.; Ge, S.; Yu, J., 3D origami-based multifunction-integrated immunodevice: low-cost and multiplexed sandwich chemiluminescence immunoassay on microfluidic paper-based analytical device. *Lab Chip* **2012,** *12*, 3150−3158.
43. Li, L.; Li, W.; Yang, H.; Ma, C.; Yu, J.; Yan, M.; Song, X., Sensitive origami dual-analyte electrochemical immunodevice based on polyaniline/Au-paper electrode and multi-labeled 3D graphene sheets. *Electrochim. Acta* **2014,** *120*, 102−109.
44. Li, W.; Li, L.; Li, M.; Yu, J.; Ge, S.; Yan, M.; Song, X., Development of a 3D origami multiplex electrochemical immunodevice using a nanoporous silver-paper electrode and metal ion functionalized nanoporous gold-chitosan. *Chem. Commun.* **2013,** *49*, 9540−9542.
45. Wang, S.; Ge, L.; Song, X.; Yu, J.; Ge, S.; Huang, J.; Zeng, F., Paper-based chemiluminescence ELISA: lab-on-paper based on chitosan modified paper device and wax-screen-printing. *Biosens. Bioelectron.* **2012,** *31*, 212−218.
46. Ge, L.; Yan, J.; Song, X.; Yan, M.; Ge, S.; Yu, J., Three-dimensional paper-based electrochemiluminescence immunodevice for multiplexed measurement of biomarkers and point-of-care testing. *Biomaterials* **2012,** *33*, 1024−1031.
47. Zhang, L.; Li, L.; Ma, C.; Ge, S.; Yan, M.; Bian, C., Detection of α-fetoprotein with an ultrasensitive electrochemiluminescence paper device based on green-luminescent nitrogen-doped graphene quantum dots. *Sens. Actuat. B: Chem.* **2015,** *221*, 799−806.
48. Wang, S.; Ge, L.; Zhang, Y.; Song, X.; Li, N.; Ge, S.; Yu, J., Battery-triggered microfluidic paper-based multiplex electrochemiluminescence immunodevice based on potential-resolution strategy. *Lab Chip* **2012,** *12*, 4489−4498.

49. Wang, P.; Ge, L.; Ge, S.; Yu, J.; Yan, M.; Huang, J., A paper-based photoelectrochemical immunoassay for low-cost and multiplexed point-of-care testing. *Chem. Commun.* **2013,** *49*, 3294−3296.
50. He, M.; Liu, Z., Paper-based microfluidic device with upconversion fluorescence assay. *Anal. Chem.* **2013,** *85*, 11691−11694.
51. Liu, W.; Guo, Y.; Zhao, M.; Li, H.; Zhang, Z., Ring-Oven Washing Technique Integrated Paper-based Immunodevice for Sensitive Detection of Cancer Biomarker. *Anal. Chem.* **2015,** *87*, 7951−7957.
52. Kumar, S.; Kumar, S.; Srivastava, S.; Yadav, B. K.; Lee, S. H.; Sharma, J. G.; Doval, D. C.; Malhotra, B. D., Reduced graphene oxide modified smart conducting paper for cancer biosensor. *Biosens. Bioelectron.* **2015,** *73*, 114−122.
53. Wang, P.; Ge, L.; Yan, M.; Song, X.; Ge, S.; Yu, J., Paper-based three-dimensional electrochemical immunodevice based on multi-walled carbon nanotubes functionalized paper for sensitive point-of-care testing. *Biosens. Bioelectron.* **2012,** *32*, 238−243.
54. Ma, C.; Li, W.; Kong, Q.; Yang, H.; Bian, Z.; Song, X.; Yu, J.; Yan, M., 3D origami electrochemical immunodevice for sensitive point-of-care testing based on dual-signal amplification strategy. *Biosens. Bioelectron.* **2015,** *63*, 7−13.
55. Wang, S.; Ge, L.; Song, X.; Yan, M.; Ge, S.; Yu, J.; Zeng, F., Simple and covalent fabrication of a paper device and its application in sensitive chemiluminescence immunoassay. *Analyst* **2012,** *137*, 3821−3827.
56. Zhao, M.; Li, H.; Liu, W.; Guo, Y.; Chu, W., Plasma treatment of paper for protein immobilization on paper-based chemiluminescence immunodevice. *Biosens. Bioelectron.* **2016,** *79*, 581−588.
57. Chu, W.; Chen, Y.; Liu, W.; Zhao, M.; Li, H., Paper-based chemiluminescence immunodevice with temporal controls of reagent transport technique. *Sens. Actuat. B: Chem.* **2017,** *250*, 324−332.
58. Yan, J.; Ge, L.; Song, X.; Yan, M.; Ge, S.; Yu, J., Paper-based electrochemiluminescent 3D immunodevice for lab-on-paper, specific, and sensitive point-of-care testing. *Chemistry* **2012,** *18*, 4938−4945.

59. Li, W.; Li, M.; Ge, S.; Yan, M.; Huang, J.; Yu, J., Battery-triggered ultrasensitive electrochemiluminescence detection on microfluidic paper-based immunodevice based on dual-signal amplification strategy. *Anal. Chim. Acta* **2013,** *767*, 66−74.

60. Gao, C.; Su, M.; Wang, Y.; Ge, S.; Yu, J., A disposable paper-based electrochemiluminescence device for ultrasensitive monitoring of CEA based on $Ru(bpy)_3^{2+}$@Au nanocages. *RSC Adv.* **2015,** *5*, 28324−28331.

61. Lan, F.; Sun, G.; Liang, L.; Ge, S.; Yan, M.; Yu, J., Microfluidic paper-based analytical device for photoelectrochemical immunoassay with multiplex signal amplification using multibranched hybridization chain reaction and PdAu enzyme mimetics. *Biosens. Bioelectron.* **2016,** *79*, 416−422.

62. Li, W.; Li, L.; Ge, S.; Song, X.; Ge, L.; Yan, M.; Yu, J., Multiplex electrochemical origami immunodevice based on cuboid silver-paper electrode and metal ions tagged nanoporous silver-chitosan. *Biosens. Bioelectron.* **2014,** *56*, 167−173.

63. Wu, K.; Zhang, Y.; Wang, Y.; Ge, S.; Yan, M.; Yu, J.; Song, X., Paper-Based Analytical Devices Relying on Visible-Light-Enhanced Glucose/Air Biofuel Cells. *ACS Appl. Mater. Interfaces* **2015,** *7*, 24330−24337.

64. Nie, J.; Zhang, Y.; Lin, L.; Zhou, C.; Li, S.; Zhang, L.; Li, J., Low-cost fabrication of paper-based microfluidic devices by one-step plotting. *Anal. Chem.* **2012,** *84*, 6331−6335.

65. Sun, G.; Liu, H.; Zhang, Y.; Yu, J.; Yan, M.; Song, X.; He, W., Gold nanorods-paper electrode based enzyme-free electrochemical immunoassay for prostate specific antigen using porous zinc oxide spheres–silver nanoparticles nanocomposites as labels. *New J. Chem.* **2015,** *39*, 6062−6067.

66. Li, L.; Xu, J.; Zheng, X.; Ma, C.; Song, X.; Ge, S.; Yu, J.; Yan, M., Growth of gold-manganese oxide nanostructures on a 3D origami device for glucose-oxidase label based electrochemical immunosensor. *Biosens. Bioelectron.* **2014,** *61*, 76−82.

67. Tang, C. K.; Vaze, A.; Rusling, J. F., Paper-based electrochemical immunoassay for rapid, inexpensive cancer biomarker protein detection. *Anal. Methods* **2014,** *6*, 8878−8881.

68. DeGregory, P. R.; Tsai, Y. J.; Scida, K.; Richards, I.; Crooks, R. M., Quantitative electrochemical metalloimmunoassay for TFF3 in urine using a paper analytical device. *Analyst* **2016,** *141*, 1734−1744.

69. Glavan, A. C.; Christodouleas, D. C.; Mosadegh, B.; Yu, H. D.; Smith, B. S.; Lessing, J.; Fernandez-Abedul, M. T.; Whitesides, G. M., Folding analytical devices for electrochemical ELISA in hydrophobic R^H paper. *Anal. Chem.* **2014,** *86*, 11999−12007.

70. Mu, X.; Zhang, L.; Chang, S.; Cui, W.; Zheng, Z., Multiplex microfluidic paper-based immunoassay for the diagnosis of hepatitis C virus infection. *Anal. Chem.* **2014,** *86*, 5338−5344.

71. Connelly, J. T.; Rolland, J. P.; Whitesides, G. M., "Paper Machine" for Molecular Diagnostics. *Anal. Chem.* **2015,** *87*, 7595−7601.

72. Ge, S.; Zhang, Y.; Zhang, L.; Liang, L.; Liu, H.; Yan, M.; Huang, J.; Yu, J., Ultrasensitive electrochemical cancer cells sensor based on trimetallic dendritic Au@PtPd nanoparticles for signal amplification on lab-on-paper device. *Sens. Actuat. B: Chem.* **2015,** *220*, 665−672.

73. Rodriguez, N. M.; Linnes, J. C.; Fan, A.; Ellenson, C. K.; Pollock, N. R.; Klapperich, C. M., Paper-Based RNA Extraction, in Situ Isothermal Amplification, and Lateral Flow Detection for Low-Cost, Rapid Diagnosis of Influenza A (H1N1) from Clinical Specimens. *Anal. Chem.* **2015,** *87*, 7872−7879.

74. Lu, J.; Ge, S.; Ge, L.; Yan, M.; Yu, J., Electrochemical DNA sensor based on three-dimensional folding paper device for specific and sensitive point-of-care testing. *Electrochim. Acta* **2012,** *80*, 334−341.

75. Wang, Y.; Wang, S.; Ge, S.; Wang, S.; Yan, M.; Zang, D.; Yu, J., Facile and sensitive paper-based chemiluminescence DNA biosensor using carbon dots dotted nanoporous gold signal amplification label. *Anal. Methods* **2013,** *5*, 1328−1336.

76. Wang, Y.; Ge, L.; Wang, P.; Yan, M.; Ge, S.; Li, N.; Yu, J.; Huang, J., Photoelectrochemical lab-on-paper device equipped with a porous Au-paper electrode and fluidic delay-switch for sensitive detection of DNA hybridization. *Lab Chip* **2013,** *13*, 3945−3955.

77. Ge, L.; Wang, P.; Ge, S.; Li, N.; Yu, J.; Yan, M.; Huang, J., Photoelectrochemical lab-on-paper device based on an integrated paper supercapacitor and internal light source. *Anal. Chem.* **2013,** *85*, 3961−3970.

78. Zhang, Y.; Gao, D.; Fan, J.; Nie, J.; Le, S.; Zhu, W.; Yang, J.; Li, J., Naked-eye quantitative aptamer-based assay on paper device. *Biosens. Bioelectron.* **2016,** *78*, 538−546.

79. Mu, X.; Xin, X.; Fan, C.; Li, X.; Tian, X.; Xu, K. F.; Zheng, Z., A paper-based skin patch for the diagnostic screening of cystic fibrosis. *Chem. Commun.* **2015,** *51*, 6365−6368.

80. Rattanarat, P.; Dungchai, W.; Siangproh, W.; Chailapakul, O.; Henry, C. S., Sodium dodecyl sulfate-modified electrochemical paper-based analytical device for determination of dopamine levels in biological samples. *Anal. Chim. Acta* **2012,** *744*, 1−7.

81. Zuk, R. F.; Ginsberg, V. K.; Houts, T.; Rabbie, J.; Merrick, H.; Ullman, E. F.; Fischer, M. M.; Sizto, C. C.; Stiso, S. N.; Litman, D. J., Enzyme immunochromatography-a quantitative immunoassay requiring no instrumentation. *Clin. Chem.* **1985,** *31*, 1144−1150.

82. Vaughan, L.; Milavetz, G.; Ellis, E.; Szefler, S.; Conboy, K.; Weinberger, M.; Tillson, S.; Jenne, J.; Wiener, M.; Shaughnessy, T.; Carrico, J., Multicentre Evaluation of Disposable Visual Measuring Device to Assay Theophylline from Capillary Blood Sample. *Lancet* **1986,** *327*, 184−186.

83. Novell, M.; Guinovart, T.; Blondeau, P.; Rius, F. X.; Andrade, F. J., A paper-based potentiometric cell for decentralized monitoring of Li levels in whole blood. *Lab Chip* **2014,** *14*, 1308−1314.

84. Bhakta, S. A.; Borba, R.; Taba, M., Jr.; Garcia, C. D.; Carrilho, E., Determination of nitrite in saliva using microfluidic paper-based analytical devices. *Anal. Chim. Acta* **2014,** *809*, 117−122.

85. Yamada, K.; Takaki, S.; Komuro, N.; Suzuki, K.; Citterio, D., An antibody-free microfluidic paper-based analytical device for the determination of tear fluid lactoferrin by fluorescence sensitization of Tb^{3+}. *Analyst* **2014,** *139*, 1637−1643.

86. Yamada, K.; Henares, T. G.; Suzuki, K.; Citterio, D., Distance-Based Tear Lactoferrin Assay on Microfluidic Paper Device Using Interfacial Interactions on Surface-Modified Cellulose. *ACS Appl. Mater. Interfaces* **2015,** *7*, 24864−24875.

87. Hsu, M. Y.; Yang, C. Y.; Hsu, W. H.; Lin, K. H.; Wang, C. Y.; Shen, Y. C.; Chen, Y. C.; Chau, S. F.; Tsai, H. Y.; Cheng, C. M., Monitoring the VEGF level in aqueous humor of patients with ophthalmologically relevant diseases via ultrahigh sensitive paper-based ELISA. *Biomaterials* **2014,** *35*, 3729−3735.

88. Jagirdar, A.; Shetty, P.; Satti, S.; Garg, S.; Paul, D., A paperfluidic device for dental applications using a novel patterning technique. *Anal. Methods* **2015,** *7*, 1293−1299.

89. Hsu, C. K.; Huang, H. Y.; Chen, W. R.; Nishie, W.; Ujiie, H.; Natsuga, K.; Fan, S. T.; Wang, H. K.; Lee, J. Y.; Tsai, W. L.; Shimizu, H.; Cheng, C. M., Paper-based ELISA for the detection of autoimmune antibodies in body fluid-the case of bullous pemphigoid. *Anal. Chem.* **2014,** *86*, 4605−4610.

90. Murdock, R. C.; Shen, L.; Griffin, D. K.; Kelley-Loughnane, N.; Papautsky, I.; Hagen, J. A., Optimization of a paper-based ELISA for a human performance biomarker. *Anal. Chem.* **2013,** *85*, 11634−11642.

91. Robinson, R.; Wong, L.; Monnat, R.; Fu, E., Development of a Whole Blood Paper-Based Device for Phenylalanine Detection in the Context of PKU Therapy Monitoring. *Micromachines* **2016,** *7*, 28.

92. Ismail, A.; Araujo, M. O.; Chagas, C. L.; Griveau, S.; D'Orlye, F.; Varenne, A.; Bedioui, F.; Coltro, W. K., Colorimetric analysis of the decomposition of S-nitrosothiols on paper-based microfluidic devices. *Analyst* **2016,** *141*, 6314−6320.

93. Pena-Pereira, F.; Lavilla, I.; Bendicho, C., Paper-based analytical device for instrumental-free detection of thiocyanate in saliva as a biomarker of tobacco smoke exposure. *Talanta* **2016,** *147*, 390−396.

94. Li, M.; Tian, J.; Al-Tamimi, M.; Shen, W., Paper-based blood typing device that reports patient's blood type "in writing". *Angew. Chem. Int. Ed.* **2012,** *51*, 5497−5501.

95. Noiphung, J.; Talalak, K.; Hongwarittorrn, I.; Pupinyo, N.; Thirabowonkitphithan, P.; Laiwattanapaisal, W., A novel paper-based assay for the simultaneous determination of Rh typing and forward and reverse ABO blood groups. *Biosens. Bioelectron.* **2015,** *67*, 485−489.

96. Bond, M.; Elguea, C.; Yan, J. S.; Pawlowski, M.; Williams, J.; Wahed, A.; Oden, M.; Tkaczyk, T. S.; Richards-Kortum, R., Chromatography paper as a low-cost medium for accurate spectrophotometric assessment of blood hemoglobin concentration. *Lab Chip* **2013,** *13*, 2381−2388.

97. Berry, S. B.; Fernandes, S. C.; Rajaratnam, A.; DeChiara, N. S.; Mace, C. R., Measurement of the hematocrit using paper-based microfluidic devices. *Lab Chip* **2016,** *16*, 3689−3694.

Achievement list

Original papers related to this thesis

(1) Kentaro Yamada; Shunsuke Takaki; Nobutoshi Komuro; Koji Suzuki; Daniel Citterio,
"An antibody-free microfluidic paper-based analytical device for the determination of tear fluid lactoferrin by fluorescence sensitization of Tb^{3+}", Analyst, **2014**, 139, 1637−1643.

(2) Kentaro Yamada; Terence G. Henares; Koji Suzuki; Daniel Citterio,
"Distance-Based Tear Lactoferrin Assay on Microfluidic Paper Device Using Interfacial Interactions on Surface-Modified Cellulose", ACS Applied Materials & Interfaces, **2015**, 7, 24864−24875.

(3) Kentaro Yamada; Koji Suzuki; Daniel Citterio,
"Text-displaying colorimetric paper-based analytical device",
ACS Sensors, **2017,** in press (DOI: 10.1021/acssensors.7b00464).

Other original papers

(1) Keisuke Tenda; Riki Ota; Kentaro Yamada; Terence G. Henares; Koji Suzuki; Daniel Citterio,
"High-Resolution Microfluidic Paper-Based Analytical Device for Sub-Microliter Sample Analysis",
Micromachines, **2016**, 7, 80.

(2) Terence G. Henares†; Kentaro Yamada†; Koji Suzuki; Daniel Citterio,
""Drop-slip" bulk sample flow on fully inkjet-printed microfluidic paper-based analytical device",
Sensors and Actuators B: Chemical, **2017**, 244, 1129−1137. († equally contributed)

(3) Hiroko Kudo; Kentaro Yamada; Daiki Watanabe; Koji Suzuki; Daniel Citterio,
"Paper-Based Analytical Device for Zinc Ion Quantification in Water Samples with Power-Free Analyte Concentration", Micromachines, **2017**, 8, 127.

Review articles

(1) Kentaro Yamada; Terence G. Henares; Koji Suzuki; Daniel Citterio,
"Paper-Based Inkjet-Printed Microfluidic Analytical Devices",
Angewandte Chemie, International Edition, **2015**, 54, 5294−5310.

(2) Kentaro Yamada†; Hiroyuki Shibata†; Koji Suzuki; Daniel Citterio,
"Toward practical application of paper-based microfluidics for medical diagnostics: state-of-the-art and challenges", Lab on a Chip, **2017**, 17, 1206−1249. († equally contributed)

Conference paper

(1) Kentaro Yamada; Shunsuke Takaki; Koji Suzuki; Daniel Citterio,
"Microfluidic Paper-Based Analytical Device for Fluorescence Detection of Lactoferrin in Tear Fluid",
Proceeding of MicroTAS 2013, **2013**, pp.895−897.

International conference presentations

Oral presentations

(1) "Reader-free paperfluidic analytical device for fluorescence-based tear lactoferrin detection",
○Kentaro Yamada; Terence G. Henares; Koji Suzuki; Daniel Citterio,
Pacifichem 2015, Honolulu (USA), December 2015.

(2) "Color printing for text-displayed colorimetry on paper-based analytical devices",
○Kentaro Yamada; Koji Suzuki; Daniel Citterio,
Gordon Research Conferences 2016 (Bioanalytical Sensors), Rhode Island (USA), June 2016.

(3) "Text-displayed colorimetric paper-based analytical devices obtained by printing",
○Kentaro Yamada; Koji Suzuki; Daniel Citterio, Pittcon 2017, Chicago (USA), March 2017.

Poster presentations

(1) "Microfluidic Paper-Based Analytical Device for Fluorescence Detection of Lactoferrin in Tear Fluid",
○Kentaro Yamada; Shunsuke Takaki; Koji Suzuki; Daniel Citterio,
The 17th International Conference on Miniaturized Systems for Chemistry and Life Sciences (MicroTAS 2013),
Freiburg (Germany), October 2013.

(2) "An Antibody-free Microfluidic Paper-Based Analytical Device (μPAD) for the Determination of Tear Fluid Lactoferrin",
○Kentaro Yamada; Shunsuke Takaki; Koji Suzuki; Daniel Citterio,
RSC Tokyo International Conference 2014, Chiba (Japan), September 2014.

(3) "Reader-free quantification of tear fluid lactoferrin on paperfluidic analytical device",
○Kentaro Yamada; Terence G. Henares; Koji Suzuki; Daniel Citterio,
RSC Tokyo International Conference 2015, Chiba (Japan), September 2015.

(4) "Paper-based microfluidic device for distance-based quantification of lactoferrin",
○Kentaro Yamada; Terence G. Henares; Koji Suzuki; Daniel Citterio,
Tokyo Paper 2015, Tokyo (Japan), October 2015.

(5) “Fluorescence-Based Optical Sensor for Lactoferrin on Paper Platform with Direct Concentration Readout”,
○Kentaro Yamada; Terence G. Henares; Koji Suzuki; Daniel Citterio,
Europt[r]ode XIII, Graz (Austria), March 2016.

(6) “Color printing for text-displayed colorimetry on paper-based analytical devices”,
○Kentaro Yamada; Koji Suzuki; Daniel Citterio,
Gordon Research Seminar (Bioanalytical Sensors), Rhode Island (USA), June 2016.

(7) “Color printing for text-displayed colorimetry on paper-based analytical devices”,
○Kentaro Yamada; Koji Suzuki; Daniel Citterio,
Gordon Research Conferences 2016 (Bioanalytical Sensors), Rhode Island (USA), June 2016.

(8) “Text-displayed colorimetric paper-based analytical devices obtained by printing”,
○Kentaro Yamada; Koji Suzuki; Daniel Citterio,
RSC Tokyo International Conference 2016, Chiba (Japan), September 2016.

(9) “Text-displayed colorimetric paper analytical device for protein sensing”,
○Kentaro Yamada; Koji Suzuki; Daniel Citterio,
International Workshop on Quantitative Biology 2017, Yokohama (Japan), April 2017.

Domestic conference presentations

Oral presentations

(1) 「ラクトフェリン測定用マイクロ流体ペーパーセンサー（μPAD）の開発」,
○山田 健太郎、髙木 俊輔、鈴木 孝治、チッテリオ ダニエル,
日本化学会第 94 春季年会，名古屋大学，東山キャンパス，2014 年 3 月.

(2) 「シグナルリーダー不要のラクトフェリン定量分析用ペーパーマイクロ流体デバイス（μPAD）」,
○山田 健太郎、ヘナレス テレンス、鈴木 孝治、チッテリオ ダニエル,
日本分析化学会第 64 年会，九州大学，伊都キャンパス，2015 年 9 月.

(3) “Text-Displayed Paper-Based Analytical Device for Urine Analysis”,
○山田 健太郎、鈴木 孝治、チッテリオ ダニエル,
日本化学会第 97 春季年会，慶應義塾大学，日吉キャンパス，2017 年 3 月.

Poster presentation

(1) 「ラクトフェリン測定用マイクロ流体ペーパーセンサ（μPAD）の開発」,
○山田 健太郎、髙木 俊輔、鈴木 孝治、チッテリオ ダニエル,
日本分析化学会第 62 年会，近畿大学，東大阪キャンパス，2013 年 9 月.

(2) 「比色法を用いた文字表示型ペーパー分析デバイス」,
○山田 健太郎、鈴木 孝治、チッテリオ ダニエル,
日本分析化学会第 65 年会，北海道大学工学部，2016 年 9 月.

Other conference activities

International conferences

(1) "Paper-based sensor for fluorescence detection of histamine",
○Yusuke Suemura; Kentaro Yamada; Koji Suzuki; Daniel Citterio,
RSC Tokyo International Conference 2014, Chiba (Japan), September 2014.

(2) "Inkjet-printed polymeric hydrogels for application on microfluidic paper-based analytical devices",
○Masanori Ishii; Kentaro Yamada; Koji Suzuki; Daniel Citterio,
RSC Tokyo International Conference 2015, Chiba (Japan), September 2015.

(3) "Parameters influencing sample transport in microfluidic paper-based analytical devices",
○Riki Ota; Kentaro Yamada; Koji Suzuki; Daniel Citterio,
RSC Tokyo International Conference 2015, Chiba (Japan), September 2015.

(4) "Histamine selective paper sensing device",
○Yusuke Suemura; Kentaro Yamada; Koji Suzuki; Daniel Citterio,
RSC Tokyo International Conference 2015, Chiba (Japan), September 2015.

(5) "Printed microfluidic paper-based analytical devices (μPADs) for ocular disease diagnostics",
Kentaro Yamada; Koji Suzuki; ○Daniel Citterio,
International Symposium on Analytical Biosensors, Fuzhou (China), November 2015.

(6) "Inkjet-printed microfluidic paper-based analytical devices (μPADs) for colorimetric cation detection",
○Daniel Citterio; Terence G. Henares; Shunsuke Takaki; Hiroyuki Shibata; Nobutoshi Komuro; Kentaro Yamada; Koji Suzuki,
Pacifichem 2015, Honolulu (USA), December 2015.

(7) "Parameters influencing the performance of inkjet-printed microfluidic paper-based analytical devices",
○Riki Ota; Kentaro Yamada; Koji Suzuki; Daniel Citterio,
Pacifichem 2015, Honolulu (USA), December 2015.

(8) "Printed (microfluidic) paper-based analytical devices (μPADs)",
Kentaro Yamada; Terence G. Henares; Nipapan Ruecha; Koji Suzuki; ○Daniel Citterio,
PACCON 2016, Bangkok (Thailand), February 2016.

(9) "Inkjet-generated ion selective optical sensing particles",
○Yoshiki Soda; Hiroyuki Shibata; Kentaro Yamada; Koji Suzuki; Daniel Citterio,
RSC Tokyo International Conference 2016, Chiba (Japan), September 2016.

(10) "Simplified metal complex stoichiometry determination by inkjet printing",
○Kento Kuwahara; Kota Kido; Kentaro Yamada; Koji Suzuki; Daniel Citterio,
RSC Tokyo International Conference 2016, Chiba (Japan), September 2016.

(11) "Printed paper-based ion-selective optode devices with integrated pH-buffer system",
○Hiroyuki Shibata; Terence G. Henares; Kentaro Yamada; Koji Suzuki; Daniel Citterio,
RSC Tokyo International Conference 2016, Chiba (Japan), September 2016.

(12) "Microfluidic paper-based analytical device (μPAD) for non-enzymatic colorimetric urea analysis",
○Daiki Watanabe; Masanori Ishii; Kentaro Yamada; Koji Suzuki; Daniel Citterio,
RSC Tokyo International Conference 2016, Chiba (Japan), September 2016.

(13) "Colorimetric Microfluidic Paper-Based Analytical Devices: Role of the Paper on Sample Transport and Analytical Performance",
○Daniel Citterio; Riki Ota; Kentaro Yamada; Hiroyuki Shibata; Yoshiki Soda; Koji Suzuki,
Pittcon 2017, Chicago (USA), March 2017.

(14) "pH-Buffer-Integrated Ion-Selective Optodes on Printed Microfluidic Paper-Based Analytical Devices (microPADs)",
○Hiroyuki Shibata; Terence G. Henares; Kentaro Yamada; Koji Suzuki; Daniel Citterio,
Pittcon 2017, Chicago (USA), March 2017.

(15) "Laminated Microfluidic Paper-Based Analytical Devices for Clinical Protein Assays",
○Keisuke Tenda; Riki Ota; Kentaro Yamada; Koji Suzuki; Daniel Citterio,
Pittcon 2017, Chicago (USA), March 2017.

(16) "Inkjet Generated Ion-Selective Optode Particles for Calibration-Free Sensing on Paper-Based Analytical Devices",
○Yoshiki Soda; Hiroyuki Shibata; Kentaro Yamada; Koji Suzuki; Daniel Citterio,
Pittcon 2017, Chicago (USA), March 2017.

(17) "With paper and office equipment to simple and lowcost analytical devices",
○Daniel Citterio; Kentaro Yamada; Terence G. Henares; Koji Suzuki,
International Workshop on Quantitative Biology 2017, Yokohama (Japan), April 2017.

(18) “Paper-based colorimetric sodium ion-selective devices integrated with pH-buffering function”,
○Hiroyuki Shibata; Terence G. Henares; Kentaro Yamada; Koji Suzuki; Daniel Citterio,
International Workshop on Quantitative Biology 2017, Yokohama (Japan), April 2017.

(19) “Inkjet-Generated Ion-Selective Optode Particles for Calibration-Free Sensing on Paper-Based Analytical Devices”,
○Yoshiki Soda; Hiroyuki Shibata; Kentaro Yamada; Koji Suzuki; Daniel Citterio,
International Workshop on Quantitative Biology 2017, Yokohama (Japan), April 2017.

(20) “Low-cost sample concentration and detection device for trace metal quantification”,
○Hiroko Kudo; Daiki Watanabe; Kentaro Yamada; Koji Suzuki; Daniel Citterio,
International Workshop on Quantitative Biology 2017, Yokohama (Japan), April 2017.

Domestic conferences

(1) 「ナトリウムイオン検出のためのイオン選択性オプトード法に基づいたマイクロ流体紙基板分析デバイス」,
○柴田 寛之、ヘナレス テレンス、山田 健太郎、鈴木 孝治、チッテリオ ダニエル,
化学とマイクロ・ナノシステム学会第 34 回研究会 (CHEMINAS 34), 幕張メッセ国際会議場, 2016 年 9 月.

(2) 「マイクロ流体紙基板分析デバイス（μPADs）のパラメータ評価」,
○太田 力、山田 健太郎、鈴木 孝治、チッテリオ ダニエル,
化学とマイクロ・ナノシステム学会第 34 回研究会 (CHEMINAS 34), 幕張メッセ国際会議場, 2016 年 9 月.

(3) 「紙基板マイクロ流体デバイスの高解像度パターニングによるサブマイクロリットル分析」,
○天田 啓介、太田 力、山田 健太郎、鈴木 孝治、チッテリオ ダニエル,
日本分析化学会第 65 年会, 北海道大学工学部, 2016 年 9 月.

(4) 「印刷技術を用いた pH 緩衝作用が内蔵された紙基板イオン選択性オプトードデバイス」,
○柴田 寛之、ヘナレス テレンス、山田 健太郎、鈴木 孝治、チッテリオ ダニエル,
日本分析化学会第 65 年会, 北海道大学工学部, 2016 年 9 月.

(5) 「インクジェット技術を用いた紙上への比色分析試薬の吐出量制御」,
○桑原 健斗、城戸 滉太、山田 健太郎、鈴木 孝治、チッテリオ ダニエル,
日本分析化学会第 65 年会, 北海道大学工学部, 2016 年 9 月.

(6) 「インクジェットプリント技術によるオプティカルセンシング粒子の創製」,
○相田 佳毅、柴田 寛之、山田 健太郎、鈴木 孝治、チッテリオ ダニエル,
日本分析化学会第 65 年会，北海道大学工学部，2016 年 9 月.

(7) 「印刷技術を用いたマイクロ流体紙基板分析デバイス上における試薬逐次流動システム」,
○石井 政憲、山田 健太郎、鈴木 孝治、チッテリオ ダニエル,
日本分析化学会第 65 年会，北海道大学工学部，2016 年 9 月.

(8) "Determination of stoichiometry for colorimetric metal indicators by inkjet printing",
○桑原 健斗、城戸 滉太、山田 健太郎、鈴木 孝治、チッテリオ ダニエル,
日本化学会第 97 春季年会，慶應義塾大学，日吉キャンパス，2017 年 3 月.

(9) "Inkjet-Generated Ion-Selective Optode Particles For Calibration-Free Sensing on Paper-Based Analytical Devices",
○相田 佳毅、柴田 寛之、山田 健太郎、鈴木 孝治、チッテリオ ダニエル,
日本化学会第 97 春季年会，慶應義塾大学，日吉キャンパス，2017 年 3 月.

(10) "Non-enzymatic urea/creatinine detection with paper-based microfluidic device",
○渡邊 大輝、石井 政憲、鈴木 孝治、山田 健太郎、チッテリオ ダニエル,
日本化学会第 97 春季年会，慶應義塾大学，日吉キャンパス，2017 年 3 月.

(11) "Low-cost sample concentration and detection device for trace metal quantification",
○工藤 弘子、渡邊 大輝、山田 健太郎、鈴木 孝治、チッテリオ ダニエル,
日本化学会第 97 春季年会，慶應義塾大学，日吉キャンパス，2017 年 3 月.

(12) "Ionophore-based colorimetric sodium ion sensing on pH-buffer-integrated paper-based devices",
○柴田 寛之、ヘナレス テレンス、山田 健太郎、鈴木 孝治、チッテリオ ダニエル,
日本化学会第 97 春季年会，慶應義塾大学，日吉キャンパス，2017 年 3 月.

Other publications

(1) 山田 健太郎、鈴木 孝治、チッテリオ ダニエル,
「家庭用インクジェットプリンタを用いた紙基板ヘルスケアセンシングチップ」 三林浩二（編）『スマート・ヒューマンセンシング』，シーエムシー出版，pp.81−90，2014 年 3 月出版.

(2) 山田 健太郎、鈴木 孝治、チッテリオ ダニエル,
「特集：ディスポーザブルセンサおよびそれを支える技術の新展開 3. 紙基板マイクロ流体分析デバイス」，Electrochemistry, **2015**, 83, 30−35.

(3) Terence Henares; Kentaro Yamada; Koji Suzuki; Daniel Citterio,
"Inkjet Printing of Biomolecules for Biorecognition" in "Design of Polymeric Platforms for Selective Biorecognition", J. Rodriguez-Hernandez, A. Lopez-Cortajarena (editors), Annia Levinson (associate editor), Springer Ed. USA, pp.197−235, published February 2015.

(4) 石井 政憲、城戸 滉太、太田 力、柴田 寛之、山田 健太郎、鈴木 孝治、チッテリオ ダニエル,
「インクジェット技術によるペーパーマイクロ流体デバイスの開発」,
日本画像学会誌, **2016**, 55, 94−105.

(5) 山田 健太郎、チッテリオ ダニエル,
「特集：広がるマイクロ流路の可能性　3. 紙製マイクロ流体デバイス」,
化学と工業, **2016**, 69, 120−122.

(6) Nipapan Ruecha; Kentaro Yamada; Koji Suzuki; Daniel Citterio,
"(Bio)Chemical Sensors Based on Paper" in "Materials for Chemical Sensing",
Thiago Regis Longo Cesar Paixão, Subrayal Medapati Reddy (editors), Springer Ed. USA, pp.29−74, published December 2016.

Patent

(1) 「紙装置を用いたトランスフェリンファミリータンパク質の検出」,
山田 健太郎、髙木 俊輔、鈴木 孝治、チッテリオ ダニエル,
特許出願 2014-037523, 2014 年 2 月 27 日出願、2015 年 3 月 19 日公開.

Awards

(1) "Hot Article", Analyst, **2014**, 139, 1637−1643.
(2) "Feature Article", Micromachines, **2016**, 7, 80.
(3) "Featured on back cover", Analyst, **2014**, Volume 139, Issue 7, published April 7, 2014.
(4) 「若手講演ポスター賞」, 日本分析化学会第 62 年会, 2013 年 9 月.
(5) "Poster Presentation Award", RSC Tokyo International Conference, September 2014.
(6) 「機能創造賞」, 慶應義塾大学マテリアルデザイン科学専修　修士論文発表会, 2015 年 3 月.
(7) "Analyst Poster Presentation Award", Gordon Research Conferences 2016 (Bioanalytical Sensors), June 2016.

Acknowledgement

I would like to offer my special thanks to my academic supervisor, Prof. Daniel Citterio, for his enormous efforts in guidance and encouragement throughout the progress of my work. Without his persistent help and extensive knowledge as a scientist, this thesis would not have been possible. I would also like to appreciate his support to give me a chance of overseas research at Colorado State University, USA.

I wish to express my great gratitude to Prof. Seimei Shiratori, Prof. Norihisa Miki and Prof. Tomoaki Okuda for their efforts as the members of the thesis committee to provide me with their valuable and constructive suggestions.

I am deeply grateful to Prof. Koji Suzuki for his kind support and encouragement as a co-supervisor. I would like to thank Ms. Mari Shoji for her solid assistance in my research as a secretary of the laboratory. Dr. Yuki Hiruta is acknowledged for his support and encouragement as a Ph.D. student as well as a lecturer of the laboratory. It was a pleasure to have the chance to work with Dr. Terence Gaba Henares and Dr. Nipapan Ruecha, very skilled, kind, and social postdoctoral fellows in the same research field.

I would like to thank my research collaborators. Prof. Kazuo Tsubota, Dr. Yoko Ogawa, and Dr. Hideki Sonobe at Keio University Hospital are acknowledged for their helpful discussion regarding the measurement of lactoferrin and for providing me with human tear samples. I received generous support from Prof. Yoshihiko Kanno at Tokyo Medical University Hospital regarding the project of urinary protein measurement. I would like to appreciate Prof. Hideko Kanazawa and Dr. Yuki Hiruta of the Faculty of Pharmaceutics, Keio University for their help in measuring paper surface ζ-potentials. The laboratory members who cooperated for the user test of the paper devices are kindly acknowledged.

This work was financially supported by the Medical Research and Development Programs Focused on Technology Transfer: Development of Advanced Measurement and Analysis Systems (SENTAN) from the Japan Agency for Medical Research and Development (AMED); a research grant provided by the Graduate School of Science and Technology, Keio University; and a Research Fellowship of the Japan Society for the Promotion of Science (JSPS) for Young Scientists.

I am grateful for the assistance and encouragement given by the laboratory students. I would like to express my special thanks to Mr. Shunsuke Takaki for his guidance and generous support as a research mentor. I am pleased that I could enjoy fruitful research life with my great colleagues. Although it is impossible to list their all names, I would like to thank the stimulating junior colleagues for their kind support, encouragement, and fruitful discussions.

Finally, I wish to show my greatest appreciation to my family for their understanding and continued support during my research life.